Elaboration of photo-responsive supramolecular nano-cylinders in solution

Luke Harvey

COLLEGE DOCTORAL PAYS DE LA LOIRE
ED MATIERE, MOLECULES MATERIAUX ET GEOSCIENCES
DOCTORAL PAYS DE LA LOIRE
MATERIAUX ET GEOSCIENCES

Le Mans Université

THESE DE DOCTORAT

DE
LE MANS UNIVERSITE
SOUS LE SCEAU DE
LA COMUE ANGERS – LE MANS

ECOLE DOCTORALE N° 596
Matière, Molécules, Matériaux et Géosciences
Spécialité : « *Chimie et physico-chimie des polymères* »

Par
Luke HARVEY

Elaboration of photo-responsive supramolecular nano-cylinders in solution

Soutenance de thèse prévue au Mans, le 19/12/2023
Unité de recherche : UMR CNRS 6283
Thèse N° : 2023LEMA1035

Rapporteurs avant soutenance :

Sébastien Perrier	Professeur	Warwick University
Rémi Métivier	Directeur de recherches	ENS Paris-Saclay

Composition du Jury :

Présidente :	Emilie Moulin	Directrice de recherches	Université de Strabourg
Examinateurs :	Sébastien Perrier	Professeur	Warwick University
	Rémi Métivier	Directeur de recherches	ENS Paris-Saclay
Dir. de thèse :	Olivier Colombani	Maître de conférences	Le Mans Université
Co-dir. de thèse :	Erwan Nicol	Maître de conférences	Le Mans Université

Acknowledgments

The work presented in this manuscript was carried out in the IMMM institute ("Institut des Molécules et Matériaux du Mans"), I would therefore like to start by thanking IMMM's directors, Prof. Laurent Fontaine, Prof. Marc Lamy De La Chapelle and Prof. Philippe Daniel, for welcoming me in the institute.

I would also like to thank Emilie Moulin, Sébastien Perrier and Rémi Métivier for accepting to review this work, and for their valuable advice.

The French Ministère de l'Enseignement Supérieur et de la Recherche is acknowledged for financing this PhD project.

An immense thanks goes out to Dr. Olivier Colombani and Dr. Erwan Nicol, who supervised this PhD project. I honestly could not have hoped for a better team, and it has been a pleasure working with you both.

Thank you Olivier for your patience, availability (despite a fairly busy agenda), and most of all, kindness. I truly appreciated how much you care for the well-being of your students. Thank you for giving me a fair amount of freedom in my work, I have learnt a lot over the last 3 years.

Thank you Erwan for your valuable guidance, availability, and having put up with my never-ending questions throughout these 3 years. Thank you for all the advice you gave me, particularly during the challenging synthesis period. These 3 years would have been a lot less enjoyable without your implication and good humor.

I also extend my thanks to Prof. Laurent Bouteiller, for his collaboration and precious advice. It was a pleasure collaborating with you during my 1st year master's internship, and I'm glad you were a part of this PhD project. Thank you for your help, which allowed the project to keep progressing.

These acknowledgements would be incomplete without thanking the people who contributed to the generally good atmosphere within the PCI team. Thanks to the other PhD students: Bastien, Yuwen, Noemie, Théo, and also post-docs: Inès, Julien, Asli and Gireesh. A particular thanks goes out to Sandra, who it was a pleasure to collaborate and exchange with.

I wish to thank Elodie Renier, the team's logistical administrator, for her help and availability, particularly during the SANS/SAXS run as well as for organizing the logistics regarding the defense of this PhD.

I also thank Prof. Sagrario Pascual for interesting discussions, and for having trusted me with master students practical work lessons.

I thank Ralf Schweins, Isabelle Morfin and Guillaume Brotons for all their help regarding SANS and SAXS measurements, from writing of the proposals to fitting the experimental data. Thanks to their implication I have learnt a lot about these techniques.

I would also like to express my gratitude towards everyone who contributed to this work: Boris, for help with SEC measurements, Sullivan, for help with NMR. A special thanks goes to Anthony Rousseau, for help with cryo-TEM measurements.

Lastly, and most importantly, I thank my friends and family for always being there for me, and particularly my brothers, Anton and Richard. I would not be where I am today without them. Blue skies

Abbreviations

^{1}H NMR - Proton nuclear magnetic resonance

AFM – Atomic force microscopy

ATRP – Atom transfer radical polymerization

Azo - Azobenzene

CD – Circular dichroism

CMC – Critical micelle concentration

Cryo-TEM – Cryogenic transmission electron microscopy

Đ – dispersity

DMF – dimethyl formamide

DMSO – dimethyl sulfoxide

DP_n – Average degree of polymerization

FRET – Forster resonance energy transfer

H-bond – Hydrogen bond

ITC – Isothermal titration calorimetry

LCST – Lower critical solubility temperature

LS, DLS, SLS – Light Scattering, Dynamic light scattering, Static light scattering

M_{app} – Weight average apparent molecular weight

MCH – Methyl cyclohexane

M_n – Number average molecular weight

N_{agg} – Weight average aggregation number

PEO – Poly-(ethylene oxide)

PISA – Polymerization induced self-assembly

PSS – Photo-stationary state

RAFT – Reversible addition fragmentation polymerization

SANS – Small angle neutron scattering

SAXS – Small angle X-ray scattering

SEC – Size exclusion chromatography

SEM – Scanning electron microscopy

SPB – Supramolecular polymer bottlebrush

THF - Tetrahydrofuran

UV-Vis – Ultraviolet-visible light absorption spectroscopy

GENERAL INTRODUCTION

Supramolecular chemistry was defined by Jean-Marie Lehn in 1987 during his Nobel prize speech as follows: « Supramolecular chemistry is the chemistry of the intermolecular bond, covering the structures and functions of the entities formed by association of two or more chemical species ». [1]

Indeed, supramolecular chemistry is the study of systems which are assembled by the means of reversible, weak interactions, such as hydrogen bonding, Van der Waals interactions, or Pi-stacking, as opposed to molecular chemistry, which is the chemistry of covalent bonds.

Supramolecular chemistry therefore allows for the design of complex structures, by self-assembly of smaller, simpler molecular units, leading to systems which would be difficult or even impossible to obtain via molecular chemistry - this approach is particularly powerful for designing nano-structures. Nano-structures, which are objects that possess at least one dimension on the nano-metric scale, can be divided into 4 categories: 0-dimensional (0D; *e.g.* quantum dots)[2], 1-dimensional (1D; rods)[3], 2-dimensional (2D; sheets)[4] and 3-dimensional (3D; networks or micelles)[5].

Imparting stimuli-responsiveness has received extensive attention in recent years, as such systems could lead to "smart" materials. In particular, light is an attractive stimulus, as it is non-invasive and allows for high spatio-temporal control. In this project, we aimed to design, synthesize and characterize supramolecular nanocylinders that may undergo reversible light-triggered disassembly in solution (**Scheme 1**). Such systems could be used for the elaboration of light-sensitive emulsions or gels, although this was not studied during this project.

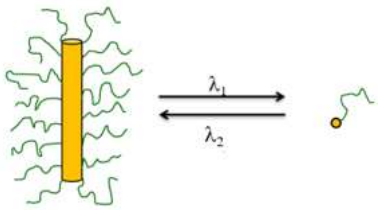

Scheme 1. Conceptual scheme of the objective of this PhD work: reversible formation and disassembly of supramolecular nanocylinders in solution upon light irradiation. The yellow core represents the self-assembling and light-responsive assembling stickers, and the green arms represent the polymer arms.

The general structure of the target compound consists in a self-assembling core, that provides both self-assembly and light-responsiveness, decorated with polymer arms, which impart solubility in water and some organic solvents.

<u>This thesis is composed of 4 chapters:</u>

- The **1st chapter** consists of a bibliographic state of the art regarding supramolecular polymer-decorated nano-cylinders, focusing respectively on self-assembly in solution driven by directional hydrogen bonding; stimuli-responsive systems; and azobenzene-containing photo-responsive assemblies.

- The **2nd chapter** presents the different synthetic pathways that were explored to access a first target molecule decorated with poly-(ethylene oxide) (PEO) arms: **Azo-(U-PEO)$_2$**.

-The **3rd chapter** presents the physico-chemical study of **Azo-(U-PEO)$_2$** in aqueous media by light scattering, UV-Vis spectroscopy, ^{1}H NMR and cryo-TEM. The results from chapters 2 and 3 have been published in Polymer Chemistry (RSC).

-The **4th chapter** presents the photo-responsive self-assembling properties of **Azo-(U-PEO)$_2$** in organic solvents (toluene and chloroform), through a combination of SANS and SAXS measurements as well as UV-Vis spectroscopy and ^{1}H NMR. These results are to be submitted for publication.

This thesis ends with the general conclusions of this work, as well as perspectives.

1. LENH, J.-M. Supramolecular Chemistry - Scope and Perspectives. *Nobel lecture* 444–491 (1987).

2. Wang, Z., Hu, T., Liang, R. & Wei, M. Application of Zero-Dimensional Nanomaterials in Biosensing. *Front Chem* **8**, 1–19 (2020).

3. Gruschwitz, F. V., Klein, T., Catrouillet, S. & Brendel, J. C. Supramolecular polymer bottlebrushes. *Chemical Communications* **56**, 5079–5110 (2020).

4. Baig, N. Two-dimensional nanomaterials: A critical review of recent progress, properties, applications, and future directions. *Compos Part A Appl Sci Manuf* **165**, 107362 (2023).

5. Verma, C., Berdimurodov, E., Verma, D. K., Berdimuradov, K., Alfantazi, A. & Hussain, C. M. 3D Nanomaterials: The future of industrial, biological, and environmental applications. *Inorg Chem Commun* **156**, 111163 (2023).

CHAPTER 1

Summary – Chapter 1

CHAPTER 1 – State of the art

The aim of this work was to design supramolecular nanocylinders that may be disrupted using light as a stimulus. Therefore, the first part of this bibliographic chapter aims to present a brief overview of the most commonly used strategies for designing 1D supramolecular nano-cylinders decorated with polymer arms in solution, with a focus on urea-based systems. Polymeric stimuli-responsive nanocylinders will also be presented. Then, azobenzene and photo-responsive systems based on this photo-switch will be presented, including some examples of azopolymers and supramolecular 1D azobenzene-based assemblies.

I. 1D Self-assembly in solution

Up until recently, the most common way to access polymer decorated nano-cylinders in solution relied on the self-assembly of amphiphilic block copolymers, however the compositional range of the blocks in which cylindrical micelles are thermodynamically favoured is fairly limited.[1–5] Furthermore, such systems are often out of thermodynamic equilibrium (i.e. kinetically frozen), implying that they do not always yield 1D structures, even when thermodynamic considerations are favorable.[5] Therefore, this approach was not used in the context of this project, due to its limited versatility, nor discussed in this bibliographic chapter. Covalent polymer bottlebrushes may also be obtained by synthesizing graft copolymers, however the synthesis can be difficult due to the steric hindrance of the arms.[6–8]

A more versatile approach consists in self-assembling polymers into nano-cylinders via weak interactions. While various weak interactions exist, the most suitable for 1D supramolecular self-assembly are generally H-bonds, due to their relatively high strength and directionality (see **Figure C1-1**).[9] The first part of this bibliographic chapter therefore presents the most commonly used self-assembling motifs for the elaboration of supramolecular polymer bottlebrushes, with a focus on hydrogen bonding systems and more particularly urea-based ones.

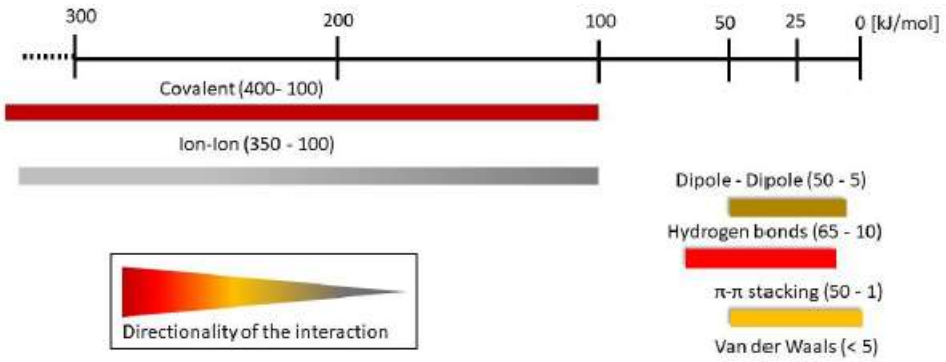

Figure C1-1. Bond energies and directionalities according to Steed et al.[9]

1. Shape persistent macrocycles

Rigid and « flat » phenylene acetylene macrocycles (PAM) decorated with polymer side chains have been described to self-assemble in a variety of solvents via Pi-stacking and solvophobic interactions, forming nano-tubes. The choice of solvent is crucial for self-assembly to occur: the solvent must be a poor solvent for the macrocycle core but a good solvent for the polymer arms. Furthermore, the self-assembly of the PAMs can be reinforced by implementing additional interactions such as H-bonding.[10]

Rosselli and coworkers have studied the self-assembly of such structures, possessing poly(styrene) (PS) arms, as can be seen in **Figure C1-2**. They studied the influence of the length of these side chains on the self-assembly in cyclohexane, which is a good solvent for the PS arms but is a non-solvent for the macrocycle core. Interestingly, when the PS arms are relatively short (1000 g/mol), the macrocycle is soluble in warm cyclohexane but forms a suspension upon cooling, suggesting that the PS arms are not long enough to provide solubility at room temperature. However, if the length of the PS arms is increased to 1500 g/mol, a gel is formed upon cooling (at concentrations above 0.5 wt.%.), and for arms of M_n = 2500 and 3500 g/mol, viscous solutions are formed. Light scattering measurements of the compound with arms of M_n = 2500 g/mol, at 0.11 wt.% in cyclohexane, revealed that long hollow nano-tubes were present, with lengths ranging from 250 to 1300 nm, and a R_h of 60 nm (which corresponds to a length of 500 nm). This work highlights the importance of using sufficiently long polymer arms to solubilize the compound, when the core is insoluble in the considered solvent. [11]

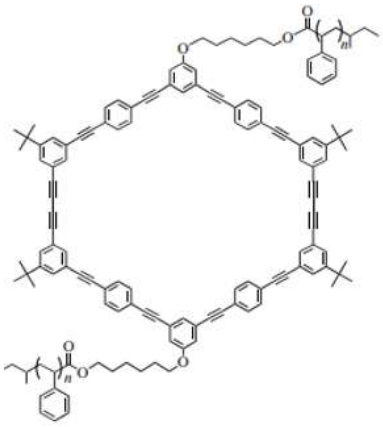

Figure C1-2. Chemical structure of PS decorated PAMs. Taken from ref[11]

More recently, PAMs consisting of hexakis(*m*-phenylene ethynylene), decorated with oligo-POE side chains, have been shown to self-assemble into nano-tubes in both polar and non-polar solvents, as demonstrated by ^{1}H NMR, UV spectroscopy and circular dichroism (CD). It is worthy to note that these side chains are linked to the macrocycle via amide bonds, which promote self-assembly via H-bonding. Interestingly, in non-polar solvents, the main driving force is reported to be H-bonding between amide groups, leading to well defined helical nano-tubes directed by the H-bonds. However, in polar solvents such as methanol or even water, it is the solvophobic interactions between hydrophobic macrocycle cores and Pi-stacking that is the driving force promoting self-assembly. Therefore, the authors report that the helicity of the nano-tubes may not be as well defined, due to a lack of directionality of the interactions.[10]

An inherent downside to this approach is the complicated synthesis which generally leads to low yields.[12,13,14]

2. Oligo cyclo-peptides

Extensive research has been carried out by the teams of Perrier and Biesalski (as well as others) on oligo-cyclopeptides as a scaffold for supramolecular nanotubes. These peptides consist of alternating R- and S- amino acids. Indeed, the alternating chirality of the amino acids leads to alternating orientation of the amide moieties within the cyclopeptide, perpendicular to the macrocycle's planar backbone, promoting stacking into β-sheets (**Figure C1-3**).[15,16] This architecture affords efficient and strong hydrogen bonding between macrocycles, ultimately leading to long, hollow nano-tubes. Macrocycles contained between 4 and 12 amino acid residues, with octapeptides leading to the highest association constants.[16]

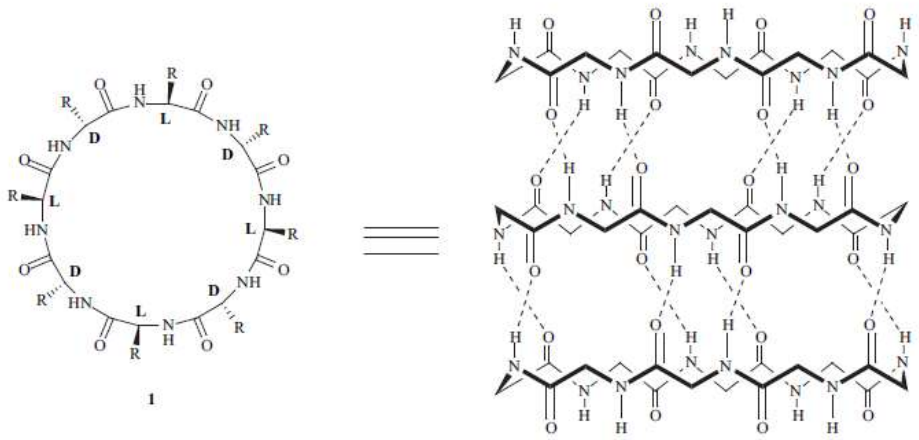

Figure C1-3. Structure of an 8-membered oligo cyclo-peptide and its supramolecular self-assembly (R groups are omitted for clarity). Taken from ref [17]

By grafting polymer arms onto the macrocycles, some degree of control over nano-tube length could be obtained, as well as fine tuning of the nano-tube solubility. Indeed, it has been shown that by increasing the grafting density and/or the molar mass of the polymer arms, the length of the cyclopeptide nano-tube decreases due to steric hindrance and the diameter increases due to longer polymeric arms. For instance, CPs decorated with PS arms of either 400 g/mol or 6000 g/mol in molecular weight were found to be on average 120 nm and 38 nm in length, respectively.[18] On the other hand, longer arms may also promote longer nano-tubes by better shielding the core from solvent that may enter into competition for H-bonding, which may be the case for systems in aqueous media.[17,18] The presence of polymer arms grafted onto the cyclopeptides also enables the obtention of isolated, distinct nano-tubes. The nature and number of amino acid residues can fine tune the properties of the inner wall of the nano-tube, as well as the internal diameter.[16]

Perrier's group also demonstrated that CP nanotubes are not kinetically frozen: polymer chains (unimers) can indeed exchange in a dynamic way between self-assembled structures. This was achieved by conjugating complementary dyes (cynanine3 and cynanine5) to the CPs. PEG-CP-Cy3 CP nanotubes and PEG-CP-Cy5 CP nanotubes were mixed in water and analysed by Förster resonance energy transfer (FRET). An increase in the FRET ratio was observed, suggesting dynamic exchange of unimers (**Figure C1-4**). Equilibrium was reached after approximately 100 minutes, as the FRET signal reached a plateau.[19]

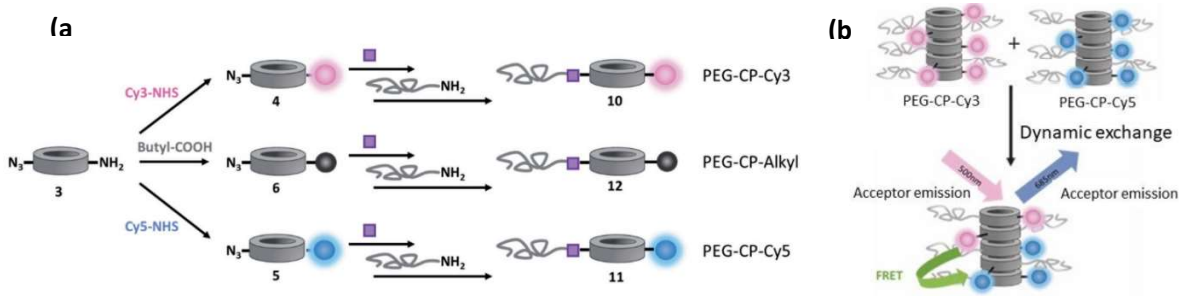

Figure C1-4. (a) Schematic representation of the dye conjugated CPs **(b)** Schematic representation of the FRET experiment. Adapted from ref[19]

In contrast to these results, Biesalski et al. reported a CP based system in which the molecular weight of the arms had little influence on the length of nano-tubes.[20] They synthesized a CP ring (containing 8 amino acid residues) possessing 3 ATRP initiator moieties, which they then self-assembled into nano-tubes, followed by subsequent ATRP polymerization of N-isopropyl acrylamide (NIPAM). They monitored the length and diameter of the nanotubes as a function of monomer conversion, using AFM. The initial nano-tubes (i.e. without polymer arms) had a diameter of 1.7 nm, which increased to 3.5 nm after polymerization (Mn = 4500 g/mol). The length of the nano-tubes, on the other hand, was found to evolve very little with polymerization, with the objects remaining around 120 nm throughout the reaction. However, at very high polymerization times, the concentration of nano-tubes appeared to decrease, and smaller particles were growingly present. This result suggests that past a certain size of polymer arm, steric repulsion starts to disrupt the assemblies. While not discussed by the authors, since the nano-tube length remains constant regardless of polymer arm length, it might indicate that this system was out of thermodynamic equilibrium.[20]

Lastly, the hollow nature of the nano-tubes could be exploited to encapsulate molecules or for selective transport, and show certain promise in drug delivery applications.[21]

3. Squaramide based nano-cylinders

More recently, squaramides have gained significant interest as self-assembling blocks in supramolecular chemistry due to their strong bidirectional H-bonding and relative ease of synthesis. Delocalization of the nitrogen lone pairs imparts aromaticity to the 4-membered cycle, and self-assembly via H-bonding has been shown to increase the aromatic character.[22] Interestingly, oxo-squaramides and thio-squaramides have been shown to self-assemble in different manners: while the first tends to self-assemble in a “head to tail” fashion, the former self-assembles in a “stacked” organisation, as can be seen in **Figure C1-5**.

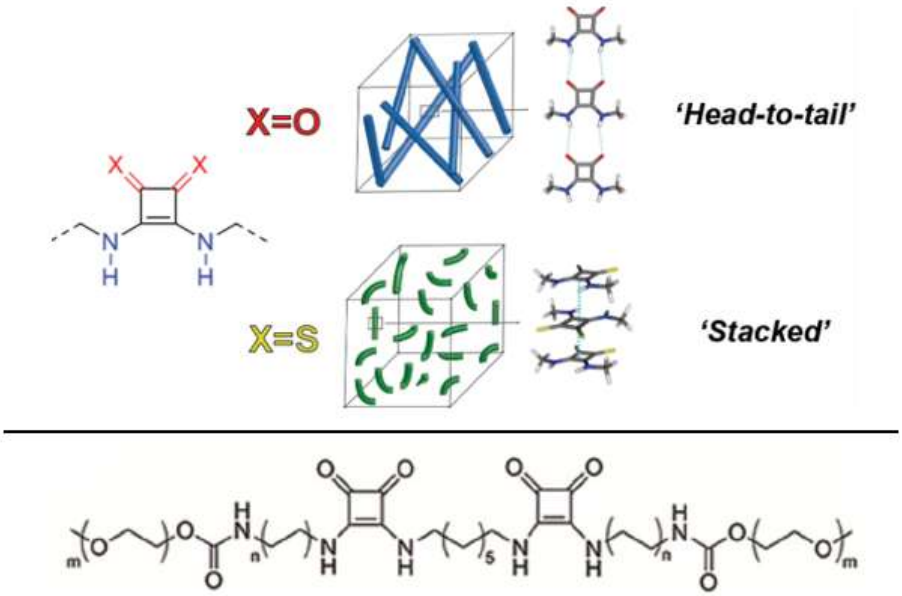

Figure C1-5. **Top**: (thio)-squaramide structure and self-assembly. Taken from ref [22]. **Bottom**: chemical structure of the bis-squaramides. Taken from ref[23]

Recently, a series of bis-squaramides, linked to oligo-PEO by alkyl spacers (both of varying lengths), have been shown to self-assemble into different morphologies in water. First, the influence of PEO arm length was studied, while keeping the alkyl length constant (n = 5). For PEO DPn = 11, long polydisperse nano-cylinders were observed by cryo-TEM, with an average length of 230 nm, but micron-long fibers were also observed. Increasing the DP_n to 17 reduced the average length down to 110 nm. At DP_n = 24, a mixture of small spheres (6-7 nm in diameter) and short nano-cylinders (50 nm in length) were observed, and at DP_n = 36, only spheres were present. Next, the influence of the alkyl linker length was studied, while keeping the PEO DP_n at 11. For C_n = 1, no aggregation was observed, and for C_n = 4, long nano-cylinders were present (around 200 nm in length), which were also polydisperse. For an even longer alkyl length of 6, a mixture of long nano-cylinders and bundles of cylinders were observed.[23]

Therefore, while nano-cylinders may be obtained with hydrogen bonding squaramides, it is important to note that it is yet only possible with fairly short polymer chains. This work does however highlight the strong influence of polymer arm length on assembly, and the fact that it is generally more difficult to achieve long nano-cylinders with long polymer arms. It also demonstrates the importance of using sufficiently long alkyl spacers for achieving self-assemblies in H-bond competing media such as water, as the alkyls protect the self-assembling core for H-bond competition.[23]

II. Urea based 1D self-assembly in solution

1. Urea based systems without polymer arms

Small molecules containing urea moieties have been extensively studied due to their facile synthesis, since they can be prepared by simply reacting an amine with an isocyanate. Ureas are particularly efficient as H-bond promoting motifs, as the two symmetrical hydrogen donating N-H groups allow for a bidentate bonding towards the carbonyl of the neighbouring urea (see **Figure C1-6**), ultimately leading towards a highly directional “stacking”

of the ureas. In particular, bis-ureas represent a powerful supramolecular sticker for promoting self-assembly into long, 1D supramolecular polymers in a wide range of solvents.

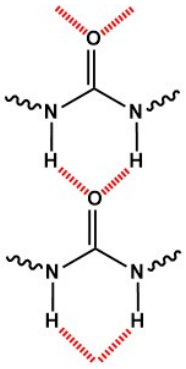

Figure C1-6. Schematic representation of the bidentate hydrogen bonding between urea groups (H-bonds in red)

Bouteiller et. al. have for example studied ethylhexyl ureotoluene (EHUT), a small-molecule bis-urea that has been shown to dynamically self-assemble into 1D structures in low polarity solvents such as dodecane, octane, heptane, or toluene to name a few. Depending on the solvent and temperature, EHUT has been shown to self-assemble into two distinct structures, as can be seen in **Figure C1-7**.[24,25,26,27,28,29,30] The authors report that the molecular size of the solvent chosen strongly influences which structure is most stable. If the solvent is small enough that it may penetrate within the cavity of the tube structure, the latter is preferred, otherwise the filament structure is favoured. The structure of the supramolecular monomer also plays an important role. A methyl on the aromatic rings in the ortho positions to the ureas favors self-assembly, by enforcing a non-coplanar configuration between the phenyl rings and the ureas. However, a methyl in the ortho position to both ureas destabilizes the tube structure, since the methyl would be pointing towards the inside of the tube, causing steric repulsion.[29,31] The assemblies were found to be highly cooperative due to two effects. The first effect is due to the polarization of the urea once assembled, thus "activating" the terminal ureas for stronger further assembly. This effects favors oligomerization (and polymerization) over dimerization. The second effect is due to the fact that in a bis-urea, once the first urea function is involved in H-bonding, the second urea group is "pre-placed" in a favourable conformation, lowering the entropic cost for assembly compared to a mono-urea, while the enthalpic gain remains the same (since the same number of H-bonds is achieved). This second effect strongly increases the strength of self-assembly for bis-ureas compared to mono-ureas (at equal concentration in urea groups).[29] Overall, bis-ureas yield very long supramolecular 1D structures in solution.

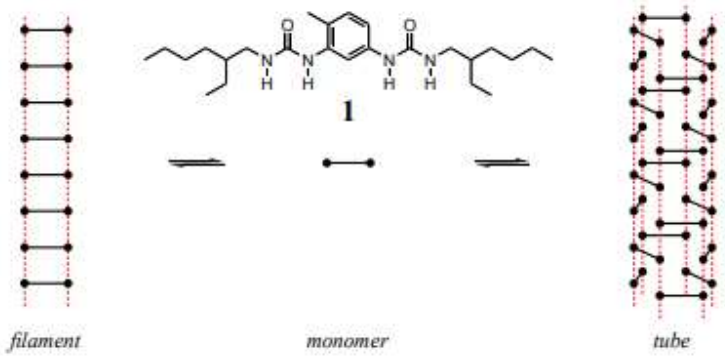

Figure C1-7. Chemical structure of EHUT, and its self-assembly into "filament" or "tube" structure. Taken from ref[24]

While many examples of low molecular weight supramolecular assemblies based on urea functions exist in the literature, the focus was put on urea systems bearing polymer arms, since the aim of this project was to elaborate nano-cylinders decorated with polymer arms.

2. Urea based systems with polymer arms

i. In organic solvents

Initial examples of polymer decorated bis-urea self-assembled systems were studied by Bouteiller's team. A tolylene-bisurea sticker decorated with two poly-(isobutylene) (PIB) arms was synthesized, yielding PIBUT (total $M_{n\ NMR}$ = 3500 g/mol – both arms). Its self-assembly was studied in a variety of organic solvents and compared to that of EHUT (**Figure C1-8**). [32]

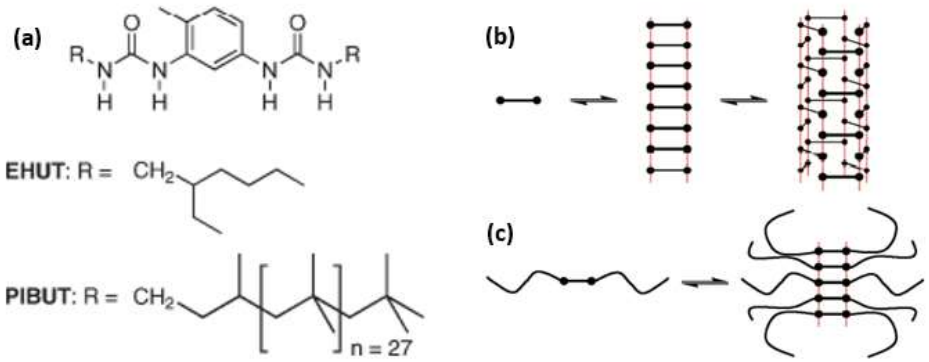

Figure C1-8. **(a)** Chemical structures of EHUT and PIBUT **(b)** Schematic representation of EHUT self-assembly in solution **(c)** Schematic representation of PIBUT self-assembly in solution. Taken from ref [32]

The authors report that in apolar solvents (such as heptane or toluene), PIBUT self-assembles into dynamic supramolecular bottlebrushes – the lower the polarity of the solvent, the higher the strength of the hydrogen bonds between ureas. In more polar solvents, such as THF, self-assembly does not occur due to H-bond competition with the solvent. PIBUT assemblies in toluene were relatively small, with SANS measurements yielding a M_{app} of 30 000 g/mol (M_{unimer} = 2700 g/mol), likely due to steric repulsion between PIB arms, which limits self-assembly. SANS measurements revealed that one molecule was present in the cross-section, suggesting the filament structure, and this was the case for all solvents tested in which the polymer self-assembles. This is likely due to the fact the tube structure is unfavorable, since 3 times more polymer arms would be present in the cross-section, drastically increasing steric repulsion. In contrast, EHUT forms very long assemblies, due to a lack of bulky polymer arms causing steric repulsion, and the structure of its self-assemblies is solvent-dependant. Concentration had very little influence on the size of the assemblies, consistent with a limited association model, and temperature also had little effect. The assemblies were however in thermodynamic equilibrium, which was demonstrated using ITC measurements. Lastly, mixing PIBUT with EHUT led to supramolecular copolymerisation, affording control over the number of PIB chains per self-assembling bis-urea unit.[32,33]

In order to increase aggregation and better overcome steric repulsion, our team, in collaboration with Bouteiller's team, used a fairly straightforward strategy: decreasing the number of PIB chains per molecule, in order to reduce steric hindrance. A bis-urea with a single polymer side chain was synthesized. While slightly longer assemblies were obtained, the entropic penalty was still too high. The number of H-bond promoting units was therefore increased. PIB (DP_n = 27) functionalized with a tris-urea sticker was synthesized (termed U_3PIB_2), which yielded

far bigger nanocylinders in cyclohexane compared to PIBUT (**Figure C1-9**). The enthalpic gain from the increased H-bonding was sufficient to overcome the entropic penalty from side chain stretching. Long nanocylinders with a persistence length bigger than 300 nm were obtained, as confirmed by light scattering.[33]

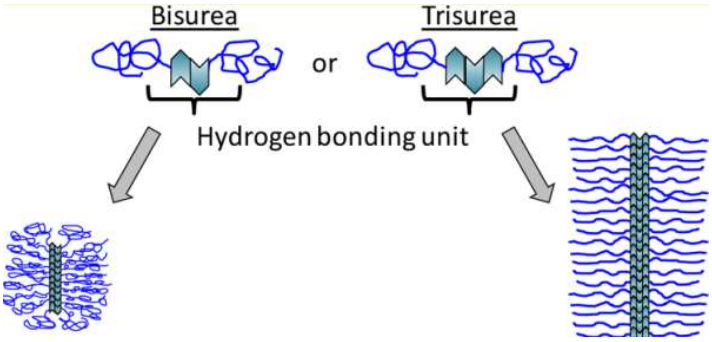

Figure C1-9. Schematic representation of bis-urea versus tris-urea decorated PIB self-assemblies. Taken from ref[33]

Following this work, our team investigated the influence of polymer arm length and nature on self-assembly. To this end, two tris-ureas decorated with two poly-(styrene) (PS) arms of various lengths, DP_n = 14 and 34, respectively termed $S_{14}U_3S_{14}$ and $S_{34}U_3S_{34}$ (**Figure C1-10**), were synthesized. This was achieved via a convergent synthetic pathway, by first polymerizing the PS arms using ATRP, followed by conversion of the terminal Br to an $–NH_2$, and finally the coupling of two PS-NH_2 arms with a urea-diisocyanate core, yielding the tris-urea sticker. The longer DP_n (34) was chosen so that comparison with the previous PIB decorated tris-urea would be possible. While $S_{14}U_3S_{14}$ self-assembled into long nanocylinders (N_{agg} = 100), $S_{34}U_3S_{34}$ yielded small star-shaped aggregates (N_{agg} = 5.5) in cyclohexane. In both cases, however, the resulting structures were much smaller than for U_3PIB_2 (N_{agg} > 600); which was attributed to the much bulkier styrene repeating units compared to isobutylene ones. Put otherwise, the entropic penalty for polymer stretching increases with increasing DP_n, and with increasing steric hindrance linked to the bulkiness of the repeating units.[34]

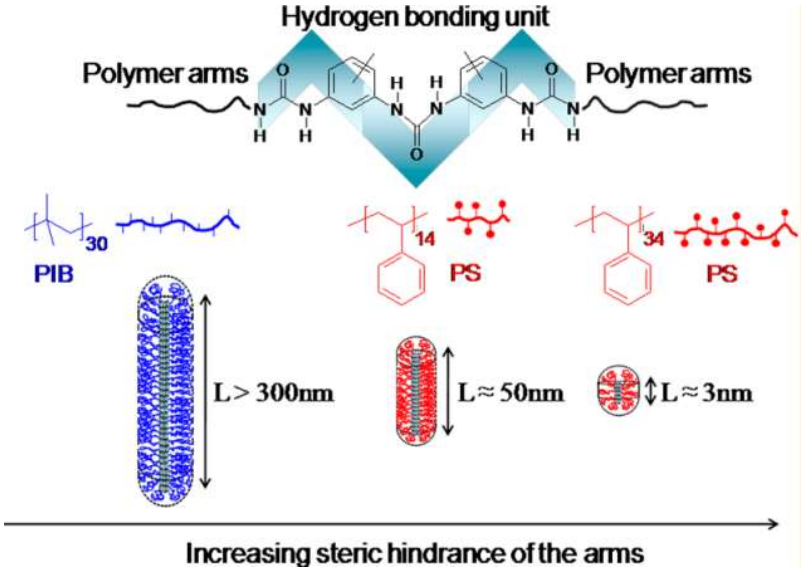

Figure C1-10. Schematic representation of self-assembly of tris-urea decorated by polymer arms of varying nature and length. Taken from ref[34]

Bouteiller's team also synthesized aromatic bis- and tris- urea stickers functionalized with ATRP initiators, allowing for convenient synthesis of polymer decorated bis- and tris-ureas via a divergent synthetic strategy, which were used to synthesize poly(*n*-butyl acrylate), and ultimately yielded nanocylinders in toluene. Such an approach allows for easy changing of monomer nature and final polymer arm length, which may allow for control over aggregation extent.[35]

In an attempt to improve the self-assembly of bulky PS decorated tris-urea, Han et al. added a flexible alkyl spacer between the sticker and the PS arms. For a DP = 10, without an alkyl spacer, spheres were formed. On the contrary, with short or long spacers, nano-cylinders were formed. It is worthy to note that the longer spacer yielded longer nano-cylinders (see **Figure C1-11**). These results highlight the importance of an alkyl spacer when the polymer arms are rather bulky, as they may otherwise interfere with 1D self-assembly of the urea stickers.[36]

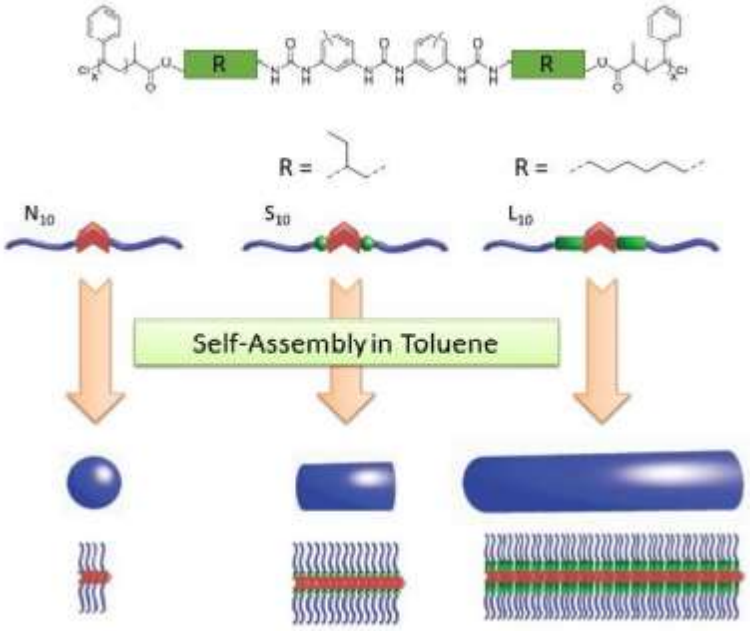

Figure C1-11. Schematic representation of the influence of flexible alkyl spacer length on self-assembly of $PS_{10}U_3PS_{10}$ in toluene. Taken from ref[36]

ii. In aqueous media

Urea stickers have also been used to promote 1D self-assembly of polymers in water – however this presents an added challenge since water is a strong H-bond competitor. To overcome this problem, placing an alkyl spacer in between the urea sticker and polymer arms now serves three purposes: 1) distancing potentially bulky polymer arms from the sticker, as seen previously, 2) protecting the urea groups from H-bond competing water and 3) reinforcing the self-assembly via hydrophobic interactions.

This is precisely what Bouteiller's team achieved in 2006, by synthesizing oligo-PEO-alkyl decorated aromatic bis-urea, as can be seen in **Figure C1-12**. They demonstrated that both the urea groups and alkyl spacers were required for self-assembly in water, while a sufficiently long oligo-PEO (DP = 9) is required to ensure solubility. This is coherent with other work carried out on similar structures.[37]

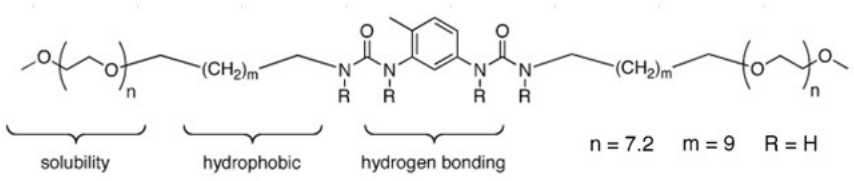

Figure C1-12. Chemical structure of oligo-PEO decorated bis-urea. Adapted from ref[38]

They then proceeded to compare the self-assembly of this compound in water with 2 other solvents: acetonitrile (ACN), as a polar aprotic solvent, and toluene, as an apolar solvent. Interestingly, the self-assembly yielded long nanocylinders in equilibrium in all solvents: Isothermal Titration Calorimetry (ITC) indeed revealed heat exchange upon dilution of self-assembled polymers in all these solvents, suggested the ability of the supramolecular structures to spontaneously disassemble at low concentration. The aggregation was quite different depending on the solvent. In water, the molecules stack along the nanocylinder axis both via H-bonding and hydrophobic interactions. Moreover, they aggregate laterally through hydrophobic interactions. In acetonitrile however, the hydrophobic effect is not strong enough to cause lateral aggregation, as revealed by a mono-molecular cross-section, measured by SANS. In toluene, the nanocylinders were shorter, and the assembly's cross section is close to mono-molecular. However, the nanocylinders were thinner than in acetonitrile, suggesting a more compact aggregation. The authors suggested that such an aggregation could be due to intramolecular H-bonds between the oligo-PEO ether groups and the ureas, since there is no hydrophobic effect protecting the ureas. ITC measurements revealed that in toluene and ACN, assembly was mainly driven by H-bonds, while in water, the main driving force was hydrophobic interactions. This work demonstrates the strong influence hydrophobic effects may have on assemblies in water.[38]

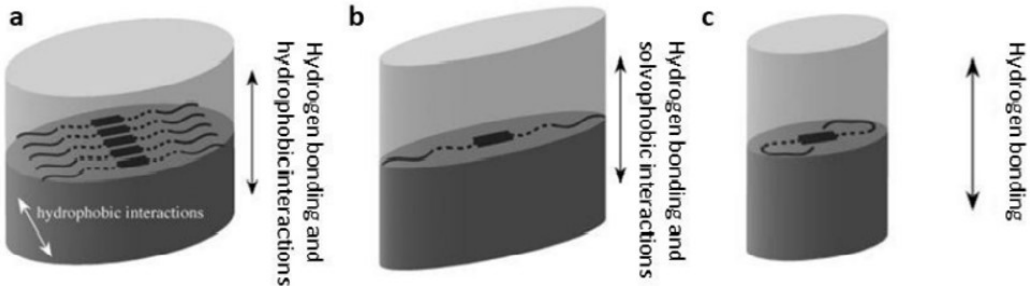

Figure C1-13. Schematic representation of self-assembly in: **a)** water, **b)** acetonitrile and **c)** toluene. Taken from ref[38]

Another strategy to ensure 1D self-assembly in water without an alkyl spacer is to simply increase the number of H-bonds within the sticker, which was reported by Han. et al. in 2018. To this end, they synthesized urea stickers decorated with PEO (M_n = 2200 g/mol, DP_n = 45) on either side, with the number of urea groups ranging from 3 to 5 (see **Figure C1-14**). Direct dissolution of the 5 urea based compound led to aggregation ($M_{app} = 2.5\times10^6$ g/mol), although not into 1D nano-cylinders, whereas compounds with 3 and 4 urea moieties hardly assembled. They then investigated the influence of solution preparation on assemblies. This was achieved by first dissolving the polymer in DMSO at 100 g/L, to ensure the polymer is in its unimer state, and then slowly adding water until reaching 1 g/L (and thus a ratio water/DMSO of 99/1 by volume). Using this procedure, they found that PEO-U_3-PEO did not aggregate, PEO-U_4-PEO weakly aggregates (N_{agg} = 16), and PEO-U_5-PEO aggregates strongly into nanocylinders ($M_{app} = 1.5\times10^7$ g/mol, N_{agg} ~ 2700, R_g = 150 nm), as determined by light scattering and cryo-TEM measurements. The solution preparation pathway dependency implies that these systems are out of

thermodynamic equilibrium. This study highlights the value of the "water/DMSO" route, which promotes the self-assembly of nano-cylinders for out-of-equilibrium assemblies.[39]

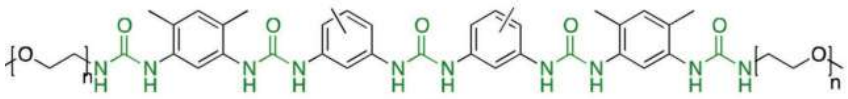

Figure C1-14. Chemical structure of PEO-U_5-PEO. Taken from ref[39]

More recently, Rieger et al. reported the synthesis of an aliphatic bis-urea functionalized with a RAFT transfer agent, allowing for the convenient synthesis of bis-urea-terminated polymers from hydrophilic monomers (see **Figure C1-15**). For short poly(dimethyl acrylamide) (PDMAc) chains (DP = 10 or 20), the polymer spontaneously self-assembles into nanocylinders in water, as is represented in the figure below. However, when the DP was increased (to 35 or 46), a mixture of spherical and cylindrical micelles was formed, with the proportion of spherical micelles increasing with the DP: for the largest DP, there were almost no nanocylinders. This is likely due to the increasing steric hindrance of the polymer arms and the entropic penalty it entails. Isothermal titration calorimetry (ITC) revealed that the self-assembly was dynamic and therefore at thermodynamic equilibrium. This approach even allowed for nano-cylinder formation with strong H-bond competing monomers such as acrylic acid at acidic pH – and disassembly was possible by increasing pH, creating electrostatic repulsion between formed carboxylates. [40]

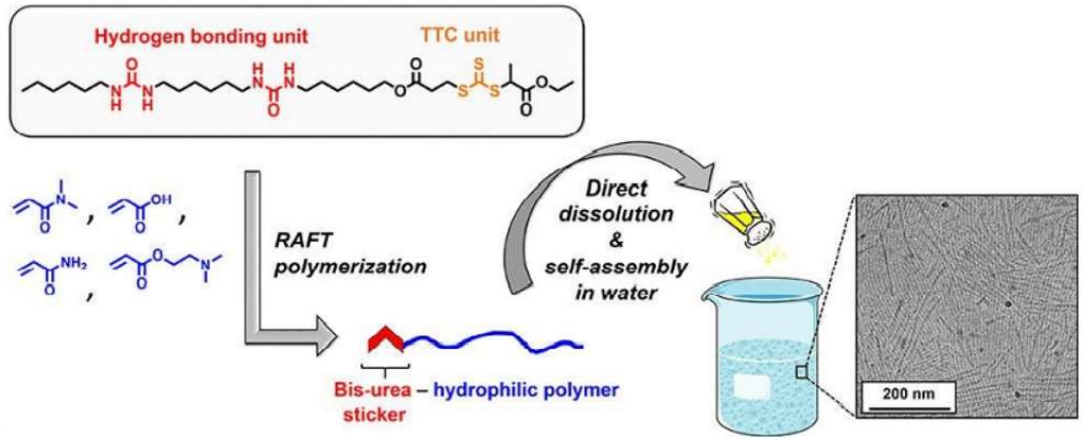

Figure C1-15. Chemical structure of the U_2-RAFT agent and self-assembly after polymerization. Taken from ref[40]

Another example of a bis-urea functionalized polymer is PEO-NDI-U_2 (see **Figure C1-16**), which was studied by our group in collaboration with Marc Sallé and David Canevet.[41] This molecule consists in a PEO chain (M_n = 2000 g/mol) end functionalized with an electron-accepting group (naphthalene-diimide) and a bis-urea, ensuring cooperative self-assembly through H-bonding. Direct dissolution of the polymer was found to yield long nano-cylinders (up to 300 nm in length), which is a rather surprising result, in contrast with previous examples, which generally required a "water/DMSO" type route. Light and neutron scattering revealed a highly aggregated system (N_{agg} = 4000), with a strong q^{-1} angular dependency, characteristic of long fibrillary objects. Cryo-TEM measurements also confirmed the formation of long, polydisperse nano-rods. Furthermore, these measurements indicated that 6 molecules were present in the cross-section (see **Figure C1-17**), as opposed to 1 molecule in the cross section, strongly hinting at lateral aggregation. This latter observation is likely due to the presence of the NDI group which further drives self-assembly through a combination of Pi-stacking and hydrophobic interactions. Indeed, the NDI group somewhat plays the role of a hydrophobic spacer, albeit a rigid one.

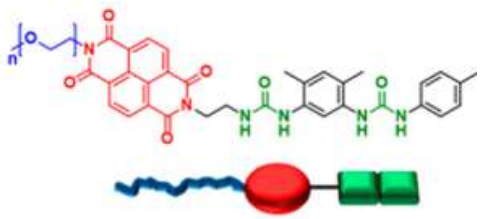

Figure C1-16. Chemical structure of PEO-NDI-U_2. Adapted from ref[41,42]

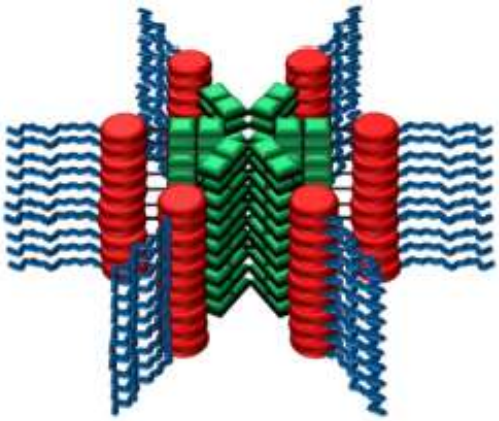

Figure C1-17. Proposed self-assembly model for PEO-NDI-U_2 in water. Taken from ref[41]

III. Stimuli-responsive polymeric supramolecular nanocylinders in solution

Now that the main strategies for accessing supramolecular polymer bottlebrushes in solution have been presented, several examples which possess stimuli-responsiveness will be presented. Imparting stimuli-responsiveness to supramolecular polymer bottlebrushes extends the scope of their potential applications, as they could be used for drug delivery, or to design stimuli-responsive emulsions.

3. pH-responsive systems

Perrier et al. reported pH-responsive oligocyclopeptide-based nano-cylinders in water, which was achieved by selecting pH-responsive polymer arms.[43] Oligocyclopeptides decorated with poly(dimethylamino ethyl methacrylate) arms led to nanotubes at high pH (N_{agg} = 15), which dissociated when acid was added due to protonation of the amine groups, leading to control over nanotube length. A similar system based on poly(2-(diisopropylamino)ethyl methacrylate) was also reported.[44] The same strategy was used with poly-(acrylic acid) conjugated CPs, where the nano-tubes are formed at low pH (around 65 nm in length), but disrupted at high pH, due to the charged carboxylates. The authors do not report if this transformation was reversible.[45] It is worthy to point out that in all these cases, the starting nano-cylinders are rather short.

Besenius et al. reported another pH-responsive system.[46] They doubly end-functionalized a polysarcosine polymer with oligopeptide units, which were shown to self-assemble into nano-rods in water (pH>6), through complementary H-bonding of the peptides, which stack into antiparallel beta-sheet like structures (**Figure C1-18**). If the pH is lowered, the imidazole moieties become protonated, and the nano-rods are disrupted. Interestingly, this process was found to be reversible, as nano-rods were recovered if the pH was increased to above 6. In contrast to the previous pH-responsive examples, this approach did not rely on the nature of the polymer – the responsivity is afforded through the self-assembling core, increasing the versatility of the strategy as it may be applied with other polymer arms.[46]

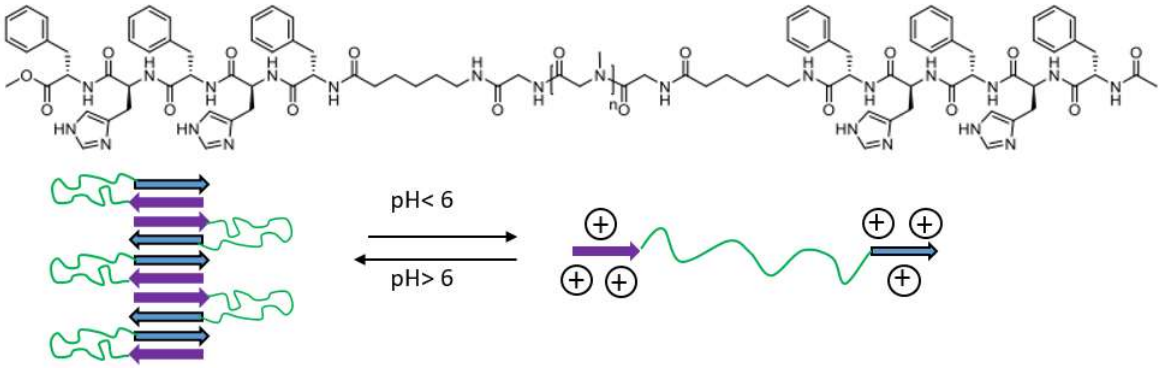

Figure C1-18. Chemical structure of the peptide-polymer-peptide conjugate, and schematic representation of the pH-responsiveness. Adapted from ref[46]

4. Temperature responsive systems

Thermo-responsive oligocyclopeptides were designed by choosing thermo-responsive polymer arms, such as poly-(N-isopropyl acrylamide) (PNIPAM), which possesses a lower critical solution temperature (LCST) of around 32°C in water.[47] The PNIPAM decorated CPs therefore formed nanotubes below the LCST, but were insoluble above this temperature. Poly(ethyl oxazoline) (PEtOx) arms were also used to impart thermo-responsiveness, leading to CPs that presented a cloud point at 70°C. Below this temperature, the PEtOx-CP conjugates formed short nanotubes, but formed micrometer sized spherical particles above the cloud point temperature.[48]

While these examples are interesting, they do not correspond to thermo-responsive disassembly of nanocylinders into their building blocks, nor to thermo-responsive assembly of elementary building blocks into supramolecular nanocylinders, but to thermally-induced aggregation/precipitation of nanocylinders. We are not aware of temperature-induced disassembly/assembly of polymeric supramolecular nanocylinders in solution except for one benzene tricarboxamide (BTA) based system discussed in section 5 because it is also light-responsive.

5. Oxidation/reduction responsive systems

Besenius et al. reported a redox responsive nano-cylinder system based on ABA polymer-peptide conjugates, which consisted in a PEO chain doubly end-functionalized with short peptide sequences, providing self-assembly into nano-rods in water, similar to the pH-responsive system described above (see **Figure C1-19**).[49] In this system, however, the peptide sequences contained thioether moieties: these units did not impede the self-assembly,

however after oxidation, sulfoxide groups were formed, which led to the disassembly of the nano-cylinders, albeit irreversibly.

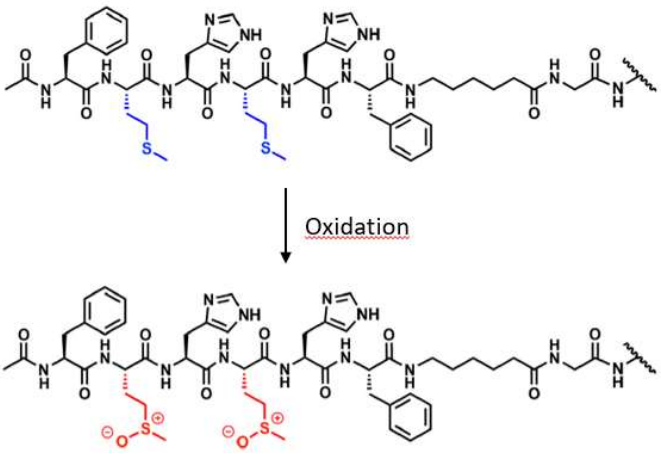

Figure C1-19. Chemical structure of the ABA polymer-peptide conjugates before and after oxidation. Adapted from ref[49]

Recently, our team, in collaboration with David Canevet and Marc Sallé, reported a polymer bottlebrush sensitive to oxidation.[50] This polymer (PEO-TTF-U_2) consists in a PEO chain (M_n = 2000 g/mol) end functionalized with a bis-urea, providing self-assembly, and a tetrathiafulvalene, which is sensitive to oxidation (**Figure C1-20**). Nano-cylinders could be formed in water using a "water/DMSO" route (direct dispersion in water did not yield nano-cylinders). The strong influence of preparation pathway indicates that the nano-cylinders are kinetically frozen (i.e. out of thermodynamic equilibrium). The nanocylinders formed were several hundreds of nanometers long, as evidenced by light scattering and cryo-TEM measurements. In water, the TTF was found to be oxidizable (using iron(III) perchlorate as oxidant), but this had little impact on the self-assemblies. This is possibly due to the fact the oxidation only goes to $TTF^{\bullet+}$ and/or to the frozen character of the assemblies. Interestingly, the oxidized TTF was found to be quite unstable in these conditions, and rapidly degraded. The nano-cylinders were then studied in acetonitrile. Oxidation led to the formation of TTF^{2+}, triggering the disruption of the vast majority of the nano-cylinders (>95%). However, due to the rapid degradation of the oxidized TTF units, this disassembly was not reversible.[50]

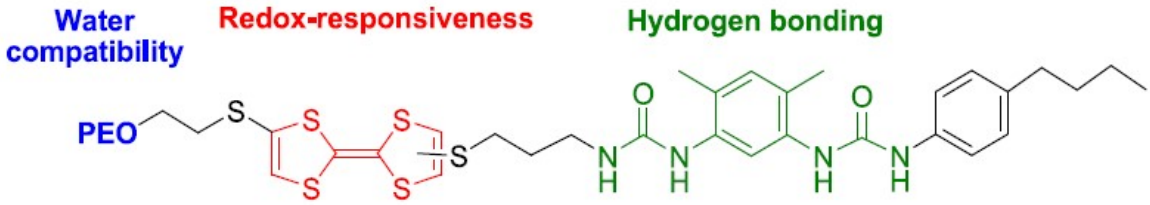

Figure C1-20. Chemical structure of TTF-U_2-PEO. Taken from ref[50]

It is worthy to note that these two examples both rely on the core for oxidation triggered disassembly, however in both cases, the disassembly is irreversible.

6. Host-guest interaction responsive systems

Another interesting example of controlled disassembly using CPs exploits host-guest interactions (see **Figure C1-21**). A CP decorated with a 5000 g/mol PEO arm was synthesized and was shown to self-assemble in water – with an average N_{agg} of 36. However, this CP was also functionalized with 2 phenylalanine moieties on opposite sides of the ring. As a consequence, when cucurbit[7]uril (CB[7]) is added, disassembly of the supramolecular bottlebrushes occurs, due to host-guest interactions between the macrocyclic CB[7] and the phenylalanines: the bulky CB[7] groups cause disassembly through steric repulsion. Re-assembly of the CPs into nanocylinders occurred if adamatanamine (ADA) was added. The latter indeed binds more strongly with CB[7] than phenylalanine, freeing up the CPs. This strategy does not rely on the nature of the polymer arms. [51]

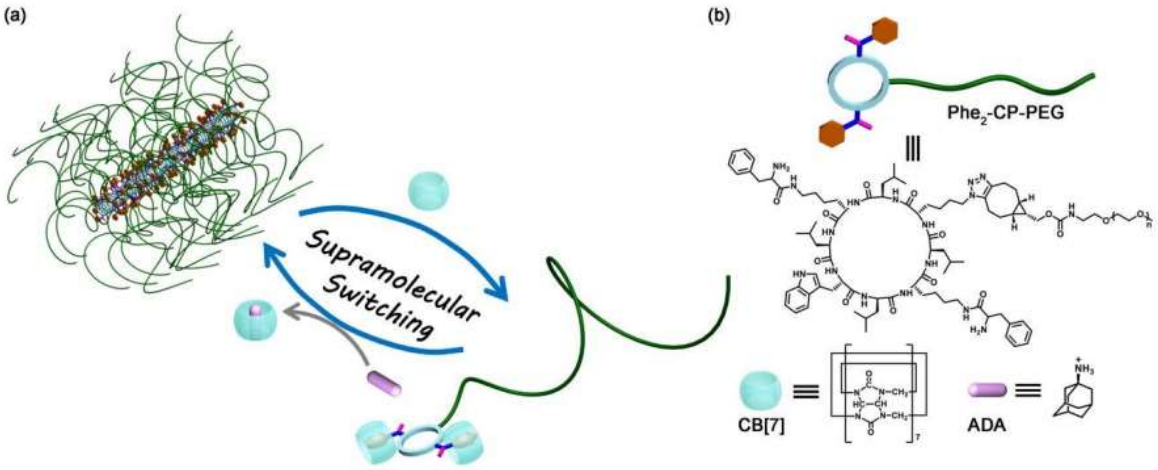

Figure C1-21. **(a)** Scheme of the reversible assembly/disassembly of CPs **(b)** Chemical structure of the compounds used. Adapted from ref [51]

7. Light-responsive systems

Photo-responsive CPs have also been described. A CP conjugate decorated with both a hydrophilic poly-(PEO acrylate) arm and a hydrophobic poly-(2-nitrobenzyl methacrylate) arm, on opposite sides of the CP ring, has been reported to self-assemble into tubisomes (**Figure C1-22**), with averages lengths of 130 nm. If this system is subjected to UV irradiation at 365 nm, the 2-nitrobenzyl methacrylate units undergo photo-cleavage, ultimately yielding methacrylic acid units, rendering the arm hydrophilic and partially charged, leading to disassembly. Since such tubisomes can be loaded with molecules, their disassembly offers potential for innovative drug delivery systems. Here, the responsiveness relies on the nature of the polymer arms, limiting the versatility of the strategy. Moreover, the disassembly is irreversible.[52]

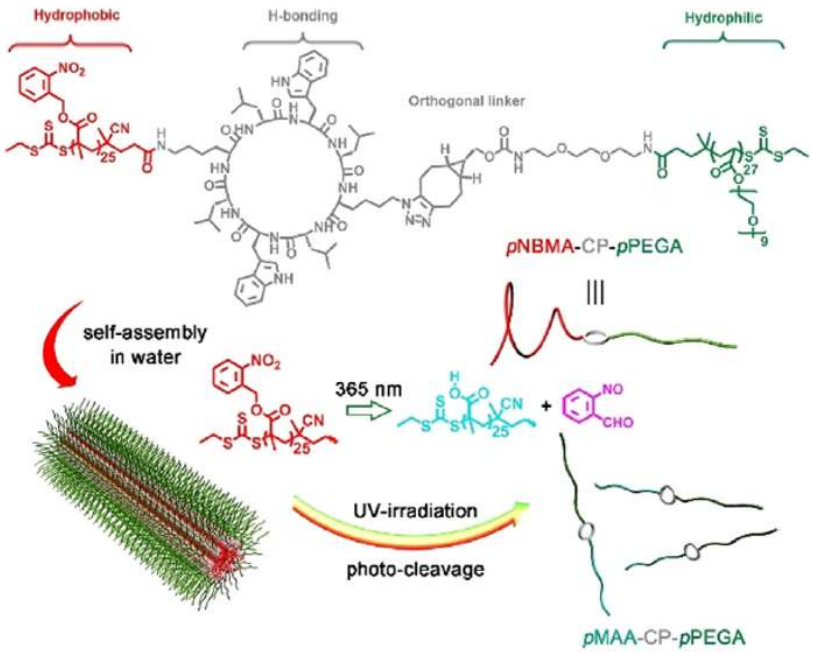

Figure C1-22. Chemical structure of the CP and schematic representation of its photo-triggered disassembly. Taken from ref[52]

8. Conclusions

To summarize, there has only been a handful of examples of stimuli-responsive supramolecular polymer bottlebrushes in solution described in the literature to this day. Of these, many rely on the nature of the polymer arms to impart responsiveness, which limits versatility. Furthermore, not all undergo reversible transformations. Lastly, only one example in which polymer decorated nano-cylinders are photo-responsive has been reported, which relied on the nature of the polymer arms as well as the disassembly being irreversible. There are, however, several examples involving the assembly of small molecules, but some relied on self-assembling motifs, such as BTAs, that may not be suitable for self-assembly with longer polymer arms.

IV. Azobenzene based photo-responsive systems

There are several photo-switches that have been used to confer light-responsive properties to a variety of materials (**Figure C1-23**). Such units are photochromic molecules, which may undergo reversible photo-isomerisation, effectively switching between the thermodynamically stable state and the metastable one, when irradiated at the appropriate wavelength. Such switches may change the geometry and/or polarity of the unit, which can lead to changes in self-assembling properties when it comes to supramolecular systems. The return to the initial, more stable form is generally possible by irradiating at a different wavelength, and in many cases, by thermal relaxation in the dark.

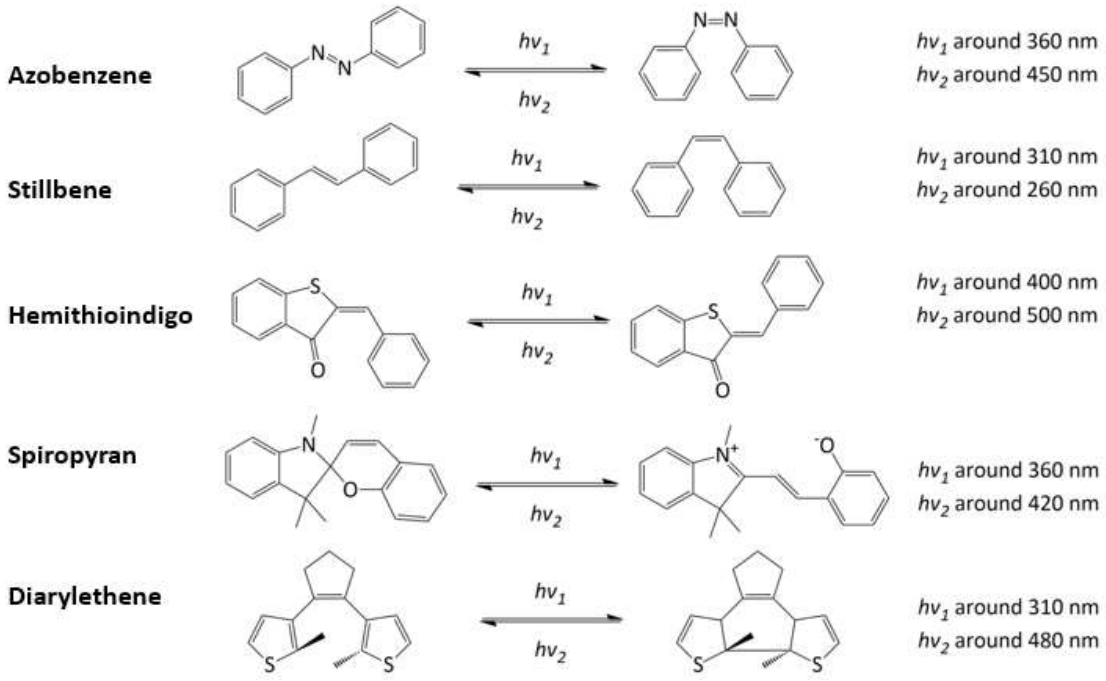

Figure C1-23. Chemical structure of commonly used photo-switches (adapted from ref[53])

While many different photo-switches have been used in various systems, azobenzene was selected for this project due to its high quantum yield (i.e. the number of times the isomerization takes place per photon absorbed by the system), fast photo-isomerization, and drastic change in geometry between its two isomers. Therefore, only azobenzene based systems will be discussed in the following.

9. Azobenzene as a photo-switch

Azobenzene is an attractive photo-switch for supramolecular assemblies due to its symmetry, ease of synthesis,[54] and relatively low bulkiness. It can be rapidly photo-isomerized to the *cis* isomer and back to the *trans* isomer (using the appropriate wavelength), with the two transformations occurring on picosecond time scale. In general terms, photo-isomerization of azobenzene, both from *trans* → *cis* and *cis* → *trans* is fast, and photo-stationary states are reached within a matter of minutes to tens of minutes, however the exact kinetics depend on the media in which the azobenzene is (solvent, temperature, etc.) as well as of the photo output of the irradiation source. A generally slow thermal relaxation allows for studying the *cis*-isomer before it goes back to its *trans* configuration.

Azobenzene, in its most stable form (*trans*) is planar, but after irradiation at the appropriate wavelength, undergoes isomerization, yielding *cis*-azobenzene. The *cis* form is no longer planar, since the C-N=N-C bond has "bent", and one benzene ring is "twisted" relative to the other, as can be seen in **Figure C1-24.** *Trans*-azobenzene goes from a length of 9 Å and a dipole moment of 0D, to a length of 6 Å and a dipole moment of 3 D (compare to water = 1.85 D or DMSO = 3.96 D) when isomerized into the *cis* form. This in turn means that *cis*-azobenzene is more hydrophilic than the *trans* isomer.[55]

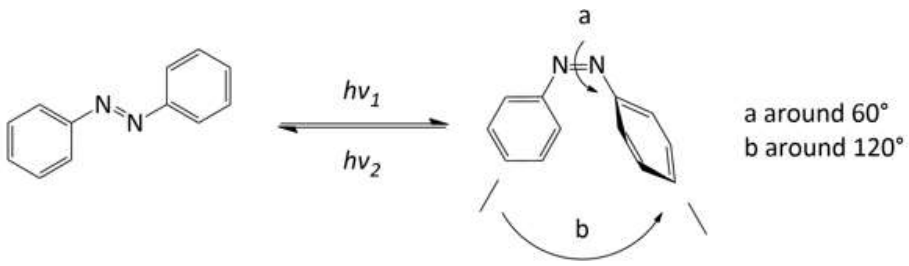

Figure C1-24. Structure of azobenzene isomers (adapted from ref[55])

After irradiating azobenzene into the *cis* form, it is possible to return to the *trans* isomer by irradiating at a different wavelength (generally with blue light). Another possibility is to leave the sample in the dark to return to the *trans* form via thermal relaxation, since the *cis* isomer is metastable. At equilibrium, after sufficiently long thermal relaxation, virtually only *trans*-azobenzene is present.[56] The *trans* isomer is 50 indeed kJ/mol more stable than the *cis*.[56]

Azobenzene possesses two absorption bands: π → π* (around 360 nm for the *trans* form) in the UV and a weaker n → π* (around 450 nm) in visible light, which makes azobenzene colored (golden-yellow in solution when unsubstituted). After irradiation, the π → π* band gets blue-shifted, that is, the band shifts to higher energies therefore lower wavelength, while the n → π* increases in intensity : therefore the color of the compound turns a deeper orange.[56]

The following first addresses the mechanisms by which unfunctionalized azobenzene may photo-isomerize, and then discusses the effect of azobenzene substitution on its properties.

i. Azobenzene photo-isomerization mechanism

Azobenzene can be found in both *trans* and *cis* configuration in the ground state, however the *trans* isomer is more stable: its energy is lower by roughly 50 kJ/mol, with the energy barrier for *trans* → *cis* isomerization having been measured at around 200 kJ/mol (see **Figure C1-25**).

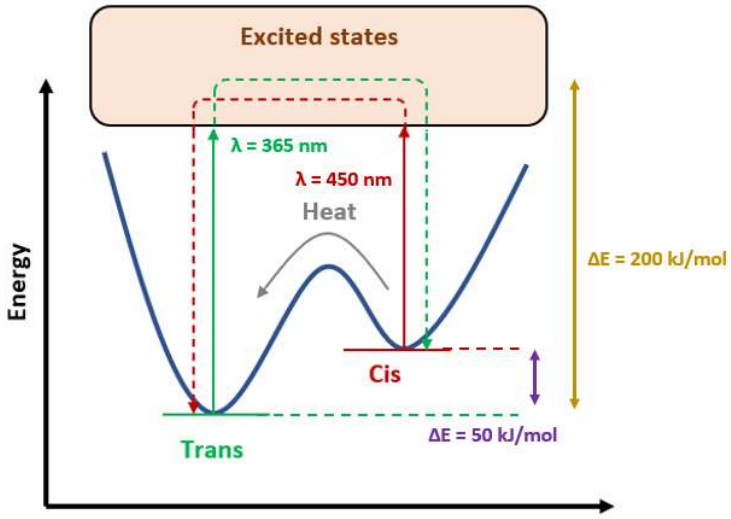

Figure C1-25. Simplified energy diagram of the *trans* – *cis* photo-isomerization

Azobenzene photo-isomerization involves the absorption of photons of a precise wavelength, inducing excitation of an electron from either the highest occupied nonbonding orbital (n) or highest occupied π orbital (π) to the lowest unoccupied π orbital (π*). The n → π* transition is considered to be the passage of an electron from its fundamental state (singlet state S_0) to its first singlet state S_1, while the π → π* is the passage from the fundamental state to its second singlet state S_2. These transitions may proceed directly, or through intermediate triplet states. *Trans* → *Cis* photo-isomerization is reported to proceed through both $S_0 \rightarrow S_2$ and $S_0 \rightarrow S_1$ excitations, while *Cis* → *Trans* photo-isomerization proceeds through the reverse path.[57]

Historically, photo-isomerization of azobenzene was believed to proceed through two mechanisms, inversion and rotation, however more recent literature suggests that there are 4 mechanisms at play: rotation, inversion, concerted inversion and inversion assisted rotation (**Figure C1-26**).[58] The rotation mechanism involves breaking the -N=N- double bond to allow for rotation around the -N-N- axis. The C-N-N-C dihedral angle is modified while the N-N-C angle remains constant, at around 120°. For the inversion mechanism, one of the two C-N=N angles increases to 180°, while the C-N=N-C dihedral angle remains at 0°, leading to a transition state in which one of the nitrogen atoms is sp hybridized. As for the concerted inversion mechanism however, both C-N=N angles increase to 180°, leading to a linear transition state. Regarding the inversion assisted rotation, both the C-N-N-C dihedral angle and C-N-N angle vary during the process.

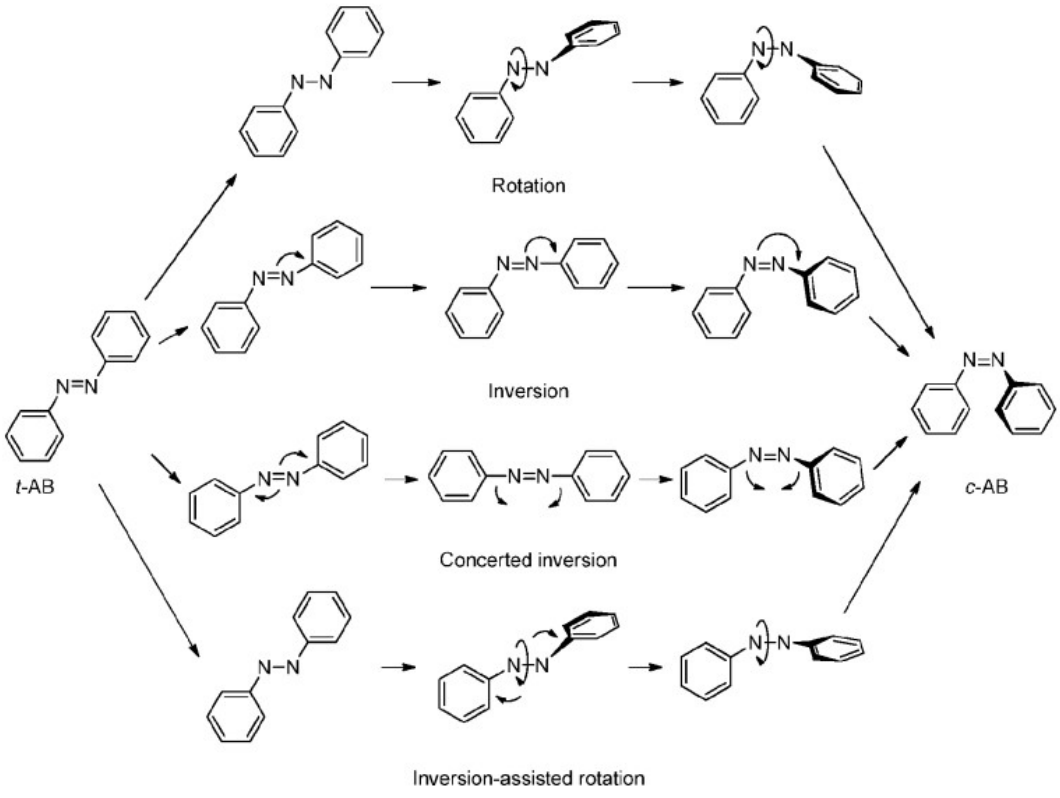

Figure C1-26. Schematic representation of the isomerization pathways. Taken from ref[58]

Thermal relaxation of *Cis* → *Trans* is believed to proceed only through inversion and rotation mechanisms.[58] The mechanisms at play during the different electronic transitions for this relaxation are still unclear. According to

Rau,[57] the inversion mechanism is linked to a n → π* transition (S_1 singlet state), and the rotation mechanism linked to the π → π* transition (S_2 singlet state).[56] Interestingly, all transition states may relax to either isomer, meaning that at photo-stationary state, a mixture of both isomers is obtained. If considering the irradiation of a mixture of trans and cis isomers with a light of energy **ω**, the two isomers will isomerize at different rates, which depend on the optical absorption and quantum yield of the given isomer at the given wavelength considered. If an isomer absorbs a photon, the quantum yield corresponds to the quantum probability of isomerization occurring. If irradiation is left to proceed for a sufficient amount of time, both rates of isomerization will become equal and the composition of *cis/trans* becomes constant: this is called the photo-stationary state. The yield of *cis* isomer at the photo-stationary state ($\mathbf{C_p(\omega)}$) can be predicted with the following formula, with **Φ(ω)** the quantum yields and **Ɛ(ω)** the optical absorptions:

$$c_p(\omega) = \frac{1}{1 + \frac{\Phi_{cis}(\omega)\epsilon_{cis}(\omega)}{\Phi_{trans}(\omega)\epsilon_{trans}(\omega)}}$$

Therefore, if a high amount of *cis* isomer is desired, it becomes apparent that the condition required is: $\mathbf{\Phi(\omega)_{trans} \; x \; Ɛ(\omega)_{trans} >> \Phi(\omega)_{cis} \; x \; Ɛ(\omega)_{cis}}$. Considering that the ratio $\mathbf{\Phi(\omega)_{trans}/\Phi(\omega)_{cis}}$ is relatively constant over the range of energies (i.e. irradiation wavelengths) relevant,[58] the condition becomes : $\mathbf{Ɛ(\omega)_{trans} >> Ɛ(\omega)_{cis}}$.

An important detail to point out is that *trans* and *cis* isomers do not have the same absorption spectra, as seen in **Figure C1-27**. For the π → π* transition, the absorption bands are well separated for the two isomers (except for the pseudo-stilbene class of azobenzenes, *vide infra*) and the trans isomer absorbs significantly more. For the n → π* transition, the bands of both isomers overlap – however the *cis* isomer absorbs approximately 3.3 times more than the *trans*.[58] This is why the n → π* transition is used for *cis* → *trans* photo-isomerization (λ ≈ 450 nm), and the π → π* transition is used for *trans* → *cis* photo-isomerization (λ ≈ 360 nm). It is worthy to note that while the *trans* → *cis* isomerization can be expected to be near quantitative since the π → π* bands are well separated for the two isomers, the same cannot be said for the *cis* → *trans* isomerization, since the n → π* bands overlap, and are overall much weaker.

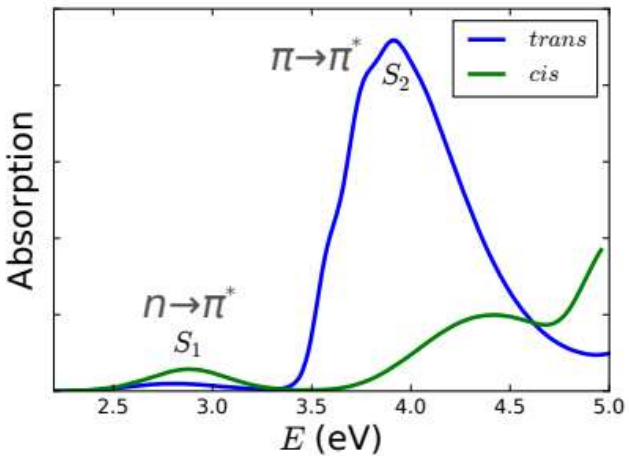

Figure C1-27. Absorption spectra of *trans*- and *cis*- azobenzene. Taken from ref[58]

ii. Azobenzene classification

The value of absorption wavelengths can vary by adding substituents on the azobenzene. For example, electron-rich substituents in the para position tend to increase $h\nu_1$ (blue-shift), and further adding an electron-withdrawing group on the other para position will increase this effect, by creating a push-pull system. This effect tends to further destabilize the *cis* isomeric form, accelerating the return to the trans isomer through thermal relaxation.[58]

In 1990, Rau proposed a simple classification of azobenzenes (i.e. azobenzene derivatives) depending on their absorption spectra and their relative π → π*, n → π* energies (**Figure C1-28**). The first class corresponds to all **azobenzenes** which share similar spectroscopic properties with unfunctionalized azobenzene, that is, two distinct π → π*and n → π* bands, and very slow thermal relaxation rate (hours to days). In this class are azobenzenes functionalized with alkyls, aryls, amides, nitriles, esters or carboxylic acids to name a few.

The second, termed **aminoazobenzenes**, class pools azobenzenes bearing electron donating groups in the ortho or para position, such as amines, alcohols or ethers. These substituents induce a red-shift of the π → π* band, where it begins to overlap with the n → π* band. Thermal relaxation of these compounds is much faster than the first class (half-life of the cis form ranging from seconds to minutes). Lastly, the third class, named "**pseudo-stilbene**", regroups push-pull azobenzenes: an electron donating group in the para/ortho position of one ring and an electron accepting group (such as $-CO_2H$, $-NO_2$) on the other. This substitution induces complete overlap of the π → π*and n → π* bands, and thermal relaxation is extremely quick (half-life ranging from milliseconds to seconds).[58]

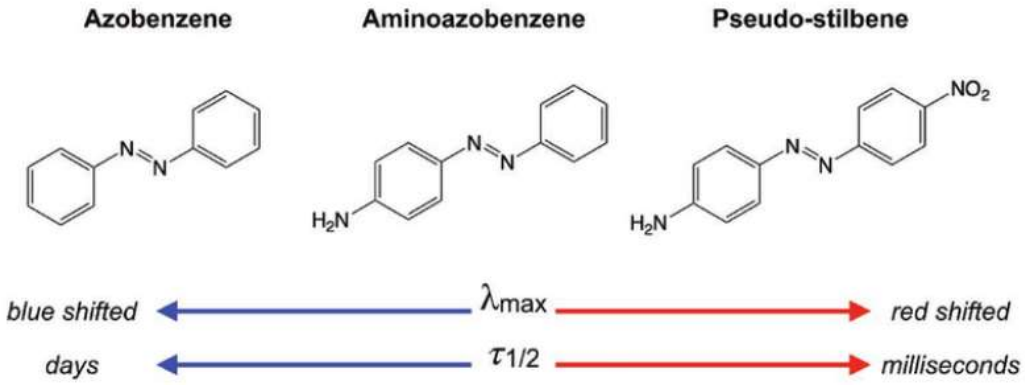

Figure C1-28. Rau's classification of azobenzenes. Taken from ref[58]

10.Photo-responsive azobenzene containing polymer assemblies in solution

Azopolymers, which are covalent polymers containing azobenzene moieties in the main chain and/or as pending side groups, represent an interesting class of materials. While the change in both geometrical configuration and polarity of the azobenzene groups after photo-isomerization can also be exploited to modify the polymers' mechanical or optical properties, this section will focus exclusively on systems in which azopolymers exhibit varying self-assemblies and morphologies in solution depending on azobenzene configuration.

In 2004, Zho's team[59] synthesized an azopolymer consisting of one block of poly(acrylic acid-co-*tert* butyl acrylate) and a second block of methacrylate functionalized with an azobenzene, using ATRP **(Figure C1-29)**. NMR measurements revealed that there were approximately 31 AA units, 19 residual tBuA units, and 33 AzoMA units, with SEC-HPLC indicating a M_n of 23100 g/mol and Đ = 1.31. Overall, the P(AA-co-tBuA) block was still found to be hydrophilic despite the presence of some hydrophobic tBuA moieties. The polymer was first dissolved in dioxane, which is a good solvent for both blocks, and water was then added, leading to the formation of micelles, since the P(AzoMA) block is hydrophobic. SEM measurements revealed there were a mixture of small, core-shell micelles (around 15 nm in diameter) with far larger micelle-like aggregates (approx. 200 nm). Upon UV irradiation, which promoted the photo-isomerization of the azobenzene to the *cis* isomer, microscopy measurements revealed that a very large portion of the big aggregates had dissociated. The authors attribute this to the fact the *cis* isomer is much more polar and less hydrophobic than the *trans* isomer. Interestingly, upon irradiation back to the *trans* isomer, the disrupted aggregates reform.

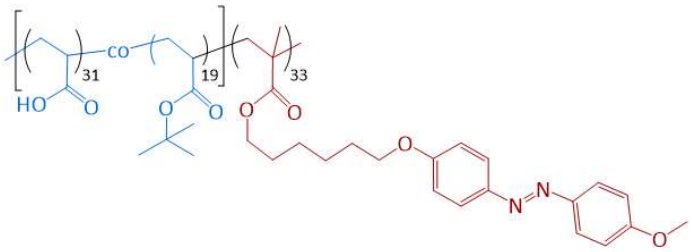

Figure C1-29. Chemical structure of PAA-b-PAzoMA (chain ends omitted for clarity). The subscripts correspond to the number average number of monomer units in the polymer chain.

A similar system was studied by Xu et al.,[60] using a block copolymer comprised of a hydrophilic PEO block, and an azobenzene-functionalized polycarbonate block, termed PMPC-Azo (**Figure C1-30**). After the synthesis, NMR analysis revealed that the carbonate units had been quantitatively functionalized with the azobenzene, yielding a final polymer of M_n = 16 000 g/mol and Đ = 1.1 (SEC-HPLC). A combination of light scattering, TEM and fluorescence spectroscopy was used to characterize the self-assembly of this polymer in water, and was found to spontaneously form spherical aggregates, and had a critical micelle concentration (CMC) very close to that of the same polymer without azobenzenes (PEO-b-poly(MPC)). DLS measurements indicated that PEO-b-poly(MPC) aggregates had an average radius of 50 nm, while PMPC formed aggregates with an average diameter of 150 nm. This increase in size was attributed to the presence of the bulky azobenzenes, which increase the size of the hydrophobic core of the aggregates. The PMPC aggregates were then irradiated with UV light, triggering the photo-isomerization of the azobenzene groups to the *cis* configuration, and after 15 minutes the photo-stationary state was reached. TEM images revealed that the aggregates had effectively disassembled, due to *cis*-azobenzene being more polar. Upon irradiation back to the *trans* isomer (λ = 450 nm), aggregates were reformed – which were larger according to DLS (190 nm in radius) than the initial aggregates. UV-vis spectroscopy indicated that the initial proportion of *trans*-azobenzene (amount not indicated by the authors) had been recovered. The aggregates

were then charged with hydrophobic Nile Red, and fluorescence spectroscopy indicated a gradual release of the compound during UV irradiation, showing the potential of this system for applications such as light-responsive drug delivery.

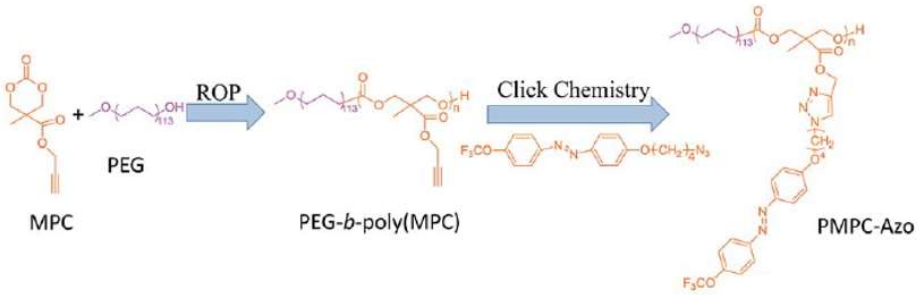

Figure C1-30. synthesis of PMPC-Azo. Taken from ref[60]

Another system, consisting of a PEO chain (1500 g/mol) end functionalized on one side with an azobenzene and on the other respectively with an amine, an NHBoc or a guanidine (Gu) group was described in the literature (see **Figure C1-31**).[61] The three polymers were directly dissolved in water and found to form spherical aggregates, due to the hydrophobic Azo groups and hydrophilic PEO chains. DLS measurements indicated that for R = NH_2, the smallest aggregates were formed, with an average radius of 100 nm. For R = Boc and Gu, the average radii were of 180 nm and 260 nm, respectively. Upon UV irradiation, photo-isomerization to the *cis* isomer occurred, and instead of dissociating, the aggregates were found to greatly increase in size. For R = NH_2, the average radius went from 100 nm to 250 nm, R = Boc going up to 470 nm and for R = Gu, 730 nm. When irradiated with visible light, isomerization back to the trans isomer occurred, and the average radii decreased, but remained slightly higher than the initial ones.

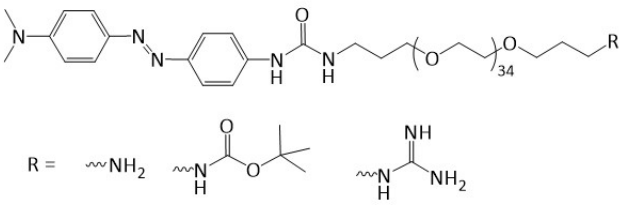

Figure C1-31. Chemical structure of Azo-PEO-R and studied –R groups.

In 2018, a system in which a photo-responsive azopolymer could adopt different morphologies depending on the ratio of *trans*/*cis*- azobenzene was reported.[62] This polymer consisted in a hydrophilic block of poly-(N,N-dimethylaminoethyl methacrylate) (PDMA), and a second hydrophobic block of poly-(benzyl methacrylate-co-azobenzene methacrylate) – and was termed $PDMA_{32}$-P($BzMA_{60}$-$AzoMA_6$). It was synthesized through polymerization induced self-assembly (PISA), by polymerizing the hydrophobic block on the already formed hydrophilic block (macro-CTA), using RAFT dispersion polymerization in EtOH (see **Figure C1-32a**). The polymer was characterized by UV-Vis spectroscopy and TEM measurements, using the dispersions obtained after the synthesis (in EtOH). The initial solution was found to contain worm-like micelles, which were formed during the synthesis as the hydrophobic block grew (PISA). UV-Vis indicated that photo-isomerization under UV light both occurred and was reversible. Photo-isomerization had a rather drastic impact on the morphology of the particles. Indeed, after 5 minutes of UV irradiation, the worm-like micelles started to partially fuse, with lamellae-like structures at the fuse points, and pending arms, which somewhat resembled “octopus-like” structures. Additional

irradiation caused the coalescence of the lamellae, leading to "jellyfish-like" particles with hemispherical heads. Upon further irradiation, vesicles were ultimately yielded (with an average diameter of approximately 200 nm) (see **Figure C1-32b**). If subjected to visible light, the transformations were fully reversible, and the initial worm-like micelles were recovered. The authors attribute this peculiar behavior to the fact that *cis*-azobenzene is bulkier than the *trans* isomer, therefore upon isomerization to *cis*-azobenzene, the packing parameter of the hydrophobic block increases (despite *cis*-azobenzene being more polar).

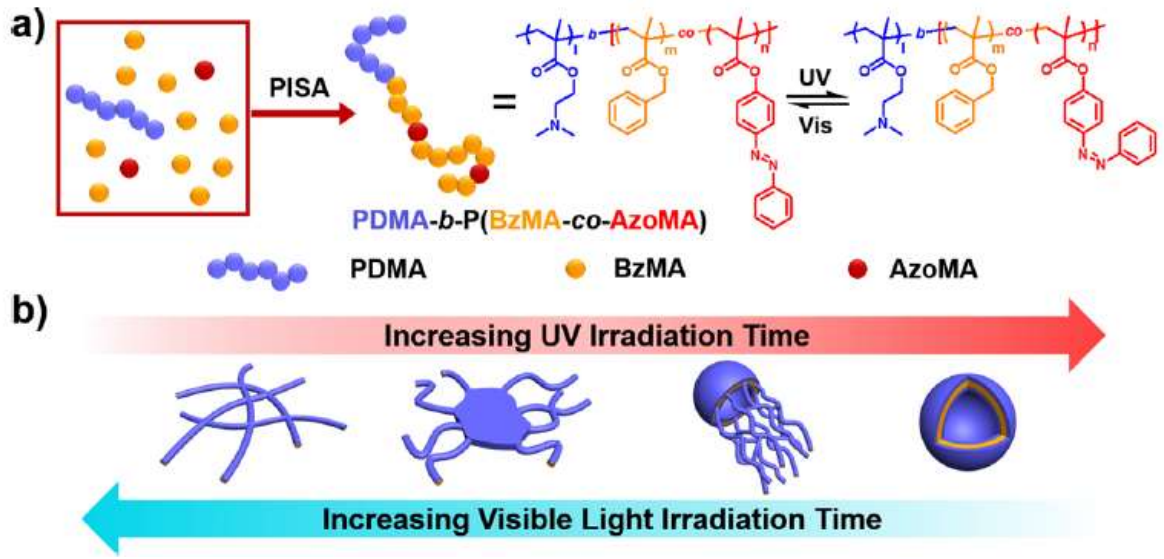

Figure C1-32. **a)** Schematic representation and chemical structure of the azopolymers. **b)** Schematic representation of morphologies obtained through UV or visible light irradiation. Taken from ref[62]

These examples of azopolymers demonstrate that azobenzene may impart a variety of photo-responsive properties to the corresponding materials, from a change in the amount of aggregation to a change in morphology. In some cases, this is due to the geometrical change of azobenzene upon photo-isomerization, while in other cases it is due to a change of polarity.

11. Photo-responsive 1D supramolecular assemblies in solution

Azobenzene represents a powerful photo-switch that can be incorporated into supramolecular structures to impart photo-responsiveness. As opposed to the previous section, where mainly spherical particles were formed, the focus of this section is put onto 1D structures. However, since the following examples do not possess polymer arms, this short review is non-exhaustive. The aim of this section is to present cases where azobenzene has been used to impart photo-responsiveness to self-assemblies, and discuss the impact of its photo-isomerization on the assemblies.

iii. In water

Kameta et al.[63] reported the synthesis and self-assembly of a rather simple azobenzene-bisamide (**Figure C1-33, top**). Aqueous solutions were prepared at a given pH, heated to reflux, and left to cool to r.t. Indeed, the compound is pH-sensitive, owing to the presence of the amine group. At pH 6.1 (protonated), fibers were formed, whereas at pH 9.2, the compound self-assembled into sheets. From pH 7.6 to 8.2, nano-tubes were formed, which were found to be self-assembled in a bilayer, with an internal diameter of 20 nm and a wall thickness of 8 nm. Upon UV irradiation, trans → cis photo-isomerization occurred within a matter of minutes, implying that photo-isomerization still occurs despite self-assembly, and was accompanied by a change in morphology: cylindrical

nano-fibers were formed. These nano-fibers were very long (several tens of µm) and had an internal diameter that was much smaller than that of the initial nano-tubes (not measurable by TEM). This change in morphology was not reversible. Indeed, after blue light irradiation (promoting isomerization back to the initial *trans* isomer), another change in morphology was observed, as helical nano-tapes were formed (see **Figure C1-33, left**). These nano-tapes were also fairly long (several hundreds of nm). These photo-triggered changes in morphology were investigated for their potential for light-responsive drug delivery. The nano-tubes were loaded with carboxyfluorescein (CF) and the release rate was measured. Without any irradiation, a slow and constant release of CF was observed. However, upon irradiation with UV, 40% of the loaded CF was rapidly released, owing to the much smaller internal diameter of the nano-fibers. Upon further irradiation with blue light, all the CF was rapidly released, due to the fact that the newly formed nano-tapes have no internal cavity whatsoever (see **Figure C1-33**, **right**).

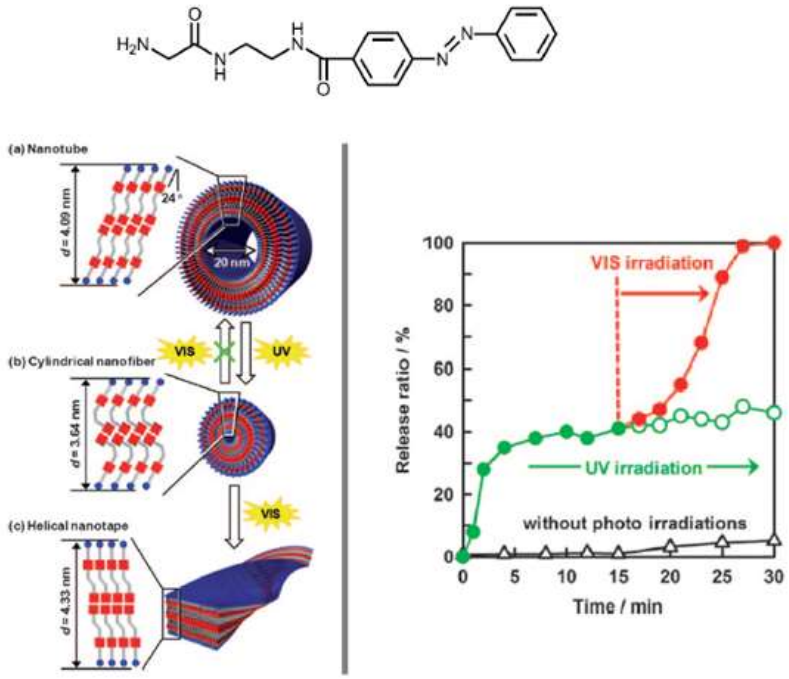

Figure C1-33. **Top**: chemical structure of the azobenzene-bisamide. **Bottom left**: schematic representation of light-responsive morphologies. **Bottom right**: release rates of CF depending on morphology of the self-assemblies Taken from ref[63]

A benzene 1,3,5-tricarboxamide (**Figure C1-34**) functionalized with azobenzenes has been reported to form various structures in aqueous solvents.[64] Samples were prepared by dissolving the Azo-BTA in organic solvent, followed by addition of water (up to 20-50% water). Interestingly, different morphologies were observed by optical microscopy depending on the starting solvent used. In DMSO, large micrometer long bundles of fibers were obtained. The same was observed in DMF, however in DMF gelation occurred. BTAs are well known for self-assembling into helical stacks (to reduce steric hindrance) via three-fold amide H-bonds.[65] However in this case, the stacks formed bundles of fibers (3-5 µm in diameter) through hydrophobic interactions, capable of gelating water/DMF mixtures. In THF/water however, spheres ranging from nm to µm diameters were obtained, and the authors report that the higher the water content, the smaller the spheres. When the DMSO/water fibers were subjected to UV irradiation, the fibers dissociated in a reversible manner, since further irradiation with blue light leads to fiber re-assembly. Note that the authors did not indicate whether the fibers were disrupted into smaller

objects or into unimers. The same observations were made for the DMF/water system, with a reversible "melting" of the gel. Surprisingly, the same cannot be said for the THF/water spheres, as UV irradiation had no effect on the assembly, despite photo-isomerization effectively taking place.

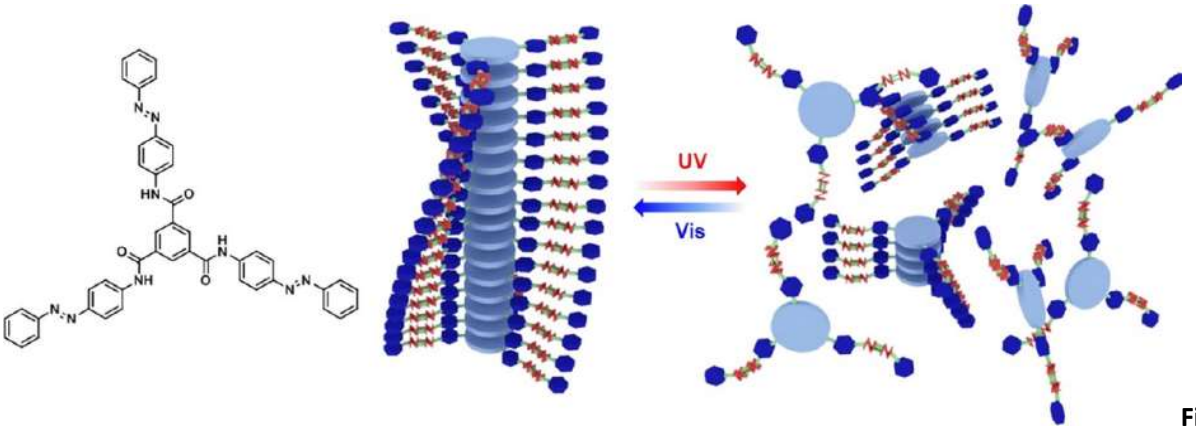

Figure C1-34. Chemical structure of Azo-BTA and schematic representation of its helical self-assembly. In reality, the helical nano-cylinders most probably aggregate laterally to form columnar aggregates since the fibers were large enough to be observed by optical microscopy. Taken from ref[64]

An azobenzene benzene tricarboxamide (BTA) was described in recent literature, containing multiple stimuli-responsive units: azobenzene, to impart photo-responsiveness, oligo-PEO to afford water solubility and thermo-responsiveness, and a lysine chain-end for pH/salt sensitivity. Two compounds were synthesized, as can be seen in **Figure C1-35**, one with the azobenzenes as pending side-groups (**a**), and the other with the azobenzenes directly incorporated close to the BTA core (**b**).[66] A DMSO/water water-route was used (final composition of water: DMSO = 99 : 1 by volume) in order to form assemblies from molecularly dissolved unimers (resolved ^{1}H NMR and TEM were used to demonstrate that the compound forms unimers in DMSO), eliminating any pre-existing assembly. While BTA (**a**) was shown to self-assemble into long, flexible micrometer long fibers, BTA (**b**) did not self-assemble in any of the tested conditions and was therefore not further studied. BTA (**a**) can actually be found in 4 different azobenzene configuration states: *trans/trans/trans*, *trans/trans/cis*, *trans/cis/cis* and *cis/cis/cis*. Initially, the authors report that the ratios of these configurations were 59% / 34% / 7% / 0%, respectively. Irradiating (**a**) with UV in both DMSO and DMSO/water led to rapid formation of cis-azobenzene in high yield (42% of *cis/cis/cis* and 42% of *trans/cis/cis*), meaning that the photo-switch is possible in both unimeric and self-assembled states. Further irradiating the samples with blue light afforded the trans isomer in high yield. After 10 isomerization cycles, no degradation was observed. Intriguingly, thermal relaxation of the cis isomer to trans in the dark was not observed, at least over the course of 24 hours, indicating that thermal relaxation was extremely slow, which was not explained by the authors. [66] UV irradiation of the self-assembled fibers led to their dissociation, which can be attributed to the fact that *cis*-azobenzene is more hydrophilic, and more sterically repulsive, disfavoring assembly and presumably favoring unimers. A kinetic measurement of isomerization using CD indicated that the amount of monomer in helical stacks was proportional to the amount of trans isomer, meaning that specific polymerization degrees can be targeted. Re-irradiating with blue light triggered re-assembly into fibers, proving the reversibility of the photo-responsiveness. [66]

The azo-BTA also showed a thermal response, with a much higher aggregation being observed at higher temperature (40-50 °C): more and longer nanorods were observed by TEM and LS. This can be explained by two phenomena: a reduced hydrophilicity of the oligo-PEO, and a larger number of trans-isomers, since heat favors a larger trans to cis ratio. Indeed, after heating, there was approximately 20% more *trans*-azobenzene than there initially was. Interestingly, if the temperature was then decreased, the initial aggregation was recovered,

indicating that the system is in thermodynamic equilibrium. Lastly, the assemblies were sensitive to pH, with few fibers being formed at low pH and none at high pH, due to the presence of pH-sensitive carboxylic acid/primary amine groups. However, adding NaCl allowed for increased aggregation under high or low pH conditions, through charge shielding effect.[66]

This example is very promising since the supramolecular nanocylinders are multi-responsive, including to a light trigger, and in a reversible way. Moreover, reversible photo-triggered disassembly was achieved in water, and the responsiveness comes from the self-assembling core. However, the polymer arms are very short. It is likely that it would be more difficult to achieve the same behaviour with longer polymer arms as the BTA motif was shown to not be a strong enough self-assembling core to form long nanocylinders with long polymer arms.[67]

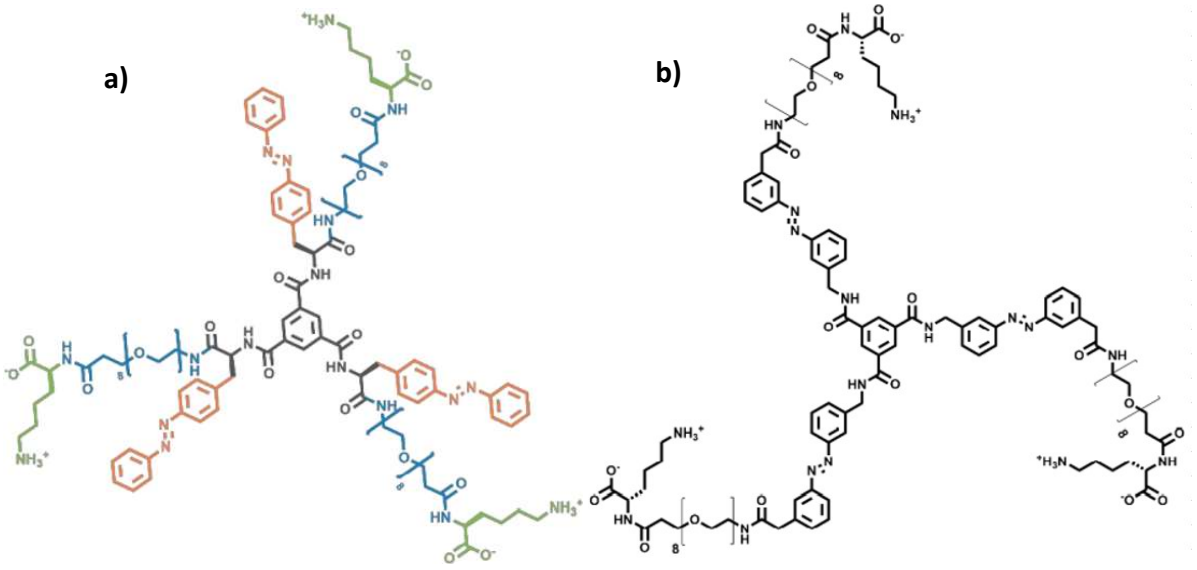

Figure C1-35. Chemical structures of the two azo-BTAs. Taken from ref[66]

iv. In organic solvent

An azo-BTA functionalized with 2 chiral dimethyloctyl arms (**Figure C1-36)** has been reported to self-assemble into long supramolecular fibers in methylcyclohexane (MCH), with a core radius of 1.38 nm (as measured by SAXS).[68] The chiral alkyl arms were chosen to induce a preferred helicity, allowing for circular dichroism (CD) analysis. The BTA cores form a helix of opposite helicity to that of the azobenzene, which forms a double helix, as represented in **Figure C1-36**. UV irradiation yielded the cis-isomer very rapidly (30 seconds) - meaning that the azobenzene still acts as a photo-switch despite being in the assembly. This in turn leads to the dissociation of the stacks – however not totally, since small stacks still remain, as evidenced using CD. This dissociation was shown to be reversible, since it was possible to reform the helical stacks via blue light irradiation or thermal relaxation, both leading to the isomerization of cis-azobenzene to its trans form. It is interesting to point out that a single azobenzene per monomer was sufficient in this case to cause supramolecular depolymerization.

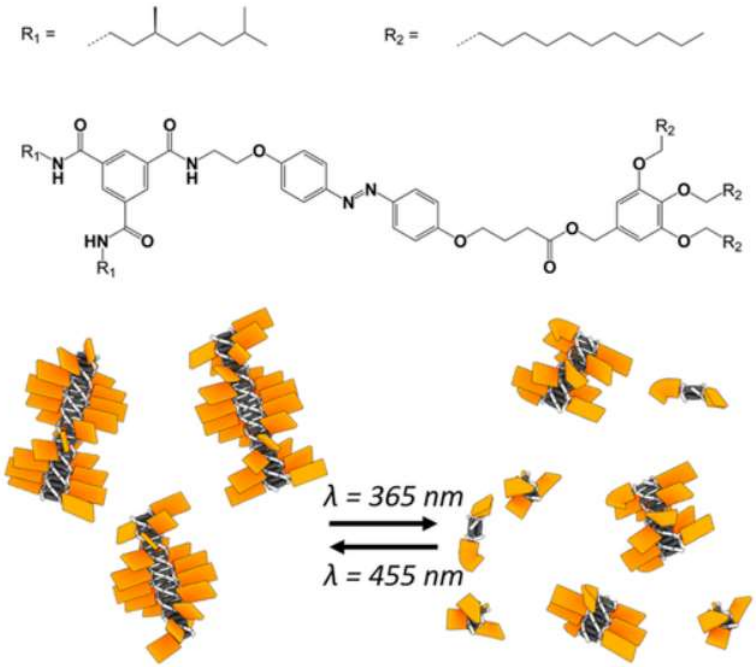

Figure C1-36. Chemical structure of the azo-BTA and schematic representation of its self-assembly. Taken from ref[68]

Arima et al.[69] designed scissor-shaped bis-azobenzene based compounds, as can be seen in **Figure C1-37,** with varying aliphatic/perfluoroalkylated tails linked to each azobenzene. Compound **2** was found to first self-assemble into toroids at 20°C in methylcyclohexane (MCH), and if the solution was further cooled to 0°C, the toroids could self-assemble into nano-tubes. On the other hand, compound **3**, which possesses perfluoroalkyl tails, was found to directly self-assemble into large fibers, without forming toroids or tubular structures. AFM measurements showed heavily entangled fibers; which could be exploited for the gelation of low polarity solvents. According to the authors, perfluoroalkyl bis-azobenzene can directly self-assemble thanks to the increased intermolecular interactions, owing to fluorophilic interactions of the tails, while the alkylated bis-azobenzene cannot. They therefore conclude that the toroidal aggregation can only be expected for molecules that weakly interact. In both cases, irradiation of the azobenzene to its *cis* isomer resulted in the reversible disassembly of the assembled structures, which could be reformed through irradiating the azobenzene back to its initial *trans* configuration.

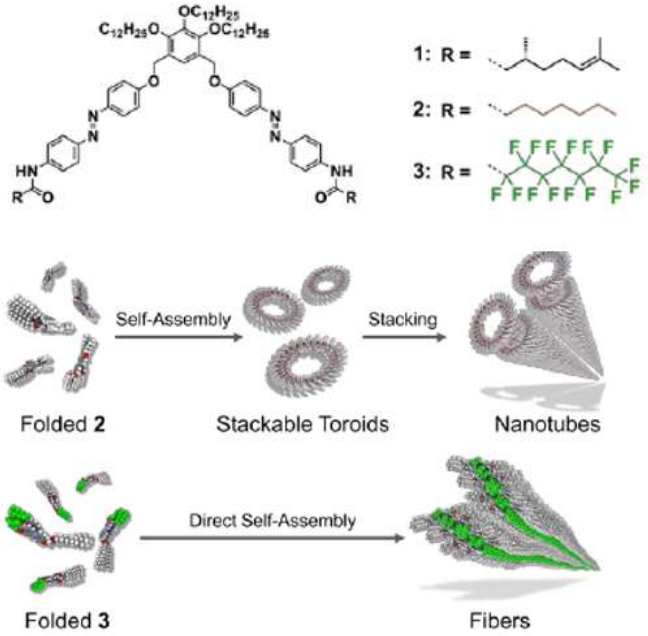

Figure C1-37. chemical structures of the bis-azobenzene compounds studied, and the schematic representation of their self-assembly. Adapted from ref[69]

Yagai et al.[70] reported an azobenzene-functionalized DAP (N,N'-disubstituted 4,6-diaminopyrimidin-2(1H)-one) (see **Figure C1-38**).[70] The azobenzene groups are initially almost quantitatively in the *trans* configuration, as measured by ^{1}H NMR. LS measurements indicated that no large assemblies were present when the compound was dissolved in THF or chloroform, however moderate self-assembly was observed in less polar media, namely cyclohexane, with an N_{agg} of 70. Self-assembly is promoted in even less polar solvents, such as heptane, and assemblies slowly grew in size (average aggregate size of 150 nm after 12 hours), suggesting that, in the apolar solvent, assembly relies on both H-bonds in addition to weaker interactions such as Van der Waals interactions. In THF, UV irradiation yielded 98% *cis*-azobenzene, whereas only 55% was formed in heptane, suggesting that self-assembly somewhat hindered photo-isomerization. As may be expected, photo-isomerization of the assemblies in cyclohexane decreased drastically the average aggregate size, down to 30 nm. Irradiating with blue light yielded 90% *trans*-azobenzene, and the same assemblies that were initially observed, were recovered.

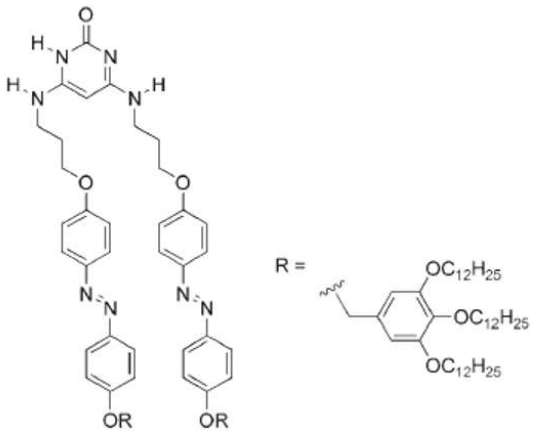

Figure C1-38. Chemical structure of azobenzene functionalized DAP. Taken from ref[70]

In some cases, photo-isomerization of azobenzene may be rendered impossible due to strong self-assembly. Such a case was reported by Inoue and coworkers,[71] who studied an azobenzene functionalized with 4 amide groups in organic media and investigated its gelation properties (see **Figure C1-39**). This compound could self-assemble into nano-fibers through H-bonding of the amides. The nano-fibers could then further aggregate between themselves and ultimately form a 3D network capable of forming gels. Indeed, it was found to be an effective gelator in a number of solvents, ranging from silicone oil to THF. TEM measurements indicated that in solvents in which gelation occurs such as cyclohexanone, an entangled network of nano-fibers was indeed present, ranging from 20 to 50 nm in diameter. In cyclohexanone, a gel was formed, but the UV-Vis spectra after irradiation revealed that no isomerization had occurred (and therefore no change in morphology). The authors used molecular modelling to demonstrate that in the gelled state, the azobenzene units were stacked – and conclude that the combination of this Pi stacking with H-bonding was too strong for the azobenzene moieties to be able to undergo photo-isomerization. In DCM, where the compound did not form a gel (the authors did not investigate whether self-assembly occurred at the nanoscale), UV irradiation triggered photo-isomerization to *cis*-azobenzene.

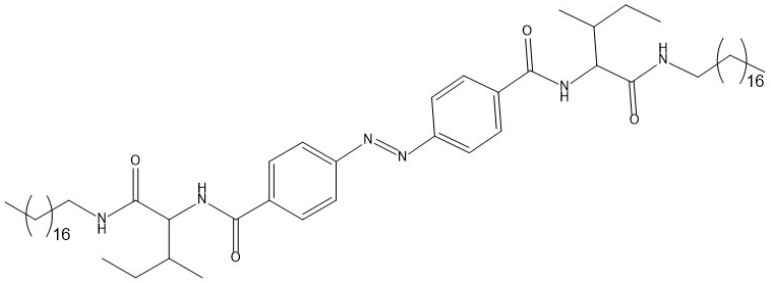

Figure C1-39. Chemical structure of the azobenzene tetra-amide organo-gelator. Adapted from ref[71]

Lastly, Feringa et al. reported a bis-urea stiff-stilbene decorated with oligo-PEO arms that could be self-assembled in both water and toluene (while not an azobenzene based example, it is quite relevant to this thesis as the structure of the polymer is somewhat similar to the polymer that was synthesized in this work). In its "inactive" cis configuration, the ureas can only bond intramolecularely, leading to no self-assembly. However, if irradiated, it can photo-isomerize to its "active" trans configuration, and undergoes self-assembly through H-bonding. In toluene, self-assembly was spontaneous, following a nucleation-elongation mechanism. The assemblies could be reversibly and quantitatively disrupted if isomerized back to the *cis* configuration.[72] In water, on the other hand, 1D self-assembly was achieved through a heat-cool cycle. The hydrophobic effect was found to significantly contribute to the self-assembly, and the authors determined a Gibbs free energy twice the value of that in toluene. However, the strong self-assembly prevented photo-isomerization from occuring at r.t. and photo-induced disassembly was not possible in water.[73]

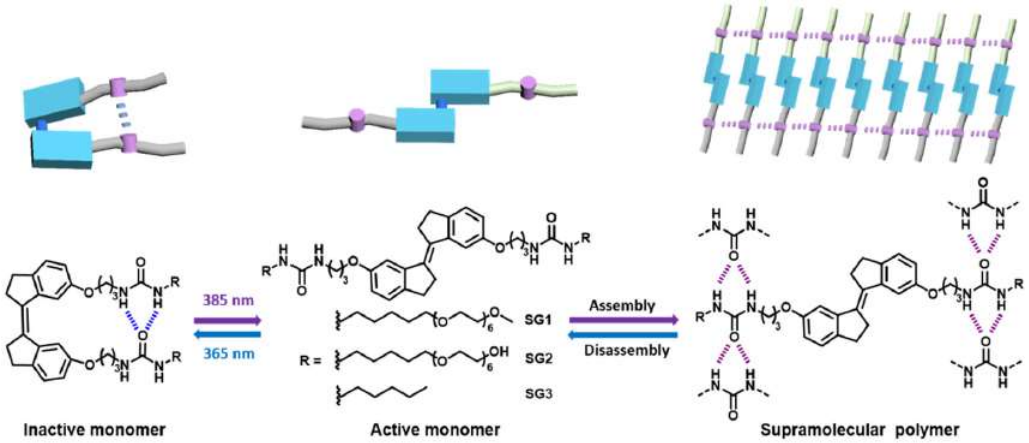

Scheme C1-41. Chemical structure of the bis-urea stillbene compound and schematic representation of its self-assembly in toluene. Taken from ref[72]

In this section, several examples of supramolecular 1D systems containing azobenzene have been presented. In azopolymers, azobenzene can induce changes in morphology through changing the hydrophilicity of a block after UV irradiation, or through changes in geometrical conformation, which can induce a change in the packing parameter of an amphiphilic polymer. In 1D assemblies however, the azobenzene generally serves the purpose of changing the shape of the molecule after UV irradiation, which prevents the molecules from being able to self-assemble (by preventing effective H-bonding for instance). This can lead to the (sometimes) reversible light-triggered disassembly of the 1D structures. In some cases, self-assembly can hinder the photo-isomerization, or completely block it, if assembly is too strong. [73]

V. Conclusions of the bibliography

The main motifs used for forming supramolecular nano-cylinders decorated with polymer arms in solution, which are oligo-cyclopeptides and bis/tris-ureas, rely on H-bonding to drive self-assembly. In particular, bis-ureas are highly cooperative, which is favorable for forming long nano-cylinders. Furthermore, their synthesis is generally quite simple and can be achieved using a variety of syntheses. Bis-urea functionalized polymers have been reported to be able to self-assemble in organic solvents, as well as in water, however extra precautions must be taken for the latter. Hydrophobic spacers in between the self-assembling core and the polymer arms are generally required for self-assembly in water, as they protect the bis-urea from both H-bond competing water, and the steric hindrance of the polymer arms. In most cases, such systems did not form nano-cylinders upon direct dissolution in water because of the frozen character of the assemblies, and an alternative protocol was used. The polymer was first dissolved in DMSO, a solvent in which it is in unimers state, followed by the slow addition of water, promoting self-assembly of the polymer into long nano-cylinders. Amongst the examples of supramolecular nano-cylinders reported in the literature, only a handful are stimuli-responsive (pH, oxidation, host-guest chemistry and light) and may undergo stimuli-triggered disassembly, and a large portion of those examples rely on the nature of the polymer arm to impart responsiveness, which limits the versatility of the approach. Moreover, most of the examples undergo irreversible disassembly, limiting the applicative potential.

Light is an attractive trigger, since it is non-invasive (i.e. the chemical composition of the solution) and easy to tune (wavelength, beam intensity, and irradiation time). Of the many light-responsive moieties that exist, azobenzene has been widely studied. In its thermodynamically favorable state, it is in the trans configuration, which is planar and non-polar. Upon irradiation at the appropriate wavelength (generally UV), it undergoes photo-isomerization to the cis isomer, which changes geometrical configuration (and is no longer planar) and becomes

more polar (therefore less hydrophobic). It can be isomerized back to trans-azobenzene either by irradiating at a second wavelength (typically 450 nm) or by rather slow (hours-days) thermal relaxation in the dark. Due to these properties, azobenzene has been used in a large number of photo-responsive systems. In this bibliographic chapter, some examples of azopolymers (polymers containing azobenzene in the main chain) have been presented, and were reported to be able to change size using light as a stimulus. Azobenzene has also been used to impart photo-responsiveness to self-assemblies of small molecules, wherein photo-triggered disassembly of 1D structures or a change in their morphology is observed upon photo-isomerization. In most cases, self-assembly does not impede photo-isomerization, but there are some cases where isomerization cannot occur due to very strong self-assembly. It is important to point out that amongst most of these azopolymers examples, many require a large number of azobenzene units per polymer to achieve the desired behavior.

The main aim of this project was to design and synthesize a polymer capable of self-assembling into long nano-cylinders decorated with polymer arms, that may undergo disassembly using light as a stimulus. To the best of our knowledge, only two examples achieving this have been previously reported: one is based on an oligo-cyclopeptide decorated with poly-(2-nitrobenzyl methacrylate) arms, which, upon UV irradiation, undergoes photo-cleavage of the nitrobenzyl groups, yielding poly(methacrylic acid) arms. Since these methacrylic acid units are charged at neutral pH, this provokes the disassembly of the nano-tubes. This approach is however limited, since it relies on the nature of the polymer arms, and is intrinsically irreversible (the chemical structure of the polymer is modified upon light exposure). The second example reported consisted in a BTA functionalized with 3 azobenzene groups and oligo-PEO, which could be assembled/disassembled in a completely reversible manner – however the polymer arms are extremely small. Considering that long polymer arms strongly hinder self-assembly as highlighted above, such a motif may not provide sufficient self-assembly if longer polymer arms are selected. Therefore, the originality targeted in this PhD work rests on three elements: 1) the nano-cylinders are decorated with fairly long polymer arms 2) the photo-triggered disassembly does not rely on the nature of the polymer arms and 3) only one azobenzene moiety per polymer is required to trigger disassembly of the nano-cylinders.

The general structure of the unimers is represented in **Scheme C1-40**. For all the reasons presented above, two urea groups were chosen to promote self-assembly via strong cooperative H-bonding. To impart photo-responsiveness, an azobenzene unit was selected and placed in between the two urea groups: the thermodynamically favorable trans isomer is planar and should favor cooperative hydrogen bonding of both urea functions, hopefully providing a sufficient driving-force for 1D stacking of unimers. However, after exposure to UV irradiation at the appropriate wavelength, azobenzene can isomerize into the cis isomer, which is no longer planar and is also more polar (and therefore slightly more hydrophilic). This should therefore prevent 1D self-assembly and break the nanocylinders for two reasons: 1) by disrupting the cooperativity between the two hydrogen bonding urea functions, and/or 2) (in water) by decreasing the additional hydrophobic character of the azobenzene unit. It is important to note that this photo-isomerization could be reversible, as *trans*-azobenzene can be recovered by irradiating at a second wavelength, or by leaving it in the dark to thermally relax. Therefore, reversibility (i.e. re-assembly of the nano-cylinders) may be achievable. Since this project aimed to study this system in both aqueous media and organic solvents, short alkyl spacers were placed in between the ureas and polymer arms, serving a dual purpose: these spacers protect the H-bond promoting ureas from both the steric hindrance that may be imparted from the polymer arms, and from H-bond competing solvent (such as water) or polymer units. The polymer arms impart solubility to the molecule (therefore a polymer soluble in both water and some organic solvents was selected), and also allow for isolated nano-cylinders to be obtained, by limiting lateral aggregation between nano-cylinders.

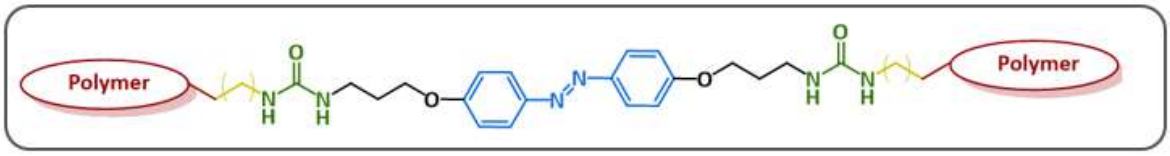

Scheme C1-40. General structure of unimers

References

1. Fielding, L. A., Derry, M. J., Ladmiral, V., Rosselgong, J., Rodrigues, A. M., Ratcliffe, L. P. D., Sugihara, S. & Armes, S. P. RAFT dispersion polymerization in non-polar solvents: Facile production of block copolymer spheres, worms and vesicles in n-alkanes. *Chem Sci* **4**, 2081–2087 (2013).

2. Grubbs, R. B. & Sun, Z. Shape-changing polymer assemblies. *Chem Soc Rev* **42**, 7436–7445 (2013).

3. Petzetakis, N., Dove, A. P. & O'Reilly, R. K. Cylindrical micelles from the living crystallization-driven self-assembly of poly(lactide)-containing block copolymers. *Chem Sci* **2**, 955–960 (2011).

4. Hayward, R. C. & Pochan, D. J. Tailored assemblies of block copolymers in solution: It is all about the process. *Macromolecules* **43**, 3577–3584 (2010).

5. Nicolai, T., Colombani, O. & Chassenieux, C. Dynamic polymeric micelles versus frozen nanoparticles formed by block copolymers. *Soft Matter* **6**, 3111–3118 (2010).

6. Feng, C., Li, Y., Yang, D., Hu, J., Zhang, X. & Huang, X. Well-defined graft copolymers: From controlled synthesis to multipurpose applications. *Chem Soc Rev* **40**, 1282–1295 (2011).

7. Sheiko, S. S., Sumerlin, B. S. & Matyjaszewski, K. Cylindrical molecular brushes: Synthesis, characterization, and properties. *Progress in Polymer Science (Oxford)* **33**, 759–785 (2008).

8. Zhang, M. & Müller, A. H. E. Cylindrical polymer brushes. *J Polym Sci A Polym Chem* **43**, 3461–3481 (2005).

9. Steed, J. W. & Atwood, J. L. Supramolecular Chemistry: Second Edition. *Supramolecular Chemistry: Second Edition* 1–970 (2009) doi:10.1002/9780470740880.

10. Wang, Q., Zhong, Y., Miller, D. P., Lu, X., Tang, Q., Lu, Z. L., Zurek, E., Liu, R. & Gong, B. Self-Assembly and Molecular Recognition in Water: Tubular Stacking and Guest-Templated Discrete Assembly of Water-Soluble, Shape-Persistent Macrocycles. *J Am Chem Soc* **142**, 2915–2924 (2020).

11. Rosselli, S., Wagner, T., Silier, B., Wiegand, S., Häuûler, W., Lieser, G. & Scheumann, V. Coil ± ring ± coil block copolymers aggregate in cyclohexane to give supramolecular hollow cylinders. *Angewandte Chemie International Edition* 3137–3141 (2001).

12. Rondeau-Gagné, S., Néabo, J. R., Desroches, M., Cantin, K., Soldera, A. & Morin, J. F. The importance of the amide configuration in the gelation process and topochemical polymerization of phenylacetylene macrocycles. *J Mater Chem C Mater* **1**, 2680–2687 (2013).

13. Smith, M. K. & Miljanić, O. S. Arylene ethynylene macrocycles: From molecular hosts to components of high-performance supramolecular architectures. *Org Biomol Chem* **13**, 7841–7845 (2015).

14. Zhang, W. & Moore, J. S. Shape-persistent macrocycles: Structures and synthetic approaches from arylene and ethynylene building blocks. *Angewandte Chemie - International Edition* **45**, 4416–4439 (2006).

15. Koh, M. L., FitzGerald, P. A., Warr, G. G., Jolliffe, K. A. & Perrier, S. Study of (Cyclic Peptide)–Polymer Conjugate Assemblies by Small-Angle Neutron Scattering. *Chemistry - A European Journal* **22**, 18419–18428 (2016).

16. Danial, M., My-Nhi Tran, C., Young, P. G., Perrier, S. & Jolliffe, K. A. Janus cyclic peptide-polymer nanotubes. *Nat Commun* **4**, (2013).

17. Pasini, D. & Ricci, M. Macrocycles as Precursors for Organic Nanotubes. *Curr Org Synth* **4**, 59–80 (2007).

18. Couet, J. & Biesalski, M. Polymer-wrapped peptide nanotubes: Peptide-grafted polymer mass impacts length and diameter. *Small* **4**, 1008–1016 (2008).

19. Rho, J. Y., Brendel, J. C., MacFarlane, L. R., Mansfield, E. D. H., Peltier, R., Rogers, S., Hartlieb, M. & Perrier, S. Probing the Dynamic Nature of Self-Assembling Cyclic Peptide–Polymer Nanotubes in Solution and in Mammalian Cells. *Adv Funct Mater* **28**, (2018).

20. Couet, J. & Biesalski, M. Surface-initiated ATRP of N-isopropylacrylamide from initiator-modified self-assembled peptide nanotubes. in *Macromolecules* vol. 39 7258–7268 (2006).

21. Wang, Q., Zhang, X., Zheng, J. & Liu, D. Self-assembled peptide nanotubes as potential nanocarriers for drug delivery. *RSC Adv* **4**, 25461–25469 (2014).

22. Saez Talens, V., Davis, J., Wu, C. H., Wen, Z., Lauria, F., Gupta, K. B. S. S., Rudge, R., Boraghi, M., Hagemeijer, A., Trinh, T. T., Englebienne, P., Voets, I. K., Wu, J. I. & Kieltyka, R. E. Thiosquaramide-Based Supramolecular Polymers: Aromaticity Gain in a Switched Mode of Self-Assembly. *J Am Chem Soc* **142**, 19907–19916 (2020).

23. Saez Talens, V., Makurat, D. M. M., Liu, T., Dai, W., Guibert, C., Noteborn, W. E. M., Voets, I. K. & Kieltyka, R. E. Shape modulation of squaramide-based supramolecular polymer nanoparticles. *Polym Chem* **10**, 3146–3153 (2019).

24. Bellot, M. & Bouteiller, L. Thermodynamic description of bis-urea self-assembly: Competition between two supramolecular polymers. *Langmuir* **24**, 14176–14182 (2008).

25. Ducouret, G., Chassenieux, C., Martins, S., Lequeux, F. & Bouteiller, L. Rheological characterisation of bis-urea based viscoelastic solutions in an apolar solvent. *J Colloid Interface Sci* **310**, 624–629 (2007).

26. Francisco, K. R., Dreiss, C. A., Bouteiller, L. & Sabadini, E. Tuning the viscoelastic properties of bis(urea)-based supramolecular polymer solutions by adding cosolutes. *Langmuir* **28**, 14531–14539 (2012).

27. Bouteiller, L., Colombani, O., Lortie, F. & Terech, P. Thickness transition of a rigid supramolecular polymer. *J Am Chem Soc* **127**, 8893–8898 (2005).

28. Shikata, T., Nishida, T., Isare, B., Linares, M., Lazzaroni, R. & Bouteiller, L. Structure and dynamics of a bisurea-based supramolecular polymer in n-dodecane. *Journal of Physical Chemistry B* **112**, 8459–8465 (2008).

29. Isare, B., Pensec, S., Raynal, M. & Bouteiller, L. Bisurea-based supramolecular polymers: From structure to properties. *Comptes Rendus Chimie* **19**, 148–156 (2016).

30. Pinault, T., Isare, B. & Bouteiller, L. Solvents with similar bulk properties induce distinct supramolecular architectures. *ChemPhysChem* **7**, 816–819 (2006).

31. Simic, V., Bouteiller, L. & Jalabert, M. Highly Cooperative Formation of Bis-Urea Based Supramolecular Polymers. *J Am Chem Soc* **125**, 13148–13154 (2003).

32. Pense, S., Nouvel, N., Guilleman, A., Creton, C., Boue, F. & Bouteiller, L. Self-assembly in solution of a reversible comb-shaped supramolecular polymer. *Macromolecules* **43**, 2529–2534 (2010).

33. Catrouillet, S., Fonteneau, C., Bouteiller, L., Delorme, N., Nicol, E., Nicolai, T., Pensec, S. & Colombani, O. Competition between steric hindrance and hydrogen bonding in the formation of supramolecular bottle brush polymers. *Macromolecules* **46**, 7911–7919 (2013).

34. Catrouillet, S., Bouteiller, L., Nicol, E., Nicolai, T., Pensec, S., Jacquette, B., Le Bohec, M. & Colombani, O. Self-assembly and critical solubility temperature of supramolecular polystyrene bottle-brushes in cyclohexane. *Macromolecules* **48**, 1364–1370 (2015).

35. Fonteneau, C., Pensec, S. & Bouteiller, L. Versatile synthesis of reversible comb-shaped supramolecular polymers. *Polym Chem* **5**, 2496–2505 (2014).

36. Han, S., Mellot, G., Pensec, S., Rieger, J., Stoffelbach, F., Nicol, E., Colombani, O., Jestin, J. & Bouteiller, L. Crucial Role of the Spacer in Tuning the Length of Self-Assembled Nanorods. *Macromolecules* **53**, 427–433 (2020).

37. Pal, A., Karthikeyan, S. & Sijbesma, R. P. Coexisting hydrophobic compartments through self-sorting in rod-like micelles of bisurea bolaamphiphiles. *J Am Chem Soc* **132**, 7842–7843 (2010).

38. Obert, E., Bellot, M., Bouteiller, L., Andrioletti, F., Lehen-Ferrenbach, C. & Boué, F. Both water- and organo-soluble supramolecular polymer stabilized by hydrogen-bonding and hydrophobic interactions. *J Am Chem Soc* **129**, 15601–15605 (2007).

39. Han, S., Nicol, E., Niepceron, F., Colombani, O., Pensec, S. & Bouteiller, L. Oligo-Urea with No Alkylene Unit Self-Assembles into Rod-Like Objects in Water. *Macromol Rapid Commun* **40**, 1–5 (2019).

40. Mellot, G., Guigner, J. M., Jestin, J., Bouteiller, L., Stoffelbach, F. & Rieger, J. Bisurea-Functionalized RAFT Agent: A Straightforward and Versatile Tool toward the Preparation of Supramolecular Cylindrical Nanostructures in Water. *Macromolecules* **51**, 10214–10222 (2018).

41. Choisnet, T., Canevet, D., Sallé, M., Nicol, E., Niepceron, F., Jestin, J. & Colombani, O. Robust supramolecular nanocylinders of naphthalene diimide in water. *Chemical Communications* **55**, 9519–9522 (2019).

42. Choisnet, T., Canevet, D., Sallé, M., Lorthioir, C., Bouteiller, L., Woisel, P., Niepceron, F., Nicol, E. & Colombani, O. Colored Janus Nanocylinders Driven by Supramolecular Coassembly of Donor and Acceptor Building Blocks. *ACS Nano* **15**, 2569–2577 (2021).

43. Catrouillet, S., Brendel, J. C., Larnaudie, S., Barlow, T., Jolliffe, K. A. & Perrier, S. Tunable Length of Cyclic Peptide-Polymer Conjugate Self-Assemblies in Water. *ACS Macro Lett* **5**, 1119–1123 (2016).

44. Larnaudie, S. C., Brendel, J. C., Jolliffe, K. A. & Perrier, S. PH-Responsive, Amphiphilic Core-Shell Supramolecular Polymer Brushes from Cyclic Peptide-Polymer Conjugates. *ACS Macro Lett* **6**, 1347–1351 (2017).

45. Chapman, R., Warr, G. G., Perrier, S. & Jolliffe, K. A. Water-soluble and pH-responsive polymeric nanotubes from cyclic peptide templates. *Chemistry - A European Journal* **19**, 1955–1961 (2013).

46. Otter, R., Klinker, K., Spitzer, D., Schinnerer, M., Barz, M. & Besenius, P. Folding induced supramolecular assembly into pH-responsive nanorods with a protein repellent shell. *Chemical Communications* **54**, 401–404 (2018).

47. Danial, M., Tran, C. M. N., Jolliffe, K. A. & Perrier, S. Thermal gating in lipid membranes using thermoresponsive cyclic peptide-polymer conjugates. *J Am Chem Soc* **136**, 8018–8026 (2014).

48. Chapman, R., Bouten, P. J. M., Hoogenboom, R., Jolliffe, K. A. & Perrier, S. Thermoresponsive cyclic peptide – poly(2-ethyl-2-oxazoline) conjugate nanotubes. *Chemical Communications* **49**, 6522–6524 (2013).

49. Otter, R., Berac, C. M., Seiffert, S. & Besenius, P. Tuning the life-time of supramolecular hydrogels using ROS-responsive telechelic peptide-polymer conjugates. *Eur Polym J* **110**, 90–96 (2019).

50. Nicolas, C., Ghanem, T., Canevet, D., Sallé, M., Nicol, E., Gautier, C., Levillain, E., Niepceron, F. & Colombani, O. Oxidation-Sensitive Supramolecular Polymer Nanocylinders. *Macromolecules* **55**, 6167–6175 (2022).

51. Song, Q., Yang, J., Rho, J. Y. & Perrier, S. Supramolecular switching of the self-assembly of cyclic peptide-polymer conjugates: Via host-guest chemistry. *Chemical Communications* **55**, 5291–5294 (2019).

52. Yang, J., Song, J. I., Song, Q., Rho, J. Y., Mansfield, E. D. H., Hall, S. C. L., Sambrook, M., Huang, F. & Perrier, S. Hierarchical Self-Assembled Photo-Responsive Tubisomes from a Cyclic Peptide-Bridged Amphiphilic Block Copolymer. *Angewandte Chemie - International Edition* **59**, 8860–8863 (2020).

53. Yang, Z., Liu, Z. & Yuan, L. Recent Advances of Photoresponsive Supramolecular Switches. *Asian Journal of Organic Chemistry* vol. 10 74–90 Preprint at https://doi.org/10.1002/ajoc.202000501 (2021).

54. Merino, E. Synthesis of azobenzenes: The coloured pieces of molecular materials. *Chem Soc Rev* **40**, 3835–3853 (2011).

55. Goulet-Hanssens, A., Eisenreich, F. & Hecht, S. Enlightening Materials with Photoswitches. *Advanced Materials* vol. 32 Preprint at https://doi.org/10.1002/adma.201905966 (2020).

56. Marturano, V., Ambrogi, V., Bandeira, N. A. G., Tylkowski, B., Giamberini, M. & Cerruti, P. Modeling of azobenzene-based compounds. *Physical Sciences Reviews* **2**, 1–11 (2019).

57. Ronayette, J., Arnaud, R. & Lemaire, J. *Isomkrisation ph~tosensibiliske par des colorants et photorkduction de l'azobenzene en solution. I1*. www.nrcresearchpress.com.

58. Bandara, H. M. D. & Burdette, S. C. Photoisomerization in different classes of azobenzene. *Chem Soc Rev* **41**, 1809–1825 (2012).

59. Wang, G., Tong, X. & Zhao, Y. Preparation of Azobenzene-Containing Amphiphilic Diblock Copolymers for Light-Responsive Micellar Aggregates. *Macromolecules* **37**, 8911–8917 (2004).

60. Hu, D., Li, Y., Niu, Y., Li, L., He, J., Liu, X., Xia, X., Lu, Y., Xiong, Y. & Xu, W. Photo-responsive reversible micelles based on azobenzene-modified poly(carbonate)s via azide-alkyne click chemistry. *RSC Adv* **4**, 47929–47936 (2014).

61. Yadav, S., Deka, S. R., Verma, G., Sharma, A. K. & Kumar, P. Photoresponsive amphiphilic azobenzene-PEG self-assembles to form supramolecular nanostructures for drug delivery applications. *RSC Adv* **6**, 8103–8117 (2016).

62. Ye, Q., Huo, M., Zeng, M., Liu, L., Peng, L., Wang, X. & Yuan, J. Photoinduced Reversible Worm-to-Vesicle Transformation of Azo-Containing Block Copolymer Assemblies Prepared by Polymerization-Induced Self-Assembly. *Macromolecules* **51**, 3308–3314 (2018).

63. Kameta, N., Masuda, M. & Shimizu, T. Photoinduced morphological transformations of soft nanotubes. *Chemistry - A European Journal* **21**, 8832–8839 (2015).

64. Lee, S., Oh, S., Lee, J., Malpani, Y., Jung, Y. S., Kang, B., Lee, J. Y., Ozasa, K., Isoshima, T., Lee, S. Y., Hara, M., Hashizume, D. & Kim, J. M. Stimulus-responsive azobenzene supramolecules: Fibers, gels, and hollow spheres. *Langmuir* **29**, 5869–5877 (2013).

65. Cantekin, S., de Greef, T. F. A. & Palmans, A. R. A. Benzene-1,3,5-tricarboxamide: A versatile ordering moiety for supramolecular chemistry. *Chem Soc Rev* **41**, 6125–6137 (2012).

66. Fuentes, E., Gerth, M., Berrocal, J. A., Matera, C., Gorostiza, P., Voets, I. K., Pujals, S. & Albertazzi, L. An Azobenzene-Based Single-Component Supramolecular Polymer Responsive to Multiple Stimuli in Water. *J Am Chem Soc* **142**, 10069–10078 (2020).

67. Gruschwitz, F. V., Klein, T., Catrouillet, S. & Brendel, J. C. Supramolecular polymer bottlebrushes. *Chemical Communications* **56**, 5079–5110 (2020).

68. Gerth, M., Berrocal, J. A., Bochicchio, D., Pavan, G. M. & Voets, I. K. Discordant Supramolecular Fibres Reversibly Depolymerised by Temperature and Light. *Chemistry - A European Journal* **27**, 1829–1838 (2021).

69. Arima, H., Saito, T., Kajitani, T. & Yagai, S. Self-assembly of alkylated and perfluoroalkylated scissor-shaped azobenzene dyads into distinct structures. *Chemical Communications* **56**, 15619–15622 (2020).

70. Yagai, S., Iwashima, T., Kishikawa, K., Nakahara, S., Karatsu, T. & Kitamura, A. Photoresponsive self-assembly and self-organization of hydrogen-bonded supramolecular tapes. *Chemistry - A European Journal* **12**, 3984–3994 (2006).

71. Inoue, D., Suzuki, M., Shirai, H. & Hanabusa, K. Novel low-molecular-weight gelators based on azobenzene containing L-amino acids. *Bull Chem Soc Jpn* **78**, 721–726 (2005).

72. Xu, F., Pfeifer, L., Crespi, S., Leung, F. K. C., Stuart, M. C. A., Wezenberg, S. J. & Feringa, B. L. From Photoinduced Supramolecular Polymerization to Responsive Organogels. *J Am Chem Soc* **143**, 5990–5997 (2021).

73. Xu, F., Crespi, S., Pfeifer, L., Stuart, M. C. A. & Feringa, B. L. Mechanistic Insight into Supramolecular Polymerization in Water Tunable by Molecular Geometry. *CCS Chemistry* **4**, 2212–2220 (2022).

CHAPTER 2

Summary – Chapter 2

CHAPTER 2 – Synthesis of Azo-(U-PEO)$_2$

I. Introduction

The aim of this work was to design photo-responsive supramolecular nano-cylinders decorated with polymer arms, via the (photo)-reversible self-assembly of molecular units in solution.

As presented in the conclusions of the bibliographic chapter, the target molecule must be composed of 4 main parts. Firstly, a bis-urea was selected as H-bond promoting unit to ensure self-assembly; and an azobenzene was chosen to impart photo-responsiveness. This self-assembling core must be functionalized with polymer arms to impart solubility, and poly-(ethylene oxide) (PEO) was chosen as it is soluble in both water and some organic solvents. Lastly, short alkyl chains were selected to link these polymer arms to the core, as they should protect the H-bond promoting groups from water (H-bond competing solvent) and possibly reinforce self-assembly through hydrophobic interactions. The general structure of the target compound is reminded in **Scheme C2-1**.

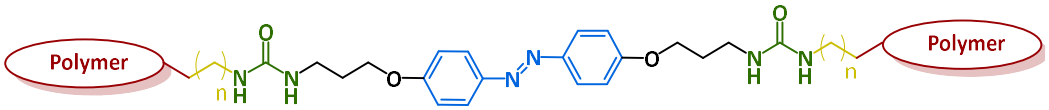

Scheme C2-1. General structure of the target molecule

In this chapter, the different synthetic routes that were explored for accessing the desired structure are presented. In the first part of this chapter, the first synthetic route that was tested is presented, which consisted in synthesizing a symmetrical azobenzene core functionalized with two amine groups as well as a PEO chain end-functionalized with an alkyl amine separately, followed by the linking of the two together, ultimately generating the urea groups. Due to difficulties in this final coupling step, an alternative route was explored, which is presented in the second part of this chapter. In this route, PEO-OH was reacted with an aliphatic diisocyanate, yielding alkyl isocyanate terminated PEO, followed by its coupling with the same azobenzene diamine core. In the third part of this chapter, the experimental protocols of the syntheses are detailed. Finally, two annexes are provided which detail two synthetic routes that were explored but not finished due to lack of time, namely the synthesis of an aromatic amine terminated PEO, and an azobenzene-bisurea RAFT agent.

II. Synthesis of Azo-(U-PEO)$_2$

1. First strategy – with urea yielding final coupling

The first synthetic pathway of the target molecule, Azo-(U-PEO)$_2$, is presented in **Scheme C2-2** and can be divided into 3 parts: the synthesis of the azobenzene core, the functionalization of the PEO arms, and finally the coupling of the two to generate the urea moieties.

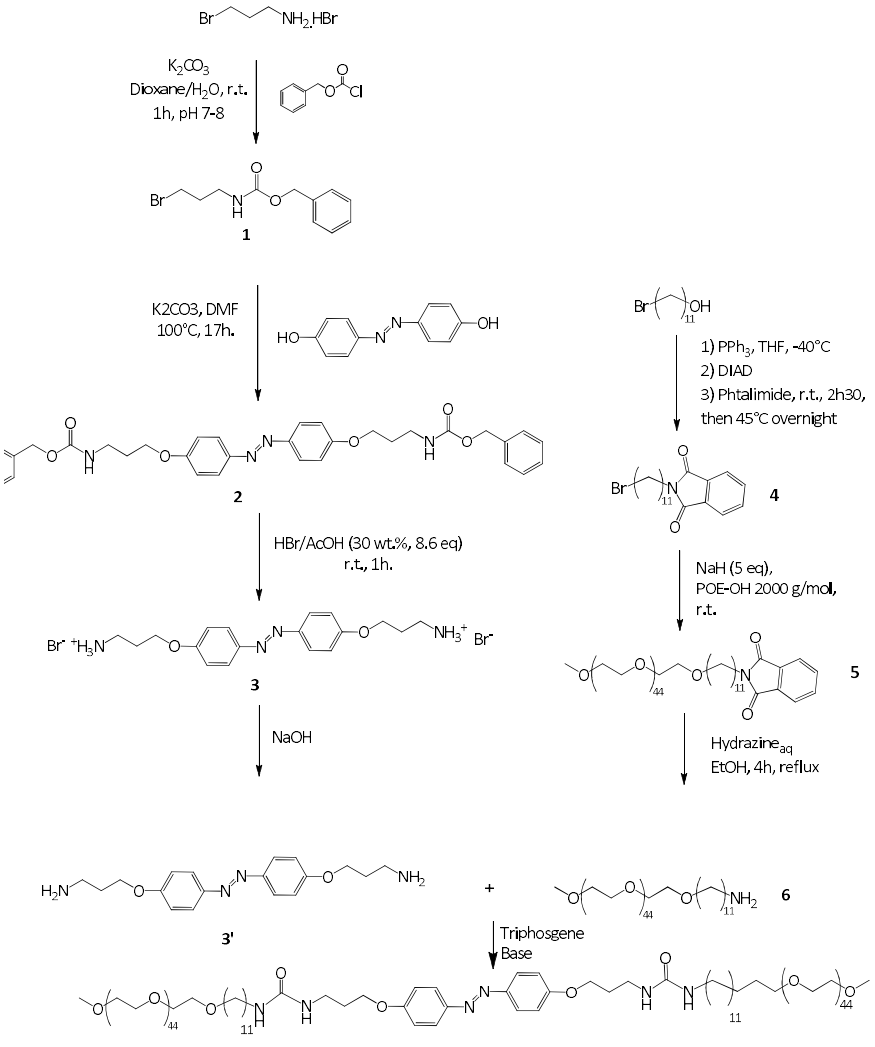

Scheme C2-2. Convergent synthetic pathway of Azo-(U-PEO)$_2$

i. Synthesis of the azobenzene core

Functionalized azobenzene **3** was prepared in three steps as depicted in **Scheme C2-3**.

The synthetic strategy to obtain azobenzene diamine 3 was based on a Williamson etherification between commercially available 4,4'-dihydroxyazobenzene and bromopropylamine. For this to work, protection and deprotection of the amine is required to avoid competition in terms of nucleophilic substitution. This was achieved using benzyl carbamate (and its acidic hydrolysis during the last step). The three steps were adapted from reported procedures and proceeded without specific difficulties.[1]

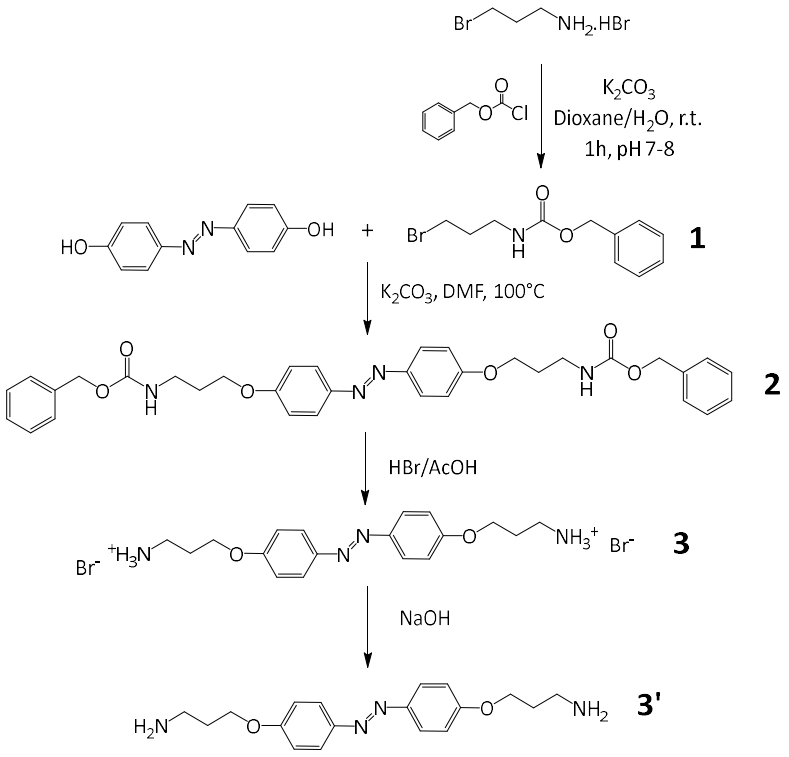

Scheme C2-3. Three step synthesis of azobenzene-diammonium **3**

Synthesis of 1 : 3-bromopropylamine was treated with benzyl chloroformate and K_2CO_3 solutions, in a water/dioxane mixture. Dioxane was required for solubility of the reagents, while water allowed for control over pH, in between 6 and 7. Control of the pH is indeed crucial to avoid any unwanted side reactions, such as nucleophilic substitution or hydrolysis of the bromine, as well as hydrolysis of the benzyl chloroformate, but avoid protonation of the ammonium and have reactive amine instead. After purification, a yellow oil was obtained (quantitative yield). ^{1}H NMR (see **Figure C2-11** in the experimental section) revealed the apparition of the benzylic -CH_2- (5.1 ppm), aromatic protons (7.4 ppm), and the -NH- signals (4.9 ppm). The -CH_2-N was shifted from a triplet at 2.85 ppm to a quadruplet (due to coupling with both the CH_2 and NH) at 3.35 ppm (in $CDCl_3$), confirming that reaction had occurred and the pure product had been obtained. 13.5 g (~100%) of product was recovered as an oil.

Synthesis of 2 : The Williamson etherification between the dihydroxy azobenzene and the protected bromopropylamine **1** proceeded smoothly in DMF at 100°C in the presence of potassium carbonate as catalytic

base. After purification, the product was obtained in good yield (80 % yield). ^{1}H NMR confirmed that the reaction had occurred since the -CH_2-Br signal (3.60 ppm) had dissapeared and the -CH_2-O- signal (4.09 ppm) had appeared (see **Figure C2-12** in the experimental section). 7.31 g of pure product (87.5%) was recovered.

Synthesis of 3 : Hydrolysis of the benzyl carbamate protecting groups proceeded efficiently by treating **2** with 30% HBr in AcOH. The product was recovered as a black powder (quantitative yield). ^{1}H NMR revealed both the dissapearance of the benzylic -CH_2- and aromatic signals, and the apparition of NH_3^+ signal at 7.85 ppm as well as a shift of the -CH_2-N- signal from 3.20 ppm to 3.00 ppm, as can be seen in the ^{1}H NMR spectrum in **Figure C2-1** (see **Figure C2-13** for full spectrum). Since neutral amines are prone to degradation (i.e. oxidization), **3** was stored as the ammonium salt (at 0 °C), and was only neutralized prior to immediate use. 3.28 g (~100%) of pure product was recovered.

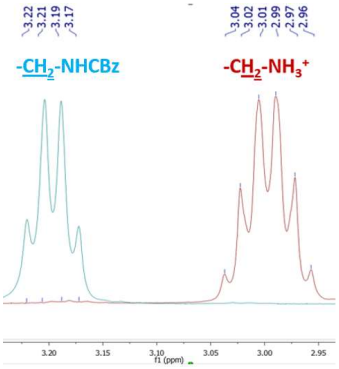

Figure C2-1. ^{1}H NMR signal of the methylene protons close to nitrogen of the reagent (2) vs. product (3) (in DMSO-d_6)

Neutralization of 3:

Since the diammonium salt **3** was insoluble in most common organic solvents, neutralization of the diammonium **3** to afford the neutral diamine **3'** (which is far more soluble) was necessary. This was achieved by mixing **3** in concentrated aqueous $NaOH_{aq}$ followed by extraction of the diamine using DCM. After solvent evaporation, a yellow powder was recovered (68%). The diamine was generally prepared and used rapidly after neutralisation, but when necessary, was stored under argon at 0°C. ^{1}H NMR confirmed that neutralization had occurred, since the ammonium peak at 7.85 ppm was replaced by the amine signal at 1.42 ppm as a broad singlet, and the -CH_2-N signal had shifted from 3.00 ppm to 2.70 ppm, as demonstrated in the ^{1}H NMR spectrum on **Figure C2-2** (complete spectrum on **Figure C2-14**). 455 mg of pure product was recovered (68%).

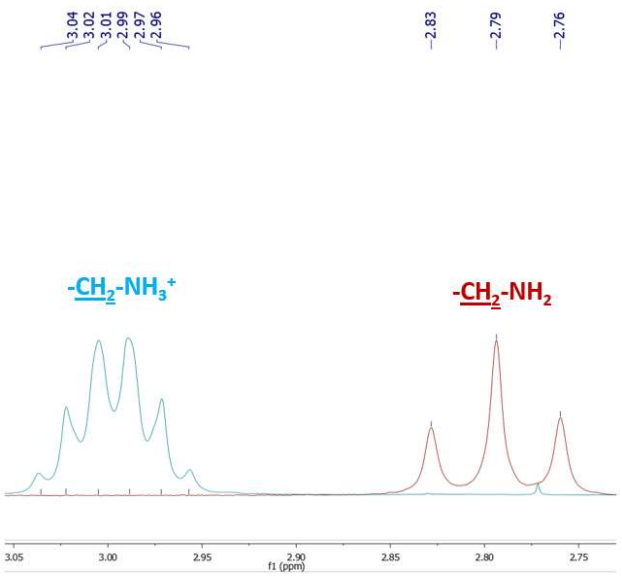

Figure C2-2. ^{1}H NMR signal of the methylene protons close to nitrogen of the reagent (protonated ammonium salt: 3) vs. product (neutral amine: 3') (in DMSO-d_6)

ii. Synthesis of the functionalized PEO arms

Synthesis of amino-alkyl-terminated PEO is achieved in three steps, as depicted in **Scheme C2-4**.

Firstly, bromoundecanol underwent a Mitsunobu reaction to convert the alcohol to phtalimide. This reaction conveniently transformed the alcohol into a protected amine in a single step, since the amino version is commercially available but is rather expensive, and would have required protection anyway. In the second step, PEO-OH (α-methoxy-ω-hydroxy-poly(ethylene oxide), M_n = 2000 g/mol, Đ = 1.05) is deprotonated using sodium hydride, and then undergoes Williamson etherification with **4**. This step turned out to be more challenging than expected since quantitative functionalization was required for the rest of the synthesis to work properly. Finally, PEO **5** is deprotected using hydrazine, yielding PEO-C_{11}-NH_2.

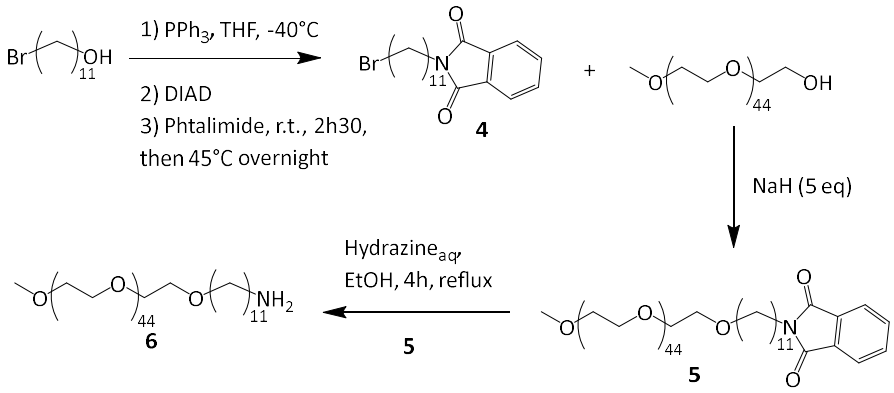

Scheme C2-4. Three step synthesis of PEO-C_{11}-NH_2 **6**

Synthesis of 4 : 1-bromo-11-undecanol was converted to **4** using typical Mitsunobu reaction conditions. Initial purification attempts by column chromatography to remove trace amounts of PPh_3 and $OPPh_3$ were unsuccessful. Instead, purification was achieved through recrystalization in methanol. Purity was confirmed by the

dissapearance of triphenylphosphine and its oxide's signals in ^{1}H NMR (**Figures C2-3** and **C2-15**), and conversion was demonstrated by the appearance of phtalimide signals as well as the dissapearance of the –C<u>H$_2$</u>-OH signal (3.64 ppm) and apparition of the –C<u>H$_2$</u>-Phtalimide signal (3.67 ppm), as can be seen in the ^{1}H NMR spectrum below. 10.45 g of product was recovered as a white powder (43.5%).

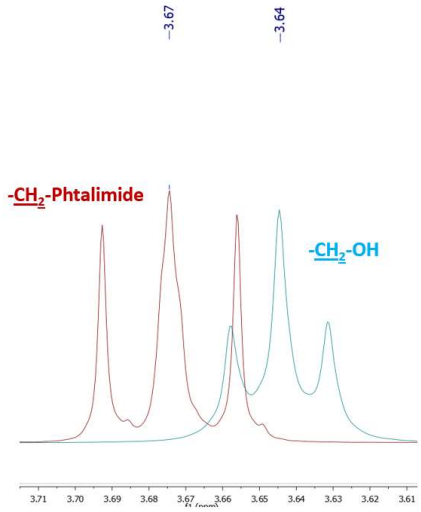

Figure C2-3. ^{1}H NMR signal of the methylene protons close to the terminal group of 1-bromo undecanol, in blue, vs. product **4**, in red (in $CDCl_3$)

<u>Synthesis of 5 :</u> PEO-OH (2000 g/mol) underwent Williamson etherification in the presence of sodium hydride with **4**.

The main challenge of this step was obtaining quantitative yields due to the difficulty of removing unreacted PEO-OH. Initially, conversion was monitored by precipitating a small portion of the reaction mixture in cold diethyl ether, and analysing it using ^{1}H NMR. Conversion was determined by comparing the integral of the PEO-OC<u>H$_3$</u> signal to the integral of the unreacted PEO-O<u>H</u> signal. However, it was found that this method was unreliable due to trace amounts of D_2O in the DMSO-d_6, leading to the dissapearance of the alcohol signal due to protonic exchange. Monitoring the conversion by looking at the –C<u>H$_2$</u>-OH signal would have been an ideal solution since this signal does not suffer from the same problem as the protons are not labile. However, this signal overlaps with the POE main chain signal. To remedy this, a drop of trichloroacetyl isocyanate (TCAI) was added into the ^{1}H NMR solution (using $CDCl_3$ as solvent), which reacts quantitatively with remaining PEO-OH (since TCAI is a highly activated isocyanate) (see **Scheme C2-5**) and deshields the –CH_2-O-Urethane signal to 4.41 ppm, allowing for reliable conversion monitoring.

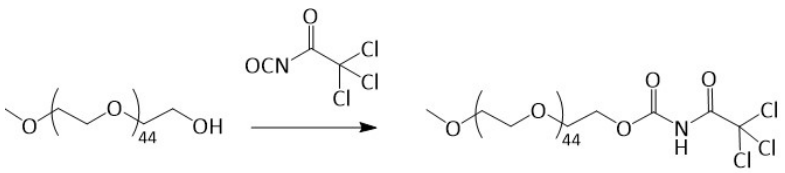

Scheme C2-5. Reaction between PEO-OH and TCAI

As can be seen in the ^{1}H NMR spectrum shown on **Figure C2-4** (PEO-OH reacted with TCAI), when the terminal methoxy is set to 3H, the -$C\underline{H_2}$-Urethane integrates for 2H. These results demonstrate that the conversion is quantitative, and can be reliably measured using proton NMR.

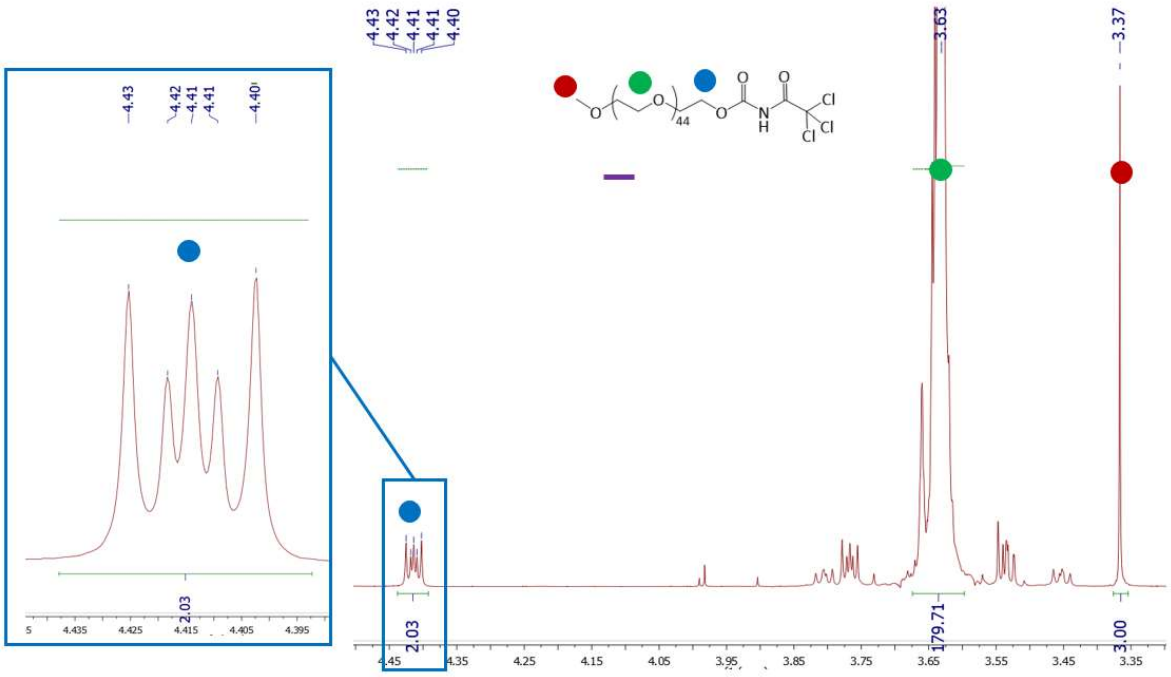

Figure C2-4. ^{1}H NMR spectrum of PEO-OH + TCAI (with the integral of the terminal methoxy set to 3H) (in $CDCl_3$)

In a typical experiment, sodium hydride (60% dispersion in mineral oil) was placed in the reaction flask and degassed with argon. A PEO-OH (1 eq.) solution was prepared either in DMF or THF, added onto the NaH and left to react for variable amounts of time (see "deprotonation time" entry, Table 1). A solution of **4** was prepared and subsequently added to the PEO-OH/NaH mixture, and was left to react for a given "reaction time". The summary of the different experiments is reported in **Table C2-1**.

Entry	Solvent	m POE (g)	Deprotonation time (h)	Eq. Br-C11-Phtal	Reaction time (h)	Temperature (°C)	Conversion
1	DMF	1	1,5	2	21	40	0% (Signal -OH)
2	THF	1	4,5	3	40	35	80% (Signal -OH)
3	THF	1	24	3 (I-C11-Phtal)	17	35	25% (Signal -OH)
4	THF	1	24	5	64	35	100% (Signal -OH)
5	THF	4	24	5	24	35	100% (TCAI)

Table C2-1: summary of synthesis conditions tested for the Williamson etherification between mono-methoxy PEO and compound **4.** Reaction time corresponds to the overall time after addition of the halogenated alkyl-phtalimide. In the conversion column, Signal –OH means that conversion was determined using the ^{1}H NMR integral of PEO-O<u>H</u> (which is not sufficient to prove quantitative reaction if the signal is not seen, but is relevant

to prove that the conversion was not total if the –OH signal is observed), while TCAI refers to use of trichloroacetylisocyanate (which must be used to prove a quantitative conversion), as described above.

The first synthesis was conducted in dry DMF (entry 1), however after 21 hours of reaction time, no conversion could be determined using ^{1}H NMR. Nonetheless, THF was tested instead, using a slightly longer deprotonation time as well as 1 eq. more of compound **4** (entry 2). After 40 hours of reaction, ^{1}H NMR indicated 80% conversion. In order to increase the electrophilicity of compound **4**, replacing the bromine by an iodine was tested, using the Finkelstein reaction. Therefore, compound 4' (I-C_{11}-Phtalimide) was synthesized by solubilizing compound **4** in acetone and adding NaI. The Williamson etherification was then carried out using 4', and after 24h of deprotonation followed by 17 hours of reaction, only 25% of conversion was observed (entry 3). Furthermore, a side reaction appeared to have occurred, which was the elimination of the iodide: 0.35 eq. underwent elimination (compared to 0.25 eq. having undergone substitution). A test synthesis was carried out in the same conditions but without polymer (only NaH), and no elimination occurred; implying that the alcoxide is responsible for the elimination. An alternative strategy to increase conversion was tested: increasing the amount of compound **4** to 5 eq. (entry 4) and the deprotonation time to 24h. After 64 hours of reaction, complete conversion was observed. A second synthesis using the same conditions but upscaling the quantities by 4 was carried out, and complete conversion was also observed and verified using the more reliable TCAI strategy (entry 5), see **Figure C2-5**.

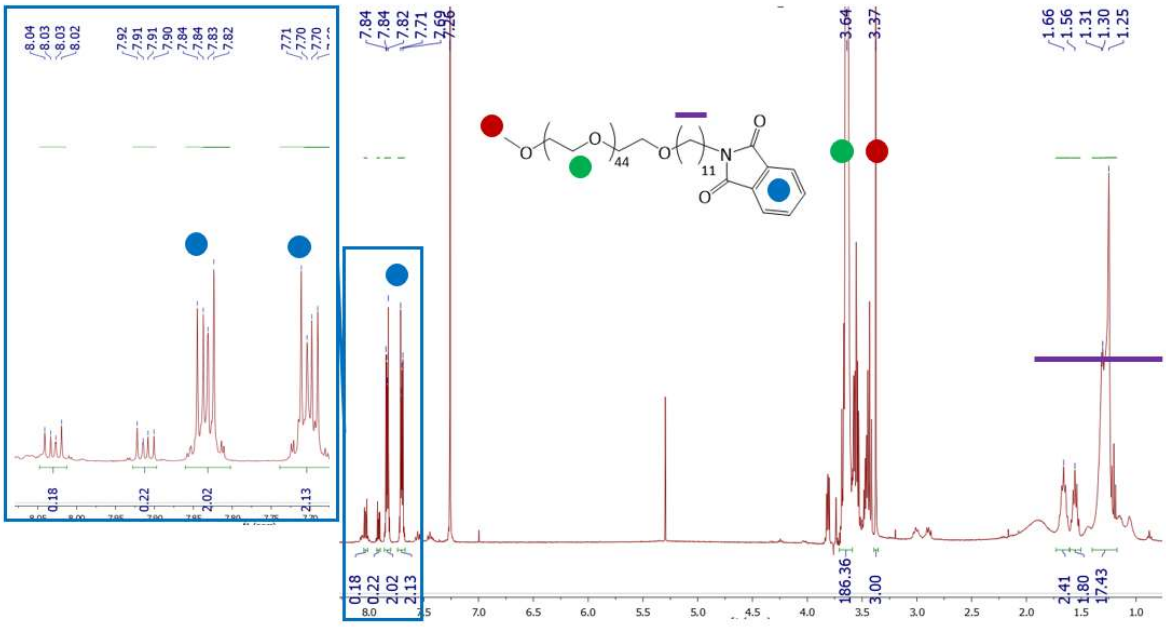

Figure C2-5. ^{1}H NMR spectrum after purification (without TCAI) (in $CDCl_3$)

It is worthy to note that during these syntheses, a small portion of the phtalimide was found to undergo ring opening (approx. 10%, corresponding to the two small multiplets are 7.91 and 8.03 ppm), but this was considered not to be problematic for the next step, so conditions were not further optimised. On the final run, the yield was of 62%.

<u>Synthesis of 6:</u>

PEO **5** was deprotected using aqueous hydrazine at reflux in EtOH for 4 hours. PEO **6** was recovered as a white powder (85%) after purification. ^{1}H NMR (**Figure C2-6**) showed the complete disappearance of the aromatic protons indicating a quantitative deprotection of the amine group. The product was recovered in 85% yield.

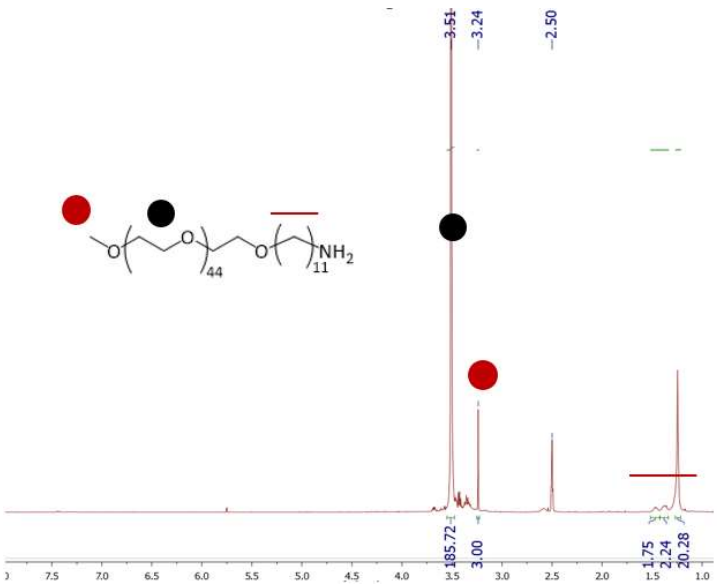

Figure C2-6. ^{1}H NMR (in DMSO-d6) of PEO-C_{11}-NH_2 **6**

iii. Investigation of coupling steps to yield the final urea functions

Triphosgene coupling

Once the synthesis of terminated alkyl-amine PEO **6** and of azobenzene-diamine **3'** had been achieved, the final step was to couple the two intermediates, generating the two urea motifs that were desired. It is important to note that this reaction must be quantitative and in near-stoichiometry, since any residual/excess PEO **6** might be difficult to eliminate during purification.

The use of triphosgene was therefore investigated, since this phosgene derivative has often been used to generate ureas from amines (both symmetrical and asymmetrical)[2,3]. Indeed, triphosgene is a crystalline solid, as opposed to the highly toxic phosgene gas, making it far more convenient and safe to work with, although claims that it is a "safe phosgene" are misleading since it is still highly toxic.

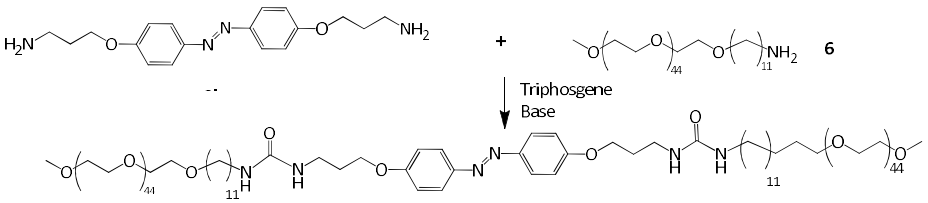

Scheme C2-6. Triphosgene coupling of PEO **6** and azobenzene **3'**

As can be seen in **Scheme C2-6**, triphosgene allows for the generation of isocyanate from amines in situ, and requires 2 eq. of catalytic base per eq. of amine. A slow addition of the 1st amine with 1 eq. catalytic base (commonly tertiary amines) to the BTC solution is required to avoid the formation of symmetrical ureas. Indeed, the first equivalent of base that is added leads to the generation of a carbamoyl chloride intermediate (in the green box in **Scheme C2-7**), that cannot further react until the second equivalent of base is added, which catalyzes the elimination of HCl proceeding through a E_1CB mechanism[4]. Therefore, isocyanate is only present once all of the first initial amine has been converted to carbamoyl chloride, preventing the formation of symmetrical ureas. The second nucleophile (in this case, a second amine) can then be added, leading in this case to the generation of urea moieties. Nevertheless, a slight excess of base is commonly used, so small amounts of isocyanate may be formed before the second addition of base (and nucleophile). Highly anhydrous conditions must be used to avoid hydrolysis of isocyanate.

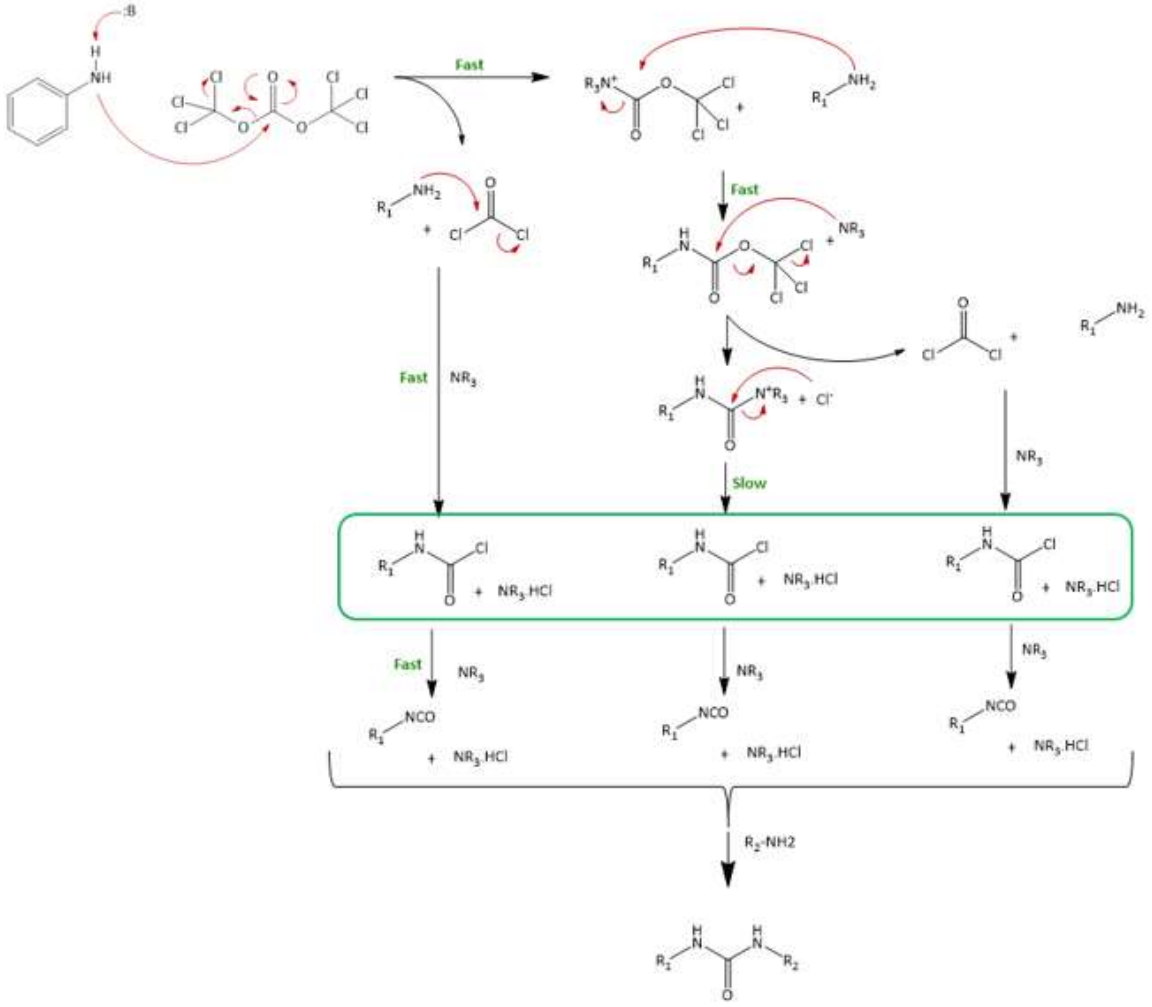

Scheme C2-7. Proposed mechanism of the formation of isocyanate from amine and BTC (NR_3: ternary amine base, R_1 = Ar, R_2 = Ar or aliphatic). Overall, 6 eq. of amine base and 3 eq. of amine are required per eq. of BTC.[3]

A typical experiment consisted in first dissolving 1 eq. of azobenzene **4** in anhydrous solvent, followed by the addition of 2.2 eq. of diethylisopropylamine (DIEA) as catalyst. This solution was added dropwise to a solution of

0.76 eq. bis-(trichloromethyl)carbonate (BTC, i.e. triphosgene) using a syringe pump, under inert atmosphere at r.t. The solution was left to react for a given amount of time, and a drop of the mixture was analyzed by FT-IR, to see if a band at 2270 cm^{-1} appeared, which should correspond to the newly formed isocyanate. A solution of 2.2 eq. of PEO-NH_2 **6** + 2.2 eq. DIEA in given solvent was then added, which should yield ureas from the addition of the amine to the in situ generated isocyanate. To monitor conversion, samples of the crude reaction mixture were precipitated in cold diethyl-ether, and analyzed by ^{1}H NMR in DMSO-d_6. Since triphosgene is soluble in THF and DCM, these solvents are commonly used for this reaction, and were both tested. After a certain amount of reaction time, the polymer was precipitated in diethyl ether. Using DCM as solvent, only 10% conversion was obtained after 162 hours of reaction time. It is worthy to point out that while a slight excess of polymer is used to ensure double functionalization of the azobenzene is achieved, a large excess cannot be used due to difficult elimination of the excess during purification.

To understand the low conversion observed, control experiments were carried out using 1,8-diaminooctane (DAO) as first amine and commercial PEO-NH_2 (M_n = 2000 g/mol), following the procedure described above, with DCM as solvent. An addition time of the DAO/DIEA solution to the BTC solution of 30 minutes was chosen (see **Scheme C2-8**). After 3 hours of reaction time, a solution of 2.2 eq. PEO-NH_2 was added and conversion was monitored using ^{1}H NMR. A very low conversion was detected (approx. 10%), even after several days of reaction time. This reference experiment therefore suggested that the low conversion was not due to the specific chemical structure of **3'** and **6** but was intrinsic to the reaction.

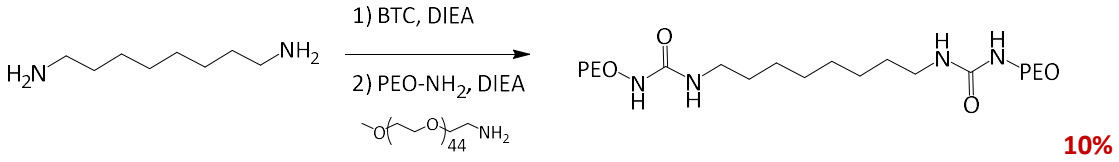

Scheme C2-8. control experiment involving DAO and PEO-NH_2

This reaction is actually generally carried out using aromatic amines for the first step[2,5]. A model reaction using 4-butylaniline as 1st amine and 2-ethylhexylamine as 2nd amine was therefore tested using the same conditions as previously (see **Scheme C2-10**). After leaving the reaction overnight, ^{1}H NMR revealed 90% conversion. Literature indicates that the formation of isocyanate from the carbamoyl chlorides proceeds through an E_1CB mechanism[4] (**Scheme C2-9**), which means that a nitrogen-anion must be generated, which then proceeds to eliminate the chlorine leaving group. In the case of aromatic carbamoyl chlorides, this anion is well stabilized through resonance, owing to the presence of an aromatic cycle. In the case of aliphatic carbamoyl chlorides, no stabilization through delocalization occurs, rendering the reaction unfavorable. This model reaction therefore suggested that using an aromatic amine to react with triphosgene was necessary.

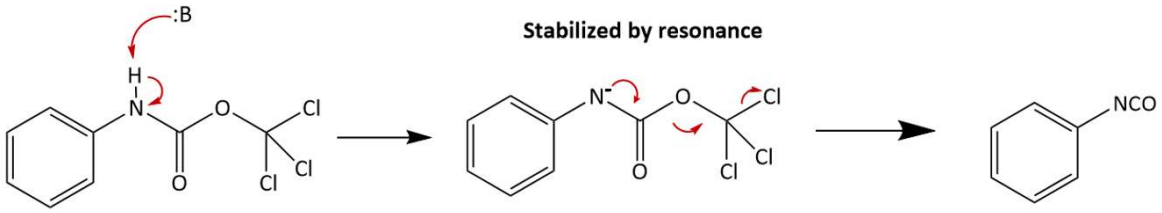

Scheme C2-9. Generation of isocyanate via E_1CB mechanism

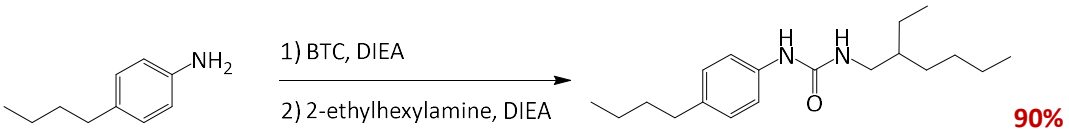

Scheme C2-10. Control experiment using aromatic 4-butylaniline and 2-ethylhexylamine

However, when the reaction presented in **Scheme C2-11** was tested, using an aromatic amine in the first step and PEO-NH_2 in the second, only 40% conversion was obtained. The isocyanate absorption band was observed by FTIR at the end of the 1st addition, but was no longer present the next day. These results suggest that the polymeric-nature of the 2nd amine hinders the reaction. It may be possible to increase PEO functionalization by using an excess of aromatic amine (in a reaction such as the one depicted in **Scheme C2-11**), but in our case, it is not possible (using an excess of azobenzene-diamine would lead to mono-functionalization of the azobenzene, and using an excess of PEO would lead to difficult elimination of the excess during purification).

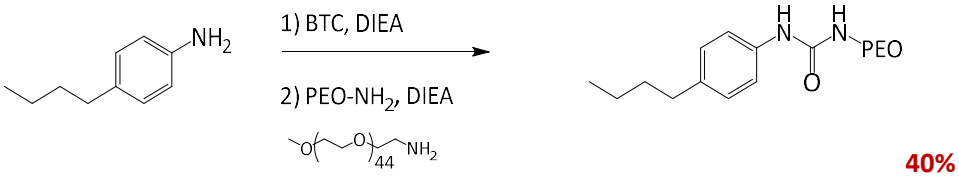

Scheme C2-11. Control experiment using aromatic 4-butylaniline and PEO-NH_2

In an attempt to remedy the problems linked to using an aliphatic amine as 1st amine (as explained above), a stronger base was tested: 1,8-diazabicyclo[5.4.0]undec-7-ene (DBU). A test was carried out using dodecylamine as 1st amine and PEO-NH_2, in anhydrous THF as solvent (see **Scheme C2-12**). 35% conversion was obtained after leaving the reaction overnight. This increase of conversion in these conditions reveals the relevance of the strategy. However, the level of conversion reached is still far from the quantitative yield required. Since the conversion appeared to be similar to the previous reaction, it appeared that the polymeric nature of the 2nd amine used (PEO-NH_2) was the limiting factor.

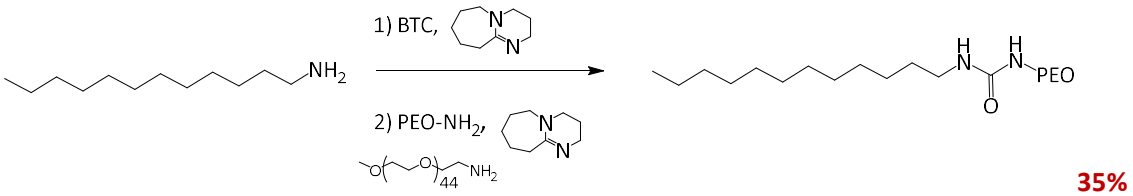

Scheme C2-12. Control experiment using dodecylamine, PEO-NH_2 and DBU as base

To conclude, using aromatic amines increases the conversion of this reaction, as does using a stronger base. However, neither allowed for quantitative functionalization of PEO. It therefore became apparent that triphosgene coupling was not a suitable synthesis for the coupling of azobenzene **3'** and PEO-NH_2 **6**. While this reaction has been used to end-functionalize PEO in previous studies[2,5], those systems used aromatic molecular amines, that could also be used in excess, which is not the case here. In the next section, an alternative urea generating coupling was therefore investigated.

Isopropenyl carbamate coupling

An attractive method for generating ureas was found in the literature and consisted of using a carbamate precursor. Carbamates may undergo dissociation into isocyanate + alcohol in basic media, and an added amine will react with the isocyanate, generating a urea. In addition, this methodology has been reported in some cases to work with aliphatic amines/carbamates.[6,7] However, all steps are reported to be in equilibrium, meaning that a mixture of symmetrical and asymmetrical ureas are commonly obtained, as can be seen in **Scheme C2-13**. A carbamate may be generated that can further react to yield symmetrical urea (in red box in **Scheme C2-13**).

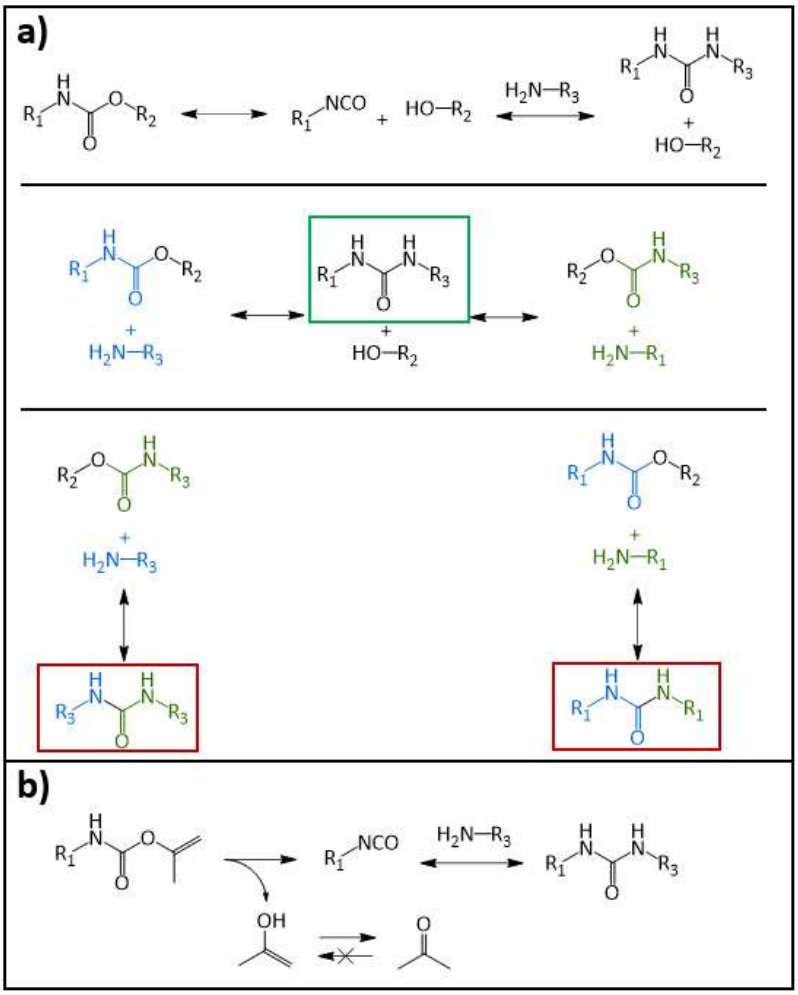

Scheme C2-13. a) Synthesis of ureas from amines and carbamates, and how a mixture of asymmetrical (green box) and unwanted symmetrical (red boxes) ureas can be obtained. **b)** How using isopropenyl carbamate can circumvent the formation of symmetrical urea.

One way of overcoming this problem (i.e. generation of symmetrical urea) is by using a carbamate that generates an alcohol that has low nucleophilicity (such as tBuOH[7], which is sterically hindered, or HO-CH_2-CF_3[8], which is electronically poor), or by transforming the generated alcohol so that it cannot react. This is precisely what Farina's team achieved, by using a peculiar isopropenyl carbamate, which liberates acetone enol upon isocyanate generation, which rapidly tautomerizes to acetone.[9] This renders the reaction non-reversible, prohibiting the formation of symmetrical ureas (as long as no isocyanate hydrolysis occurs) (see **Figure C2-13b**).

A new key intermediate was therefore synthesized, following two synthetic strategies (**Scheme C2-14**). The first consisted in repeating the same initial synthesis but with isopropenyl chloroformate instead of benzyl chloroformate, which proceeded smoothly (≈100 % yield). However, the carbamate was lost during Williamson etherification, even if the reaction is carried out at r.t. instead of 100 °C (top part of **Scheme C2-14**). Therefore, a second synthesis was carried out by reacting the azobenzene diamine **4** with isopropenyl chloroformate, yielding azobenzene-di-(isopropenyl carbamate) in 76% yield (bottom part of **Scheme C2-14**).

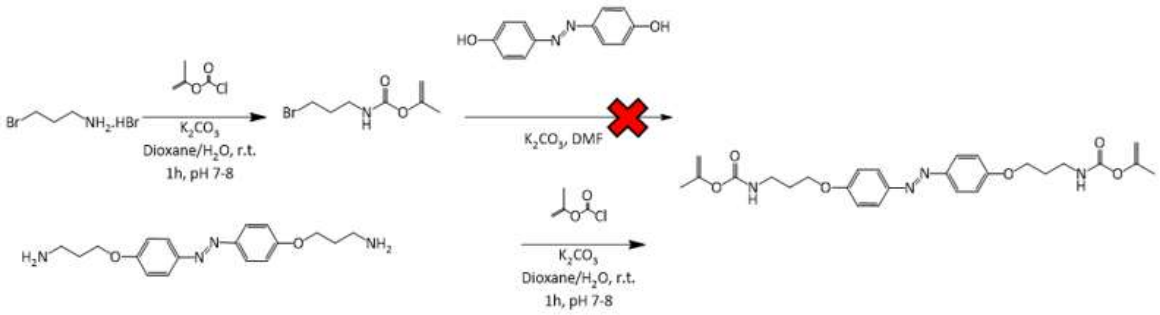

Scheme C2-14. Synthetic strategies for accessing azobenzene-bis-(isopropenyl carbamate)

Synthesis of isopropenylcarbamatepropyl bromide

The same procedure used for the synthesis of CBz protected bromopropylamine **1** were used for this synthesis (i.e. in water/dioxane mixture with K_2CO_3 as catalytic base) but with commercially available isopropenyl chloroformate. After purification, a yellow oil was obtained (quantitative yield). ^{1}H NMR (DMSO-d_6) revealed the apparition of a triplet at 7.53 ppm corresponding to the NH proton of the carbamate, peaks at 4.60 ppm and 4.59 ppm had also appeared, corresponding to the alkene protons. The –$\underline{CH_2}$-N peak also went from 2.90 ppm (–$\underline{CH_2}$-NH_3^+) to 3.53 ppm, confirming the reaction had taken place (**Figure C2-20**). The product was recovered as a yellow oil (1.10 g, ~100%).

Williamson etherification between isopropenylcarbamatepropyl bromide and 4,4'-dihydroxyazobenzene

The same conditions used for the synthesis of azobenzene **2** were used here (overnight in DMF at 100°C with K_2CO_3). ^{1}H NMR (**Figure C2-21**) revealed the elimination of the isoproprenyl carbamate during the reaction, as only the peaks corresponding to the azobenzene-diamine were present. The reaction was repeated at r.t., but despite the decrease in temperature, the carbamate still degraded. Therefore, it was decided to use azobenzene **4** as already synthesized previously, and react it with isopropenyl chloroformate.

Synthesis of azobenzene bis-isopropenyl carbamate from azobenzene diammonium

The same conditions that were employed for the synthesis of CBz protected bromopropylamine **1** were again used here, however in these conditions, a yield of only 4% was obtained. It was found that increasing the amount of water used remedied this (2/1 water/dioxane instead of 1/1), and the product was obtained in 76% yield. ^{1}H NMR (**Figure C2-22**) indicated that the –$\underline{CH_2}$-N peak had shifted from 2.79 ppm to 3.18 ppm.

Now that the new isopropenyl carbamate intermediate had successfully been synthesized, attempts to couple it with the previously synthesized PEO-C_{11}-NH_2 were realized (**Scheme C2-15**).

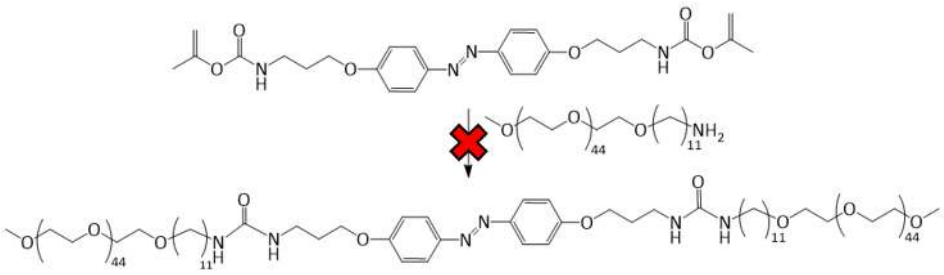

Scheme C2-15. Final coupling reaction using the isopropenyl carbamate intermediate

The reaction was conducted in anhydrous THF and using DBU as catalyst base, at 55 °C under argon atmosphere. After a week of reaction time, the polymer was precipitated in diethyl ether, and ^{1}H NMR revealed that there was approximately 5-10% of urea relative to the PEO methoxy chain end (**Figure C2-23**). SEC measurements indicated that there was only 20% of bi-substituted product, the rest being either mono-adduct or the initial PEO (**Figure C2-24**).

It is possible that this reaction suffers from the same problems as the triphosgene coupling, where only aromatic carbamates provide suitable reactivity. The last strategy that was partly explored (see Annex 1) was synthesize an aromatic amine terminated PEO for used in trisphosgene coupling, in the aim of increasing reactivity.

iv. Conclusions

The successful synthesis of the azobenzene diamine (or dicarbamate) and of PEO-C_{11}-NH_2 was achieved, but the coupling of the two together to generate urea was found to be rather challenging. Triphosgene coupling gave low yields when a polymer was used in the synthesis. Higher yields could perhaps have been obtained by combining the use of an aromatic amine with the stronger DBU base, however this was not tested. Coupling using the isopropenyl carbamate methodology also gave poor conversions. Since quantitative yields were required, and a considerable excess of a reagent cannot be used, this overall "final urea generating coupling from two amines" strategy was not further pursued, as generating isocyanate appeared to be difficult. Instead, a different approach was explored, presented in the next section, where the isocyanate was already formed.

2. Second strategy – involving the use of diisocyanates

Due to the difficulties met in forming ureas with the previous strategy, a rather different strategy was explored. It consisted in first reacting PEO-OH with an excess of aliphatic diisocyanate, yielding end-functionalized isocyanate PEO, which could then be reacted with azobenzene diamine to yield the final polymer, as described in **Scheme C2-16**. Due to its low cost relative to other diisocyanates, hexamethylene diisocyanate (HMDI) was selected to optimize the reaction, before using other diisocyanates of varying alkyl length.

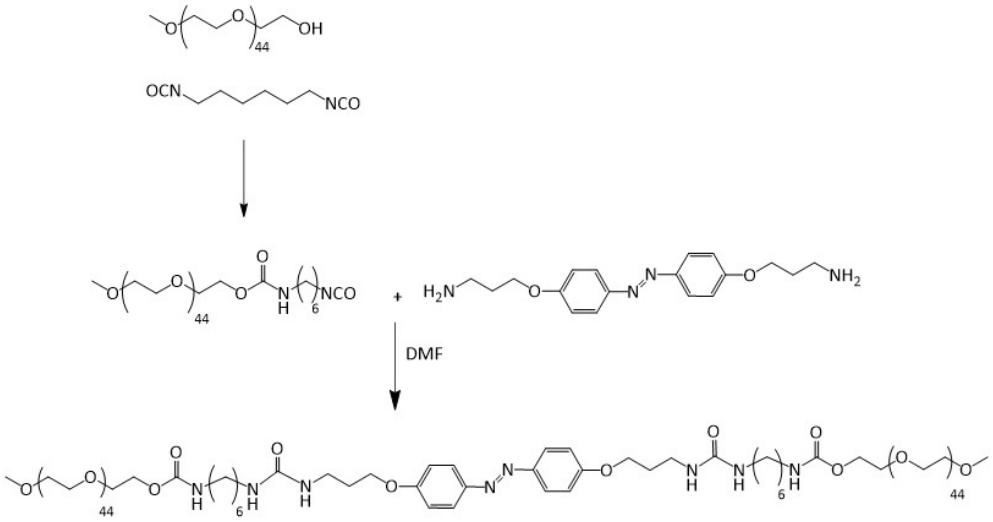

Scheme C2-16. Synthesis of Azo-(U-PEO)$_2$ using diisocyanate

<u>Synthesis of isocyanate terminated PEO using HMDI:</u>

For this reaction, it is important to use an excess of HMDI in order to avoid the addition of two PEO chains onto the same HMDI, yielding a polymer which would be difficult to separate from the product. To further limit this side-reaction, it was chosen to slowly add the PEO to the HMDI. It is also important to work in highly anhydrous conditions to limit isocyanate hydrolysis.

Therefore, a solution of PEO-OH in anhydrous DCM was slowly added to a solution of 5 eq. HMDI in anhydrous DCM using a syringe pump (4-hour long addition) and the mixture was left to react overnight at r.t. to remove excess isocyanate and recover the product. The crude was first concentrated by bubbling argon, and then precipitated in dry Et_2O using a cannula system in order to never expose the moisture-sensitive product to air. The precipitate was then washed with dry Et_2O using the same cannula system, and residual solvent was evaporated under reduced pressure.

In order to measure conversion and purity, a ^{1}H NMR tube in DMSO-d_6 was prepared and a drop of benzylamine was quickly added in order to neutralize all isocyanate groups. Anhydrous benzylamine/DMSO-d_6 were not used due to the fact that benzylamine is far more reactive than water with regards to the isocyanate moieties, limiting risks of isocyanate hydrolysis. The alkyl and urethane ^{1}H-NMR signals allow to quantify PEO functionalization, and the newly formed benzylurea generates a characteristic signal – the benzylic C<u>H$_2$</u> – that allow to determine whether or not the isocyanate groups are still present. In all runs, quantitative functionalization of the PEO was found to occur (a representative example is shown in **Figure C2-26**). The product was recovered as a white powder (2.3 g, 76%).

However, the isocyanate moieties were found to be highly unstable in time, despite careful measures being taken to prevent their hydrolysis (purification steps in anhydrous conditions, storing under static vacuum or under argon at -18°C). It was therefore decided that the isocyanate intermediate had to be used shortly after being prepared.

Furthermore, the presence of an impurity was observed as there was an extra peak in ^{1}H NMR at 5.70 ppm. A potential explanation could be that this impurity (which we termed “bis-PEO”) was formed through the partial hydrolysis of isocyanate, yielding amine which could then react with remaining isocyanate (see **Scheme C2-17**). To confirm this hypothesis, non-neutralized PEO-C_6-NCO was put in DMSO-d_6 to react with residual water

overnight. The ^{1}H NMR of this solution revealed that the signal at 5.70 ppm had greatly increased, to 0.70 H (i.e. 70% bis-PEO) (compared to the neutralized version), confirming this hypothesis. Another experiment was conducted, where non-neutralized PEO-C_6-NCO was stored under argon at -18°C for 5 days, and then neutralized with $BnNH_2$ and subjected to ^{1}H NMR analysis, which revealed that 33% of the isocyanate had already been hydrolyzed. To further confirm the formation of bis-PEO, SEC-HPLC experiments were carried out. After purification, the polymer was neutralized with benzylamine, and the resulting product was analyzed by SEC-HPLC with the UV detector at either 254 nm or 340 nm. If a mixture of bis-PEO + PEO-Benzylurea is obtained, 1 UV peak and 2 RI peaks are expected if the UV detector is at 254 nm (since bis-PEO is not expected to absorb at this wavelength), however no UV peaks should be observed at 340 nm. This is precisely what was measured, as can be seen in **Figure C2-7**. Since the LS signal of the SEC analysis was unexploitable, SEC analysis of two commercial non-functionalized PEO (M_n = 2000 g/mol and M_n = 4600 g/mol) was performed, and afforded retention times of 20 and 18 minutes, respectively. The retention times of the two peaks on the chromatogram of **Figure C2-7** are therefore coherent with the presence of the product (M_n = 2000 g/mol, retention time 20 minutes) + bis-PEO (M_n = 4000 g/mol, retention time 18.2 minutes). After purification, 10-15 mol.% of bis-PEO was present, which is problematic, since it is likely difficult to eliminate. It therefore became apparent that finding ways to limit the formation of this impurity would be important.

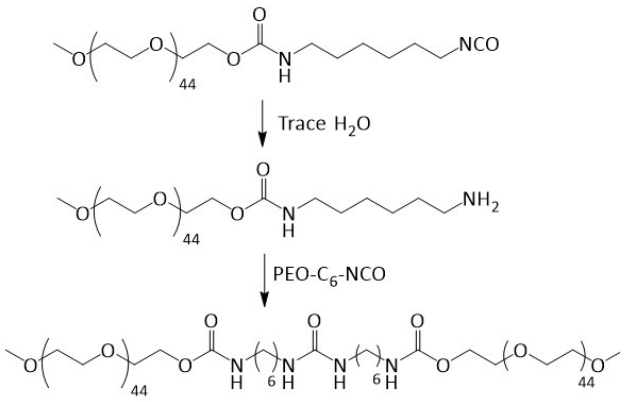

Scheme C2-17. Formation of bis-PEO via isocyanate hydrolysis

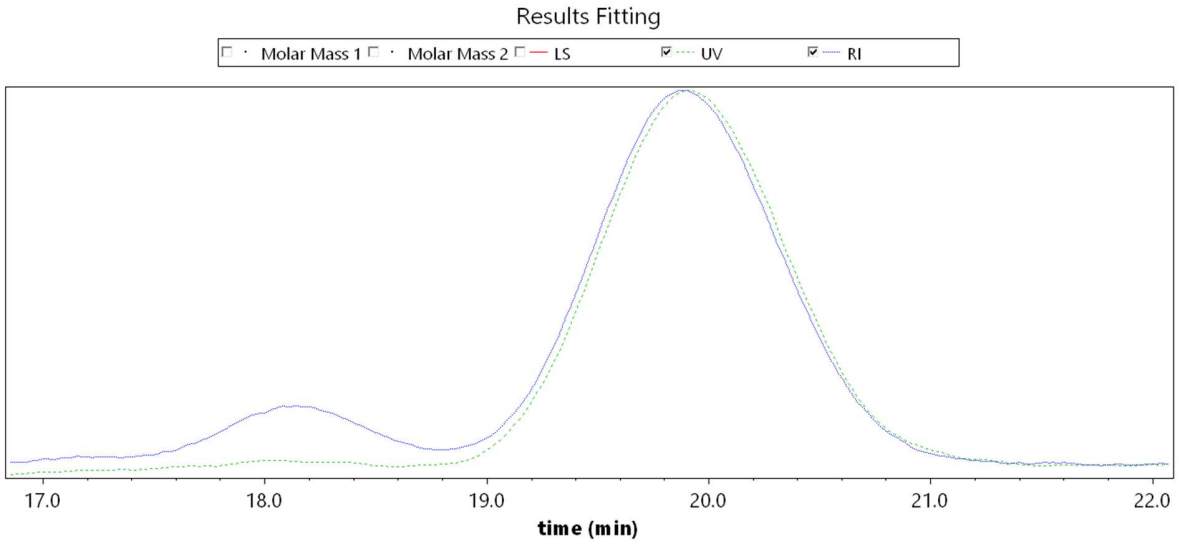

Figure C2-7. SEC analysis of PEO-Benzylurea containing bis-PEO, UV detector set at 254 nm (THF as eluent)

A simple solution to remedy this issue was using activated molecular sieves (MS) in powder form, to capture any traces of water to limit isocyanate hydrolysis. Therefore, both individual solutions (of PEO-OH and diisocyanate) were stirred over the MS in dry solvents before the addition of PEO to the diisocyanate. This strategy allowed to reduce the amount of generated bis-PEO down to low amounts (typically less than 5%). However, its formation was nonetheless inevitable. It was decided to proceed with the next step, and purify the final product. Overall, typical yields on this reaction were around 70%, suggesting a portion of product is lost during precipitation.

Synthesis of isocyanate terminated PEO using C4 and C8 diisocyanates:

A reaction was conducted using the conditions established for HMDI, but by replacing HMDI by the 4 carbon equivalent, 1,4-tetramethylene diisocyanate (TMDI). After quenching with $BnNH_2$, ^1H NMR revealed two urea peaks integrating for 0.40 H each (instead of 1), and integration of the $-C\underline{H_2}$-Urethane signal indicated that only 40-50% of the PEO had been functionalized (see **Figure C2-8**). These results suggest that the functionalization was not quantitative using this diisocyanate. However, all (or most) of the isocyanate appeared to survive purification. The reaction was repeated using this time the 8 carbon diisocyanate, 1,8-octamethylene diisocyanate (OMDI). After purification and $BnNH_2$ quench, ^1H NMR indicated that all the PEO had been functionalized, but only 40% of isocyanate survived purification to react with benzylamine. It is unclear why the reaction gave such different results depending on the choice of diisocyanate. It appeared that the shorter alkyl diisocyanates were more difficult to functionalize PEO with, but the isocyanate moieties are less prone to hydrolysis, while the opposite could be said for longer alkyl diisocyanates. A comparison of the ^1H NMR spectra are presented in **Figure C2-8**. Due to lack of time, further syntheses involving TMDI or OMDI were not pursued, but further investigation is required to better understand the differences that were observed.

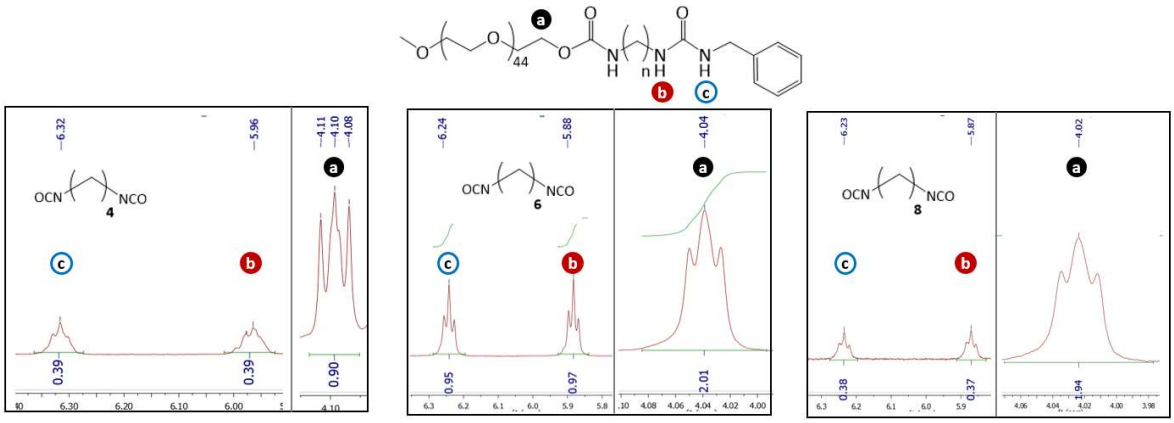

Figure C2-8. ^1H NMR (DMSO-d6, 400 MHz) urea and $-C\underline{H_2}$-Urethane peaks of the polymers after benzylamine quench, using C_4 TMDI (left), C_6 HMDI (middle) or C_8 OMDI (right) as diisocyanate for the synthesis (using the terminal methoxy signal of the PEO chain as reference).

Coupling of PEO-C_6-NCO with neutral azobenzene 3:

The final product was synthesized by solubilizing the isocyanate terminated PEO (slight excess) and azobenzene diamine separately in anhydrous DMF, and stirred in the presence of powdered molecular sieves. DMF was selected as solvent due to it being the only solvent (other than DMSO) in which the azobenzene diamine showed decent solubility. The azobenzene solution was then added to the PEO solution and left to react for 5 minutes,

followed by addition of a large excess of $BnNH_2$ to quench any remaining isocyanate. The crude was filtered to remove molecular sieves, and then precipitated in Et_2O/pentane 50/50. ^1H NMR of the crude precipitate revealed that approximately 10% of bis-PEO was present, and no benzylurea PEO was detected. However, the azobenzene had quantitatively reacted, as the newly formed ureas integrated correctly with the aromatic azobenzene protons, as seen in the crude ^1H NMR spectrum below.

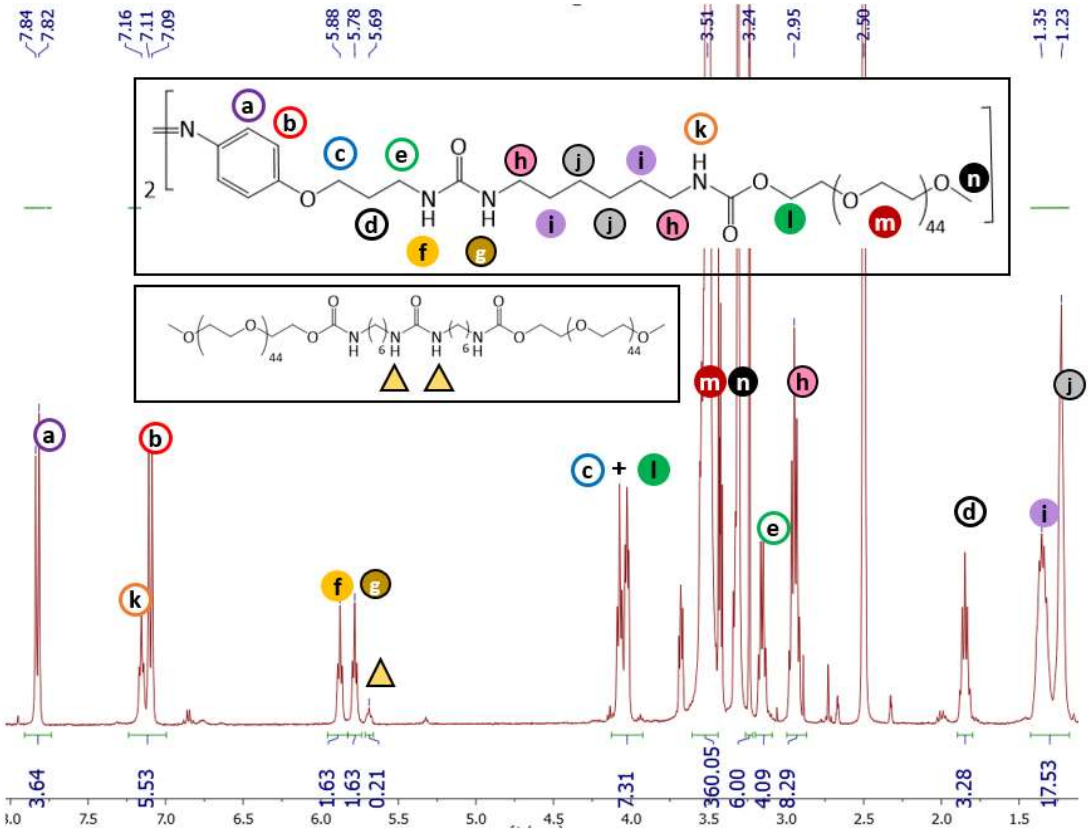

Figure C2-9. ^1H NMR spectrum of the crude product in DMSO-d_6

While the reaction appeared to work, the remaining challenge was eliminating the unwanted bis-PEO. Therefore, selective precipitations were explored, in which only (or almost only) the product precipitated, using different ratios of Et_2O/EtOH from a concentrated EtOH solution. The idea here was that the azobenzene imparts higher insolubility to the product in this solvents mixture, compared to the bis-PEO. The ratio that worked the best was Et_2O/EtOH 7/1. However, the precipitate was un-filterable (fine suspension). It was therefore recovered by centrifugation, further washed with the same solvent mixture followed by pure Et_2O. While this method effectively yielded (almost) pure product (see **Figure C2-10**), as there were only trace amounts of bis-PEO left, as confirmed by SEC-HPLC and ^1H NMR, significant loss of product occurred (1.31 g, 69 % of product recovered).

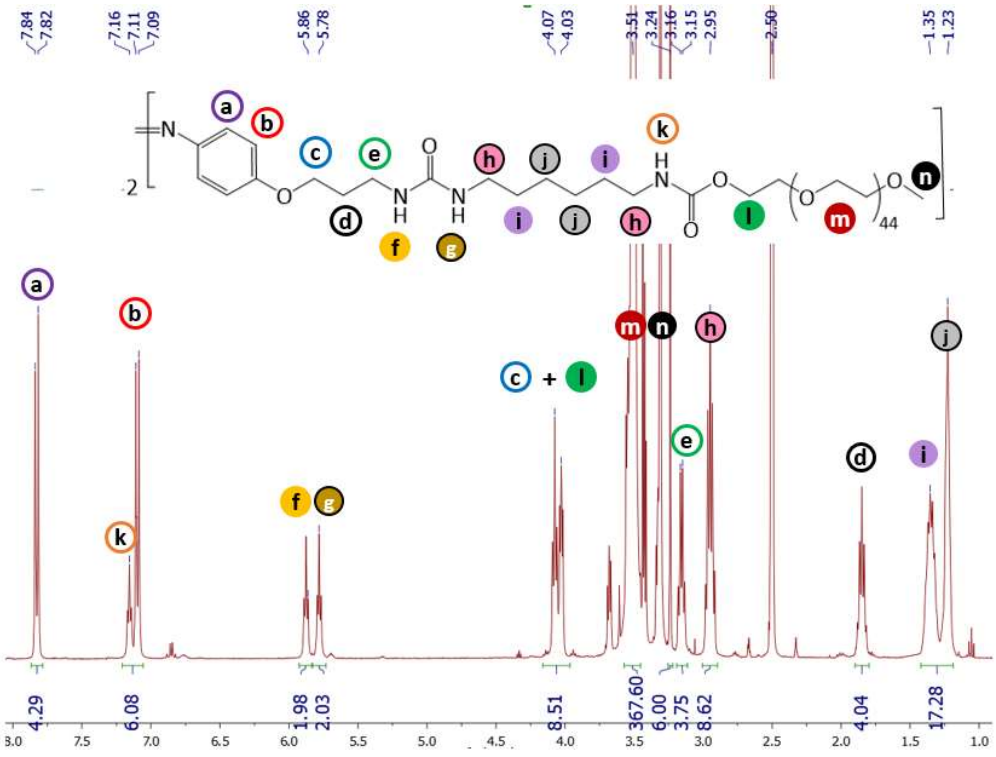

Figure C2-10. ^{1}H NMR (in DMSO-d_6) of the pure product

III. Conclusions and perspectives

In light of these results, it would appear that the convergent syntheses involving a final urea generating coupling step, such as triphosgene coupling, were not adapted to the synthesis of aliphatic ureas. Instead of trying to generate isocyanate during the reaction, a different approach turned out to work rather well: using commercially available isocyanates. Therefore, the 5-step convergent synthesis involving the use of hexamethylene diisocyanate led to the succesful synthesis of Azo-(U-PEO)$_2$ despite a somewhat challenging purification to remove polymeric side products. Initial attempts to synthesize the same polymer but with shorter (C_4) or longer (C_8) alkyl chains were unsucessful, but would merit further investigation, as they could have interesting impacts on self-assembling properties, such as extent of association (by more or less protecting the self-assembling core from H-bond competing water for instance).

Attempts to synthesize an aromatic amine-terminated PEO were also carried out, in the aim of improving reactivity for triphosgene coupling step, and are presented in **Annex 1**. However, since these experiments were conducted in parallel to the HMDI based route, they were not pursued once succesful synthesis using HDMI had been achieved. It would nonetheless be interesting to finish this synthesis, in order to compare the effect of an aromatic spacer (versus an alkyl one) on self-assembly.

Another perspective to this work would be the synthesis of the Azo-(U-TTC)$_2$ RAFT agent, which would give direct access to azobenzene-bisureas decorated with a range of different polymer arms. This would allow for the effect of polymer arm nature and length to be conveniently probed. Some attempts in synthesizing such a RAFT agent are presented in **Annex 2**.

IV. Experimental details

Nuclear magnetic resonance (NMR). ^{1}H NMR spectra were recorded on either a Bruker DPX-200 or Bruker AC-400 spectrometer, using deuterated chloroform ($CDCl_3$) or dimethyl sulfoxide (DMSO-d_6) as solvents. Chemical shifts (δ) are expressed in parts per million (ppm) relative to the reference (tetramethylsilane (TMS), δ = 0 ppm) and were calibrated using the residual solvent peak. Multiplicities are reported as follows: singlet (s), doublet (d), triplet (t), quadruplet (q), quintet (qt), sextet (sext), multiplet (m), and broad signal (br s).

i. Synthesis of the azobenzene core

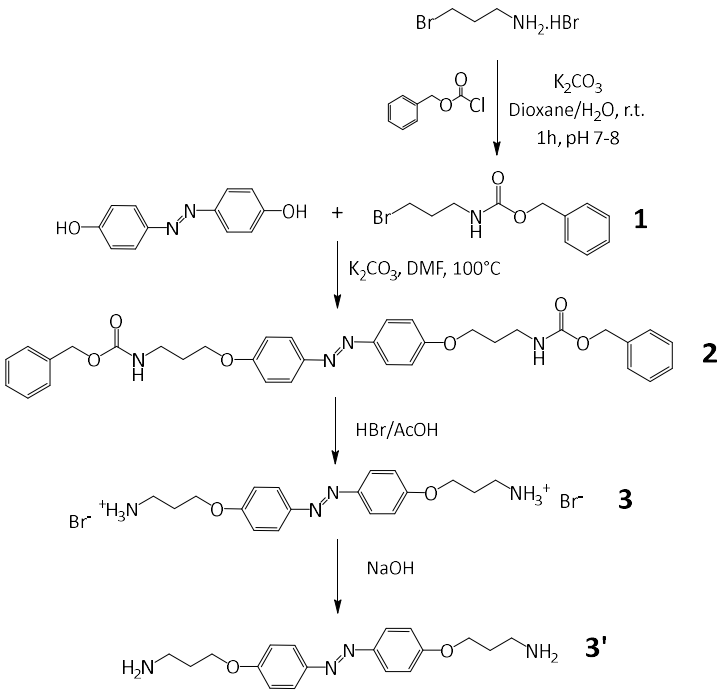

Scheme C2-18. Synthetic pathway to access **azobenzene 3'**

<u>Synthesis of protected bromopropylamine 1: adapted from ref</u>[1]

3-bromopropylamine hydrobromide (10.95 g, 50 mmol, 1 eq) was dissolved in 50 mL of a 50/50 v/v mixture of water and dioxane in a beaker equipped with a stir-bar. A solution of benzyl chloroformate (10.50 g, 61.5 mmol, 1.23 eq) in 25 mL of dioxane was prepared, as well as an aqueous 3.5M K_2CO_3 solution. A pH-meter was placed in the reaction beaker. Successive dropwise additions of the benzyl chloroformate solution and potassium carbonate solution into the beaker were carried out while maintaining the pH in between 6 and 7, until all the benzyl chloroformate solution had been added, under heavy stirring. The solution became cloudy once approximatively half of the benzyl chloroformate solution had been added. The solution pH was then adjusted in between 7 and 8, and the mixture was left to react for 1 hour under heavy stirring. 5 mL of 2M aqueous NaOH were then added to hydrolyze the excess benzyl chloroformate, and the mixture was left to react for two additional hours. The reaction mixture was then extracted with 3 x 100 mL diethyl ether, and the organic phases were combined and washed with 100 mL 1 M aqueous NaOH followed by 2 x 100 mL water. The organic phase was then dried over $MgSO_4$, and the solvent was removed under reduced pressure. The crude product was further purified using silica gel chromatography with DCM/cyclohexane 10/1 as eluent, yielding 13.5 g (~100 %) of product as a light yellow oil.

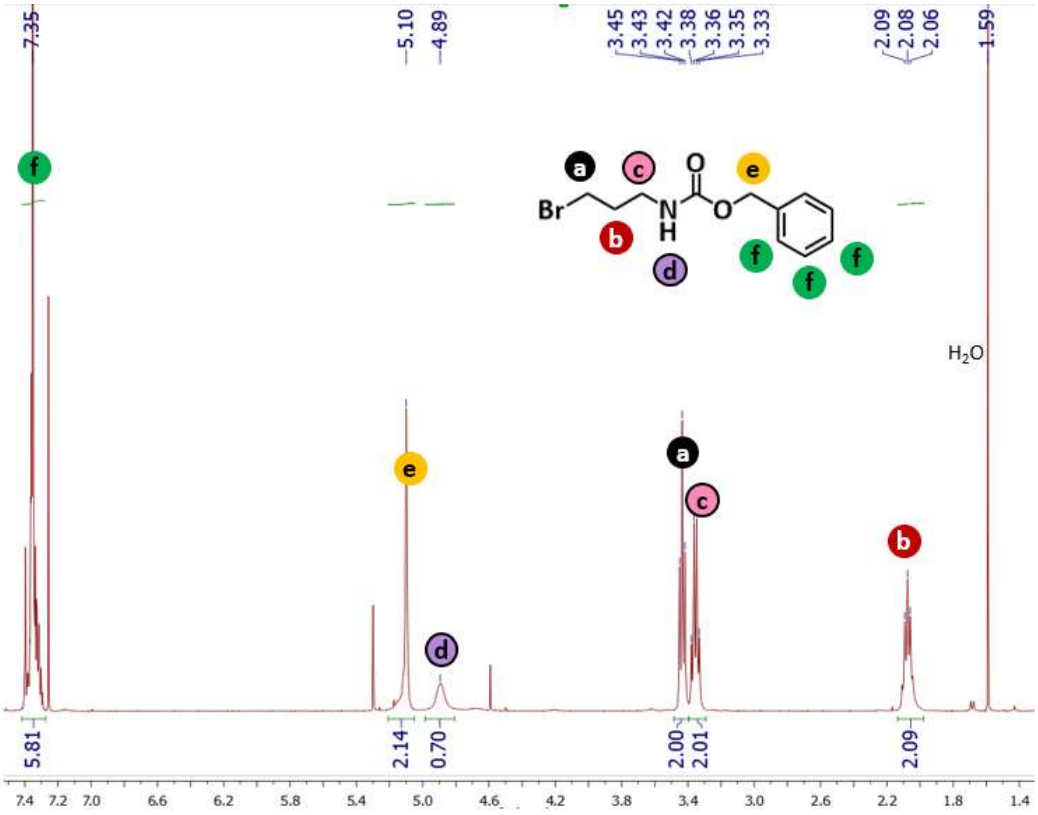

Figure C2-11. ^{1}H NMR (in $CDCl_3$) of the pure product **1**

^{1}H NMR ($CDCl_3$, 400 MHz): δ (ppm) 7.35 (m, **H^{f}**, 5H), 5.10 (s, **H^{e}**, 2H), 4.89 (br s, **H^{d}**, 1H), 3.42 (t, **H^{a}**, J = 6.4 Hz, 2H), 3.35 (q, **H^{c}**, J = 6.4 Hz, 2H), 2.08 (qt, **H^{b}**, J = 6.4 Hz, 2H)

Synthesis of azobenzene 2: adapted from ref[1]

In a round bottom flask equipped with a water condenser, septum and stir-bar, 4,4'-dihydroxyazobenzene (3 g, 14.0 mmol, 1 eq), Cbz-protected bromopropylamine (8.35 g, 30.8 mmol, 2.2 eq) and K_2CO_3 (9.68 g, 70 mmol, 5 eq) were mixed in 60 mL DMF. The reaction vessel was degassed with argon, and the mixture was left to react overnight at 100 °C. The solution was then left to cool, and was filtered. The recovered precipitate was washed with water followed by diethyl ether, dissolved in THF, dried over $MgSO_4$, and concentrated until the product was barely soluble in hot THF. The product was then left to recrystallize and the supernatant solvent was re-concentrated, in order to carry out a second recrystallization. The recrystallized fractions were combined, affording 7.31 g (87.5%) of pure product as a dark orange powder.

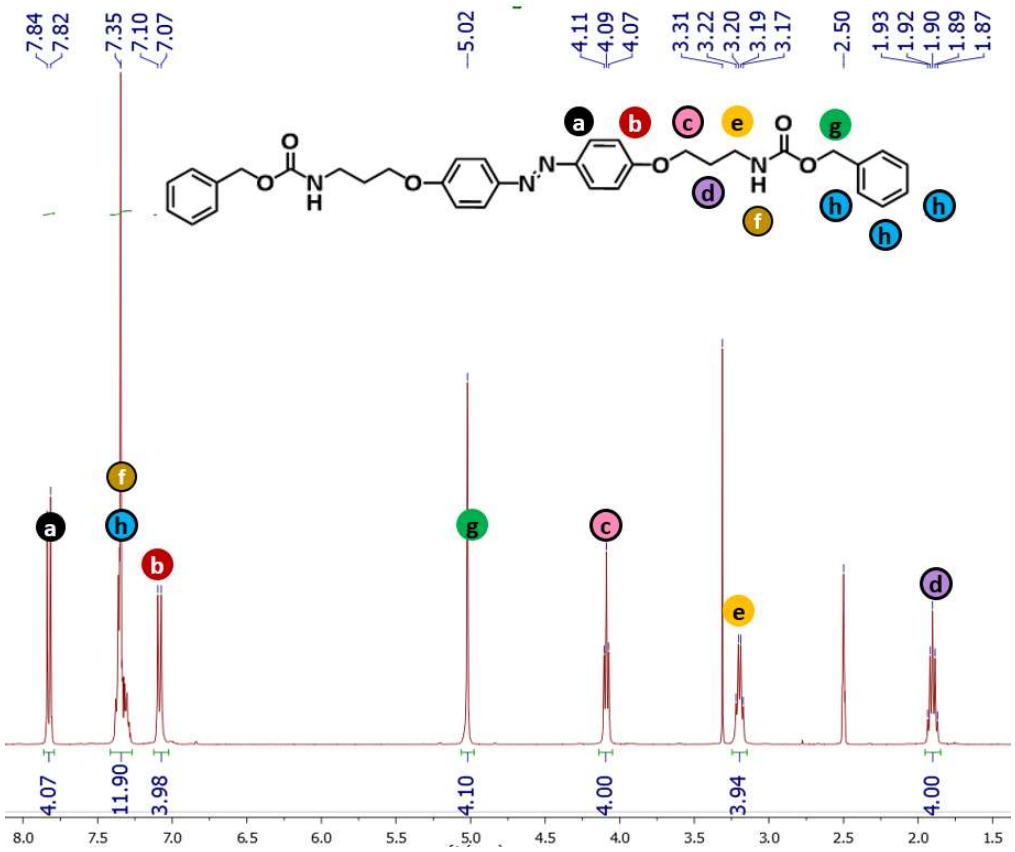

Figure C2-12. ^{1}H NMR (in DMSO-d_6) of the pure azobenzene **2**

^{1}H NMR (DMSO-d_6, 400 MHz): δ (ppm) 7.83 (d, **H^{a}**, J = 9.2 Hz, 4H), 7.35 (m, **H^{h} + H^{f}**, 12H), 7.08 (d, **H^{b}**, J = 9.2 Hz, 4H), 5.02 (s, **H^{g}**, 4H), 4.09 (t, **H^{c}**, J = 6,2 Hz, 4H), 3.20 (q, **H^{e}**, J = 6,2 Hz, 4H), 1.90 (qt, **H^{d}**, J = 6,2 Hz, 4H)

Synthesis of azobenzene 3:

In a round bottom flask equipped with a stir bar, azobenzene **2** (4 g, 6.71 mmol, 1 eq) was placed and 30% HBr in AcOH (15.52 g, 57,6 mmol, 8.85 eq) was added. The mixture immediately turned dark red/black, and was left to react for 1 hour. 50 mL of diethyl ether was then added, and the mixture was stirred for 5 minutes before being filtered. The precipitate was washed with diethyl ether. Traces of solvent were removed under reduced pressure, yielding 3.28 g (~100 %) of a black powder.

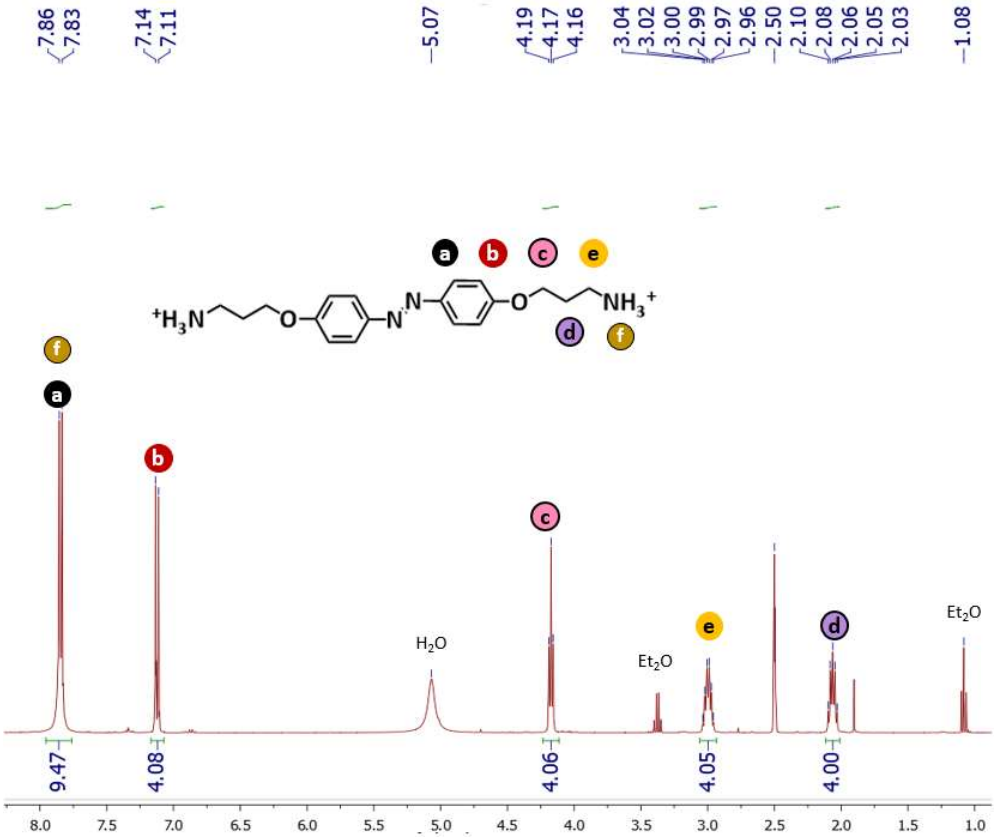

Figure C2-13. ^{1}H NMR (in DMSO-d_6) of the pure azobenzene **3**

^{1}H NMR (DMSO-d_6, 400 MHz): δ (ppm) 7.84 (m, **H^a + H^f**, J = 9.2 Hz, 10H), 7.12 (d, **H^b**, J = 9.2 Hz, 4H), 4.17 (t, **H^c**, J = 6,4 Hz, 4H), 3.00 (sext **H^e**, J = 6,4 Hz, 4H), 2.05 (qt, **H^d**, J = 6.4 Hz, 4H)

Neutralization of azobenzene 3:

Azobenzene **3** (1 g, 2.04 mmol) was placed in a round bottom flask and NaOH (5 g, 0,125 mol) dissolved in 10 mL of water was added. The mixture was stirred for an hour, 200 mL of DCM was added, followed by 30 mL of water. The mixture was stirred until the aqueous phase was clear (approximatively 2 hours). The organic phase was separated and the aqueous phase was further washed with 2 x 100 mL DCM. The solvent was removed under reduced pressure, and 455 mg (68%) of yellow powder was obtained, which was stored under argon at 0 °C.

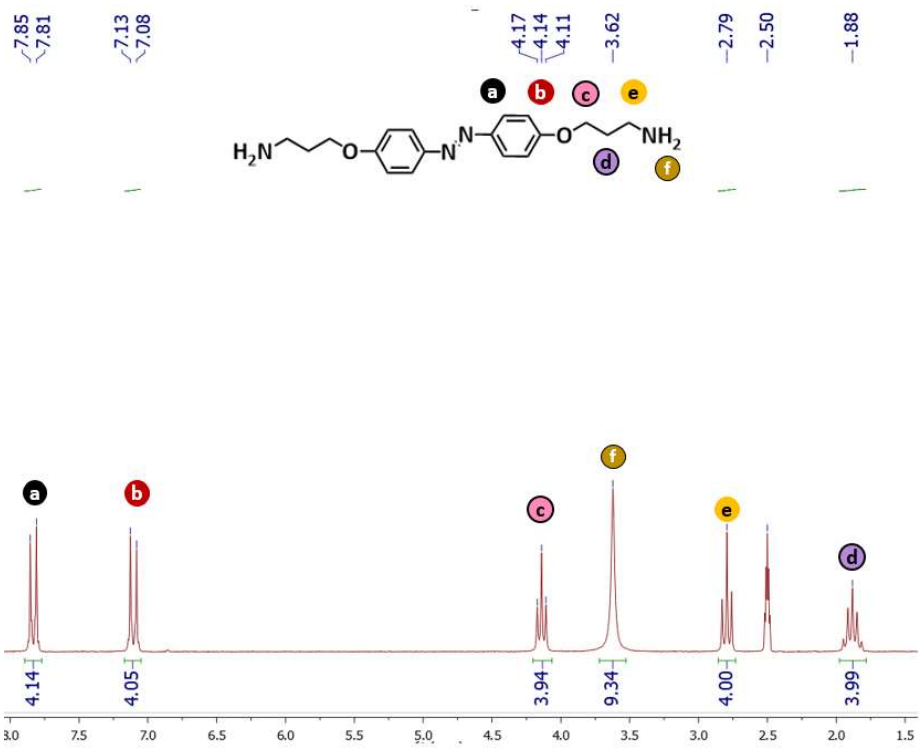

Figure C2-14. ^{1}H NMR (in DMSO-d_6) of neutralized azobenzene **3'**

^{1}H NMR (DMSO-d_6, 200 MHz): δ (ppm) 7.83 (d, **H^{a}**, J = 9 Hz, 4H), 7.10 (d, **H^{b}**, J = 9 Hz, 4H), 4.14 (t, **H^{c}**, J = 6.6 Hz, 4H), 3.62 (br s, **H^{f}**, 2H) 2.79 (t, **H^{e}**, J = 6.6 Hz, 4H), 1.88 (qt, **H^{d}**, J = 6.6 Hz, 4H)

ii. Synthesis of POE-C_{11}-NH_2

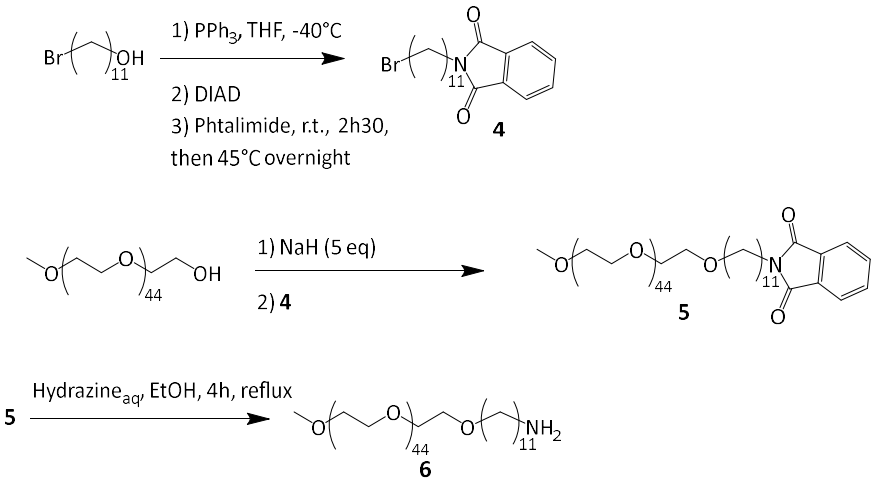

Scheme C2-19. Synthesis of PEO-C_{11}-NH_2 **6**

Synthesis of 4:

In a vial, DIAD (15.5 mL, 76 mmol, 1.2 eq) was solubilized in 25 mL of toluene under argon atmosphere. In a round bottom flask equipped with a stir-bar, 11-bromoundecanol (15.58 g, 63.3 mmol, 1 eq) and triphenylphosphine (19.93 g, 76 mmol, 1.2 eq) were dissolved in 200 mL of anhydrous THF under argon atmosphere, and the solution was cooled to -40 °C using a iPrOH / liquid N_2 bath. The DIAD solution was then added dropwise. After 5 minutes, phthalimide (11.18 g, 76 mmol, 1.2 eq) in suspension in 75 mL of anhydrous THF was added to the reaction medium. The cold bath was removed and the reaction mixture was left to come back to r.t. and left to react for 2.5 h. The mixture was then heated to 45 °C overnight. The crude mixture was filtered (to remove triphenylphosphine and its oxide), and the solvent was removed from the supernatant under reduced pressure. A yellow oil was obtained, and the product was recrystallized from MeOH several times to remove residual amounts of triphenylphosphine and its oxide. 10,45 g (43.5 %) of white powder were obtained.

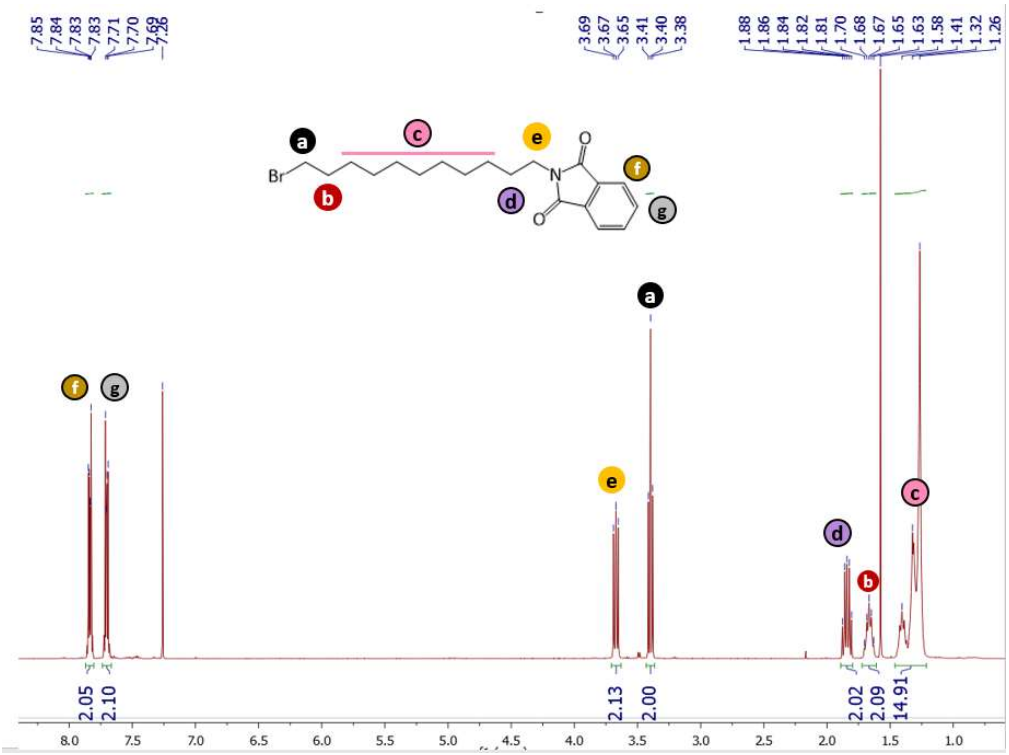

Figure C2-15. ^{1}H NMR ($CDCl_3$, 400 MHz) of pure compound **4**

^{1}H NMR ($CDCl_3$, 400 MHz): δ (ppm) 7.84 (m, **H^f**, 2H), 7.70 (m, **H^g**, 2H), 3.67 (t, **H^e**, J = 7.2 Hz, 2H), 3.40 (t, **H^a**, J = 6.8 Hz, 2H), 1.84 (qt, **H^d**, J = 7.2 Hz, 2H), 1.66 (qt, **H^b**, J = 7.2 Hz, 2H), 1.26 (m, **H^c**, 14H)

Scheme C2-20. Synthesis of **4'**

Synthesis of 4'

The Finkelstein reaction was carried out on compound **4** by solubilizing 1.5 g of the latter in 10 mL of acetone in a round bottom flask, followed by the addition of 3.22 g of NaI (5.4 eq.). The solution was refluxed for 2 days.

Acetone was then removed by evaporation under reduced pressure, and 30 mL of DCM was added. The organic solution was extracted with 3 x 30 mL H_2O to remove salt. The organic phase was then dried over $MgSO_4$, and the solvent was removed under reduced pressure, yielding 1.55 g of yellow oil (92% yield).

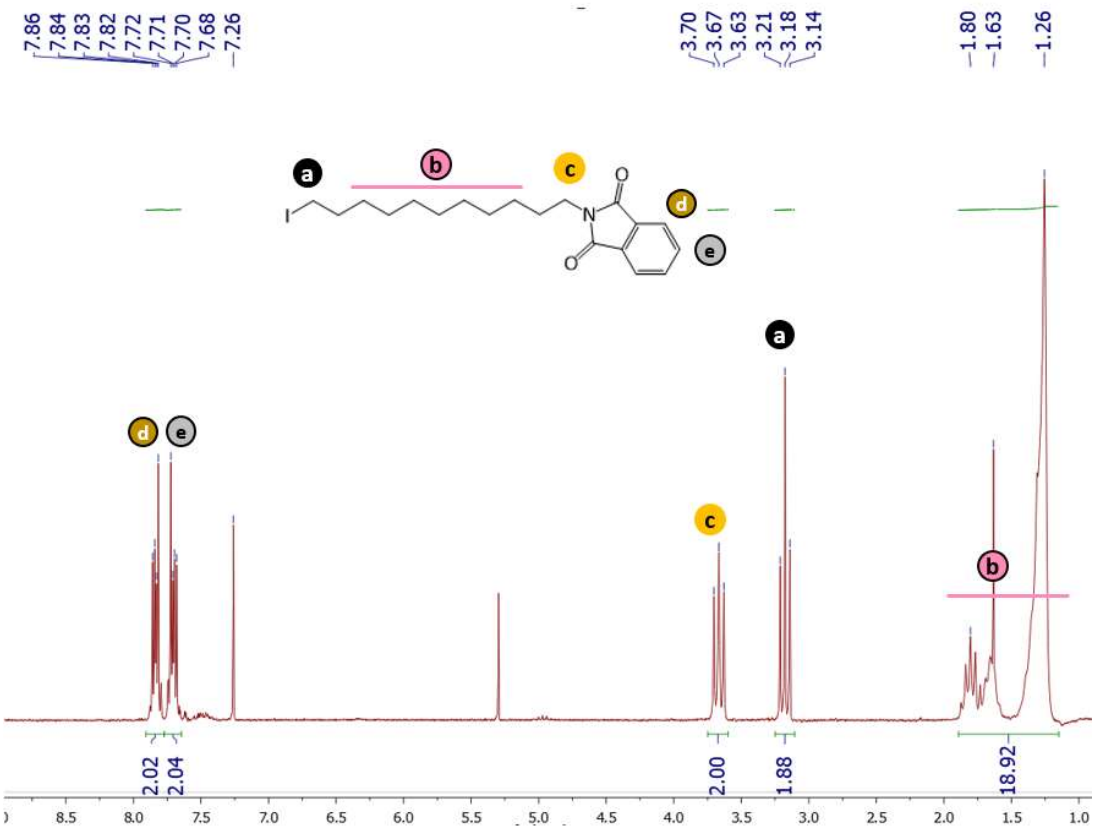

Figure C2-16. ^{1}H NMR ($CDCl_3$, 200 MHz) of pure compound **4'**

^{1}H NMR ($CDCl_3$, 200 MHz): δ (ppm) 7.84 (m, **H^d**, 2H), 7.70 (m, **H^e**, 2H), 3.67 (t, **H^c**, J = 7.2 Hz, 2H), 3.18 (t, **H^a**, J = 7.0 Hz, 2H), 1.87-1.26 (m, **H^b**, 18H)

Synthesis of 5:

A typical procedure for the Williamson etherification involving monomethyl hydroxy poly-(ethylene oxide) (PEO-OH) and brominated compound **4** consisted in stirring NaH (5 eq.) in a solution of 4 g of PEO-OH (1 eq., 2 mmol) in 8 mL of anhydrous THF for a given amount of time in a round bottom flask, under argon atmosphere, followed by addition of a solution of 2.45 g of **4** in 6 mL anhydrous THF. Conversion was monitored by precipitating a small amount of the reaction mixture in cold diethyl ether, and analyzing the resulting precipitate in ^{1}H NMR (in DMSO-d_6). During the first runs, conversion was monitored via the integration of the PEO-O*H* signal. However, this proved to be unreliable. Therefore, a drop of trichloroacetyl isocyanate (TCAI) was added into the NMR tube, which reacts with any remaining alcohol, shifting the -C*H*$_2$-O- signal due to the formation of a urethane. Once the reaction was complete, purification was achieved by first filtering the crude reaction mixture to remove salts, followed by two precipitations in Et_2O/pentane 70/30, silica gel chromatography ($CHCl_3$ -> $CHCl_3$/EtOH 75/25 gradient eluent), and a final precipitation in cold Et_2O. The final yield was of 62 % on the successful run.

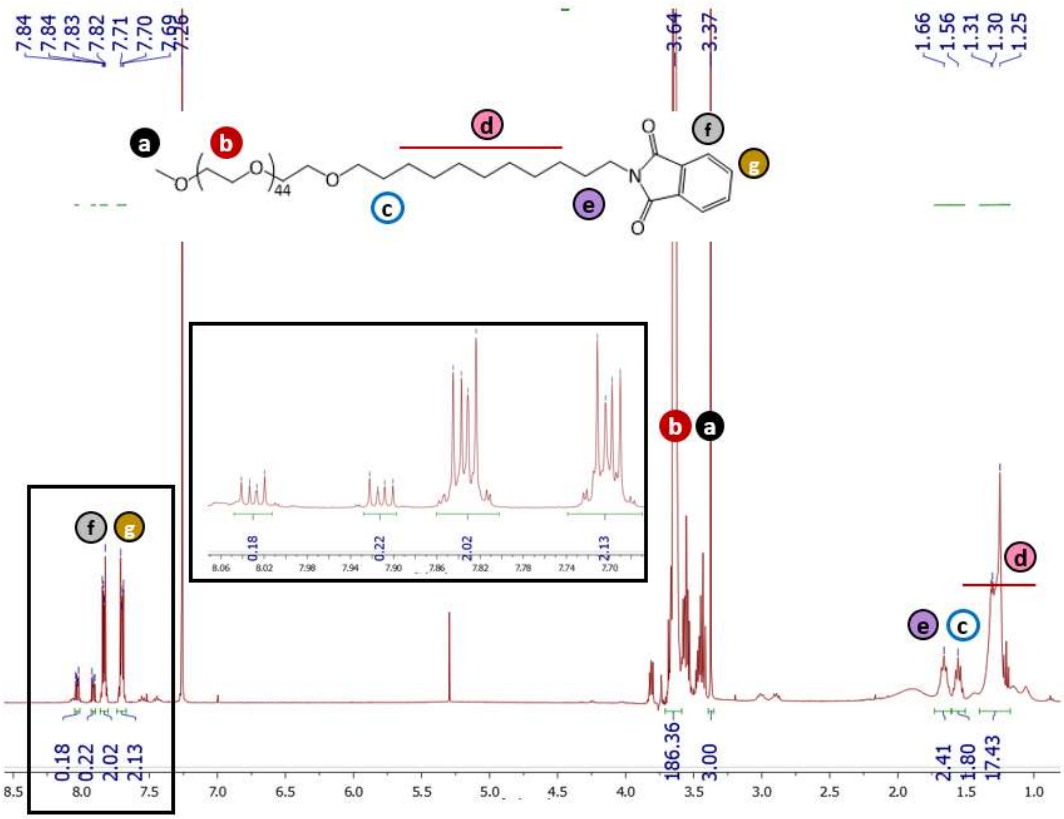

Figure C2-17. ^{1}H NMR ($CDCl_3$, 400 MHz) of compound **5**

^{1}H NMR ($CDCl_3$, 400 MHz): δ (ppm) 7.83 (m, **H^{f}**, 2H), 7.70 (m, **H^{g}**, 2H), 3.64 (s br, **H^{b}**, 180H), 3.37 (s, **H^{a}**, 3H), 1.66 (m, **H^{e}**, 2H), 1.56 (m, **H^{c}**, 2H), 1.25 (m, **H^{d}**, 14H)

Note: the smaller aromatic peaks integrating for 0.18 and 0.22H are presumably opened phtalimide.

Synthesis of 6:

In a round bottom flask, 0.763 g of polymer **4** was dissolved in 3.3 mL EtOH and 0.2075 g of an aqueous solution of hydrazine (80 %) was added. The solution was refluxed for 4 h, followed by addition of 1M HCl until a pH of 1 was reached. The solution was centrifuged and the supernatant was recovered, which was neutralized with 1M NaOH. The solution was saturated with NaCl, and the polymer was extracted with 4 x 50 mL DCM. The combined organic phases were dried over $MgSO_4$, and the solution was then concentrated by evaporating solvent under reduced pressure. The polymer was finally precipitated in Et_2O/pentane 70/30, yielding a white powder (85 % yield).

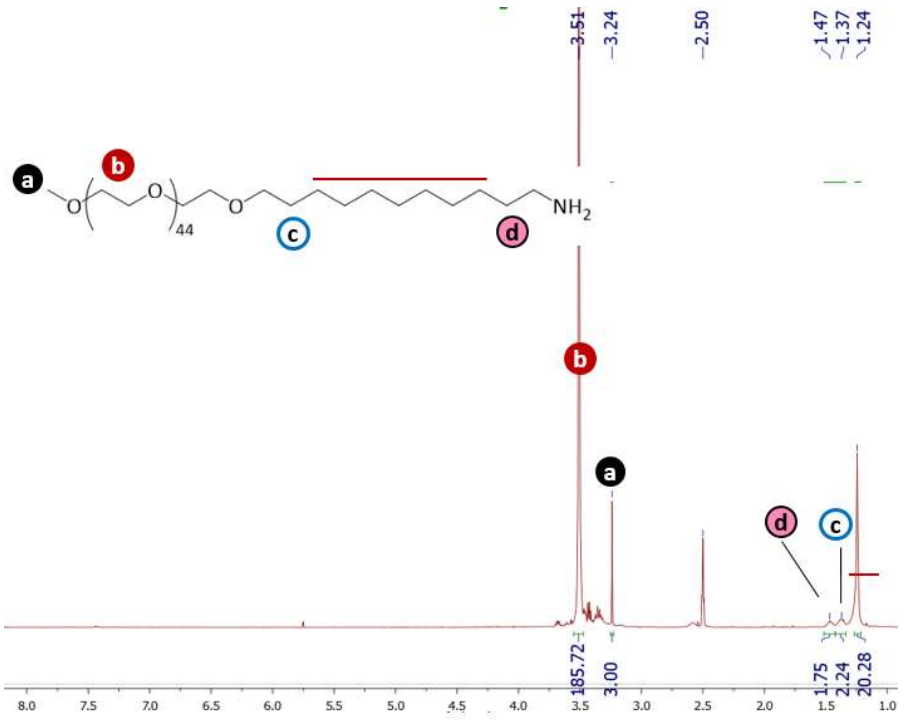

Figure C2-18. ^{1}H NMR (DMSO-d_6, 400 MHz) of pure PEO-C_{11}-NH_2 **6**

^{1}H NMR (DMSO-d_6, 400 MHz): δ (ppm) 3.51 (s br, **H^{b}**, 180H), 3.24 (s, **H^{a}**, 3H), 1.47 (m, **H^{d}**, 2H), 1.37 (m, **H^{d}**, 2H), 1.24 (m, **H^{e}**, 14H)

iii. Triphosgene coupling

This section covers the experiments conducted relative to the coupling of two amines to form a urea, using triphosgene.

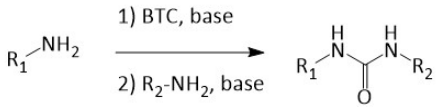

Scheme C2-21. General principle of the triphosgene coupling.

<u>General protocole:</u>

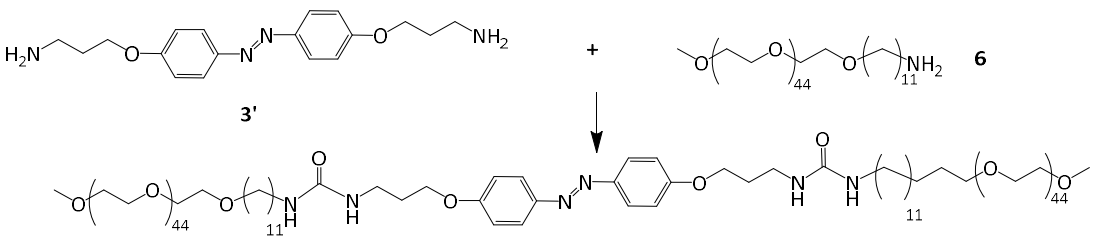

Scheme C2-22. Triphosgene mediated coupling of azobenzene diamine **3'** and PEO-C_{11}-NH_2

1 eq (36 mg) of azobenzene **3'** (in the neutralized form) was placed in a vial, with 5 mL anhydrous solvent and 2.2 eq. of diisopropylethylamine (DIEA, 42.1 µL), and was put under argon atmosphere. In another vial, 0.38 eq. triphosgene (24.8 mg) was solubilized in 0.8 mL anhydrous solvent under argon atmosphere. The first solution was added dropwise to the second over the course of 30 min using a syringe pump, and the solution was then left to react for 3 h. PEO-C_{11}-NH_2 **6** (524 mg, 2.2 eq.) was dissolved under argon atmosphere in 2.5 mL of anhydrous solvent, and 2.8 eq. DIEA (53.5 µL) was added. This solution was added to the reaction mixture, and left to react. Conversion was monitored by ^{1}H NMR, by taking a small amount of the reaction mixture, precipitating the polymer in dry diethyl ether, and centrifuging to removing the supernantant. Conversion was determined by integration of the newly formed urea peaks towards 6 ppm. The polymer was then washed twice with dry diethyl ether, and was finally dried and analyzed. After 162 h of reaction, only 10-15% conversion was obtained.

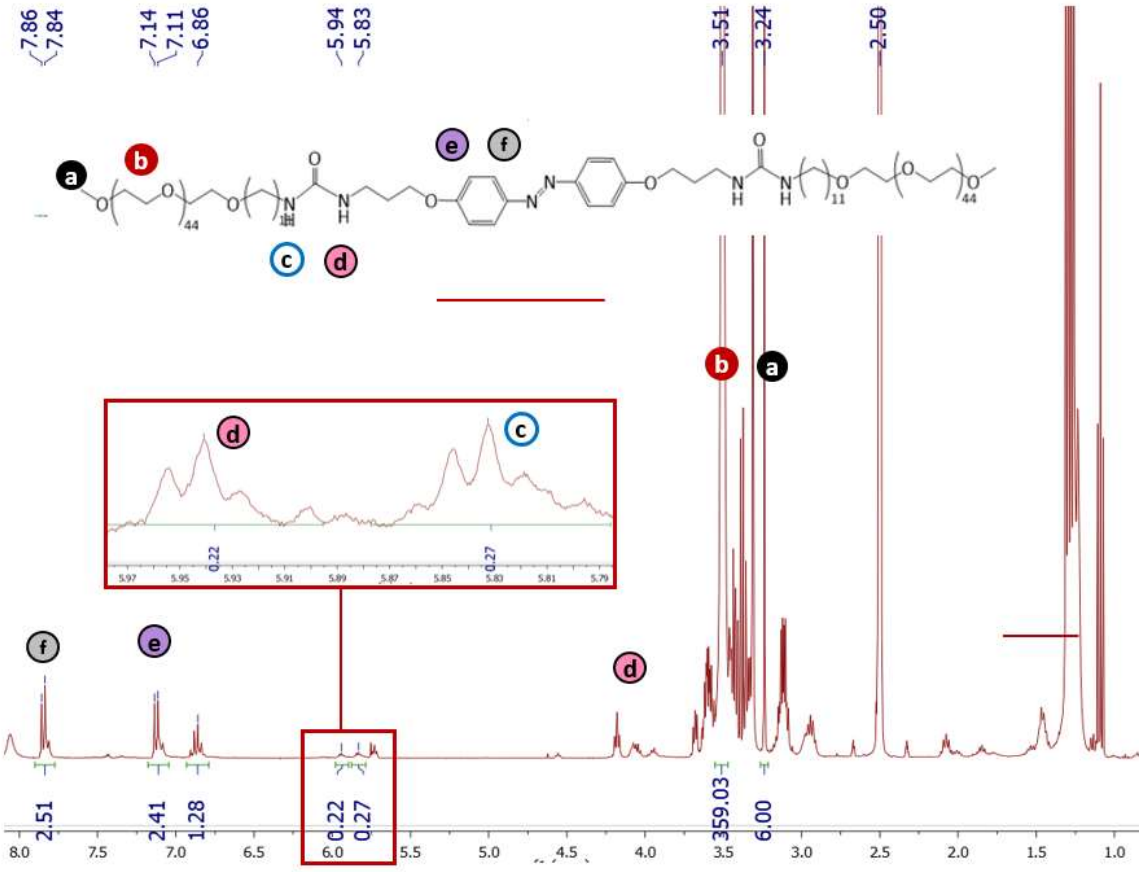

Figure C2-19. ^{1}H NMR (DMSO-d_6, 400 MHz) of the crude reaction mixture after precipitation in dry diethyl ether.

For control syntheses involving only mono-amines, the stoiechiometry was adapted in consequence.

iv. Isoproprenyl carbamate coupling

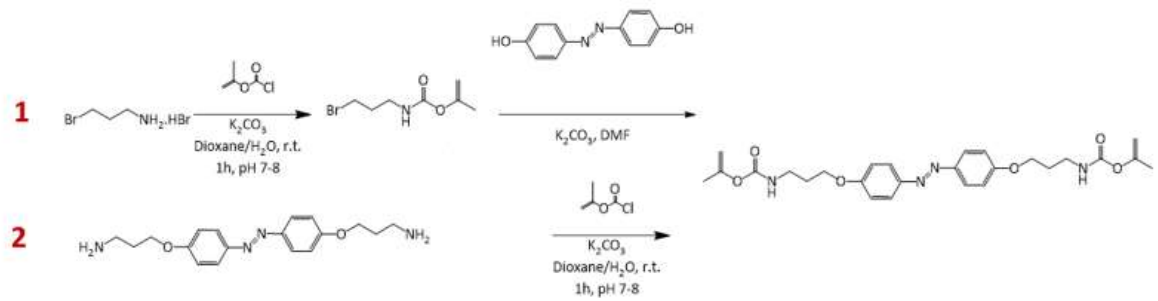

Scheme C2-23. Synthetic routes to access azobenzene-bis isopropenyl carbamate

Synthesis following route 1

Synthesis of isopropenylcarbamatepropyl bromide

1.095 g of 3-bromopropylammonium bromide was dissolved in a mixture of 6 mL water and 6 mL of dioxane in a beaker equipped with a stir bar and a pH-meter. Another solution containing 0.723 g (2.4 eq.) of isopropenyl chloroformate in 2 mL of dioxane was prepared as well as a 3.5 M aqueous solution of K_2CO_3 (2.42 g K_2CO_3 in 5 mL of water). The two solutions were alternatingly added to the first solution in order to maintain a pH between 6 and 7 (addition of chloroformate would decrease pH whereas addition of K_2CO_3 would increase pH), until all the chloroformate solution had been added. The pH was then adjusted to 7.5 and the reaction was left to proceed under stirring for 1 h. 1 mL of 1M NaOH aqueous solution was then added, and the reaction was left for two additional hours under stirring. At the end of the reaction time, it was observed that an oily yellow layer was present at the bottom of the beaker. The crude reaction mixture was extracted 3 times with diethyl ether (3 x 30 mL), and the combined organic phases were washed with 1 x 20 mL NaOH 1M aq. + 2 x 20 mL water. The organic phase was dried over $MgSO_4$, and solvent was removed under vacuum, affording 1.10 g (≈100% yield) of pure product as a yellow oil.

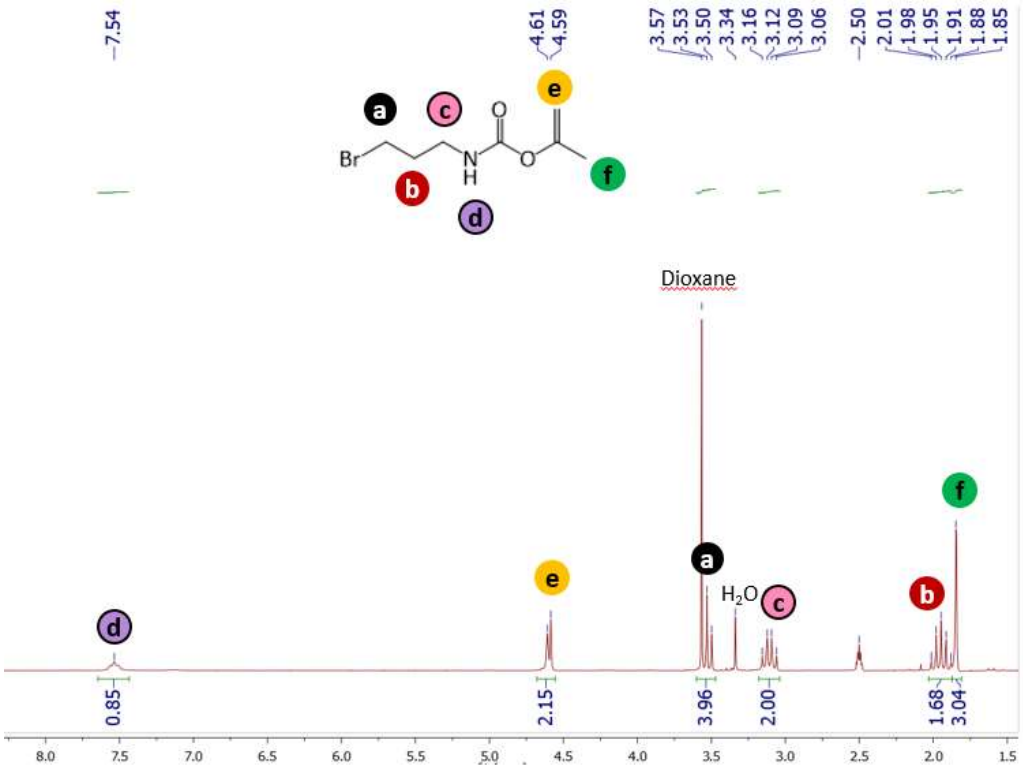

Figure C2-20. ^{1}H NMR (DMSO-d_6, 200 MHz) of the product

^{1}H NMR (DMSO-d_6, 200 MHz): δ (ppm) 7.54 (t, **H^{d}**, J = 5.8 Hz, 1H), 4.60 (m, **H^{e}**, 1H+1H), 3.53 (t, **H^{a}**, J = 6.6 Hz, 2H), 3.10 (q, **H^{c}**, J = 5.8 Hz, 2H), 1.95 (qt, **H^{b}**, 2H), 1.85 (s, **H^{f}**, 3H)

<u>Williamson etherification between isopropenylcarbamatepropyl bromide and 4,4'-dihydroxyazobenzene</u>

305 mg of 3-bromopropyl isopropenyl carbamate (2.2 eq.) were placed in a small round bottom flask with a stir bar, with 133 mg of 4,4'-dihydroxyazobenzene (1 eq.), 5 eq. of dry K_2CO_3, under argon atmosphere. 3 mL of DMF were then added, and the reaction was left overnight at 100 °C. The next day, the crude reaction mixture was left to cool to r.t., and the precipitate was filtered and washed with water. ^{1}H NMR revealed that no carbamate was left despite the etherification appearing to have taken place (which would otherwise have been present at 4.60 ppm). The reaction was re-conducted but without heating, and the carbamate once again had degraded and was no longer present.

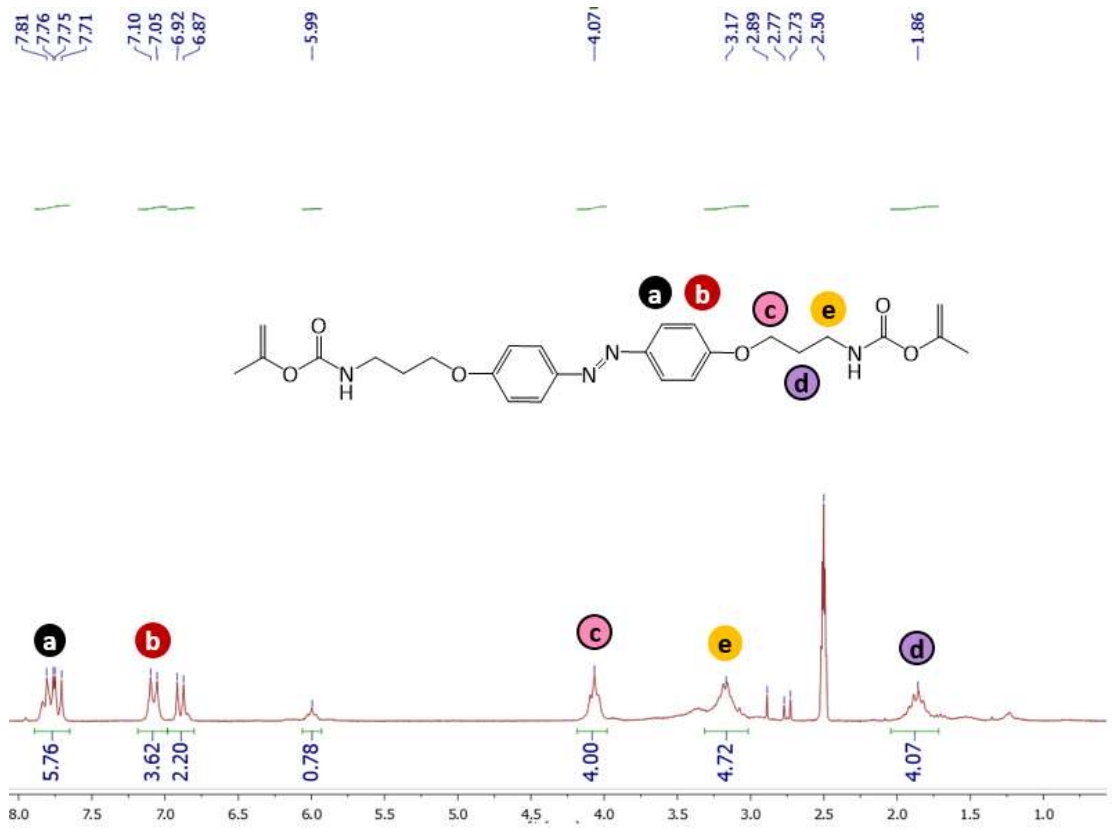

Figure C2-21. ^{1}H NMR (DMSO-d6, 200 MHz) of the product after workup (reaction conducted at 100 °C)

Synthesis following route 2

<u>Synthesis of azobenzene bis-isopropenyl carbamate from azobenzene diammonium:</u>

0.300 g (1 eq.) of neutralized azobenzene diamonnium **3** was dissolved in a mixture of 24 mL water and 12 mL of dioxane in a beaker equipped with a stir bar and a pH-meter. Another solution containing 0.177 g of isopropenyl chloroformate (2.4 eq.) in 5 mL of dioxane was prepared as well as a 3.5 M aqueous solution of K_2CO_3 (2.42 g K_2CO_3 in 5 mL of water). The two solutions were alternatingly added to the first solution, while maintaining a pH in between 6 and 7 (addition of chloroformate would decrease pH whereas addition of K_2CO_3 would increase pH), until all the chloroformate solution had been added. The solution was initially clear and was at pH = 2, but became cloudy once the pH had been adjusted to 6-7. At the end of the additions, the pH was then adjusted to 7.5 and the reaction was left to proceed under stirring for 1 hour. 0.25 mL of 1 M NaOH aqueous solution was then added, and the reaction was left for two additional hours under stirring. At the end of the reaction, the product was recovered by filtration followed by washing with water. After drying under vacuum, 192 mg of yellow powder are obtained, and confirmed pure by ^{1}H NMR.

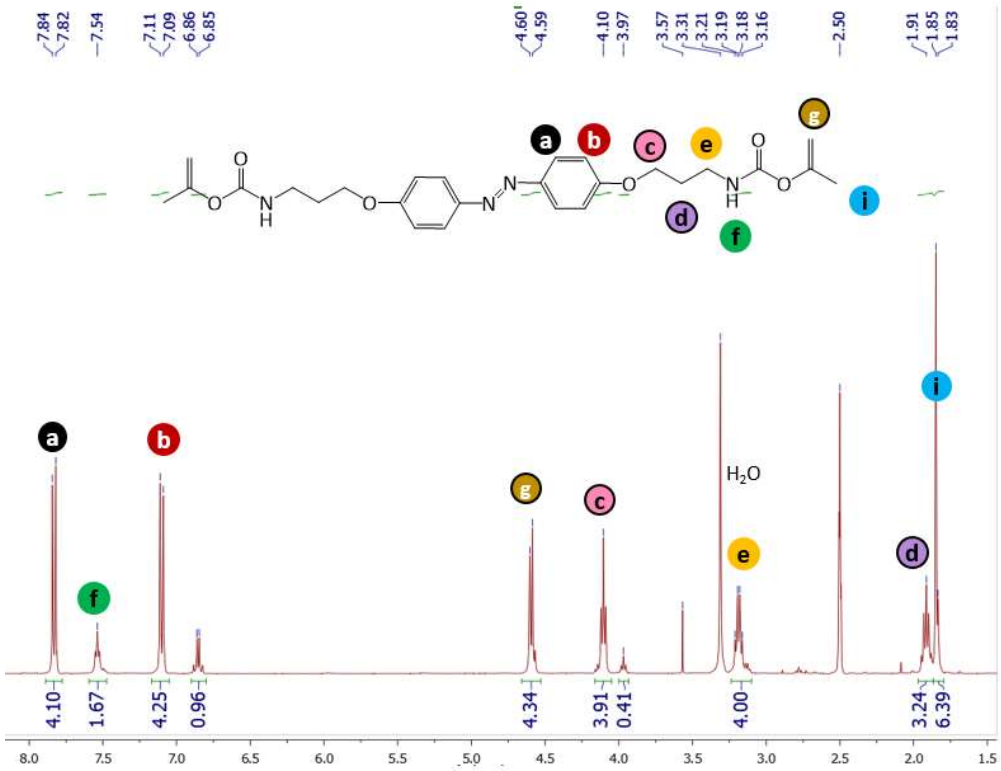

Figure C2-22. ^{1}H NMR (DMSO-d_6, 400 MHz) of the pure product. The peak at 6.85 ppm corresponds to the aromatic protons of a small amount of the *cis* isomer.

^{1}H NMR (DMSO-d_6, 400 MHz): δ (ppm) 7.83 (d, **H^{a}**, J = 8.8 Hz, 4H), 7.54 (t, **H^{f}**, 2H), 7.10 (d, **H^{b}**, J = 8.8 Hz, 4H), 4.60 (m, **H^{g}**, 1H+1H), 4.10 (t, **H^{c}**, J = 6 Hz, 4H), 3.19 (q, **H^{e}**, J = 6 Hz, 4H), 1.91 (qt, **H^{d}**, J = 6.4 Hz, 4H), 1.85 (s, **H^{i}**, 6H)

Coupling of azobenzene bis-isopropenyl carbamate and PEO-C_{11}-NH_2:

The protocol tested was adapted from ref[9]. In a round bottom flask, 185 mg of PEO-C_{11}-NH_2 **6** (2 eq.) were mixed with 17.7 mg of azobenzene bis-isopropenyl carbamate and 2.70 µL of DBU (0.5 eq.) in 1 mL of dry THF under argon atmosphere. The mixture was heated at 55 °C, and the polymer was precipitated in diethyl ether after a week of reaction time. ^{1}H NMR revealed that a small amount of urea had formed (less than 10 %, see **Figure C2-23**), and SEC measurements indicated 2 populations, with mostly mono or un-substituted PEO present (80 %).

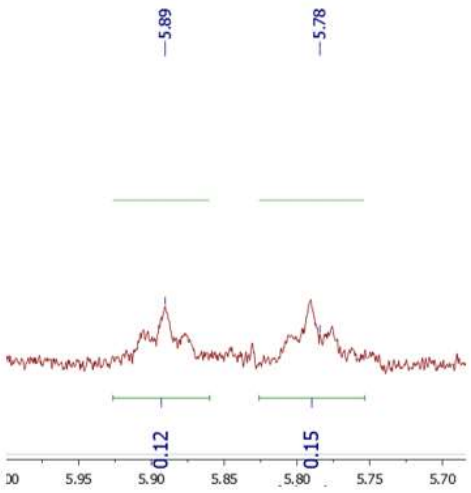

Figure C2-23. ^{1}H NMR (DMSO-d_6, 400 MHz) of the purified product, urea peaks (integral reference set on the PEO-OMe chain ends at 6H)

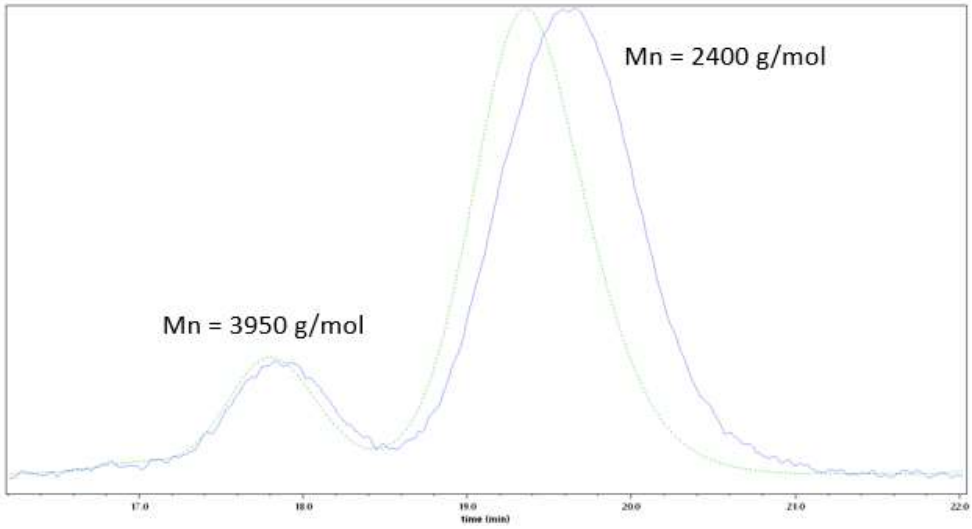

Figure C2-24. SEC chromatogram of the purified product, green curve is the UV signal and blue curve is the RI signal.

v. Diisocyanate based syntheses

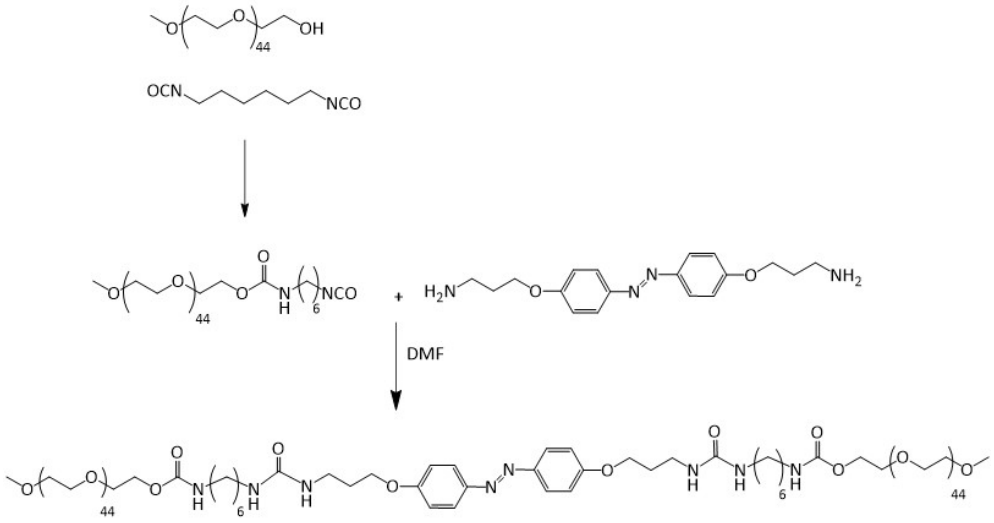

Scheme C2-24. Synthesis route involving the use of diisocyanate

Synthesis of PEO-C_6-NCO:

Prior to use, the PEO-OH was dried by azeotropic distillation with toluene to remove trace amounts of water. This was achieved by preparing a 20% wt./vol.% solution of PEO-OH in toluene, which was refluxed under argon for 1 h, and toluene was then distilled off. The polymer was then dried overnight in a vacuum oven at 50 °C and stored under argon.

The reaction was conducted at room temperature. **Typical procedure**: in a 50 mL round bottom flask, 3 g of PEO-OH (1.5 mmol) were solubilized in 30 mL anhydrous DCM under argon atmosphere. In a 100 mL round bottom flask, 20 mL of anhydrous DCM were mixed with hexamethylene diisocyanate (HMDI, 5 eq., 1.260 g) under argon atmosphere. The PEO solution was injected into the HMDI solution over the course of 4 h using a syringe pump and the mixture was left to react overnight.

The next day, the reaction mixture was concentrated by bubbling argon until approximately 15 mL of solution was remaining. The concentrated crude mixture was precipitated in 500 mL of anhydrous diethyl ether (DEE) under argon atmosphere and heavy stirring, and the precipitate was then left to decant. As much supernatant as possible was removed with a canula. The vessel was filled back up with fresh anhydrous Et_2O (around 400 mL), mixed, decanted, and the supernatant was removed. This operation was repeated three times in total to afford 3 washings (see **Figure C2-25**).

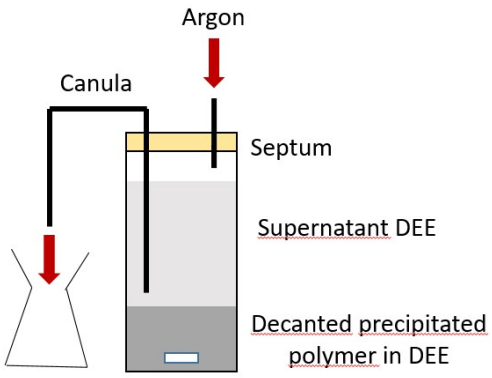

Figure C2-25. Schematic representation of the precipitation setup under argon atmosphere

The precipitate was then dried under vacuum, and a white powder was obtained (2.3g, 76%).

To verify the conversion and purity of **4**, 10 mg of the polymer was rapidly solubilized in DMSO-d_6 and a drop of benzylamine was quickly added, in order to quench the isocyanates by forming benzylurea moieties. The solution was then analyzed by ^{1}H NMR.

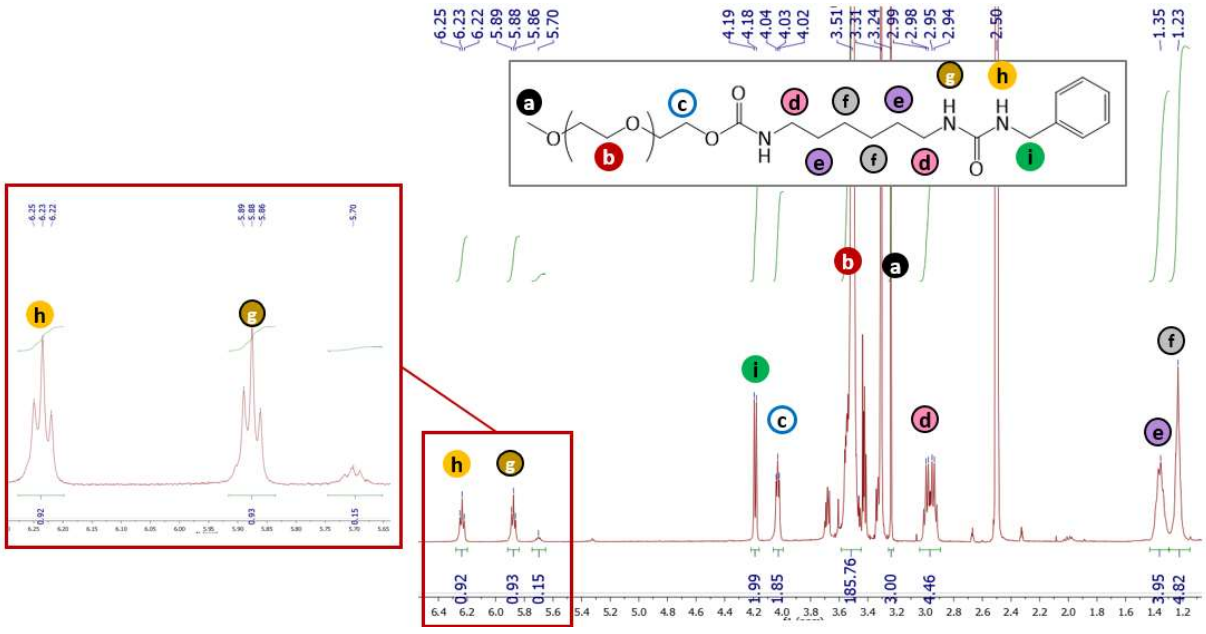

Figure C2-26. ^{1}H NMR spectrum of PEO-C_6-Benzylurea

When molecular sieves (4 Å) in powder form were used, a spatula point of it were added to the initial PEO-OH solution and to the DCM before adding HMDI. Both were stirred separately for 30 minutes, HMDI was then added

into the dried DCM and further stirred for another 30 minutes. The rest of the protocol was then carried out, yielding 2.15 g of product (70 %).

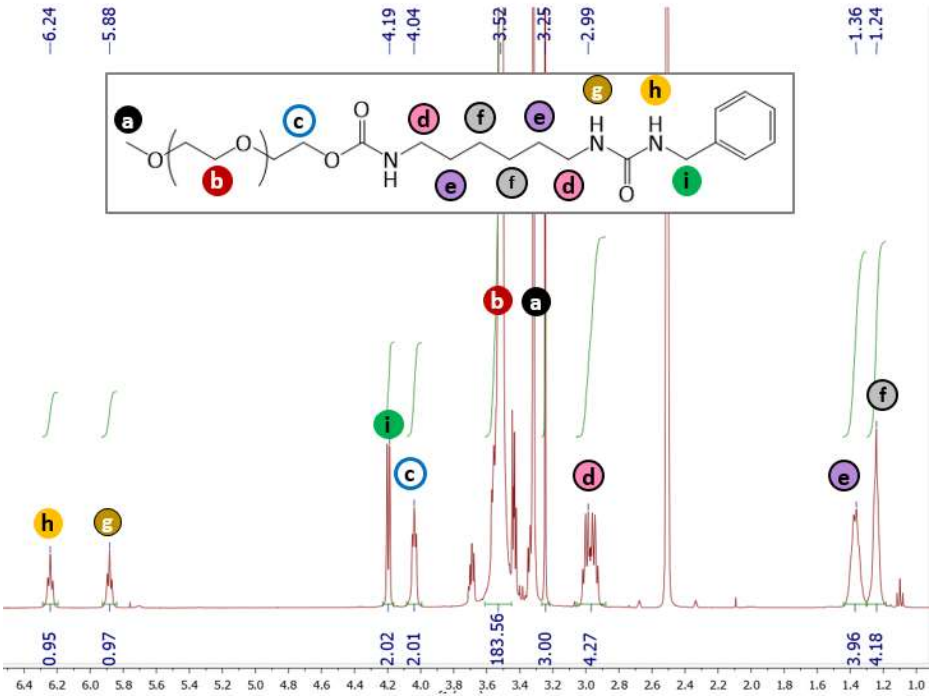

Figure C2-27. ^{1}H NMR of PEO-C_6-Benzylurea with use of powder molecular sieves

^{1}H NMR (DMSO-d_6, 400 MHz): δ (ppm) 6.24 (t, **H^{h}**, J = 6 Hz, 1H), 5.88 (t, **H^{g}**, J = 6 Hz, 1H), 4.19 (d, **H^{i}**, J = 6 Hz, 2H), 4.04 (t, **H^{c}**, J = 4.8 Hz, 2H), 3.52 (m, **H^{b}**, 180H = DP_n x 4H), 3.25 (s, **H^{a}**, 3H), 2.99 (m, **H^{d}+H$^{d'}$,** 2H+2H), 1.36 (m, **H^{e}+H$^{e'}$**, 2H+2H), 1.24 (m, **H^{f}+H$^{f'}$**, 2H+2H).

<u>Synthesis of Azo-(U-PEO)$_2$:</u>

In a 25 mL round bottom flask, 6 mL of dry DMF and a spatula point of molecular sieves (4 Å) in powder form were stirred under argon for 20 min. In parallel, 0.144 g (1 eq.) of azobenzene diamine **<u>3'</u>** were solubilized in 3 mL of dry DMF with a spatula point of molecular sieves (4 Å) in powder form and stirred for 20 min. 2 g (2.1 eq) of PEO-C_6-NCO were quickly added to the first solution, and put back under argon. Once the polymer was solubilized, the azobenzene solution was added to the polymer solution via a syringe and was left to react for 5 min. The slight excess of isocyanate-terminated PEO was then quenched by adding 0.3 mL of benzylamine, and the reaction was left to proceed for 5 more min. The crude polymer was then precipitated in 300 mL of DEE/pentane 50/50 (v/v). ^{1}H NMR revealed that the product had indeed formed, and that no PEO-benzylurea was present. However, another side reaction had occurred, due to partial hydrolysis of isocyanate moieties. This led to the formation of more PEO-U-C_6-U-PEO. The ^{1}H NMR spectrum showed that a third urea peak was present, representing approximately 10 % of the impurity, and signals of the product integrated approximately 10 % less than expected (**Figure C2-28**). In order to remove this unwanted impurity, 1.9 g of the crude polymer was solubilized in 2 mL EtOH, and precipitated in 40 mL of DEE/EtOH 7/1 v/v, washed twice with this solvent mixture, and then finally washed with pure DEE. After drying, 1.31 g of pure product was recovered (61 % yield), as confirmed by ^{1}H NMR

(**Figure C2-29**). An extremely small amount of PEO-C_6-U-C_6-PEO may still be present since a very small signal is still present after purification, but it is so small that no reliable integration may be done.

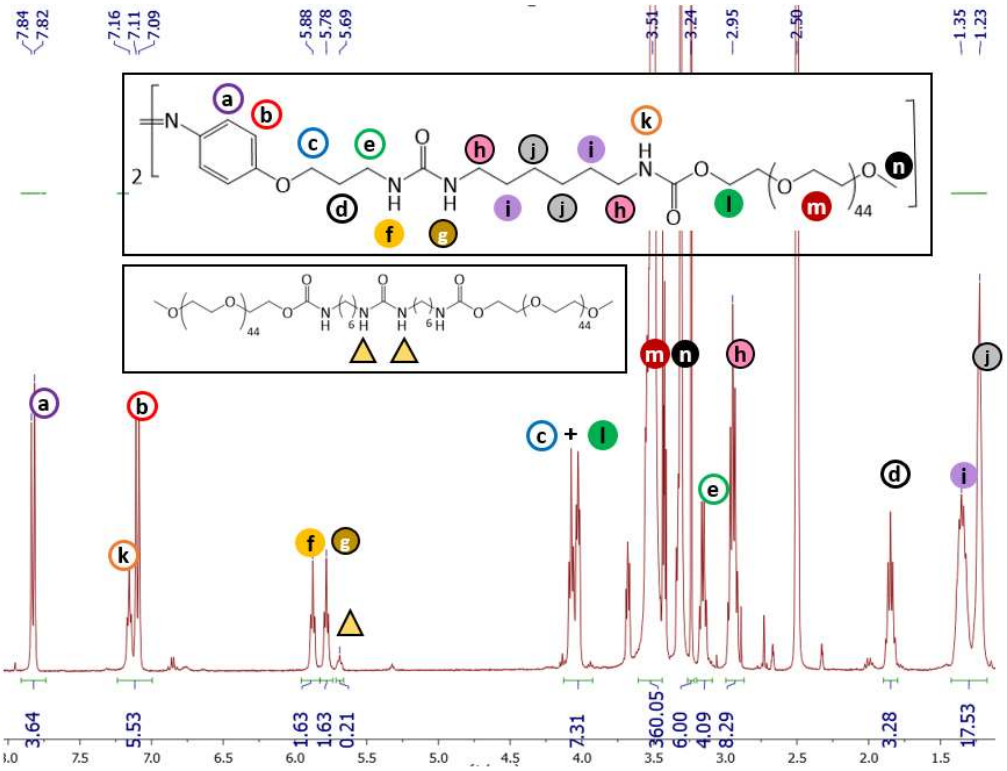

Figure C2-28. ^{1}H NMR (in DMSO-d_6) of the crude product with the impurity PEO-C_6-U-C_6-PEO

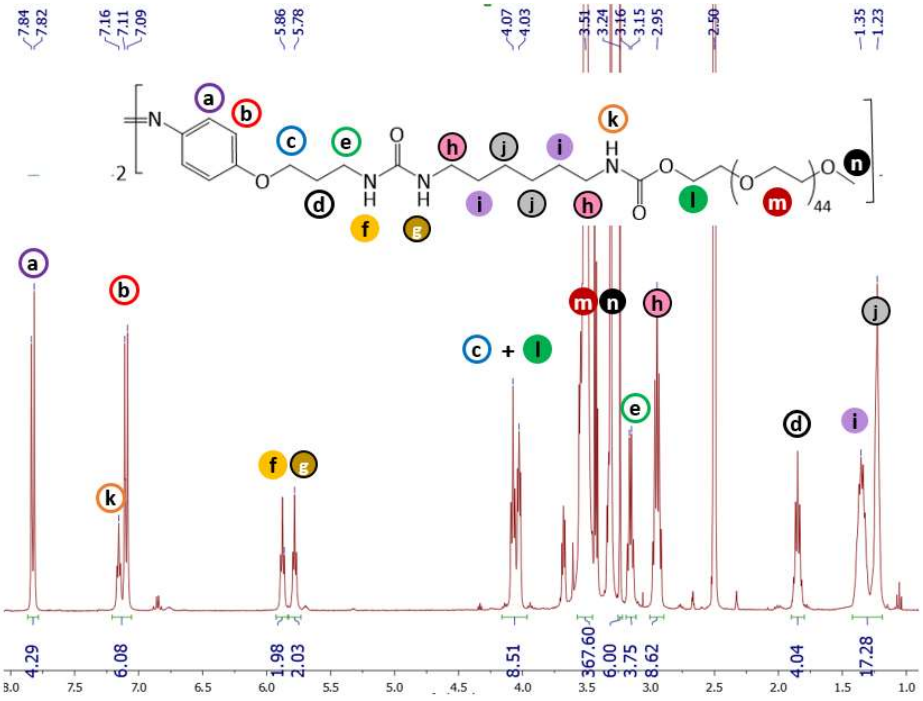

Figure C2-29. ^{1}H NMR (in DMSO-d_6) of the pure product

^{1}H NMR (DMSO-d_6, 400MHz): δ (ppm) 7.83 (d, **H^{a}**, J = 9.2 Hz, 4H), 7.16 (t, **H^{k}**, J = 5.6 Hz, 2H), 7.10 (d, **H^{b}**, J = 9.2 Hz, 4H), 5.86 (t, **H^{f}**, J = 6 Hz, 2H), 5.78 (t, **H^{g}**, J = 6 Hz, 2H), 4.07 (t, **H^{c}**, J = 6Hz, 4H), 4.03 (t**, H^{l}**, 4H), 3.51 (s br, **H^{m}**, 360H = DP_n x 4H), 3.24 (s, **H^{n}**, 6H), 3.15 (q, **H^{e}**, J = 6 Hz, 4H), 2.95 (m **H^{h}+H$^{h'}$**, J = 6 Hz, 4H+4H), 1.85 (qt, **H^{d}**, J = 6 Hz, 4H), 1.35 (m, **H^{i}+H$^{i'}$**, 4H+4H), 1.23 (m, **H^{j}+H$^{i'}$**, 4H+4H).

Note: the H^{h} signals appears as a quintuplet, while the expected multiplicity would have been a dedoubled triplet, or quadruplet (if the coupling constants were identical). A hypothesis to explain why it appears as a quintuplet, is that in fact the two CH_2 are not equivalent and they have a difference in chemical shift equal to their coupling constant, so while on their own, they should give quadruplets, the two together give a quintuplet.

SEC measurements also indicated that the product was pure, although SEC in DMF showed a slight shouldering of the signal towards lower molecular weights, which could be due to trace amounts of PEO-C_6-U-C_6-PEO. Nevertheless, the retention time is similar but slightly smaller than PEO-$_{4K}$, consistent with the expected molecular weight (~4500 g/mol).

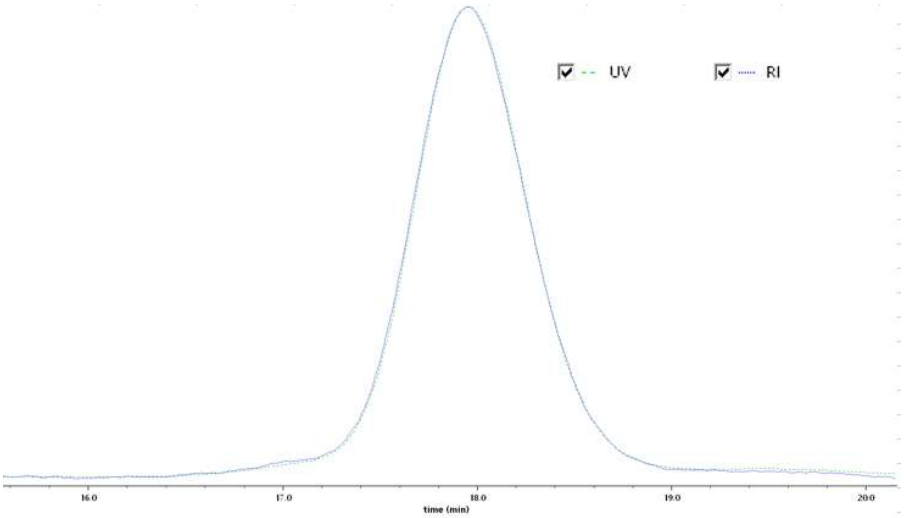

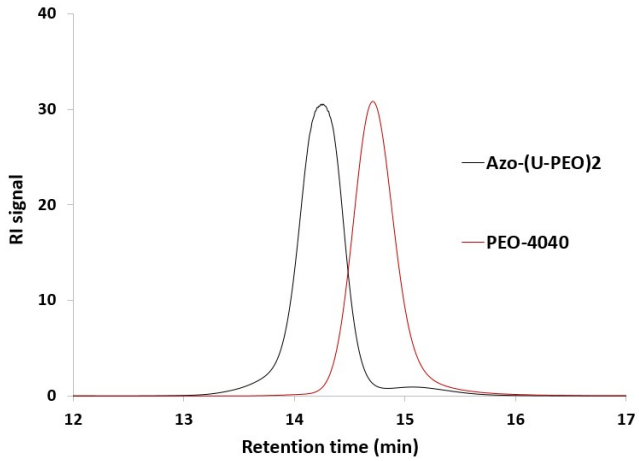

Figure C2-30. SEC-HPLC chromatogram of the purified product (in THF) (UV detector at 254 nm) (**top**), and in DMF (with 1 g/L LiBr), with a PEO-4K for comparison (**bottom**).

V. Annex 1 – Synthesis of an aromatic amine-terminated PEO

Attempts to synthesize an aromatic amine terminated PEO were carried out, in the aim of being able to couple it using triphosgene to the azobenzene diamine **3'**. However, these syntheses were carried out in a similar timeframe as the syntheses involving diisocyanates as well as the test reactions with triphosgene; and since the diisocyanate related syntheses appeared to be giving more promising results compared to those with triphosgene (even with aromatic amines), this route was not fully explored. Nonetheless, the results that were obtained are presented in this annex.

1. Results and discussion

Since the synthesis of ureas from amines using triphosgene appeared to work better when starting with an aromatic amine, a new strategy was explored, involving the synthesis of a PEO chain end-functionalized with an aromatic amine.

To this end, a first synthetic pathway was explored, described in **Scheme C2-25**. The strategy was to first end-functionalize a PEO with an aromatic nitro group, which could then be reduced to an amine, and finally couple to the azobenzene-diamine **3** through triphosgene urea synthesis.

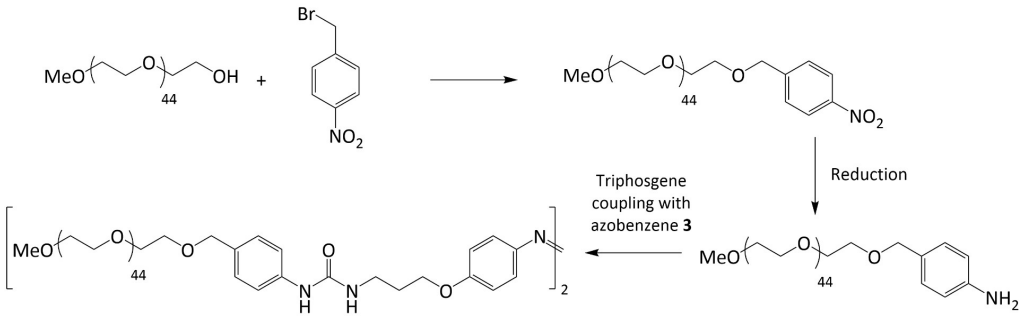

Scheme C2-25. Synthesis route to target compound through the synthesis of aromatic amine terminated PEO followed by triphosgene coupling

<u>Synthesis of PEO-Ar-NO_2:</u>

The first conditions tested consisted in solubilizing 1 eq. of PEO-OH (M_n = 2000 g/mol) in anhydrous THF, followed by the addition of 20 eq. of NaH, in order to deprotonate the terminal hydroxyl group. After two hours of stirring at r.t., 10 eq. of para-nitrobenzylbromide were added, and the initially colorless solution instantly became black. After two days of reaction, the polymer was precipitated, and no conversion whatsoever was observed in ^{1}H NMR. Two test syntheses were repeated using these conditions, one with the polymer and one without. The one containing the polymer became once again black as soon as the nitrobenzylbromide was added, and the one without polymer turned yellow upon nitrobenzylbromide addition, and the solution was black the next day. Another test was performed using the same initial reaction conditions, but with benzyl bromide (without the nitro group), and the solution did not turn black (even with the polymer present). The results seem to indicate that an unidentified side reaction occurred, that was somehow accelerated when the polymer was present, and only took place if the benzyl bromide had a nitro group.

Since the unwanted side-reaction seemed to occur between the hydride and the nitro group, alternative bases were tested. To this end, trimethylamine (TEA) was employed instead of NaH, all other conditions remaining

constant. After 17 hours of reaction time, ^{1}H NMR revealed that it was in fact the TEA that had reacted with the nitrobenzylbromide. Replacing the TEA by tBuOK led to the solution once again turning black upon addition of nitrobenzylbromide, and after 17 hours of reflux, no conversion was measured.

Since the nitro group appeared to be somewhat problematic, a slightly different approach was explored, involving NHBoc protected amines, based on already described literature (see **Scheme C2-26**). On one hand, tosylated PEO-OH was prepared, transforming the initial hydroxyl moiety into a good leaving group. On the other hand, the amine of 4-aminophenol was protected with Boc_2O, allowing for the phenolic alcohol to then undergo a SN reaction with the tosylated PEO. The protected amine could then be deprotected through acidic hydrolysis, which could be coupled to the azobenzene-diamine core **3** using triphosgene.

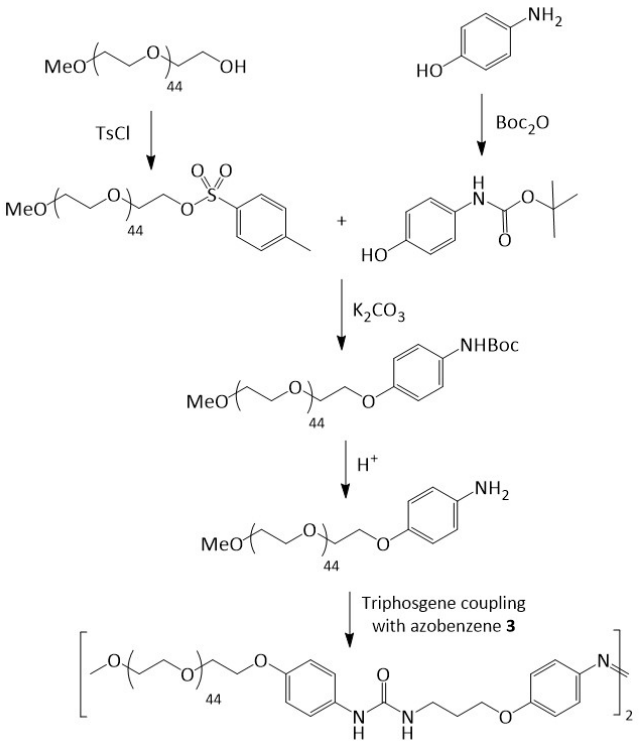

Scheme C2-26. Second synthetic route involving aromatic amine terminated PEO

<u>Synthesis of NHBoc protected phenol:</u>

The protection of the amine proceeded smoothly by slowly adding 1 eq. of Boc_2O in THF to a solution of 1 eq. of 4-aminophenol in THF at 0°C, and then letting it react for 24 hours. At the end of the reactions, the solvent was removed under vacuum, yielding the pure product in quantitative yield, as indicated by ^{1}H NMR which revealed the apparition of a singlet at 1.50 ppm, corresponding to the t-butyl protons, and large singlet at 6.36 ppm, corresponding to the NH signal of the carbamate (**Figure C2-32).**

<u>Synthesis of PEO-OTs:</u>

1 eq. of PEO-OH (M_n = 2000 g/mol) was solubilized in a mixture of DCM/pyridine (8/2 v/v), and a solution of TsCl (5 eq.) in pyridine was slowly added to the polymer solution at 0°C. The reaction was then left to pursue, and after 19 hours of reaction time, ^{1}H NMR revealed a conversion of 90%. Workup was performed by transferring the crude to cold 6M aq. HCl, and the product was extracted using DCM. The combined organic phases were further washed with 2M HCl, followed by drying over $MgSO_4$. ^{1}H NMR of the purified product revealed a conversion of 90-95%, with the apparition of aromatic signals of the tosyl part as well as the $–CH_2$-OTs being deshielded to 4.15 ppm (**Figure C2-31**). Addition of TCAI to the product indicated that no PEO-OH was left.

Synthesis of PEO-Ar-NHBoc:

This protocol was adapted from the literature.[10] 10 eq. of Boc protected amino-phenol was solubilized in dry DMF at 80°C, leading to a brown solution. 10 eq. K_2CO_3 were added, which turned the solution dark green, and 1 eq. PEO-OTs was added. The solution was slightly concentrated under vacuum, and precipitated in diethyl ether. ^{1}H NMR indicated quantitative functionalization of the PEO, although further purification would have been required to remove salts. Due to the success of the second synthetic strategy using HMDI that had been carried out in parallel, this synthetic route was not further pursued. Furthermore, the control experiment consisting in coupling butyl-aniline and PEO-NH_2 with triphosgene was carried out in a similar timeframe as this synthetic route had been explored, and since its conversion was of only 40%, triphosgene based routes were deemed insufficient for this project. Despite previous projects in our team having relied on the use of triphosgene based coupling of amines to yield ureas with quantitative yields, we are not quite sure why a conversion of only 40% was obtained while using exactly the same experimental protocol. It was also deemed preferable to have alkyl spacers, both due to their flexibility, and the ability to tailor their length in order to have some degree of control of the hydrophobicity of the core.

2. Experimental details

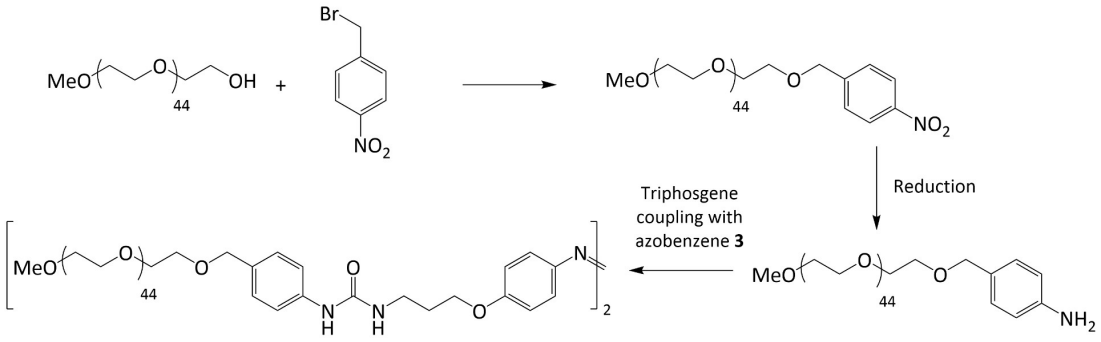

Scheme C2-27. First synthetic route explored involving the synthesis of aniline terminated PEO

Synthesis of aromatic nitro terminated PEO

A typical procedure consisted in placing 20 eq. of base in the round bottom flask, under argon atmosphere, followed by the addition of a solution of 3.2 g of PEO-OH (M_n = 2000 g/mol, 1 eq.) in 40 mL of anhydrous THF. The solution was stirred for 2 h, and then 10 eq. of p-nitrobenzyl bromide (3.46 g) was added. When the chosen base was NaH or tBuOK, the solution instantly became black upon addition of the nitrobenzyl bromide, and no

conversion was measured using ^{1}H NMR after two days of reaction time at 30°C. When TEA was selected as base, the solution did not become black.

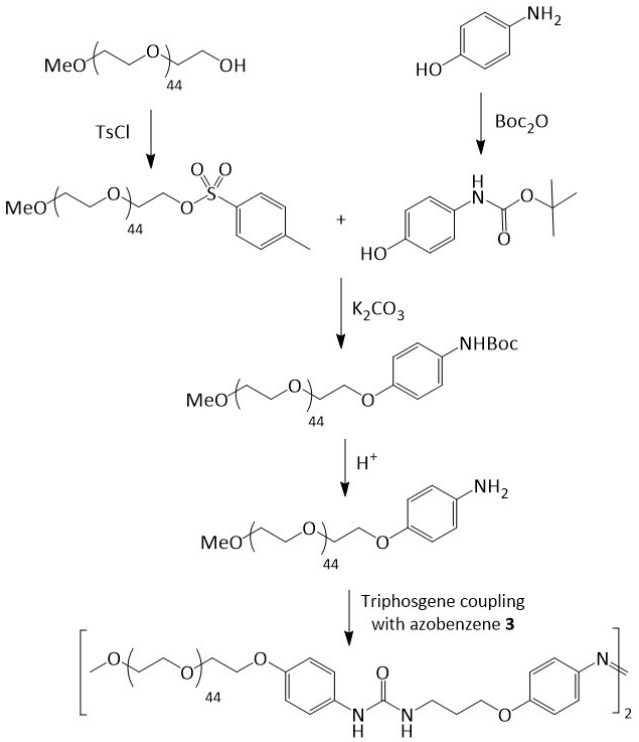

Scheme C2-28. Second synthetic route explored involving the synthesis of aniline terminated PEO

<u>Synthesis of tosylated PEO:</u>

This protocole was adapted from ref[10]. In a round bottom flask, 3 g of PEO-OH (M_n = 2000 g/mol, 1 eq.) were solubilized in 2.4 mL of pyridine and 0.6 mL of DCM under argon atmosphere, and was then cooled in an ice bath to 0 °C. A solution of 5 eq. of tosyl chloride (1.425 g) in 5 mL of pyridine was added to the PEO solution over the course of 24 h using a syringe pump. The solution was maintained for as long as possible at 0 °C. The reaction was left for 19 more hours, after which ^{1}H NMR indicated 90 % conversion. The reaction mixture was treated by pouring it into 50 mL of cold 6 M aqueous HCl, and the polymer was extracted using DCM (3 x 30 mL). The combined organic phases were washed twice with 2 M aqueous HCl (2 x 50 mL), dried over magnesium sulfate, and DCM was evaporated under reduced pressure. ^{1}H NMR indicated 90-95% conversion and addition of TCAI revealed that no PEO-OH was left. 2.9 g of product were obtained, corresponding to a yield of 91 %. The ^{1}H NMR spectrum also revealed that trace amounts of TsOH were present, but no further purification was done.

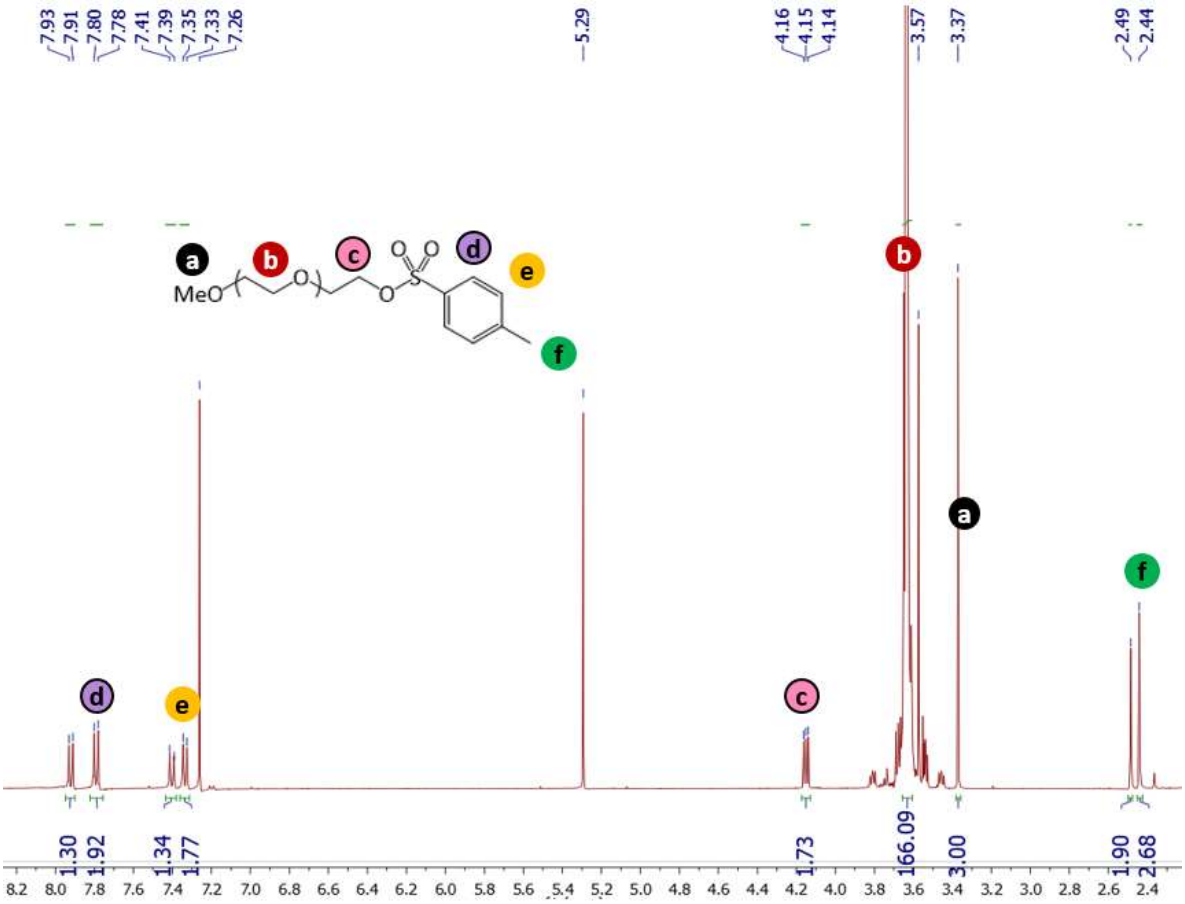

Figure C2-31. ^{1}H NMR ($CDCl_3$, 400 MHz) of the product. The extra peaks at 7.92, 7.39 and 2.49 ppm correspond to traces of TsOH

^{1}H NMR ($CDCl_3$, 400 MHz): δ (ppm) 7.79 (d, **H^{d}**, J = 8.8 Hz, 2H), 7.34 (t, **H^{e}**, J = 8.8 Hz, 2H), 4.15 (t, **H^{c}**, J = 4.8 Hz, 2H), 3.63 (s, **H^{b}**, 180H), 3.37 (s, **H^{a}**, J = 6, 3H), 2.44 (s, **H^{f}**, 3H)

<u>Boc protection of amino phenol:</u>

12 g of 4-amino phenol were solubilized in 300 mL of anhydrous THF in a round bottom flask under argon atmosphere. The solution was cooled to 0 °C in an ice bath, and 24 g (1 eq.) of Boc_2O were added. The mixture was vigorously stirred for 24 h at r.t., followed by evaporation of the solvent under reduced product, affording pure product in quantitative yield (23 g).

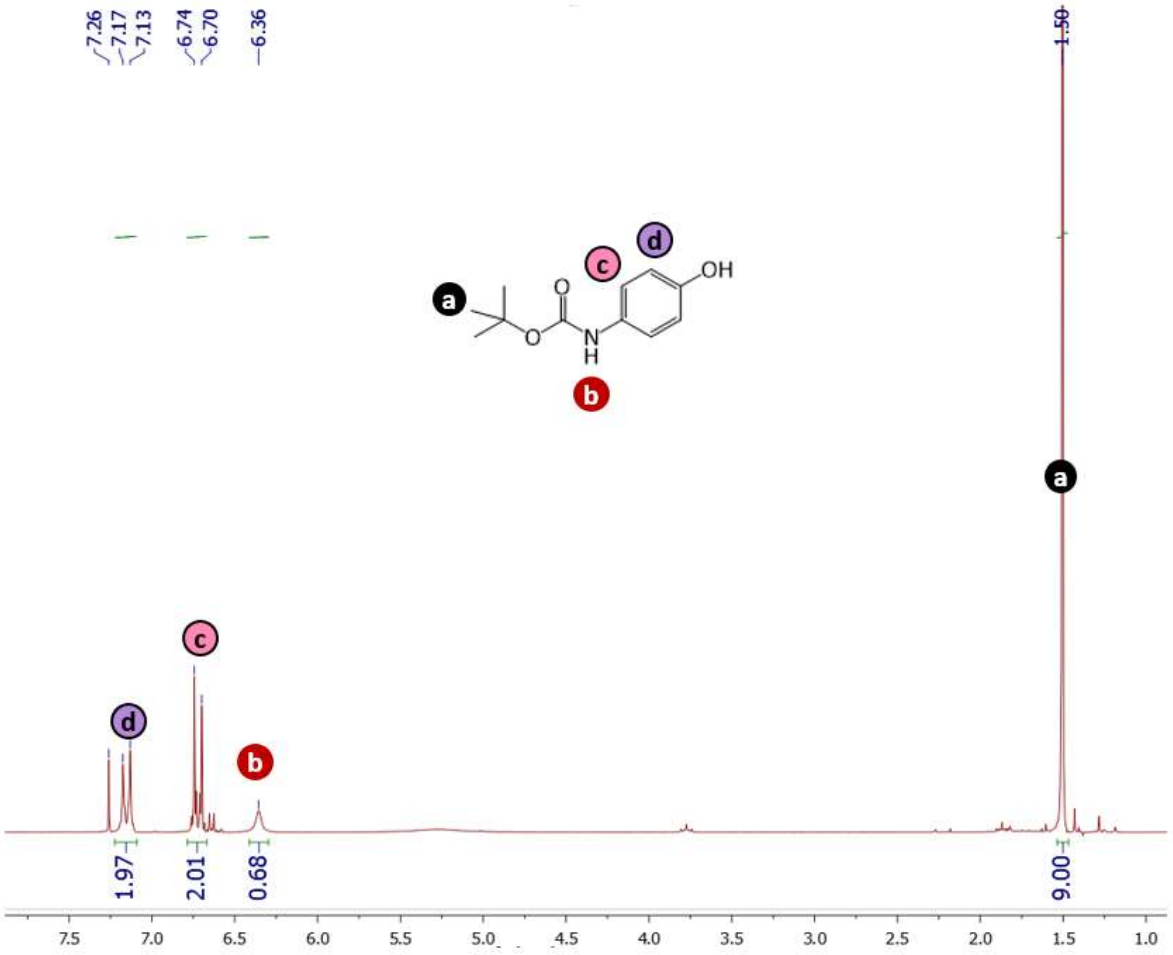

Figure C2-32. ^{1}H NMR ($CDCl_3$, 200 MHz) of the product

^{1}H NMR ($CDCl_3$, 200 MHz): δ (ppm) 7.15 (d, **H^{d}**, J = 9.0 Hz, 2H), 6.72 (t, **H^{c}**, J = 9.0 Hz, 2H), 6.36 (s, **H^{b}**, 1H), 1.50 (s, **H^{a}**, 9H)

Synthesis of PEO-Ar-NHBoc

250 mg (10 eq.) of Boc protected phenol were dissolved in 6 mL of dry DMF in a round bottom flask under argon atmosphere and were heated to 80 °C. 10 eq. of K_2CO_3 were added under argon flow, followed by 250 mg (1 eq.) of PEO-OTs. The solution went from brown to dark green after the addition of K_2CO_3. The reaction was left overnight, and the solution was concentrated under vacuum and then precipitated in diethyl ether. ^{1}H NMR revealed quantitative functionalization due to the shift of the –CH_2-O signal, however further purification was not done.

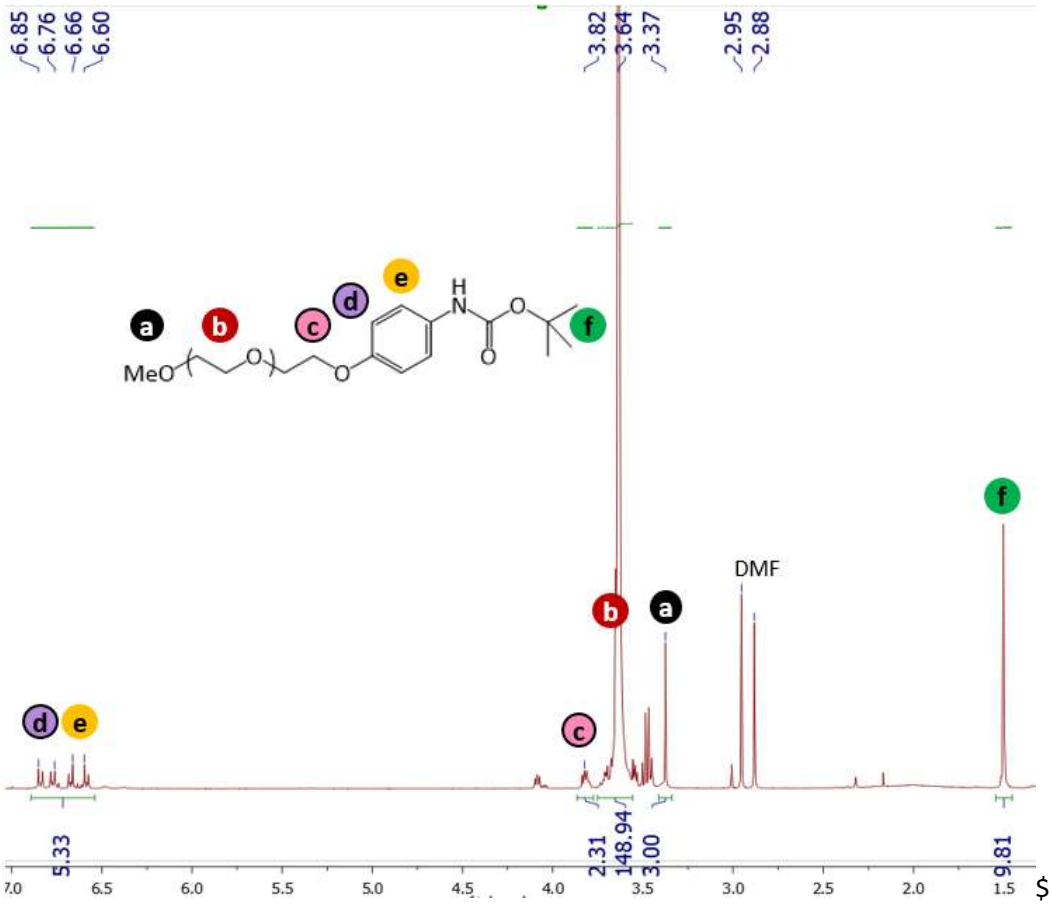

Figure C2-33. ^{1}H NMR ($CDCl_3$, 400 MHz) of the crude polymer

VI. Annex 2 – Synthesis of an azobenzene-bisurea RAFT agent

The aim here was to synthesize a RAFT agent containing an azobenzene and a bis-urea. The general structure resembles the one of Azo-(U-PEO)$_2$ but with a trithiocarbonate as RAFT agent instead of PEO polymer arms: Azo-(U-TTC)$_2$. Two synthetic routes were explored, the first being the synthesis of an aliphatic amine-functionalized trithiocarbonate and its coupling to the azobenzene diamine **3'** using triphosgene. These syntheses were carried out in parallel to the triphosgene coupling attempts involving PEO, and also did not work unfortunately. An alternative synthetic strategy was investigated, involving the use of commercially available 3-chloropropyl isocyanate. This synthetic route appeared to be promising, but was not fully finished due to lack of time, and no RAFT polymerizations were carried out.

1. Results and discussion

i. First strategy – with urea yielding final coupling

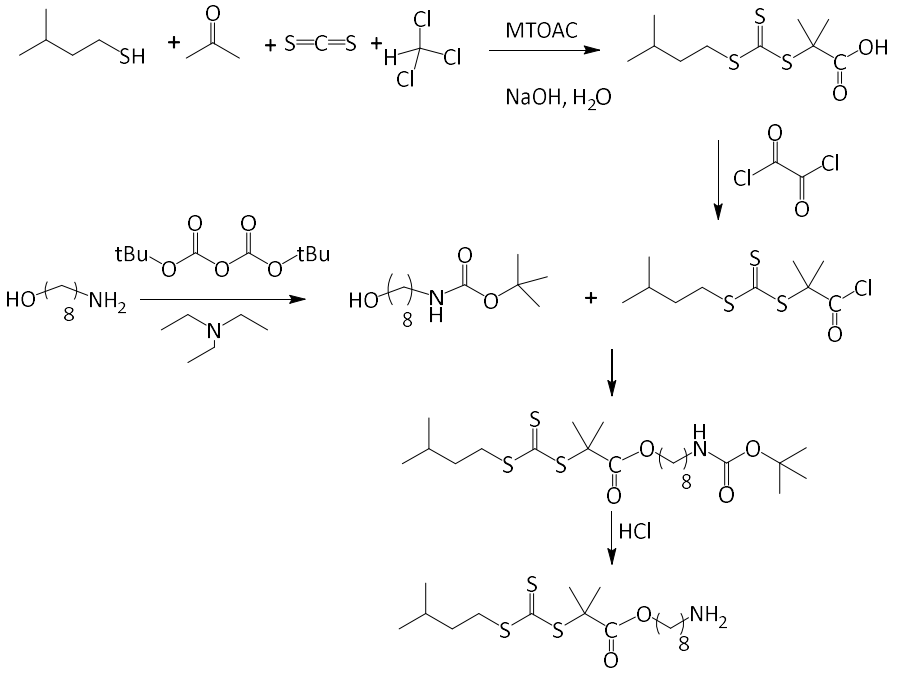

Scheme C2-29. First synthetic strategy to access Azo-(U-TTC)$_2$

As can be seen in **Scheme C2-29**, the first synthetic strategy consisted in first synthesizing a trithiocarbonate functionalized with a carboxylic acid, its activation with oxalyl chloride to esterify it with Boc-protected amino-hexanol, and finally the deprotection of the amine through acidic hydrolysis. The aim was to then couple it with azobenzene diamine **3'** using triphosgene. All steps were adapted from ref[11].

Synthesis of TTC-COOH:

This reaction was carried out using chloroform, acetone, carbon disulfide with concentrated aqueous NaOH, and tributylmethyl ammonium chloride as phase transfer agent. First, a mixture of thiol, acetone, and phase transfer agent is prepared. Concentrated NaOH is then added, which deprotonates the thiol. CS_2 is then added, onto which the thiolate undergoes nucleophilic addition. Chloroform is then added, which reacts with NaOH to form a carbene, which in turn reacts with acetone to form a dichloro-epoxyde through cycloaddition. Finally, the

trithiocarbonate anion opens the epoxyde ring through nucleophilic addition, and the carboxylate is formed through hydrolysis of the chlorines.

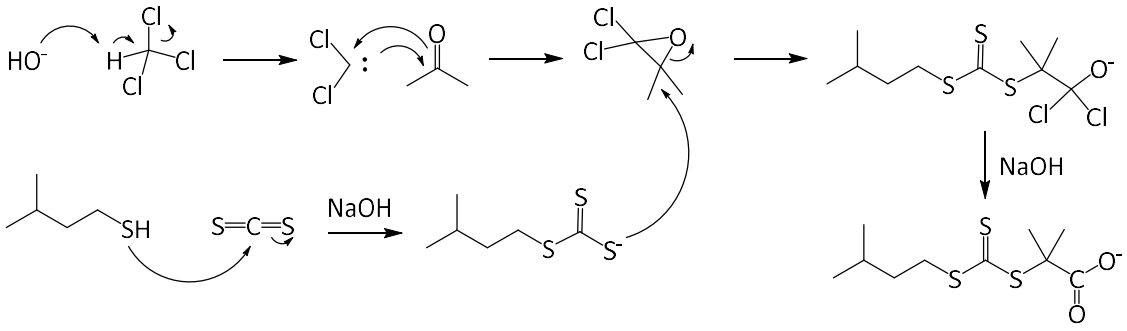

Scheme C2-30. Proposed mechanism leading to the formation of TTC-COOH

After purification, 58,3 g (49.5%) of yellow powder is obtained **(Figure C2-34**).

Boc protection of HO-C_8-NH_2:

The reaction proceeded smoothly in anhydrous DCM using 1.05 eq. Boc_2O with 1.05 eq. TEA as catalytic base. After purification, 2.54 g of pure product were recovered (quant. yield). ^{1}H NMR indicated the apparition of a singlet at 1.30 ppm, corresponding to the tert-butyl methyls, confirming the reaction had occurred (**Figure C2-35**).

Esterification of TTC-COOH with HO-C_8-NHBoc:

This reaction was performed in two steps: firstly, TTC-COCl was formed through reaction with oxalyl chloride in DCM, and then the esterification was performed by introducing a solution of HO-C_8-NHBoc. After a night at reflux, purification was achieved, yielding pure product as a yellow oil (63% yield). ^{1}H NMR indicated that the methylene in alpha position to the hydroxyl group had shifted from 3.63 ppm to 4.07 ppm, confirming the success of the reaction (**Figure C2-36**).

Deprotection of TTC-C_8-NHBoc:

The NHBoc protecting group was removed by treating the compound with 4M HCl in dioxane at 0°C. After a night of reaction, the product was recovered as a yellow oil in quantitative yield. ^{1}H confirmed that the reaction had occurred, as a new peak at 8.24 ppm integrating for 3H had appeared, corresponding to the newly formed ammonium protons (**Figure C2-37**).

The next step involved the coupling of the amine functionalized TTC with the azobenzene diamine core (see **Scheme C2-31**).

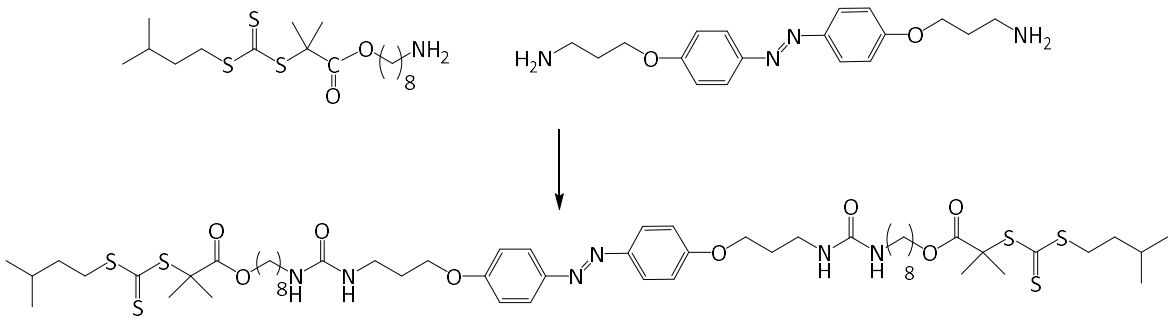

Scheme C2-31. Coupling of TTC-C_8-NH_2

The same conditions that were used for the triphosgene coupling with PEO were tested (using DBU as base), but ^{1}H NMR indicated no urea formation. While the reaction could have been carried out using an excess of the TTC-NH_2, no further attempts of this reaction were carried out due to lack of time and considering the conclusions reached in parallel on this coupling strategy.

ii. Second strategy – involving the use of isocyanate

An alternative strategy was explored, consisting in using commercially available isocyanate for the synthesis (see **Scheme C2-32**). Firstly, 6-aminohexanol was reacted with 3-chloropropylisocyanate to form the urea. Note that no protection of the alcohol was required due to the amine being far more nucleophilic. Then, Williamson etherification was achieved between 4,4'-dihydroxyazobenzene and chlorinated urea, note again that no protection of the aliphatic alcohol was required (to avoid competition in terms of nucleophilic substitution) since the base that was used (K_2CO_3) is strong enough to deprotonate the phenols but not aliphatic alcohols. Lastly, an attempt to esterify the azobenzene-diol with TTC-COOH was carried out, using carbonyl-diimidazole (CDI) to activate the alcohol. Since the azobenzene diol was only soluble in DMSO at 80°C, CDI mediated esterification was selected as it had been used in previous work by our team in these conditions.

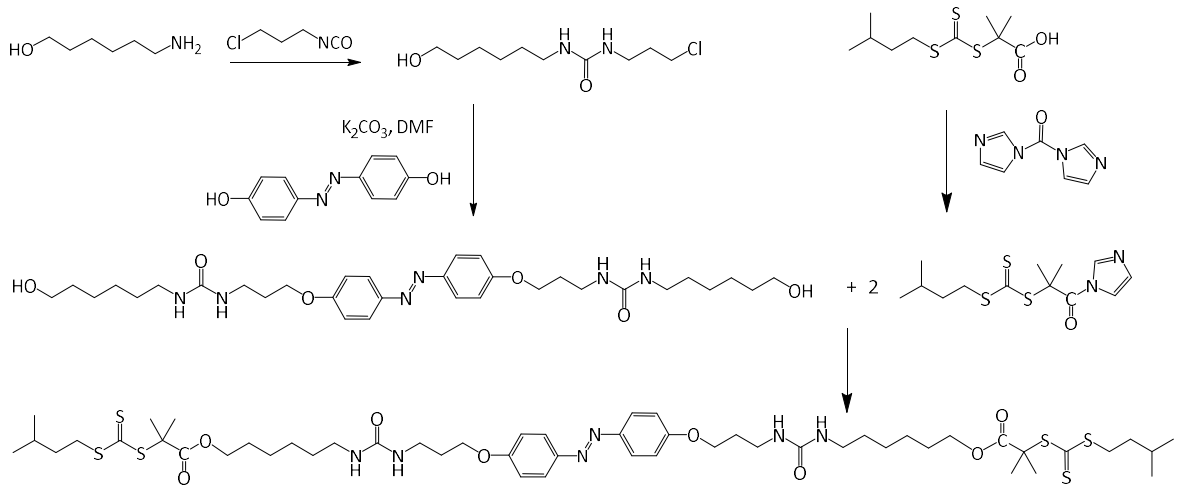

Scheme C2-32. Synthesis of Azo-(U-TTC)$_2$ involving the use of chloropropylisocyanate

<u>Synthesis of HO-C_6-U-C_3-Cl:</u>

This reaction was achieved by reaction of 6-aminohexanol in DCM with 3-chloropropyl isocyanate. After a minute of reaction time, the solution solidified into a white block. More DCM was added, and the product was filtered and pure product was recovered after solvent evaporation (85% yield), see **Figure C2-38**.

Williamson etherification between dihydroxyazobenzene and HO-C_6-U-C_3-Cl:

The same conditions that were used for the Williamson etherification for the synthesis of azobenzene **2** were used here. After purification, ^{1}H NMR was conducted at 80°C (the product was otherwise insoluble), which revealed that the reaction had taken place, since the –CH_2-Cl peak at 3.60 ppm had disappeared and the newly formed –CH_2-O-Azo peak appeared at 4.11 ppm (**Figure C2-39**). The product was recovered as a golden powder in 91% yield.

Due to lack of time, the last step has not yet been investigated.

2. Experimental details

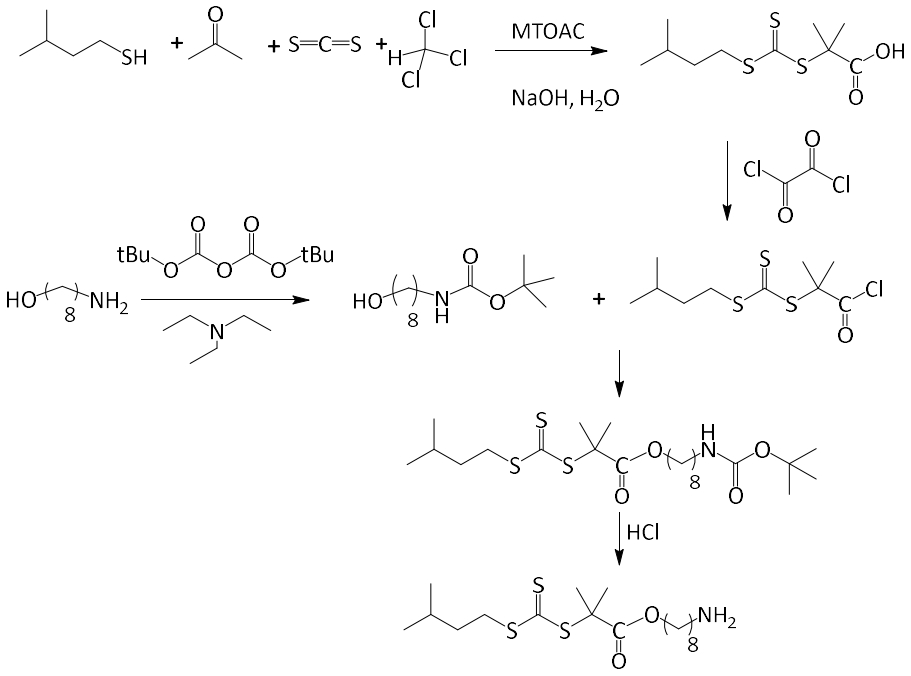

Scheme C2-33. First synthetic strategy for accessing Azo-(U-TTC)$_2$

Synthesis of TTC-COOH – adapted from ref[11]

In a round bottom flask, a solution of 55.2 mL of 3-methylbutanethiol in 280 mL of acetone and 10.6 g of tributylmethylammonium chloride was prepared at 0°C under argon atmosphere. Then, 50 mL of an aqueous NaOH (50 wt.%) solution was slowly added over the course of 10 minutes. The solution was vigourously stirred for 20 minutes, after which 28 mL of carbon disulfide in 80 mL acetone was added to the reaction mixture over the course of 5 minutes. The mixture was further mixed for 30 minutes, and 56 mL of $CHCl_3$ were then added followed by 130 mL of the same aqueous NaOH solution (50 wt.%) dropwise. The solution was left to react at r.t. overnight. The next day, solvent was removed under reduced pressure, and 31% aqueous HCl was added (140 mL) at 0°C to neutralize the crude. The mixture was filtered to remove salt, and then the product was extracted using DCM (150 mL, 100 mL and finally 50 mL DCM). The combined organic phases were washed with saturated

aqueous NaCl solution, dried over $MgSO_4$, and solvent was evaporated. The product was purified by recrystallization in pentane (10 g of crude product for 10 mL of pentane). ^{1}H NMR indicated the desired structure had been obtained. Since the product still smelled bad, it is possible that trace amounts of thiol were still present, but weren't detected by NMR.

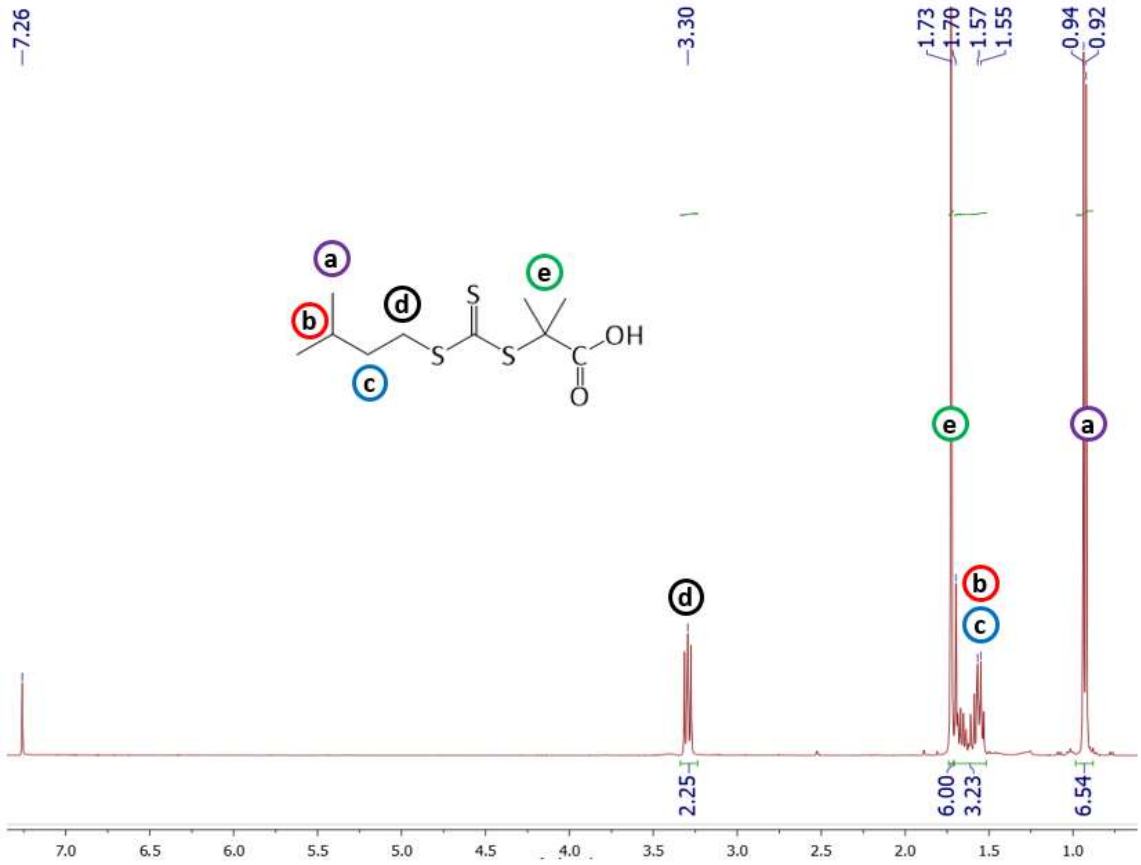

Figure C2-34. ^{1}H NMR ($CDCl_3$, 400 MHz) of pure TTC-COOH

^{1}H NMR ($CDCl_3$, 400 MHz): δ (ppm) 3.30 (t, **H^d**, J = 7.6 Hz, 2H), 1.73 (s, **H^e**, 6H), 1.70-1.55 (m, **H^b+H^c**, 1+2=3H), 0.93 (d, **H^a**, J = 6.4 Hz, 6H).

<u>Boc protection of HO-C_8-OH - adapted from ref</u>[11]

1 g of 8-aminooctanol (1 eq., 6.89 mmol) was solubilized under argon atmosphere in 17 mL anhydrous DCM in a round bottom flask at 0°C. Then, 1.05 eq. of TEA (1 mL) was slowly added dropwise followed by 1.05 eq. of Boc_2O (1.6 mL), again dropwise. The reaction was left overnight at r.t. The next day, solvent was evaporated, and Et_2O was added, leading to a turbid mixture. The organic phase was washed with 15 mL 1M HCl, after which the phase was no longer turbid. The organic phase was further washed with 3 x 15 mL water, dried over $MgSO_4$, and solvent was removed, yielding 1.44 g of pure product.

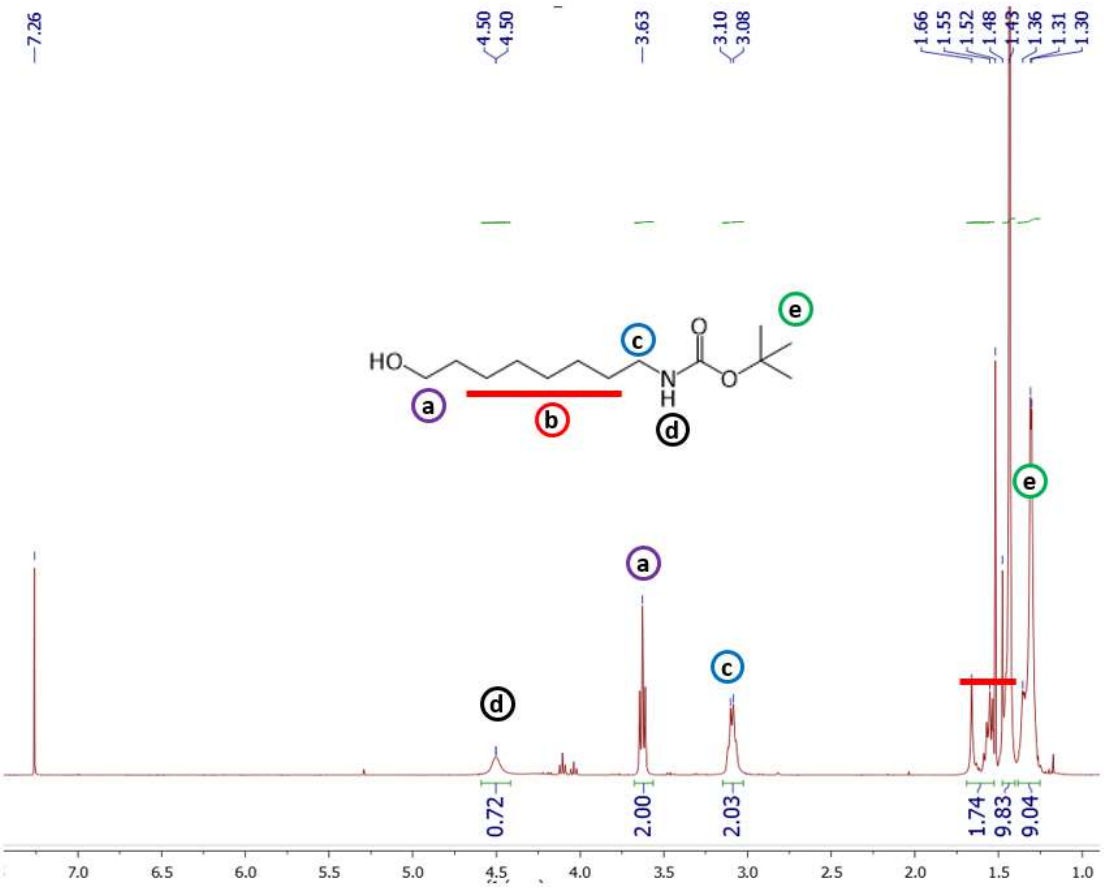

Figure C2-35. ^{1}H NMR ($CDCl_3$, 400 MHz) of the pure, Boc protected product

^{1}H NMR ($CDCl_3$, 400 MHz): δ (ppm) 4.50 (s br, **H^{d}**, 1H), 3.63 (t, **H^{a}**, J = 6.4 Hz, 2H), 3.09 (q, **H^{c}**, J = 6.8 Hz, 2H), 1.66-1.43 (m, **H^{b}**, 12H), 1.30(m, **H^{e}**, 9H)

<u>Esterification of TTC-COOH with HO-C_8-NHBoc – adapted from ref</u>[11]

1.07 g of TTC-COOH (1 eq., 4 mmol) was solubilized in 4 mL of dry DCM under argon atmosphere. 3 eq. (1 mL) of oxalyl chloride was slowly added, and the solution was refluxed for a few hours until the solution turned dark red. DCM and excess oxalyl chloride were then removed under vacuum. A solution of 1.5 eq. HO-C_8-NHBoc in 4 mL of anhydrous DCM was then added, and the solution was refluxed overnight. The next day, solvent was evaporated, and the resulting oil was dissolved in 40 mL Et2O, and washed with 40 mL saturated aqueous NaHCO3 solution, 40 mL saturated aqueous NaCl solution, and finally 40 mL water. The organic phase was dried over $MgSO_4$, and solvent was removed under vacuum. The crude product still contained 25% of the initial alcohol (according to 1H NMR), and was therefore purified by column chromatography, using EtOAc/Petroleum Ether (40-60°C fraction) 1:4 (v/v), yielding 1.26 g pure product as a yellow oil (63%).

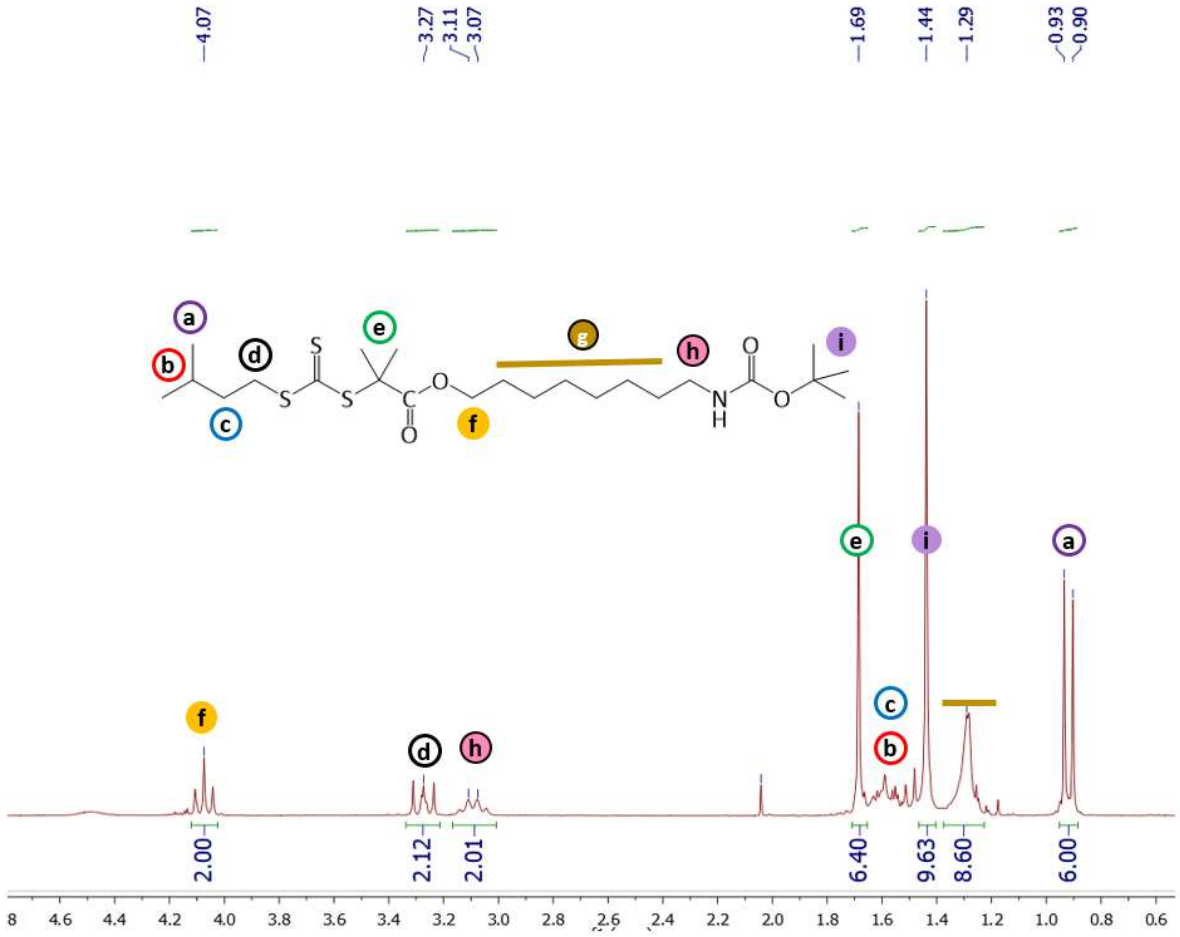

Figure C2-36. ^{1}H NMR (CDCl3, 200 MHz) of pure TTC-C_8-NHBoc

^{1}H NMR ($CDCl_3$, 200 MHz): δ (ppm) 4.07 (t, **H^{f}**, J = 6.4 Hz, 2H), 3.27 (t, **H^{d}**, J = 7.6 Hz, 2H), 3.09 (q, **H^{h}**, J = 7.0 Hz, 2H), 1.69 (s, **H^{e}**, 6H), 1.69-1.44 (m, **H^{b}+H^{c}**, 1+2=3H), 1.44 (s, **H^{i}**, 9H), 1.29 (s br, **H^{g}**, 6H), 0.91 (s, **H^{a}**, 6H).

<u>Deprotection of TTC-C_8-NHBoc – adapted from ref</u>[11]

1 g of TTC-C_8-NHBoc (1 eq., 2.15 mmol) was mixed with 1.63 mL of 4M HCl in dioxane under argon at 0°C. The reaction was left to proceed overnight at r.t. The next day, workup was performed by sampling evaporating solvent and acid, yielding pure product in quantitative yield as a yellow oil.

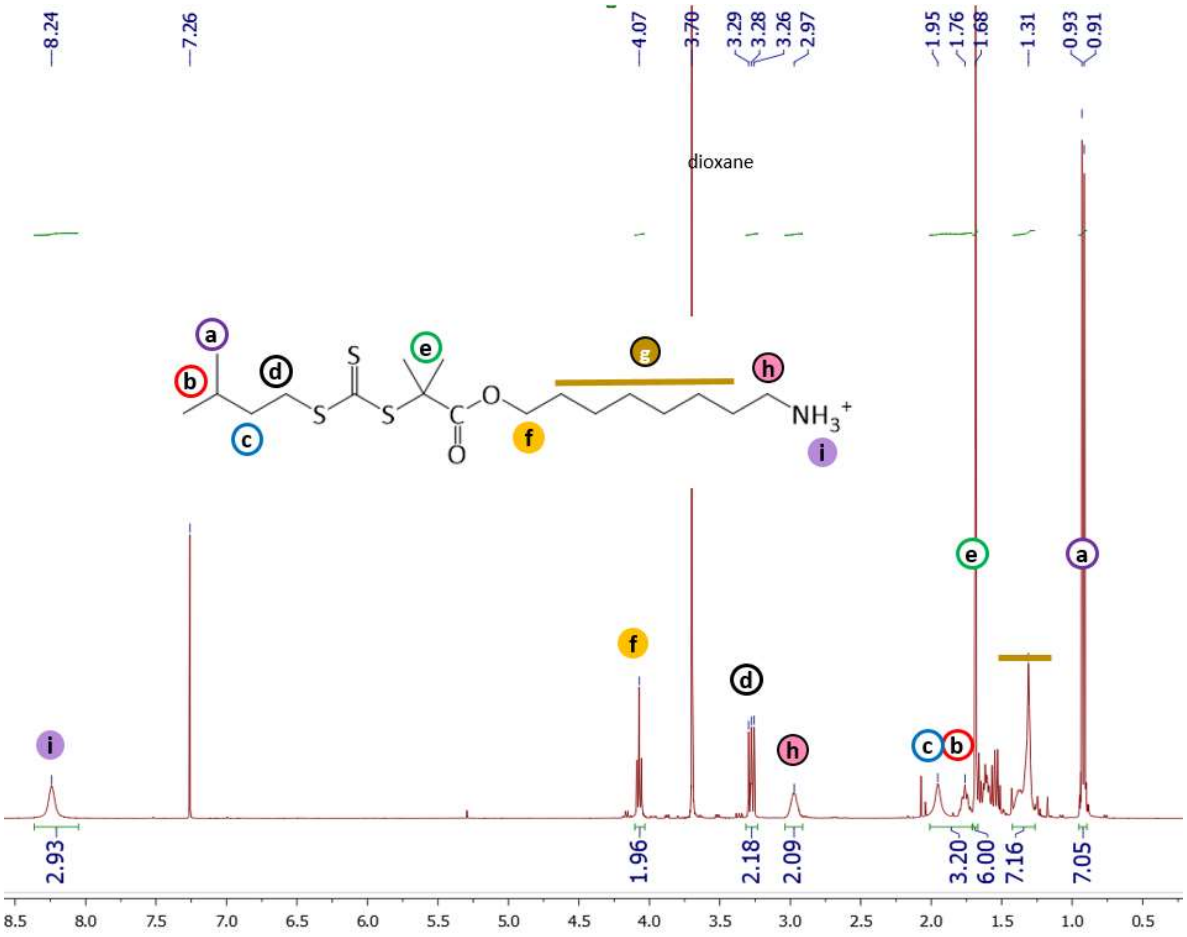

Figure C2-37. ^{1}H NMR (CDCl3, 400 MHz) of pure TTC-C_8-NH_3^+

^{1}H NMR ($CDCl_3$, 400 MHz): δ (ppm) 8.24 (s br, **H^{i}**, 1H), 4.07 (t, **H^{f}**, J = 6.4 Hz, 2H), 3.28 (t, **H^{d}**, J = 7.6 Hz, 2H), 2.97 (hex, **H^{h}**, J = 6 Hz, 2H), 1.95-1.76 (m, **H^{b}+H^{c}**, 1+2=3H), 1.68 (s, **H^{e}**, 6H), 1.31 (s br, **H^{g}**, 6H), 0.91 (s, **H^{a}**, 6H).

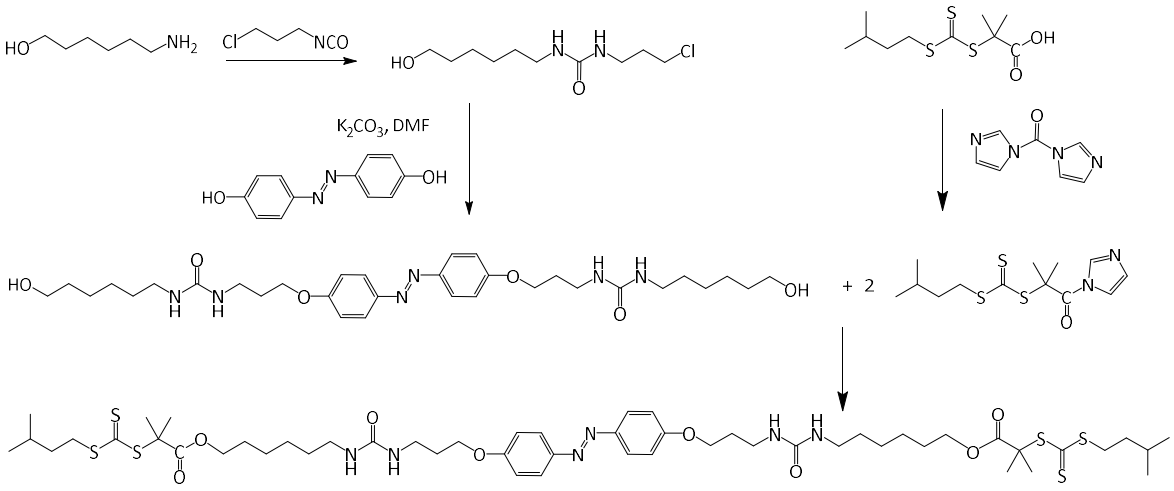

Scheme C2-34. Second synthetic strategy for accessing Azo-(U-TTC)$_2$

Synthesis of HO-C_6-U-C_3-Cl:

1 g (1,1 eq.) of 6-aminohexanol was solubilized in 10 mL of anhydrous DCM with a spatula point of powder molecular sieves under argon atmosphere. The mixture was stirred for 30 minutes, and 0.92 g (0.8 mL, 1 eq.) of 3-chloropropyl isocyanate was added dropwise. The mixture rapidly solidified, and 10 mL of additional DCM were added, and the round bottom flask was placed in a warm water bath for a few minutes. The mixture was then left to return to r.t. for 20 minutes, filtered, and washed with DCM. The product was recovered as a white powder in 85% yield.

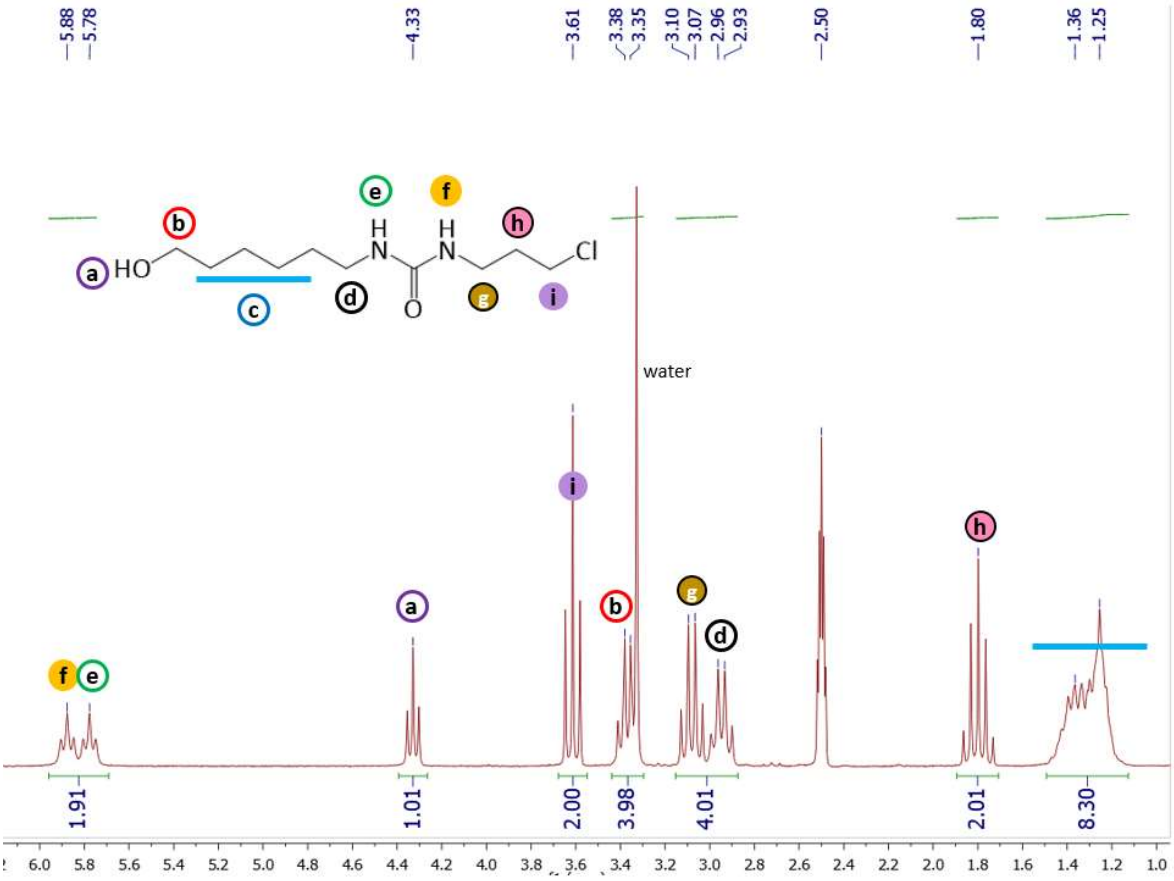

Figure C2-38. ^{1}H NMR (DMSO, 200 MHz) of pure HO-C_6-U-C_3-Cl

^{1}H NMR (DMSO, 200 MHz): δ (ppm) 5.88 (t, **H^f**, J = 6 Hz, 1H), 5.78 (t, **H^e**, J = 5.8 Hz, 1H), 4.33 (t, **H^a**, J = 5.0 Hz, 1H), 3.61 (t, **H^i**, J = 6.6 Hz, 2H), 3.36 (q, **H^b**, J = 5.0 , 2H), 3.08 (q, **H^g**, J = 6 Hz, 2H), 2.95 (t, **H^d**, J = 5.8 Hz, 2H), 1.80 (qt, **H^h**, J = 6.6 Hz, 2H), 1.36-1.25 (m, **H^c**, 8H).

Williamson etherification between dihydroxyazobenzene and HO-C_6-U-C_3-Cl:

In a round bottom flask were placed 300 mg of 4,4'-dihydroxyazobenzene (1 eq., 1.4 mmol), 732 mg of HO-C_6-U-C_3-Cl (2.2 eq.), 970 mg K_2CO_3 (5 eq.) and 6 mL of DMF, under argon atmosphere. The reaction was left to proceed overnight at 100°C. The next day, the mixture was left to cool down to r.t., and a precipitate formed, which was filtered off and washed with water followed by Et_2O. The powder was then dried, and ^{1}H NMR indicated that

product had been recovered in 91% yield. ^{1}H NMR indicated two small aromatic doublets that might correspond to unreacted azobenzene, but further purification was not pursued due to lack of time.

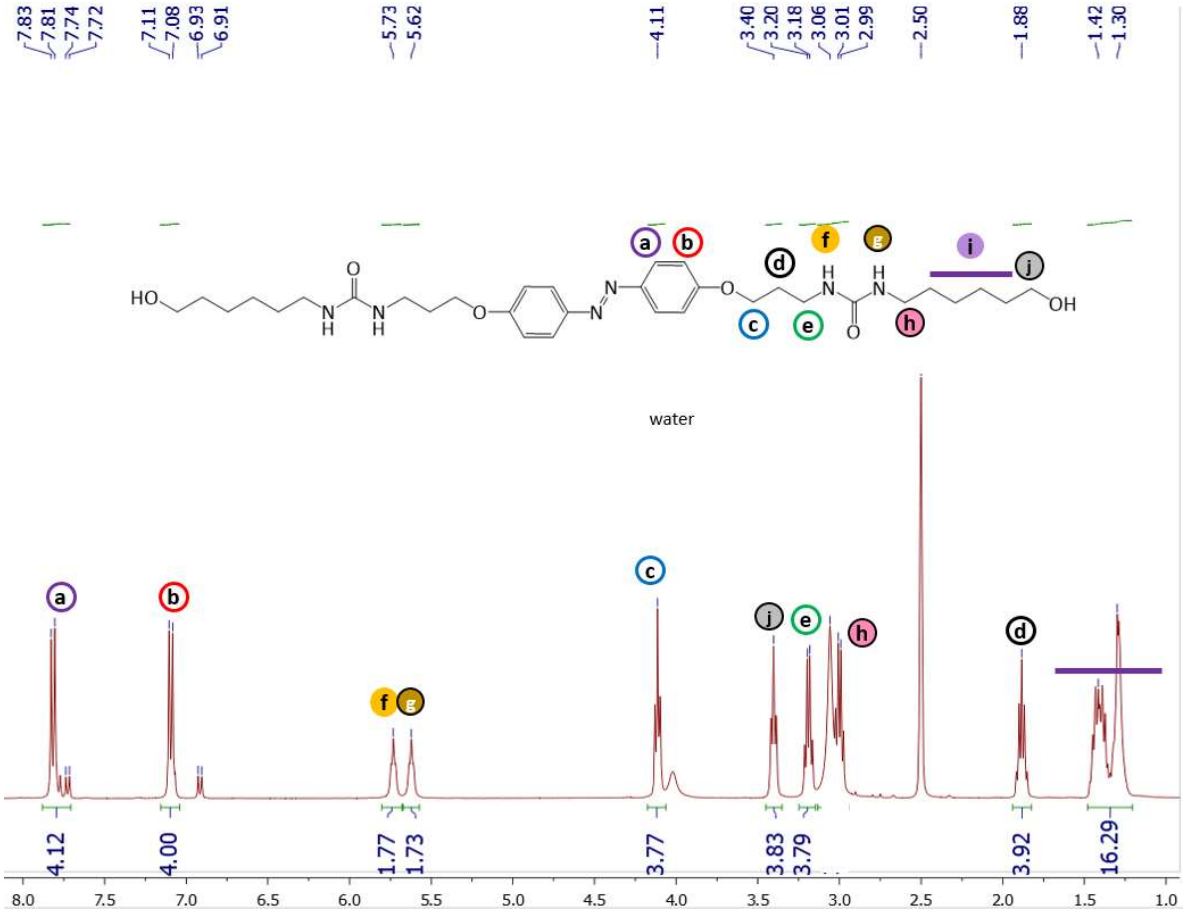

Figure C2-39. ^{1}H NMR (DMSO, 400 MHz, 80°C) of Azo-(C_3-U-C_6-OH)$_2$

^{1}H NMR (DMSO, 400 MHz): δ (ppm) 7.82 (d, **H^{a}**, J = 8.8 Hz, 4H), 7.10 (d, **H^{b}**, J = 8.8 Hz, 4H), 5.73 (t, **H^{f}**, J = 6.4 Hz, 2H), 5.62 (t, **H^{g}**, J = 6.4 Hz, 2H), 4.11 (t, **H^{c}**, J = 6.0 Hz, 4H), 3.40 (t, **H^{j}**, J = 6.4 Hz, 4H), 3.19 (q, **H^{e}**, J = 6.4 Hz, 4H), 3.00 (q, **H^{h}**, J = 6.4 Hz, 4H), 1.88 (qt, **H^{d}**, J = 6.4 Hz, 4H), 1.42-1.30 (m, **H^{i}**, 16H).

Note: the water peak has almost the same chemical shift as peak **H^{h}**, and the integral is therefore not measureable.

Bibliography

1. Wei, W., Tomohiro, T., Kodaka, M. & Okuno, H. Selective Synthesis and Kinetic Measurement of 1 : 1 and 2 : 2 Cyclic Azobenzene Units. 8979–8987 (2000) doi:10.1021/jo000926p.

2. Choisnet, T., Canevet, D., Sallé, M., Nicol, E., Niepceron, F., Jestin, J. & Colombani, O. Robust supramolecular nanocylinders of naphthalene diimide in water. *Chemical Communications* **55**, 9519–9522 (2019).

3. Leroyer, L., Prat, L., Cabassud, M., Gourdon, C., Dechy-Cabaret, O., Barthes, M., Camus, P. & Hattou, S. Transposition of a triphosgene-based process for pharmaceutical development: From mg · h-1 to kg · h-1 of an unsymmetrical urea. *Green Processing and Synthesis* **2**, 239–250 (2013).

4. Yamasaki, R., Honjo, Y., Ito, A., Fukuda, K. & Okamoto, I. Spontaneous and direct transformation of N,O-diaryl carbamates into N,N'-diarylureas. *Chem Pharm Bull (Tokyo)* **66**, 880–884 (2018).

5. Nicolas, C., Ghanem, T., Canevet, D., Sallé, M., Nicol, E., Gautier, C., Levillain, E., Niepceron, F. & Colombani, O. Oxidation-Sensitive Supramolecular Polymer Nanocylinders. *Macromolecules* **55**, 6167–6175 (2022).

6. Kim, H. K. & Lee, A. Facile one-pot synthesis of unsymmetrical ureas, carbamates, and thiocarbamates from Cbz-protected amines. *Org Biomol Chem* **14**, 7345–7353 (2016).

7. Bui, T. T. & Kim, H. K. Lanthanum(III) Trifluoromethanesulfonate Catalyzed Direct Synthesis of Ureas from N-Benzyloxycarbonyl-, N -Allyloxycarbonyl-, and N -2,2,2-Trichloroethoxycarbonyl-Protected Amines. *Synlett* **31**, 997–1002 (2020).

8. Bogolubsky, A. V., Ryabukhin, S. V., Pipko, S. E., Lukin, O., Shivanyuk, A., Mykytenko, D. & Tolmachev, A. A facile synthesis of unsymmetrical ureas. *Tetrahedron* **67**, 3619–3623 (2011).

9. Gallou, I., Eriksson, M., Zeng, X., Senanayake, C. & Farina, V. Practical Synthesis of Unsymmetrical Ureas from Isopropenyl Carbamates approach is particularly efficient for symmetrical ureas . synthetic efficiency is limited by the formation of symmet- rical urea side products . Another method of choice for urea form. *J. Org. Chem* **70**, 6960–6963 (2005).

10. Lutz, E., Moulin, E., Tchakalova, V., Benczédi, D., Herrmann, A. & Giuseppone, N. Design of Stimuli-Responsive Dynamic Covalent Delivery Systems for Volatile Compounds (Part 1): Controlled Hydrolysis of Micellar Amphiphilic Imines in Water. *Chemistry - A European Journal* **27**, 13457–13467 (2021).

11. Han, S., Pensec, S., Yilmaz, D., Lorthioir, C., Jestin, J., Guigner, J. M., Niepceron, F., Rieger, J., Stoffelbach, F., Nicol, E., Colombani, O. & Bouteiller, L. Straightforward preparation of supramolecular Janus nanorods by hydrogen bonding of end-functionalized polymers. *Nat Commun* **11**, 2–7 (2020).

CHAPTER 3

Summary – Chapter 3

CHAPTER 3 – Physico-chemical study of Azo-(U-PEO)$_2$ in aqueous media

I. Introduction

Once the successful synthesis of Azo-(U-PEO)$_2$ had been achieved, as described in the previous chapter, several physical chemistry questions arose. Firstly, does the polymer self-assembles into the desired 1D nano-structures in water? If so, under which conditions? What are the dimensions of the assemblies? Secondly, are the azobenzene moieties able to photo-switch despite the self-assembly, and if so, what effect does it have on the assemblies?

This chapter is split into two main parts. The first presents the major results from the physico-chemical study of the polymer in aqueous medium, followed by the article accepted in *Polymer Chemistry* (RSC). A second part details some problems that were encountered related to the analysis of the self-assembled structures by light scattering.

II. Initial Results

In order to investigate the self-assembling properties of Azo-(U-PEO)$_2$, the polymer was directly dissolved in water at 1 g/L and the solution was probed by light scattering (LS) and Cryo-TEM. LS measurements indicated a weakly aggregated system, with an average aggregation number of approximately 70, and no nano-cylinders were observed by Cryo-TEM. It therefore became apparent that direct dissolution of the polymer in water did not yield the desired nano-structures.

To remedy this, an alternative pathway was tried, which had been used in previous work by our team on similar systems.[1–4] This route, that was termed the "water/DMSO" route, consisted in first dissolving the polymer in DMSO at high concentration (90 g/L), which is a strong H-bond competitor where the polymer dissolves as unimers. Water was then slowly added to the concentrated DMSO solution, until a final ratio of water/DMSO 99/1 (v/v) was achieved. Cryo-TEM images revealed that many long, polydisperse nano-cylinders were present, and this result was confirmed by light scattering, which indicated that the system was highly aggregated ($N_{agg} \approx 800$, $M_{app} \approx 4.10^6$ g/mol), and showed a clear q^{-1} angular dependency, which is characteristic of long 1D nano-cylinders. These results indicated that the system was out of thermodynamic equilibrium (i.e. kinetically frozen), due to the strong pathway dependency.

UV-Vis measurements indicated that despite the strong self-assembly, photo-isomerization of the azobenzene still occurred, and in a rather fast manner, with photo-stationary states being reached within a matter of minutes, both for the *trans* → *cis* (λ = 365 nm) and *cis* → *trans* (λ = 450 nm) isomerizations.

Once again using a combination of LS and cryo-TEM, it was shown that UV irradiation (λ = 365 nm) triggered the disassembly of the nano-cylinders into much smaller, less aggregated particles (possibly spheres and/or small bits of nano-cylinders), due to photo-isomerization of the azobenzene to its *cis* configuration. Despite *trans*-

azobenzene being recovered after irradiation at 450 nm (or by thermal relaxation), no nano-cylinders were recovered, possibly due to the out of thermodynamic equilibrium nature of this system.

III. Article 1: "Photo-triggered disassembly of supramolecular polymer bottlebrushes in water", accepted for publication in Polymer Chemistry (RSC)

Luke Harvey[a], Jean-Michel Guigner[b], Laurent Bouteiller[c], Erwan Nicol[a*], Olivier Colombani[a*]

[a] *Institut des Molécules et Matériaux du Mans (IMMM), UMR 6283 CNRS, Le Mans Université, 72085 Le Mans, Cedex 9, France*

[b] *Sorbonne Université, CNRS, Institut de Minéralogie, de Physique des Matériaux et de Cosmochimie, 4 Place Jussieu, F-75005 Paris, France*

[c] *Sorbonne Université, CNRS, Institut Parisien de Chimie Moléculaire, Equipe Chimie des Polymères, 4 Place Jussieu, F-75005 Paris, France*

ABSTRACT: We report the 5-steps synthesis and self-assembly of an azobenzene-bisurea sticker flanked by two alkyl spacers and poly-(ethylene oxide) arms. In the trans-azobenzene configuration, long nano-cylinders can be obtained by first molecularly dissolving the polymer in DMSO, followed by the slow addition of water. Addition of water triggers 1D self-assembly through a combination of strong, cooperative H-bonding between urea motifs and hydrophobic effect. UV-light irradiation triggers photo-isomerization of the azobenzene units to their non-planar cis configuration, rapidly and irreversibly disrupting the photo-responsive assemblies.

1. Introduction

Polymer bottlebrushes[5–9] consist of a long linear polymer backbone so densely grafted with polymer side-chains, typically on every monomer unit, that it becomes rigid and extended, affording a cylindrical (1D) morphology. The anisotropic shape and high persistence length of polymer bottle-brushes coupled with the possibility to tune their functionality and solubility by playing with the chemical structure of the side-chains makes these polymers relevant for applications in anti-fouling, nanolithography, templates for the design of inorganic nanocylinders, design of supersoft thermoplastic elastomers or medicine (drug delivery, sensing, signaling, detection). Nature also uses polymer bottlebrushes for joints lubrication, cell protection and lung clearance.[5,7,9]

Initially, polymer bottlebrushes have been prepared by covalent strategies (grafting through, grafting from or grafting to).[5,7,9] More recently, supramolecular polymer bottlebrushes[6] (SPB) have been obtained where the backbone is built by strong and directional non covalent interactions such as π-stacking or hydrogen bonding. This strategy grants more versatility to control the length, diameter and chemical functionality of the bottlebrushes compared to covalent approaches. SPB with lengths up to several hundreds of nanometers have been obtained. Additionally, the use of non-covalent interactions opens the door to the design of stimuli-responsive SPBs. Imparting stimuli-responsiveness to SPBs is of growing interest, as it broadens their applicative potential in stimuli-triggered drug delivery[10], responsive gels or emulsion stabilization[11] for example. There are however up to now very few examples of SPBs which can be disrupted in response to stimuli such as light[10], pH[12], oxidation[1,13,14] or host-guest interactions[15]. Moreover, most rely on the nature of the polymer arms for responsiveness, limiting versatility and applicative potential. For instance, Perrier et al. prepared light responsive SPBs where the 1D self-assembly is granted by strong cooperative hydrogen bonding in water between cyclic oligopeptides,[16] whereas the responsiveness results from the use of poly(2-nitrobenzyl methacrylate) arms. The latter

become irreversibly transformed into poly(methacrylic acid) when exposed to UV irradiation, thereby triggering irreversible disassembly through electrostatic repulsion between the polymer arms.[10] This strategy clearly depends on the chemical structure of the polymer arms and does not allow modifying the chemical structure and functionality of the SPB while maintaining their responsive character.
A more versatile and attractive strategy would be to rely on the hydrogen bonding self-assembling part to impart responsiveness independently of the polymer arms. To the best of our knowledge, only five examples achieving this have been described in the literature (three examples responsive to oxidation[1,13,14], one to pH[17], and one based on host-guest chemistry[15]). No SPBs where the self-assembling core is light-responsive have been reported to the best of our knowledge. A few examples involving the assembly of non-polymeric small molecules in solution into 1D supramolecular structures have been described.[18–20] For instance, Feringa et. al. reported the 1D self-assembly of a stiff-stilbene functionalized with a bis-urea and oligo-PEO arms in water, which proceeded through kinetic control, driven by H-bonding, π-stacking and hydrophobic effect. Assembly was so strong that photo-isomerization of assemblies of the *trans* isomer was not possible at r.t.[20] Another study reported a benzene-tricarboxamide (BTA) functionalized with azobenzene moieties, responsible for the light sensitivity and, octa-(ethylene glycol) units responsible for water solubility has been shown to undergo reversible fiber assembly/disassembly upon light irradiation.[21] However, BTAs have been reported to be unsuitable for 1D self-assembly with long polymer arms on their own,[6] requiring additional H-bonding units to drive self-assembly.[22] Indeed, 1D-supramolecular self-assembly of polymers in solution into SPBs requires very strong non covalent interactions to overcome the high entropic penalty caused by the stretching of the polymer side-chains within the SPBs,[23] a penalty that BTA are not able to overcome unless they are functionalized with short peptides; which has not been attempted in the context of light-responsive SPBs.
In the present work, we present the synthesis, characterization and supramolecular self-assembly of a poly-(ethylene oxide)-based polymer containing an azobenzene central core and urea moieties promoting the establishment of intermolecular hydrogen bonding driving the formation of SPB in aqueous solution. The effect of light (triggering the conformational switch of the azobenzene groups) on the assemblies was investigated by light scattering and cryo-electron microscopy.

2. Experimental section

Materials

4,4'-dihydroxyazobenzene (TCI, 98%), bromopropylamine hydrobromide (Br-C_3-NH_2.HBr, TCI, 98%), benzyl chloroformate (Acros Organics, 97%), hexamethylene diisocyanate (HMDI, Aldrich, synthesis grade), HBr in acetic acid (TCI, 30 wt.%, 5.1 mol/L), DMF (Fischer, >99%, reagent grade), dichloromethane (DCM, Carlo Erba), cyclohexane (Aldrich, >99,5%), dioxane (Honeywell, >99.5%), aqueous NaOH and HCl solutions (Aldrich), and NaOH pellets (Aldrich, 98%) were purchased and used as received. $MgSO_4$ (Fluka) and powder molecular sieves (Aldrich, 4Å) were dehydrated by heating in an oven overnight at 300°C. K_2CO_3 (Aldrich) was dried under vacuum at 40°C overnight. Deionized water was obtained using a MilliQ IQ 7000 system. Monomethoxy-hydroxy-poly-(ethylene oxide) (PEO-OH) (M_n=2000 g/mol, Đ = 1.05) was purchased from Sigma-Aldrich, and dried by azeotropic distillation using toluene. For that, a 20% wt./vol.% solution of PEO-OH in toluene was prepared, refluxed under argon for 1 hour, and toluene was then distilled off. The polymer was finally dried overnight in a vacuum oven at 50°C and stored under argon. Analytical thin-layer chromatography (TLC) was carried out using aluminium plates coated with Merck Silica gel 60 F254 (Aldrich) and observation was done under a UV lamp (254 nm). Column gel chromatography was carried out using silica gel 60 from Aldrich (SiO_2, pore size 60 Å, 40-63 μm).

Characterizations

Nuclear magnetic resonance (NMR). ^{1}H NMR spectra were recorded on either a Bruker DPX-200 or Bruker AC-400 spectrometer, using deuterated chloroform ($CDCl_3$) or dimethyl sulfoxide (DMSO-d_6) as solvents. Chemical shifts (δ) are expressed in parts per million (ppm) relative to the reference (tetramethylsilane (TMS), δ = 0 ppm). Multiplicities are reported as follows: singlet (s), doublet (d), triplet (t), quadruplet (q), quintet (qt), sextet (sext), multiplet (m), and broad signal (br s).

Size exclusion chromatography. SEC measurements in DMF were conducted on an apparatus composed of a Waters 1515 Isocratic HPLC Pump, a Waters 2707 plus Autosampler, 1 PL gel 5µm guard column and 2 PL gel 5 µm mixed-d columns (the 3 columns are stored in an oven at 60 °C), a Waters 2998 Photodiode Array Detector, a minidawn TREOS Wyatt MALS detector, a Waters 2414 Differential Refractometer (at 40 °C), using DMF with LiBr 1 g/L as eluent. The flow rate was 1 mL/min. The conventional calibration was achieved with PMMA standards polymers with apex molecular weight M_p from 904 g/mol to 304000 g/mol. Samples were prepared by dissolving the polymer in an eluent/toluene mixture (1000/1 v/v) and then filtered with 0.22 µm PTFE filters.

Light irradiations

LED irradiations were carried out using a Thor Labs DC2200 High-Power LED Driver, with Thor Labs M365LP1 and Thor Labs M450LP1 LEDs, operating at 365 nm and 450 nm, respectively. The LEDs were linked to the driver using a waveguide. Irradiation of solutions was carried out with the waveguide placed 4.5 cm above the solution. The LED irradiance at this distance was measured using a Thor Labs PM160T optical power meter, and the irradiances were measured as follows: 215 $mW.cm^{-2}$ for the 365 nm LED and 515 $mW.cm^{-2}$ for the 450 nm LED.

Cryogenic transmission electron microscopy

For cryo-TEM images, a 5 µL drop of the initial sample solution was deposited on "quantifoil"® (Quantifoil Micro Tools GmbH, Germany) carbon membrane grids. The excess of liquid on the grid was absorbed with a filter paper and the grid was quench-frozen quickly in liquid ethane to form a thin vitreous ice film using a homemade mechanical cryo-plunger. Once placed in a Gatan 626 cryo-holder cooled with liquid nitrogen, the samples were transferred in the microscope and observed at low temperature (-180 °C). Cryo-TEM images were recorded on ultrascan 1000, 2k x 2k pixels CCD camera (Gatan, USA), using a LaB_6 JEOL JEM2100 (JEOL, Japan) cryo-microscope operating at 200kV with a JEOL low dose system (Minimum Dose System, MDS, JEOL, Japan) to protect the thin ice film from any irradiation before imaging and reduce the irradiation during the image capture.

UV-Vis absorption spectroscopy

UV-Vis spectra were measured on a Jasco V760 spectrometer using glass cuvettes with an optical pathway of 1 mm at room temperature.

Light scattering

Measurements were done with a standard ALV-CGS3 system equipped with an ALV-5003 multi tau correlator system (ALV GmbH, Germany) with a vertically polarized helium-neon laser with wavelength λ = 633 nm as light source. The measurements were done at 20 ° C over a large range of scattering wave vectors q varying from ca. 2.8 × 10^{-4} $Å^{-1}$ to 2.6 × 10^{-3} $Å^{-1}$. $q = \frac{4\pi n}{\lambda}\sin(\frac{\theta}{2})$, with θ the angle of observation, n the refractive index of the solvent and λ = 633 nm the wavelength of the laser. The apparent hydrodynamic radius was determined by dynamic light scattering and the apparent radius of gyration and molecular weight were determined by static light scattering. It is worthy to note that

samples did not absorb at 633 nm, making these solutions appropriate for LS measurements in these conditions. The dn/dc of PEO in water (0.13 mL/g) was used for Azo-(U-PEO)$_2$ in aqueous media (i.e. water/DMSO 99/ v/v).

Treatment of light scattering data.

Static light scattering (SLS). The normalized excess scattered light R, in cm^{-1}, scattered by the polymer was determined according to **Equation E1**.

$$R = \frac{R_{solution}(\theta) - R_{solvant}(\theta)}{R_{toluene}(\theta)} \times \left(\frac{n_{solvant}}{n_{toluene}}\right)^2 \times R_{toluene} \qquad \textbf{E1}$$

With $R_{solution}$, $R_{solvent}$ and $R_{toluene}$ the average intensities scattered, respectively, by the solution, the solvent, and the reference (toluene) at angle θ; $n_{solvent}$ = 1.33 for water, $n_{toluene}$ = 1.496 correspond to the respective refractive indexes of water and of toluene; and $R_{toluene} = 1.35 \times 10^{-5}$ cm^{-1} the Rayleigh ratio of toluene for a wavelength λ = 633 nm. For water/DMSO (99/1 v/v) solutions, $n_{solvent}$ was taken equal to n_{water}.

The normalized excess scattered light R obtained from SLS experiments depends on the polymer concentration C (in g.cm^{-3}), on a contrast factor K, on the apparent weight average molecular weight of the scatterers extrapolated to q → 0, and on a form factor P(q), which depends on the size and shape of the scatterers. The apparent molecular weight M_{app} can be approximated to the true M_w of the scatterers since interactions between scatterers may be neglected in such diluted solutions.

$$R = K \times C \times M_{app} \times P(q) \qquad \textbf{E2}$$

$$K = \frac{4\pi^2 {n_{solvant}}^2}{\lambda^4 N_a} \times \left(\frac{\partial n}{\partial c}\right)^2 \qquad \textbf{E3}$$

N_a is Avogadro's number and $\left(\frac{\partial n}{\partial c}\right)$ is the refractive index increment of the polymer in the chosen solvent.

Determination of the number of molecules in the cross-section. In the q-region where R/KC varies proportionally to q^{-1}, the molecular weight per unit length M_L can be determined according to equation **E4**.

$$M_L = \frac{q \times R}{\pi \times \mathrm{KC}} \qquad \textbf{E4}$$

C corresponds to the polymer concentration (g.cm^{-3}), R is the excess scattered light, K is the contrast as defined previously, and M_L is the molecular weight per unit length.

Considering that the average distance between two urea units has been reported to be 0.46 nm,[23] the number of molecules in the cross-section can be calculated according to equation **E5**.

$$\text{Number of molecules in the cross} - \text{section} = \frac{M_L \times 0.46}{M_{uni}} \qquad \textbf{E5}$$

With M_{uni} the weight average molecular weight of the unimers. M_{uni} was calculated by multiplying the M_n of the unimers determined by ^{1}H NMR with their dispersity measured by SEC. $DP_{n,NMR}$ = 370/4 ≈ 92 (a total of 370 protons in the polymer chains, and 4 protons per repeat unit); $M_{n,NMR}$ = 92 x 44 + 664 ≈ 4700 g/mol (44 g/mol per repeat unit and the central core has a M = 664 g/mol), and finally M_{uni} = 4700 x 1.05 ≈ 4900 g/mol).

Dynamic light scattering (DLS). The normalized electric field autocorrelation functions ($g1(t)$) obtained by DLS measurements were analyzed in terms of a relaxation time (τ) distribution:

$$g_1(t) = \int A(\tau) e^{\left(\frac{-t}{\tau}\right)} d\tau \qquad \textbf{E6}$$

The apparent diffusion coefficient D was calculated from the average relaxation rate of this relaxation mode as $D = \langle \tau^{-1} \rangle / q^2$. The apparent hydrodynamic radius R_{app} is related to D through the Stokes-Einstein equation:

$$R_{app} = \frac{k_b T}{6\pi\eta D} \qquad \textbf{E7}$$

With k_b Boltzmann's constant, T the absolute temperature and η the viscosity of the solvent. When the particles are small compared to q^{-1} and the solutions are sufficiently diluted so that interactions can be neglected (i.e. at 0.9 or 1 g/L), R_{app} is equal to the z-average hydrodynamic radius, R_h.

Synthesis

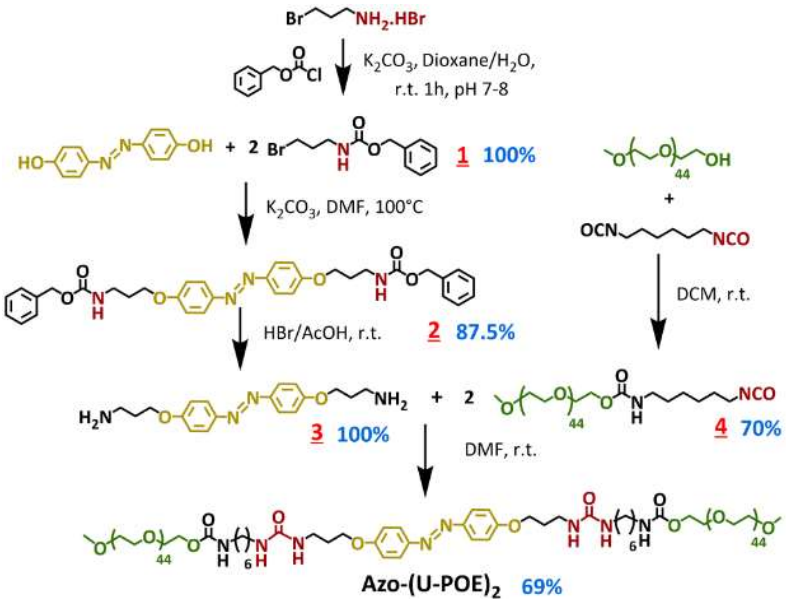

Scheme 3.1: **Synthetic scheme of Azo-(U-PEO)$_2$. The percentages in blue correspond to the yields of the corresponding steps.**

Synthetic protocols of azobenzenes (**1**), (**2**) and (**3**) were adapted from the literature[24] (see SI for details).

Synthesis of PEO-C_6-NCO (4)

The reaction was conducted at room temperature. In a 100 mL round bottom flask, 20 mL of anhydrous DCM was stirred under argon atmosphere with a spatula tip of activated molecular sieves (4 Å) in powder form for 30 min. Then, hexamethylene diisocyanate (HMDI, 5 eq., 1.26 g) was added to it and the solution was stirred for 30 more min. In parallel, in another (50 mL) round bottom flask, 3.00 g of dry monomethoxy-hydroxy-PEO (1.50 mmol) was solubilized in 30 mL anhydrous DCM under argon atmosphere, a spatula tip of activated molecular sieve (4 Å) in powder form was added and the solution was stirred for 30 min. The PEO-OH solution was then decanted to get rid of the molecular sieve, transferred to a 60 mL syringe, and injected into the HMDI solution over the course of 4 hours, using a syringe pump. The mixture was then left to react overnight.

The next day, the reaction mixture was concentrated without exposure to air by bubbling argon until approximately 15 mL of solution was remaining. The concentrated crude mixture was precipitated in 500 mL of anhydrous diethyl ether (DEE) under argon atmosphere and vigorous stirring, and the precipitate was then left to decant. As much supernatant as possible was removed with a canula. The vessel was filled back up with fresh anhydrous DEE, mixed, decanted, and the supernatant was removed. This operation was repeated three times in total to afford 3 washings. The precipitate was then dried under vacuum, and a white powder was obtained (2.15 g, 70 %).

It is worthy to note that this isocyanate polymer was found to be highly unstable and prone to hydrolysis, even if stored under argon at -18°C for a few days. For this reason, it was necessary to use it for the next step straight after purification. For the same reason, this polymer could not be analyzed directly by ^{1}H NMR. To verify the conversion and purity of **4**, 10 mg of the polymer was rapidly solubilized in DMSO-d_6 and a drop (large excess) of benzylamine was quickly added in order to quench the isocyanate functions

by forming benzylurea moieties. The solution was then analyzed by ^{1}H NMR, revealing that the product had indeed formed quantitatively since urea peaks, alkyl peaks and the benzylic –CH_2– peak of the benzylurea were present and all integrated correctly with respect to the PEO methoxy chain end.
^{1}H NMR (DMSO-d_6, 400 MHz): δ (ppm) 6.24 (t, J_3 = 6.0 Hz, 1H), 5.88 (t, J_3 = 6.0 Hz, 1H), 4.19 (d, J_3 = 6.0 Hz, 2H), 4.04 (t, J_3 = 4.8 Hz, 2H), 3.52 (m, 180H = DP_n x 4H), 3.25 (s, 3H), 2.99 (m**,** 2H+2H), 1.36 (m, 2H+2H), 1.24 (m, 2H+2H).

Synthesis of Azo-(U-PEO)$_2$

In a 25 mL round bottom flask, 6 mL of dry DMF and a spatula point of molecular sieve (4 Å) in powder form were stirred under argon for 20 min. In parallel, 0.144 g (1 eq.) of azobenzene diamine **3** was solubilized in 3 mL of dry DMF with a spatula point of molecular sieve (4 Å) in powder form and stirred for 20 min. 2.00 g (2.1 eq) of PEO-C_6-NCO (**4**) were quickly added to the first solution under argon circulation. Once the polymer was solubilized, the azobenzene solution was added to the polymer solution via a syringe and was left to react for 5 min. The slight excess of isocyanate-terminated PEO was then quenched by adding 0.3 mL of benzylamine (large excess), and the reaction was left to proceed for 5 more min. The crude polymer was then precipitated in 300 mL of DEE/pentane 50/50 (v/v). ^{1}H NMR revealed that the product had indeed formed, and that no PEO-benzylurea was present. However, another side reaction seemed to have occurred, leading to the formation of an impurity (triangles on **Figure C3-S8**). We hypothesize that the partial hydrolysis of isocyanate moieties happened, in turn leading to the formation of PEO-U-C_6-U-PEO (see **Figure C3-S7** for details). The ^{1}H NMR spectrum showed that a third urea peak was present, representing approximately 10% of the impurity, and the specific proton signals of the product integrated systematically ~10 % lower than expected (**Figure C3-S8**). In order to remove this unwanted impurity, 1.9 g of the crude polymer was solubilized in 2 mL EtOH, precipitated in 40 mL of DEE/EtOH 7/1 v/v, washed twice with this solvent mixture and then finally washed with pure DEE. After drying, 1.31 g of product was recovered (61 % yield), as confirmed by ^{1}H NMR (**Figure C3-1**), with all signals integrating as expected with the azobenzene and PEO methoxy chain end.

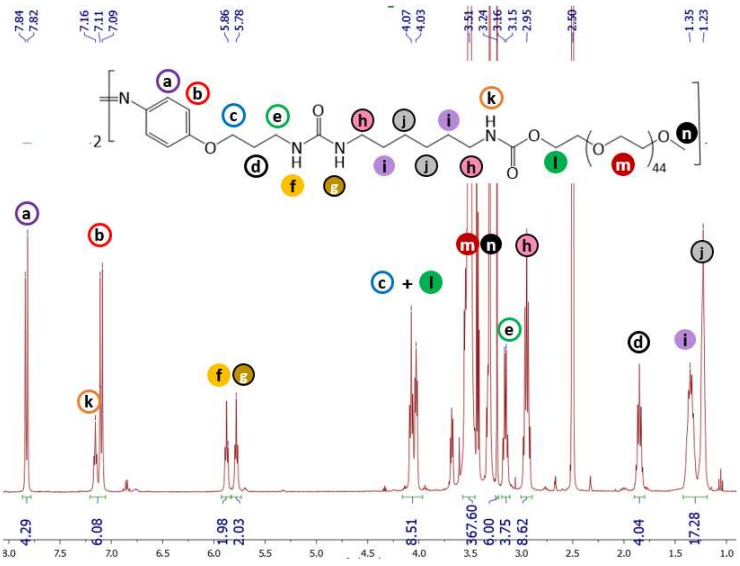

Figure C3-1. ^{1}H NMR (in DMSO-d_6) of the purified **Azo-(U-PEO)$_2$ (5).**

^{1}H NMR (DMSO-d_6, 400MHz): δ (ppm) 7.83 (d, **H^a**, J_3 = 9.2 Hz, 4H), 7.16 (t, **H^k**, J_3 = 5.6 Hz, 2H), 7.10 (d, **H^b**, J_3 = 9.2 Hz, 4H), 5.86 (t, **H^f**, J_3 = 6.0 Hz, 2H), 5.78 (t, **H^g**, J_3 = 6.0 Hz, 2H), 4.07 (t, **H^c**, J_3 = 6.0 Hz, 4H), 4.03 (t, **H^l**, 4H), 3.51 (s br, **H^m**, 360H = DP_n x 4H), 3.24 (s, **H^n**, 6H), 3.15 (q, **H^e**, J_3 = 6.0 Hz, 4H), 2.95 (q **H^h+H$^{h'}$**, J_3 = 6.0 Hz, 4H+4H), 1.85 (qt, **H^d**, J_3 = 6.0 Hz, 4H), 1.35 (m, **H^i+H$^{i'}$**, 4H+4H), 1.23 (m, **H^j+H$^{j'}$**, 4H+4H).

SEC measurements were carried out in DMF (and LiBr 1 g/L) with PMMA calibration. The product gave a retention time of 14.71 minutes, which corresponds to a M_n = 8300 g/mol in PMMA equivalents, which is much higher than the expected molar mass, and Đ = 1.06. Therefore, a PEO of M_n = 4000 g/mol was analyzed for comparison, and gave a similar but slightly higher retention time; which is consistent with the expected M_n = 4700 g/mol of **Azo-(U-PEO)$_2$**. Note that there is a very slight shouldering at around 15 min retention time, which indicates that trace amounts of PEO-U-C_6-U-PEO may still be present. This is coherent with ^{1}H NMR (**Figure C3-1**), in which an extremely small peak at 5.70 ppm is still present, which corresponds to the PEO-U-C_6-U-PEO urea signal. The peak is however not big enough for reliable integration. It was chosen to proceed the study with this level of purity.

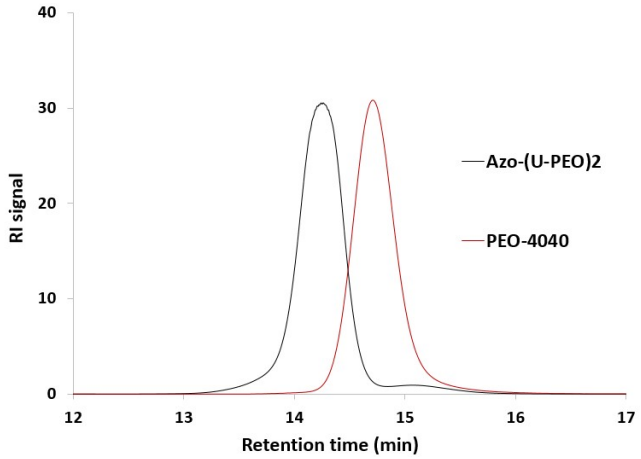

Figure C3-2. SEC chromatogram of the purified **Azo-(U-PEO)$_2$** and of PEO_{4k} in DMF (with LiBr 1 g/L).

Sample preparation

Direct dispersion in water. The polymer was directly dispersed at 1 g/L in ultrapure milli-Q water (which was filtered over 0.02 µm filter before use), lightly heated (approx. 40 °C) for a few minutes to accelerate dissolution, and left to stir in the dark for 1 hour. The solution was then filtered over 0.45 µm prior to LS. The loss of matter upon filtration was found to be negligible according to UV-Vis spectroscopy before and after filtration (by comparing the absorption peaks at 365 nm).

Water-DMSO route. 30 mg of polymer was solubilized in 300 µL (330 mg) of DMSO (that was filtered over 0.02 µm prior to use), heated slightly (approx. 40 °C) for a few minutes to accelerate dissolution, and left to cool to r.t. (approx. 10 min). The polymer/DMSO solution was then filtered over 0.2 µm. 200 µL of this solution were placed in a 7 mL vial, and 1.8 mL ultrapure milli-Q water (which was filtered over 0.02 µm) was added to this solution at a rate of 5 mL/h using a syringe pump, in the dark, and with a stirring of 200 rpm to reach a concentration of 9 g/L and a DMSO/water content of 10/90 v/v. 3 mL of this solution was then diluted manually by addition of water down to 0.9 g/L and a final water/DMSO ratio of 99/1 v/v. The final solution was filtered over 0.45 µm prior to light scattering measurements, and loss of matter was verified using UV-Vis (at 365 nm) and was of 8%.

3. Results and discussion

In order to prepare light-responsive supramolecular polymer bottlebrushes where the disruption of the self-assembled structures is controlled by the self-assembling core, we designed **Azo-(U-PEO)$_2$** (see **Scheme 3.1.**). This approach should therefore leave the choice of polymer arms unrestrained, as long as they do not interfere with self-assembly. A bis-urea sticker,[25] which was shown to self-assemble strongly in solution, was selected as H-bond promoting unit. It was shown with small molecules that bis-ureas self-assembled several orders of magnitude more strongly than mono-ureas provided that the two urea functions were oriented in the same direction, affording a cooperative self-assembly.[25] Our strategy was therefore to separate both urea functions of **Azo-(U-PEO)$_2$** by an azobenzene moiety to impart light-responsiveness: the planar *trans* isomer should allow 1D stacking by granting cooperative self-assembly of the two urea functions, while photo-isomerization to the non-planar *cis*-azobenzene should break the cooperativity of the two urea functions and disrupt the nano-cylinders. Poly(ethylene oxide) arms (PEO, M_n=2000 g/mol per arm, Đ = 1.05) were connected on each side of the bis-urea core to impart solubility in water. These arms were linked to the core with C_6 alkyl spacers to protect the bis-ureas from H-bond competing water and reinforce the self-assembly through hydrophobic interactions.[26]

i. Synthesis of Azo-(U-PEO)$_2$

The gram-scale synthesis of **Azo-(U-PEO)$_2$** was achieved in a 5-step convergent synthesis, as described in **Scheme 3.1**. The critical step was the synthesis of PEO-C_6-NCO (**4**), because this required to functionalize only one function of 1,6-hexanediisocyanate by a PEO arm and to keep the remaining water-sensitive isocyanate function of (**4**) intact during purification. This was achieved by slowly adding a solution of PEO-OH to a 5-fold excess of 1,6-hexanediisocyanate in water-free conditions, followed by precipitation of the polymer in dry solvents. (**4**) was strongly moisture-sensitive and its partial hydrolysis (< 10%) occurred, requiring a selective precipitation of the final **Azo-(U-PEO)$_2$** to get rid of impurities. 1.31 g (69%) of purified **Azo-(U-PEO)$_2$** was finally obtained (see experimental section and SI for details).

ii. Self-assembly of Azo-(U-PEO)$_2$ in its *trans* configuration

Next, the self-assembling properties of **Azo-(U-PEO)$_2$** were studied in aqueous medium at 1 g/L by cryoTEM and light scattering (LS). Upon direct dispersion of **Azo-(U-PEO)$_2$** in water, LS indicated a weakly aggregated system (R_h = 15 nm, N_{agg} ≈ 70, see SI, **Figure C3-S9**), with no angular dependence, suggesting that this route does not lead to the formation of 1D assemblies. Aging the solution for 10 days did not lead to re-organization into nano-cylinders either.

A so-called "water/DMSO" route[1,3,4] was then used to favor a higher extent of aggregation: the polymer was first dissolved at high concentration in DMSO (90 g/L), a strong hydrogen bond competitor in which the polymer molecularly dissolves, followed by slow addition of water (until a final ratio of 99/1 water/DMSO (v/v) and polymer concentration of 0.9 g/L) which should trigger self-assembly.

Cryo-TEM measurements indicated that many long, polydisperse nanocylinders were present (see **Figure C3-3a**) confirming the targeted morphology of the self-assemblies. Additionally, some small spheres could be observed by improving the quality of the cryoTEM images (see **Figure C3-S11** for details). Light scattering measurements confirmed the presence of nano-cylinders, since there was a q^{-1} angular dependency of the scattered intensity, characteristic of anisotropic 1D assemblies. Large dimensions (R_h = 80 nm, R_g = 140 nm) and molar mass (M_w = 4.10^6 g/mol, corresponding to an aggregation number N_{agg} ≈ 800) confirmed the large extent of aggregation compatible with the formation of long nanocylinders (see **Figure C3-3c**). LS measurements were also used to determine the number of molecules self-assembled within the cross-section of the nanocylinders. For that purpose R.q/KCπ was plotted as a function of q, revealing the formation of a plateau at high q (**Figure C3-S14**), corresponding to M_L with a

value of $9.0x10^3$ $g.mol^{-1}.nm^{-1}$ (calculated using **Equation E4** as explained in the experimental section). Using **Equation E5**, the number of molecules in the cross-section was calculated to be 1.0. The data were fitted using Sasview (see **Figure C3-3c**, red curve), with an average length of 520 nm and a diameter of 10 nm, which is consistent with cryo-TEM (L ≈ 500 nm). Considering the distance of a fully stretched PEO monomer unit of 0.28 nm[27] and an Azo core length around 2 nm, stacked **Azo(-U-PEO)$_2$** molecules with fully stretched PEO_{44} arms should lead to nanocylinders with a diameter of 27 nm ($d_{stretched}$ = 0.28 x 44 x 2 + 2). The smaller experimental diameter of the nanocylinders (~10 nm as determined via cryo-TEM) implies that the PEO_{44} arms in the self-assemblies are stretched approximately to one third of their maximum length, which seems reasonable for SPBs decorated by neutral polymer arms. As long as the azobenzene units were in their *trans* configuration, the "DMSO-route" therefore successfully led to the formation of long, thin and isolated SPBs consisting of **Azo-(U-PEO)$_2$** stacked upon each other by hydrogen bonds and protected from bundling by the polymer arms. Since direct dispersion in water hardly led to assembly, the strong influence of the preparation pathway indicates that the system is kinetically frozen (i.e. out of thermodynamic equilibrium), which was also observed with similar systems in aqueous medium.[1,3,4] Acetone and ethanol were also used as potential subsitutes for DMSO (see **Figure C3-S16** for details) to prepare SPBs with the "DMSO-like preparation route", but did not yield nano-cylinders. This could be due to the fact that while these solvents are good H-bond competitors, they are bad solvents for the self-assembling core, whereas DMSO is a good solvent. Therefore they probably do not allow molecular solubilization of **Azo-(U-PEO)$_2$** as unimers prior to water addition; which prevents its well-organized assembly into supramoecular SPBs.

iii. Light response of the self-assemblies

The light responsiveness of **Azo-(U-PEO)$_2$** was studied both by UV-Vis to determine whether the *trans* → *cis* isomerization occurred, and by cryoTEM and LS to determine the consequence it had on the self-assembled structures. Initially, the polymer contained almost 100% *trans*-azobenzene (<3% *cis*) according to ^{1}H NMR (see **Figure C3-1,** the aromatic peaks at 7.83 and 7.10 ppm correspond to the *trans*-azobenzene protons). Irradiation under gentle stirring of a 0.9 g/L "water/DMSO" (99/1) solution at 365 nm resulted in the progressive decrease of the absorption band at 365 nm, corresponding to the $\pi \rightarrow \pi^*$ transition of *trans*-azobenzene, and a simultaneous appearance of two absorption bands at 315 nm and 450 nm corresponding respectively to the $\pi \rightarrow \pi^*$ and $n \rightarrow \pi^*$ transitions of *cis*-azobenzene (**Figure C3-4a**).[28] Visually, the solution turned a deeper orange, allowing for direct macroscopic observation of the isomerization. The *trans* → *cis* isomerization therefore occurs, and is rather quick, with the photo-stationary state being reached after only a few minutes and corresponding to a *trans*/*cis* molar ratio of 25/75 (according to ^{1}H NMR, see **Figure C3-S19** for details).

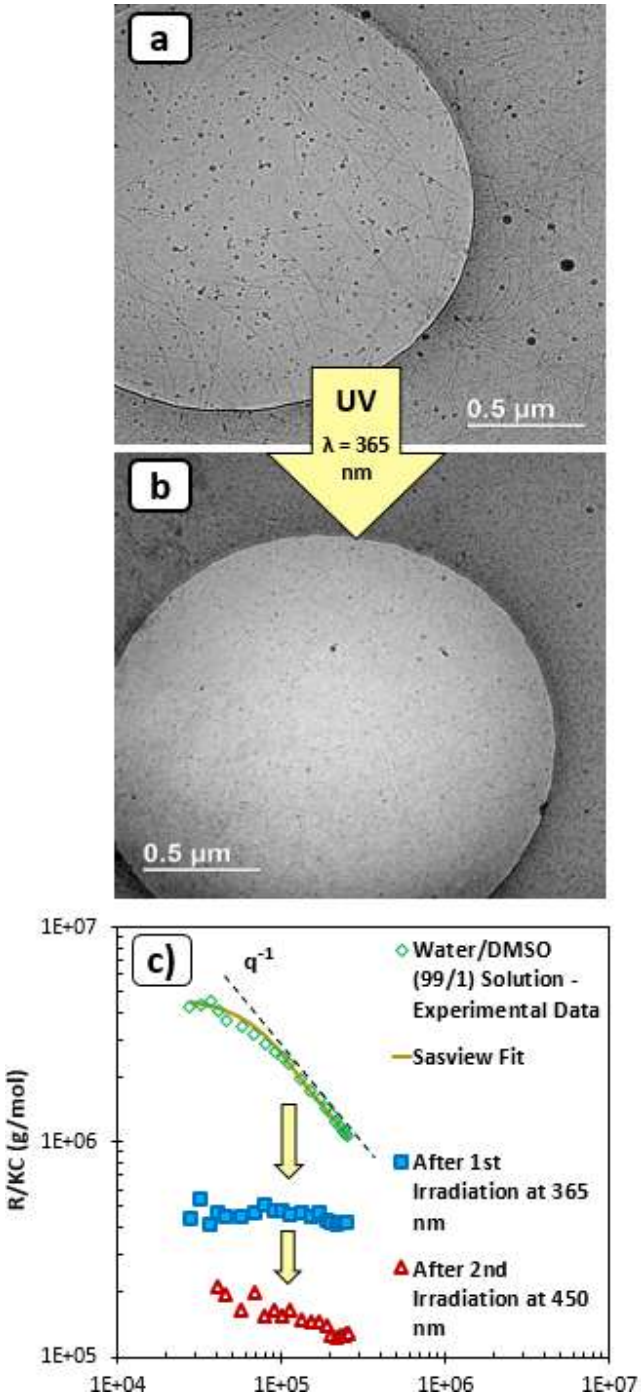

Figure C3-3. Cryo-TEM images using the water/DMSO route (at 0.9 g/L) **(a)** before UV irradiation - and **(b)** after UV irradiation (λ = 365 nm). The large highly contrasted black dots are ice crystals. **(c)** R/KC ratio as a function of q measured by SLS prior to irradiation (green diamonds, the data were fitted using Sasview, with L = 520 nm, r = 5 nm, —), after UV irradiation at λ = 365 nm (blue squares), and after a second irradiation at λ = 450 nm (red triangles). The black dotted line is a q^{-1} visual aid.

Subjecting the latter solution to irradiation at 450 nm allowed reappearance of the *trans* absorption band and disappearance of the *cis* ones. The new stationary state was reached within a minute (see **Figure C3-4b**) and corresponded to a *trans*/*cis* ratio of 75/25 by mol (according to ^{1}H NMR, see **Figure C3-S19**). 100% of *trans* isomer could not be achieved by irradiation at 450 nm; which was attributed to the fact that both

cis → *trans* and *trans* → *cis* isomerization are triggered at this wavelength, the quantum yield for the latter transition being much lower, but not negligible.[21] It was verified that 365 nm/450 nm irradiation cycles led to identical ratios of isomers, indicating no degradation occurs (see **Figure C3-4c**). Moreover, heating a *cis*-rich solution at 80°C for 30 minutes led again to an amount of *trans*-isomer close to 100% through thermal relaxation (see **Figure C3-S18** for details). Thermal relaxation also occurred at r.t., but it was rather slow ($\tau_{1/2} \approx$ 22 hours) (see **Figure C3-S17** for details).

To conclude, *trans* → *cis* and *cis* → *trans* photo-induced isomerization occurred very rapidly and reversibly in aqueous medium even though the polymer was involved in 1D supramolecular structures. It was additionally verified that photo-isomerization occurs on a similar timescale in aqueous medium after direct dispersion in water (photo-stationary states being reached within a matter of minutes), where **Azo-(U-PEO)$_2$** weakly assembles and forms spherical particles (see **Figure C3-S10** for details). This implies that the *trans* → *cis* photo-isomerization is not strongly hindered by the self-assembly of **Azo-(U-PEO)$_2$** into 1D structures. This result is quite relevant as it has been reported that self-assembly into fibers may prevent photo-isomerization in some cases,[20,29] although this is not systematic.

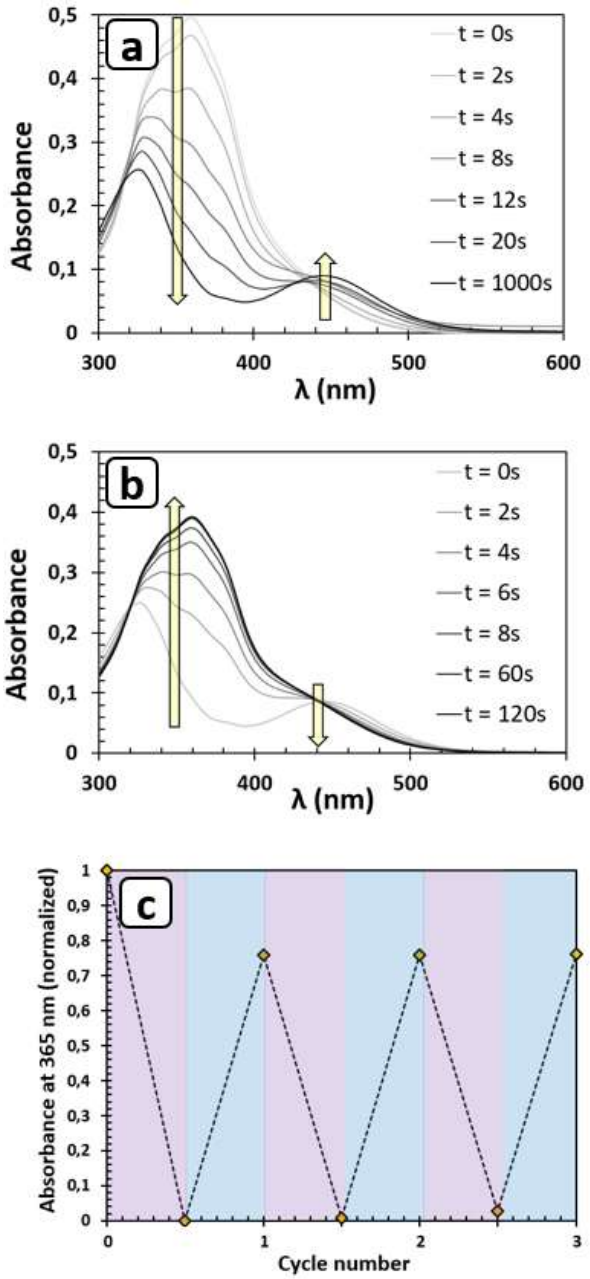

Figure C3-4. (a) *Trans* →*Cis* photo-isomerization (365 nm) of Azo-(U-PEO)$_2$,**(b)** *Cis* → *Trans* photo-isomerization (450 nm) of Azo-(U-PEO)$_2$ and **(c)** Photo-isomerization cycles of Azo-(U-PEO)$_2$, (at 0.9 g/L following the "water/DMSO" route)

To probe the effect of photo-isomerization on the assemblies, a solution prepared by the "water/DMSO" route was irradiated at 365 nm and analyzed by cryo-TEM and LS (see **Figure C3-3b** and **C3-3c**) revealing disruption of the nanocylinders: $N_{agg} \approx 90$, R_h = 40 nm, no more angular dependency of the scattered intensity. The still large N_{agg} and R_h however suggest that the cylinders are not fully disrupted into unimers but into small objects, which may be spheres and/or small bits of the initial nanocylinders (see **Figures C3-3b and C3-S12** which indeed reveals the presence of small spherical particles as well as a few very short 1D structures). Further irradiating at 450 nm triggered isomerization back to *trans*-azobenzene as mentioned above, but was not accompanied by the re-assembly of nano-cylinders (see **Figure C3-3c**). Actually, irradiating at 450 nm even led to a decrease in assembly (N_{agg} = 30, R_h = 15 nm), and cryo-TEM

revealed that only small spherical particles were present. These latter particles are similar to those obtained with **Azo-(U-PEO)$_2$** in its trans configuration by direct dispersion in water (see above). To confirm that the cis-isomer does not self-assemble into 1D structures, a "water/DMSO" solution was prepared by irradiating with UV-light (365 nm) the initial DMSO solution to form *cis*-**Azo-(U-PEO)$_2$** before adding water. LS indicated weak aggregation (N_{agg} = 20, R_h ~ 15 nm) with no q^{-1} angular dependence (see **Figure C3-S15**), confirming that *cis*-**Azo-(U-PEO)$_2$** cannot form nanocylinders even with the "water/DMSO" route. We actually note that the self-assembled structures formed in these conditions are even less aggregated than those obtained upon irradiation at 365 nm of a solution of nanocylinders of *trans*-**Azo-(U-PEO)$_2$** (N_{agg} ≈ 90, R_h = 40 nm). This suggests that *cis*-**Azo-(U-PEO)$_2$** also formed out-of-equilibrium structures with pathway-dependent characteristics.

From these results, we hypothesize that both the preparation pathway and the configuration of the azobenzene units influence the organization of the polymer as depicted on **Figure C3-5**.

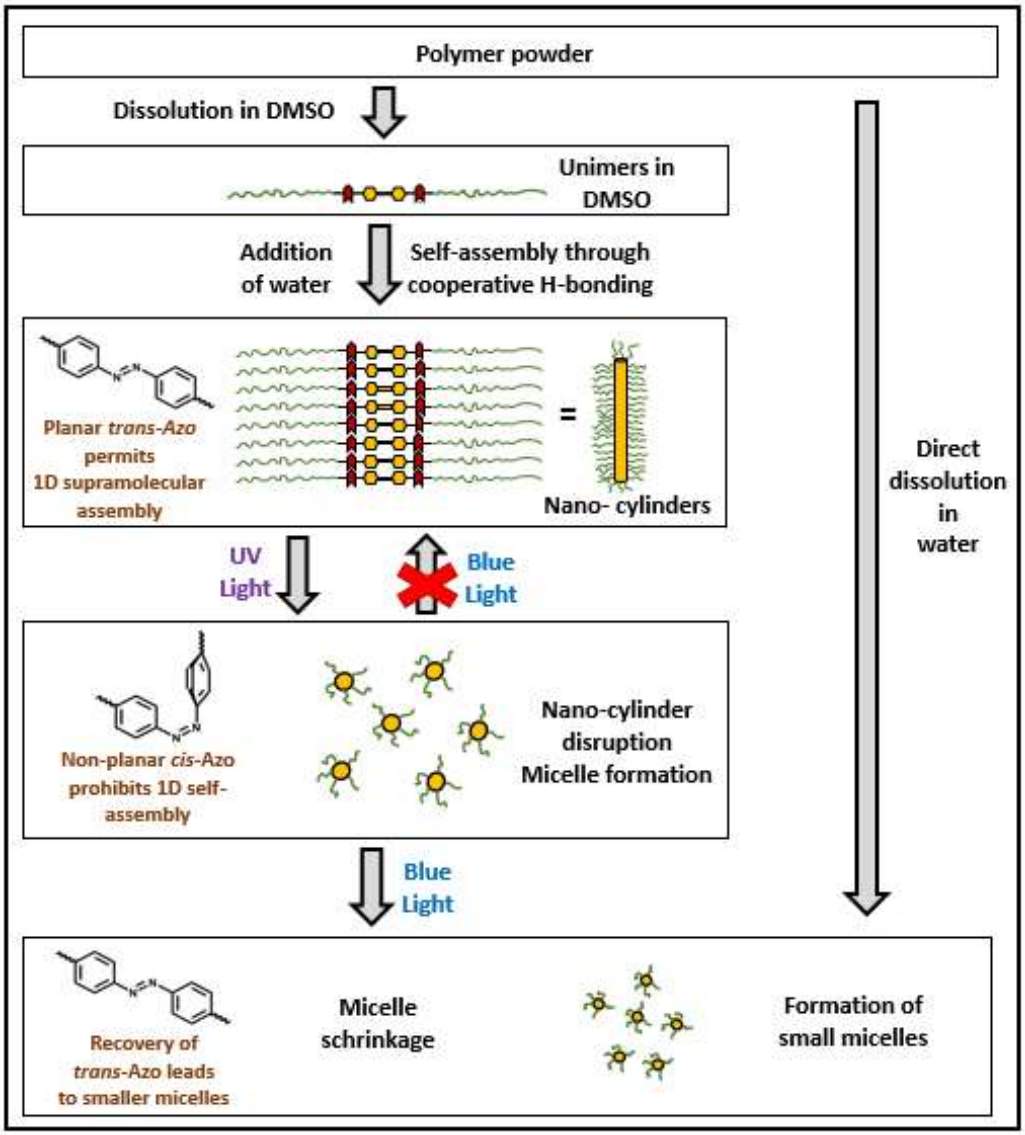

Figure C3-5. Schematic representation of the physico-chemical behavior of **Azo-(U-PEO)$_2$** in water following the "water/DMSO" route.

The *cis*-**Azo-(U-PEO)$_2$** apparently disfavors the formation of long nanocylinders, as expected, because it certainly suppresses the cooperative hydrogen bonding of both urea functions for geometrical reasons,

thereby leading to relatively weak hydrogen bonds. The *trans*-**Azo-(U-PEO)$_2$** may lead to the formation of long nanocylinders thanks to cooperative hydrogen bonding, but only with certain preparation conditions, namely the "DMSO-route". Indeed, the "DMSO-route" allows the initial dissolution of **Azo-(U-PEO)$_2$** as unimers, which probably helps them stack one on top of the other through directional and cooperative hydrogen bonds when water is added. In these conditions, hydrogen bonding is probably the main driving force for the formation of elongated supramolecular nanocylinders, the hydrophobic interactions only playing a protecting role over the hydrogen bonds from H-bond competing water. Now, if *trans*-**Azo-(U-PEO)$_2$** is obtained by irradiating at 450 nm a solution of small spherical micelles of *cis*-**Azo-(U-PEO)$_2$**, it starts from a supramolecular organization mainly driven by hydrophobic interactions which are not directional. Those hydrophobic interactions probably disfavor for kinetic reasons the reorganization of the *trans*-**Azo-(U-PEO)$_2$** into hydrogen bonded stacks of molecules required to reform nanocylinders. It should be noted that some examples in the literature report weakly dynamic assemblies which slowly evolve from spheres to elongated structures over time. It could therefore have been expected that the transition from *cis* back to *trans* might lead again to nanocylinders after prolonged time. However, direct dispersion of *trans*-**Azo-(U-PEO)$_2$** did not lead to nanocylinders even after ten days; suggesting a strong kinetic hurdle preventing self-assembly of *trans*-**Azo-(U-PEO)$_2$** into 1D structures unless starting with unimers as enabled by the "DMSO-route".
The *cis*-*trans* isomerization of **Azo-(U-PEO)$_2$** therefore does not allow the reformation of nanocylinders. Still, changing the configuration of the azobenzene units from *cis* to *trans* seems to slightly impact the packing parameter of the molecules, which would explain why spherical particles of *cis*-**Azo-(U-PEO)$_2$** become slightly less aggregated upon irradiation at 450 nm into *trans*-**Azo-(U-PEO)$_2$**. This argument is further supported by the fact that the micelles of *trans*-**Azo-(U-PEO)$_2$** have roughly the same characteristics as those obtained by direct dispersion in water. A similar variation of the aggregation state of micelles upon *cis*-*trans* isomerization was reported in the literature for an azobenzene-urea terminated PEO, which underwent an increase in micelle radius upon UV irradiation.[30]

4. Conclusions

To summarize, we report the successful synthesis of **Azo-(U-PEO)$_2$**, a polymer which combines a self-assembling bis-urea sticker with a photo-responsive azobenzene core and PEO polymer arms. This compound can self-assemble in aqueous medium into long SPBs following an appropriate strategy ("water/DMSO route"). The use of rather long PEO arms affords the formation of very thin and isolated nanocylinders (diameter ~ 10 nm) formed by mono-molecular hydrogen-bonded stacks of **Azo-(U-PEO)$_2$** in the cross-section of the nanocylinders and no significant lateral aggregation. The very high specific surface area and aspect ratio of these particles makes them potentially relevant for applications as Pickering emulsion stabilizers or to interact with biological material such as DNA or proteins.
Exposing the nanocylinders to UV irradiation at 365 nm rapidly triggers photo-isomerization to *cis*-azobenzene, which in turn provokes the disruption of the nanocylinders. This represents the first light-sensitive SPB where the light-responsiveness is intrinsic to the self-assembling core rather than to the specificity of the polymer arm. This may allow changing the functionality and chemistry of the polymer arms without losing their response to light. Further irradiating at 450 nm rapidly triggers photo-isomerization back to the *trans* isomer, but does not lead to nano-cylinder reassembly, which could be explained by the frozen character of the assemblies in water. Efforts are thus required in the future to develop reversibly-responsive SPBs.

Acknowledgments

Le Mans Université is acknowledged for funding LH's PhD work. The authors thank Sandra Kalem and Clémence Nicolas for fruitful discussions. Anthony Rousseau and Frédérick Niepceron and plateforme "Microscopy" at IMMM are thanked for their help with cryo-TEM measurements, Boris Jacquette and platerforme "Matière molle" are thanked for SEC measurements, and Sullivan Bricaud and plateforme "RMN" are thanked for help with NMR measurements.

Conflicts of interest

There are no conflicts to declare.

References

1. Nicolas, C., Ghanem, T., Canevet, D., Sallé, M., Nicol, E., Gautier, C., Levillain, E., Niepceron, F. & Colombani, O. Oxidation-Sensitive Supramolecular Polymer Nanocylinders. *Macromolecules* **55**, 6167–6175 (2022).

2. Han, S., Nicol, E., Niepceron, F., Colombani, O., Pensec, S. & Bouteiller, L. Oligo-Urea with No Alkylene Unit Self-Assembles into Rod-Like Objects in Water. *Macromol Rapid Commun* **40**, 1–5 (2019).

3. Choisnet, T., Canevet, D., Sallé, M., Lorthioir, C., Bouteiller, L., Woisel, P., Niepceron, F., Nicol, E. & Colombani, O. Colored Janus Nanocylinders Driven by Supramolecular Coassembly of Donor and Acceptor Building Blocks. *ACS Nano* **15**, 2569–2577 (2021).

4. Han, S., Pensec, S., Yilmaz, D., Lorthioir, C., Jestin, J., Guigner, J. M., Niepceron, F., Rieger, J., Stoffelbach, F., Nicol, E., Colombani, O. & Bouteiller, L. Straightforward preparation of supramolecular Janus nanorods by hydrogen bonding of end-functionalized polymers. *Nat Commun* **11**, 2–7 (2020).

5. Verduzco, R., Li, X., Pesek, S. L. & Stein, G. E. Structure, function, self-assembly, and applications of bottlebrush copolymers. *Chem Soc Rev* **44**, 2405–2420 (2015).

6. Gruschwitz, F. V., Klein, T., Catrouillet, S. & Brendel, J. C. Supramolecular polymer bottlebrushes. *Chemical Communications* **56**, 5079–5110 (2020).

7. Sheiko, S. S., Sumerlin, B. S. & Matyjaszewski, K. Cylindrical molecular brushes: Synthesis, characterization, and properties. *Progress in Polymer Science (Oxford)* **33**, 759–785 (2008).

8. Zhang, M. & Müller, A. H. E. Cylindrical polymer brushes. *J Polym Sci A Polym Chem* **43**, 3461–3481 (2005).

9. Tu, S., Choudhury, C. K., Luzinov, I. & Kuksenok, O. Recent advances towards applications of molecular bottlebrushes and their conjugates. *Curr Opin Solid State Mater Sci* **23**, 50–61 (2019).

10. Yang, J., Song, J. I., Song, Q., Rho, J. Y., Mansfield, E. D. H., Hall, S. C. L., Sambrook, M., Huang, F. & Perrier, S. Hierarchical Self-Assembled Photo-Responsive Tubisomes from a Cyclic Peptide-Bridged Amphiphilic Block Copolymer. *Angewandte Chemie - International Edition* **59**, 8860–8863 (2020).

11. Tang, J., Quinlan, P. J. & Tam, K. C. Stimuli-responsive Pickering emulsions: Recent advances and potential applications. *Soft Matter* **11**, 3512–3529 (2015).

12. Larnaudie, S. C., Brendel, J. C., Jolliffe, K. A. & Perrier, S. PH-Responsive, Amphiphilic Core-Shell Supramolecular Polymer Brushes from Cyclic Peptide-Polymer Conjugates. *ACS Macro Lett* **6**, 1347–1351 (2017).

13. Otter, R., Berac, C. M., Seiffert, S. & Besenius, P. Tuning the life-time of supramolecular hydrogels using ROS-responsive telechelic peptide-polymer conjugates. *Eur Polym J* **110**, 90–96 (2019).

14. Baram, J., Shirman, E., Ben-Shitrit, N., Ustinov, A., Weissman, H., Pinkas, I., Wolf, S. G. & Rybtchinski, B. Control over self-assembly through reversible charging of the aromatic building blocks in photofunctional supramolecular fibers. *J Am Chem Soc* **130**, 14966–14967 (2008).

15. Song, Q., Yang, J., Rho, J. Y. & Perrier, S. Supramolecular switching of the self-assembly of cyclic peptide-polymer conjugates: Via host-guest chemistry. *Chemical Communications* **55**, 5291–5294 (2019).

16. Song, Q., Cheng, Z., Kariuki, M., Hall, S. C. L., Hill, S. K., Rho, J. Y. & Perrier, S. Molecular Self-Assembly and Supramolecular Chemistry of Cyclic Peptides. *Chemical Reviews* vol. 121 13936–13995 Preprint at https://doi.org/10.1021/acs.chemrev.0c01291 (2021).

17. Otter, R., Klinker, K., Spitzer, D., Schinnerer, M., Barz, M. & Besenius, P. Folding induced supramolecular assembly into pH-responsive nanorods with a protein repellent shell. *Chemical Communications* **54**, 401–404 (2018).

18. Gerth, M., Berrocal, J. A., Bochicchio, D., Pavan, G. M. & Voets, I. K. Discordant Supramolecular Fibres Reversibly Depolymerised by Temperature and Light. *Chemistry - A European Journal* **27**, 1829–1838 (2021).

19. Lee, S., Oh, S., Lee, J., Malpani, Y., Jung, Y. S., Kang, B., Lee, J. Y., Ozasa, K., Isoshima, T., Lee, S. Y., Hara, M., Hashizume, D. & Kim, J. M. Stimulus-responsive azobenzene supramolecules: Fibers, gels, and hollow spheres. *Langmuir* **29**, 5869–5877 (2013).

20. Xu, F., Crespi, S., Pfeifer, L., Stuart, M. C. A. & Feringa, B. L. Mechanistic Insight into Supramolecular Polymerization in Water Tunable by Molecular Geometry. *CCS Chemistry* **4**, 2212–2220 (2022).

21. Fuentes, E., Gerth, M., Berrocal, J. A., Matera, C., Gorostiza, P., Voets, I. K., Pujals, S. & Albertazzi, L. An Azobenzene-Based Single-Component Supramolecular Polymer Responsive to Multiple Stimuli in Water. *J Am Chem Soc* **142**, 10069–10078 (2020).

22. Klein, T., Ulrich, H. F., Gruschwitz, F. V., Kuchenbrod, M. T., Takahashi, R., Fujii, S., Hoeppener, S., Nischang, I., Sakurai, K. & Brendel, J. C. Impact of amino acids on the aqueous self-assembly of benzenetrispeptides into supramolecular polymer bottlebrushes. *Polym Chem* **11**, 6763–6771 (2020).

23. Catrouillet, S., Fonteneau, C., Bouteiller, L., Delorme, N., Nicol, E., Nicolai, T., Pensec, S. & Colombani, O. Competition between steric hindrance and hydrogen bonding in the formation of supramolecular bottle brush polymers. *Macromolecules* **46**, 7911–7919 (2013).

24. Wei, W., Tomohiro, T., Kodaka, M. & Okuno, H. Selective Synthesis and Kinetic Measurement of 1 : 1 and 2 : 2 Cyclic Azobenzene Units. 8979–8987 (2000) doi:10.1021/jo000926p.

25. Simic, V., Bouteiller, L. & Jalabert, M. Highly Cooperative Formation of Bis-Urea Based Supramolecular Polymers. *J Am Chem Soc* **125**, 13148–13154 (2003).

26. Obert, E., Bellot, M., Bouteiller, L., Andrioletti, F., Lehen-Ferrenbach, C. & Boué, F. Both water- and organo-soluble supramolecular polymer stabilized by hydrogen-bonding and hydrophobic interactions. *J Am Chem Soc* **129**, 15601–15605 (2007).

27. Darko, C. An Experimental Approach of Introducing Polymer Crystallization to Students using Diblock Copolymer Thin Films An Experimental Approach of Introducing Polymer Crystallization to Students using. (2021) doi:10.17632/hry2mscm54.1.

28. Baroncini, M. & Bergamini, G. Azobenzene: A Photoactive Building Block for Supramolecular Architectures. *Chemical Record* **17**, 700–712 (2017).

29. Inoue, D., Suzuki, M., Shirai, H. & Hanabusa, K. Novel low-molecular-weight gelators based on azobenzene containing L-amino acids. *Bull Chem Soc Jpn* **78**, 721–726 (2005).

30. Yadav, S., Deka, S. R., Verma, G., Sharma, A. K. & Kumar, P. Photoresponsive amphiphilic azobenzene-PEG self-assembles to form supramolecular nanostructures for drug delivery applications. *RSC Adv* **6**, 8103–8117 (2016).

IV. Supporting information – Article 1

While the synthesis is detailed in Chapter 2, despite being somewhat redundant, we decided to still include the synthesis as it is presented in the article for ease of reading.

1. Synthesis

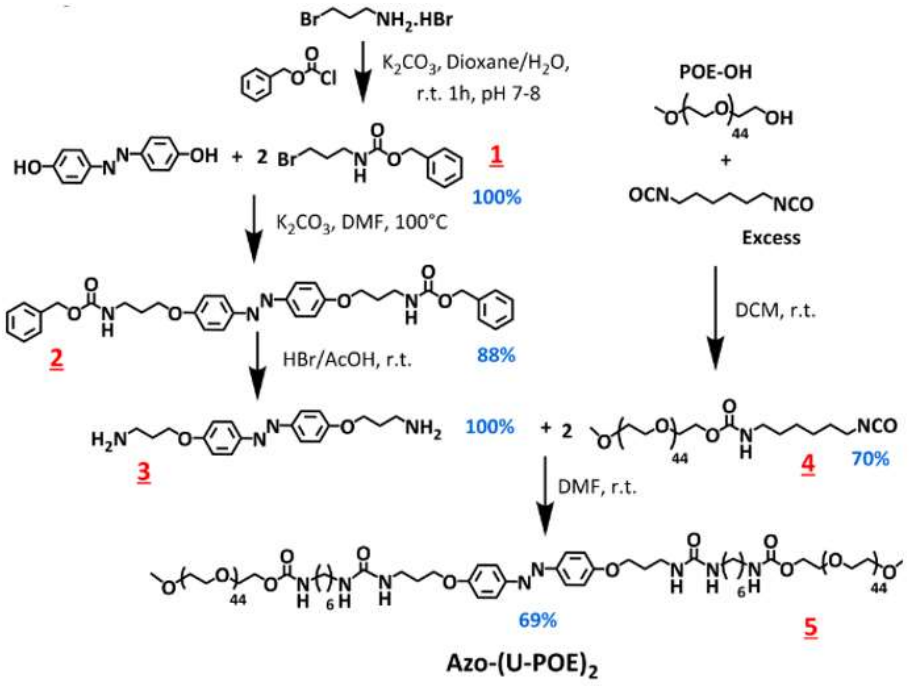

Figure C3-S1. Synthetic scheme of **Azo-(U-PEO)$_2$ (5).** The percentages in blue correspond to the yields of the corresponding steps.

Synthesis of Boc-protected bromopropylamine 1: adapted from ref[1]

3-bromopropylamine hydrobromide (10.9 g, 50 mmol, 1 eq) was dissolved in 50 mL of a 50/50 v/v mixture of water and dioxane in a beaker equipped with a stir-bar. A solution of benzyl chloroformate (10.5 g, 61.5 mmol, 1.23 eq) in 25 mL of dioxane was prepared, as well as an aqueous 3.5 M K_2CO_3 solution. A pH-meter was placed in the reaction beaker. Successive dropwise additions of the benzyl chloroformate solution and potassium carbonate solution into the beaker were carried out at room temperature under vigorous stirring while maintaining the pH between 6 and 7 until all the benzyl chloroformate solution had been added. The solution became cloudy once approximatively half of the benzyl chloroformate solution had been added and remained so until the end of the addition, presumably due to the product precipitating. The solution pH was then adjusted between 7 and 8, and the mixture was left to react for 1 subsequent hour under vigorous stirring. 5 mL of 2 M aqueous NaOH were then added to hydrolyze the excess benzyl chloroformate and the mixture was left to react for 2 additional hours. The reaction mixture was then extracted with 3 x 100 mL diethyl ether, the aqueous phase becoming limpid upon extraction. The organic phases were combined and washed with 100 mL 1 M aqueous NaOH followed by 2 x 100 mL water. The organic phase was then dried over $MgSO_4$ and the solvent was removed under reduced pressure. The crude product was further purified using silica gel chromatography with

DCM/cyclohexane 10/1 vol/vol as eluent, yielding 13.5 g (~ 100 %) of product as a light yellow oil. Its chemical structure was confirmed by ^{1}H NMR (**Figure C3-S2**).

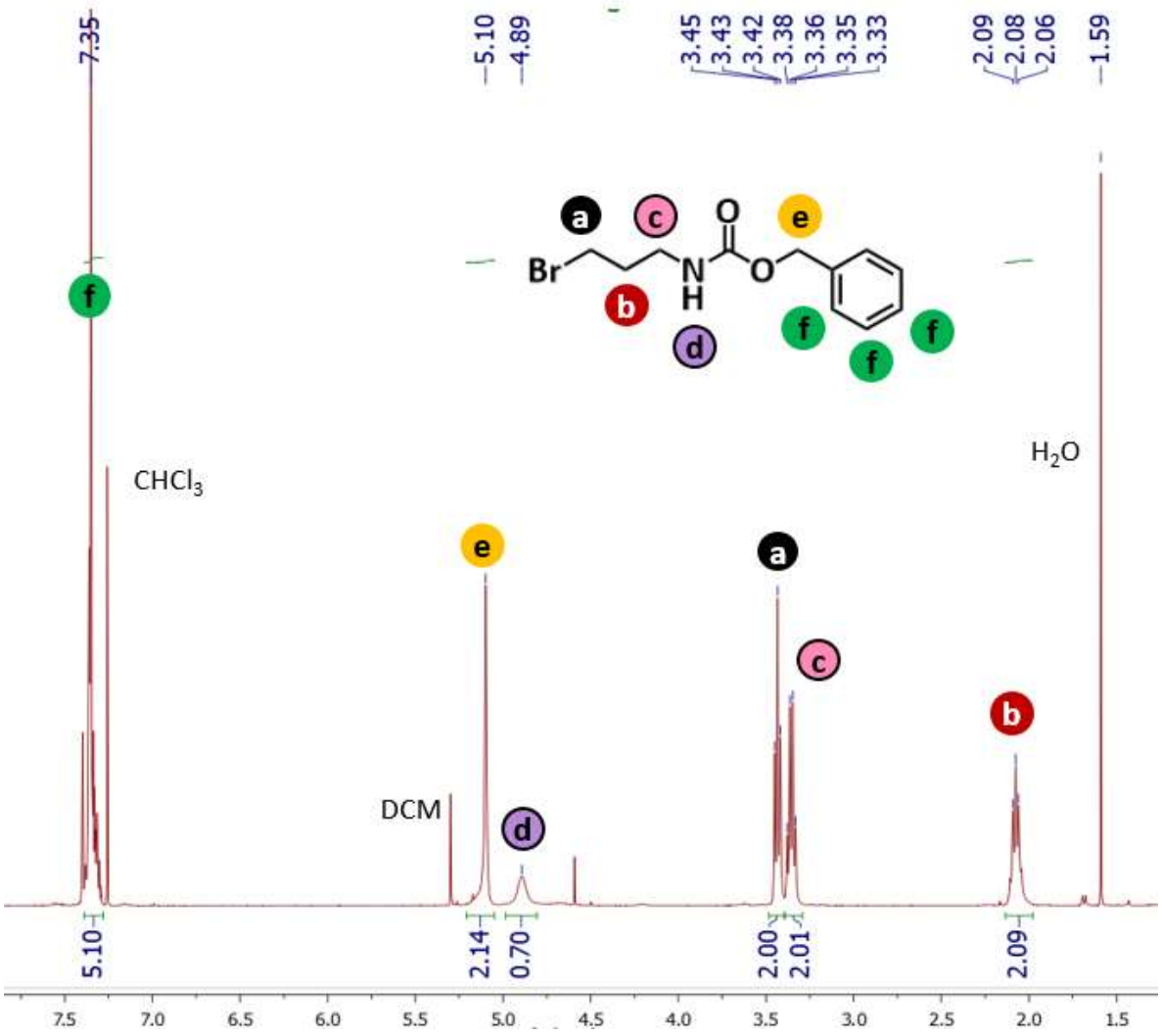

Figure C3-S2. ^{1}H NMR (in $CDCl_3$) of product **1**

^{1}H NMR ($CDCl_3$, 400 MHz): δ (ppm) 7.35 (m, **H^f**, 5H), 5.10 (s, **H^e**, 2H), 4.89 (br s, **H^d**, 1H), 3.42 (t, **H^a**, J_3 = 6.4 Hz, 2H), 3.35 (q, **H^c**, J_3 = 6.4 Hz, 2H), 2.08 (qt, **H^b**, J_3 = 6.4 Hz, 2H)

Synthesis of Azobenzene 2: adapted from ref[1]

In a round bottom flask equipped with a water condenser, septum and stir-bar, 4,4'-dihydroxyazobenzene (3,00 g, 14.0 mmol, 1 eq), Cbz-protected bromopropylamine **1** (8.35 g, 30.8 mmol, 2.2 eq) and K_2CO_3 (9.68 g, 70 mmol, 5 eq) were mixed in 60 mL DMF. The reaction vessel was degassed with argon and the mixture was left to react overnight at 100 °C. The solution was then left to cool, and upon cooling, a precipitate formed, which was filtered off. The recovered precipitate was washed with water and diethyl ether, dissolved in THF, dried over $MgSO_4$, and concentrated until the product was barely soluble in hot THF. The product was then left to recrystallize and recovered by filtration. The supernatant was re-concentrated in order to carry out a second recrystallization. The

two recrystallized fractions were combined, affording 7.31 g (87 %) of pure product as a dark orange powder, see **Figure C3-S3** for ^{1}H NMR characterization.

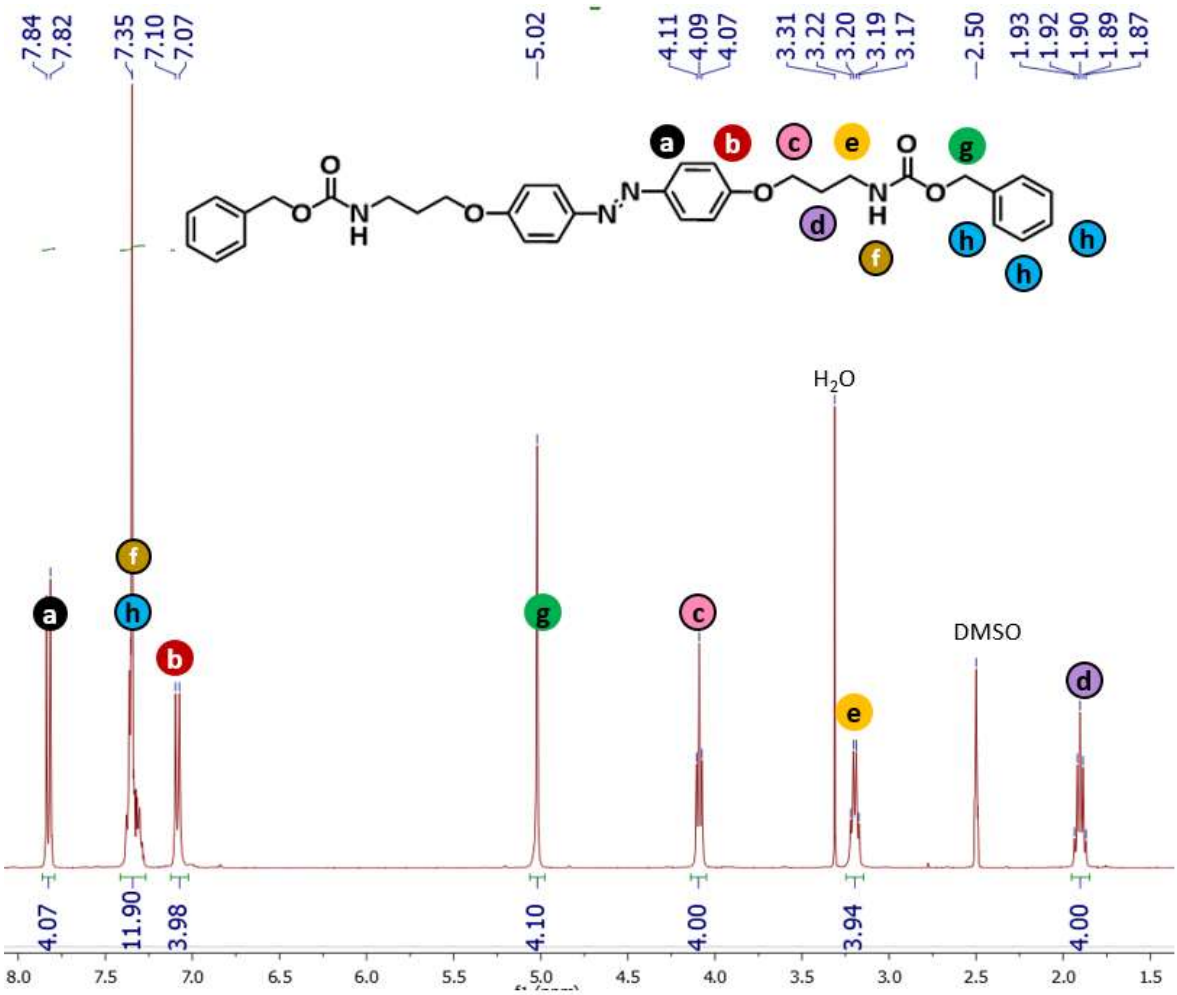

Figure C3-S3. ^{1}H NMR (in DMSO-d_6) of azobenzene **2**

^{1}H NMR (DMSO-d_6, 400 MHz): δ (ppm) 7.83 (d, **H^a**, J_3 = 9.2 Hz, 4H), 7.35 (m, **H^h + H^f**, 12H), 7.08 (d, **H^b**, J_3 = 9.2 Hz, 4H), 5.02 (s, **H^g**, 4H), 4.09 (t, **H^c**, J_3 = 6,2 Hz, 4H), 3.20 (q, **H^e**, J_3 = 6,2 Hz, 4H), 1.90 (qt, **H^d**, J = 6,2 Hz, 4H)

Synthesis of Azobenzene-diammonium 3: adapted from ref[1]

Azobenzene **2** (4,00 g, 6.71 mmol, 1 eq) was introduced in a round bottom flask equipped with a stir bar and 30% HBr in AcOH (15.5 g, 57,6 mmol, 8.85 eq) was added quickly. The mixture immediately turned dark red/black and was left to react for 1 hour. 50 mL of diethyl ether was then added, and the mixture was stirred for 5 minutes before being filtered. The precipitate was washed with diethyl ether. Traces of solvent were removed under reduced pressure, yielding 3.28 g (~ 100 %) of a black powder, see **Figure C3-S4** for ^{1}H NMR characterization. It is noteworthy that while some traces of solvents were present, these were eliminated during the next step (ammonium neutralization) and therefore weren't problematic.

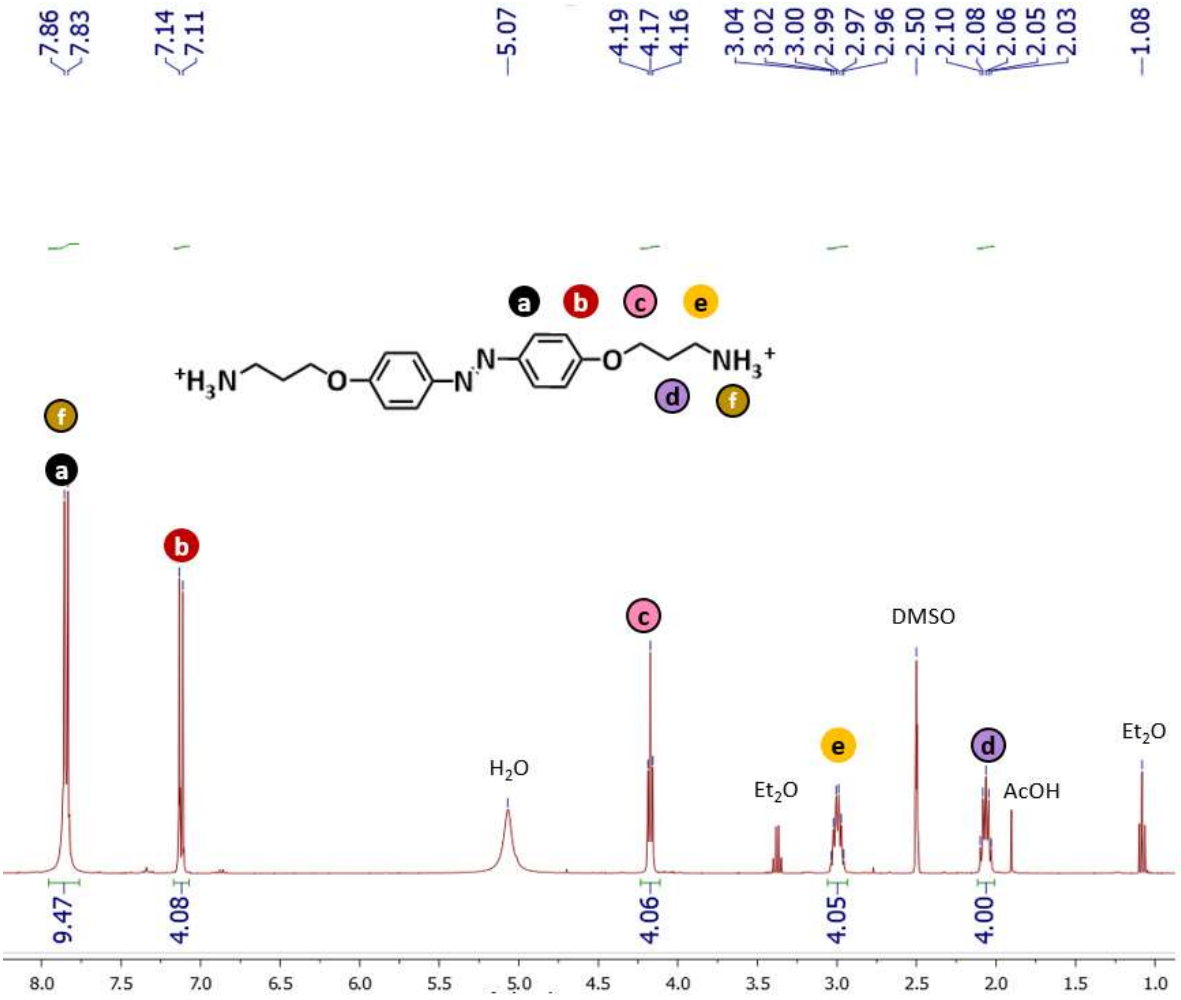

Figure C3-S4. ^{1}H NMR (in DMSO-d_6) of azobenzene **3**

^{1}H NMR (DMSO-d_6, 400 MHz): δ (ppm) 7.84 (m, **H^a + H^f**, 10H), 7.12 (d, **H^b**, J_3 = 9.2 Hz, 4H), 4.17 (t, **H^c**, J_3 = 6,4 Hz, 4H), 3.00 (sext **H^e**, J_3 = 6,4 Hz, 4H), 2.05 (qt, **H^d**, J_3 = 6.4 Hz, 4H)

Neutralization of 3:

Azobenzene **3** (1.00 g, 2.04 mmol) was placed in a round bottom flask immersed in an ice bath and NaOH (5.00 g, 61 eq.) dissolved in 10 mL of water was added. The mixture was stirred for one hour at room temperature. Then, 200 mL of DCM was added, followed by 30 mL of water. The mixture was stirred until the aqueous phase was clear (approximatively 2 hours). The organic phase was separated and the aqueous phase was further washed with 2 x 100 mL DCM. The organic phases were gathered, dried over molecular sieves (4 Å, powder form), filtered, and DCM was removed under reduced pressure, affording 0.455 g (68 %) of a yellow powder, which was stored under argon at 0 °C. Its chemical structure was confirmed by ^{1}H NMR (**Figure C3-S5**).

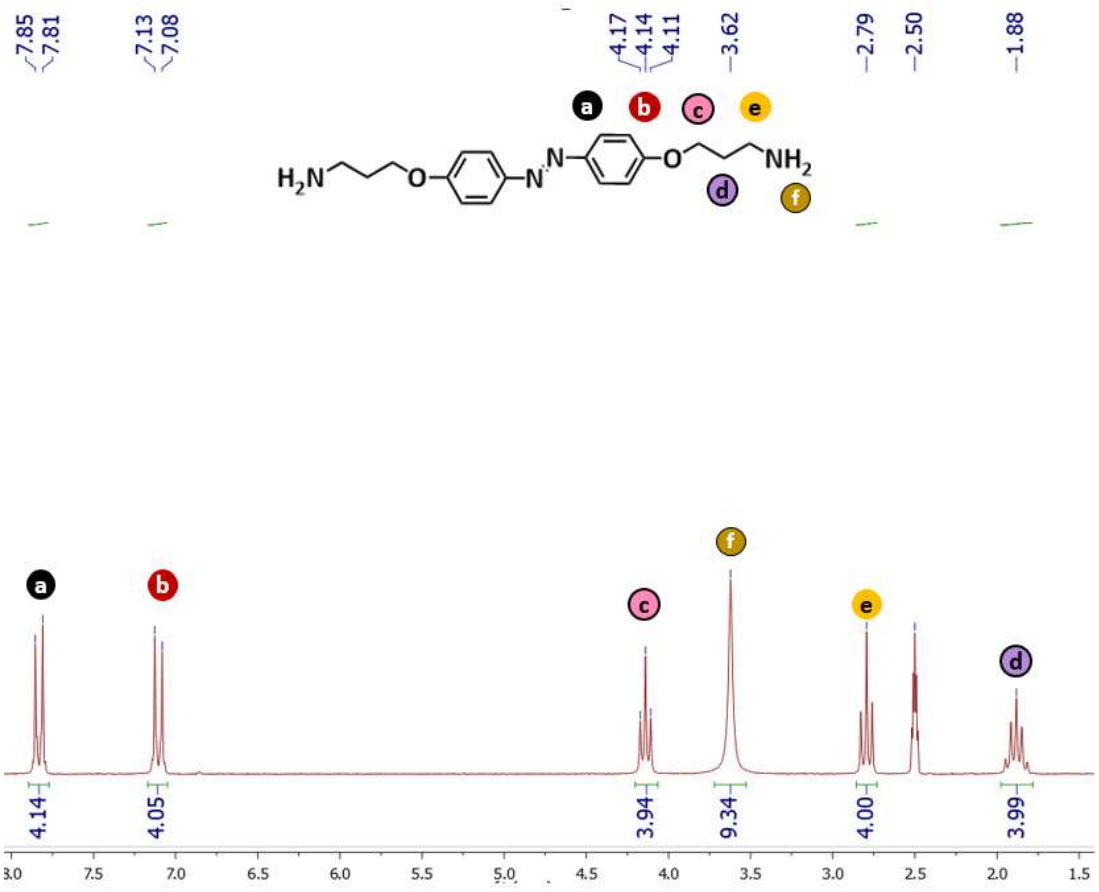

Figure C3-S5. ^{1}H NMR (in DMSO-d_6) of neutralized azobenzene **3**.

^{1}H NMR (DMSO-d_6, 200 MHz): δ (ppm) 7.83 (d, **H^a**, J_3 = 9.0 Hz, 4H), 7.10 (d, **H^b**, J_3 = 9.0 Hz, 4H), 4.14 (t, **H^c**, J_3 = 6.6 Hz, 4H), 3.62 (br s, **H^f** + H_2O, 4H coming from H_f) 2.79 (t, **H^e**, J_3 = 6.6 Hz, 4H), 1.88 (qt, **H^d**, J_3 = 6.6 Hz, 4H)

Note: the peak at 3.62 ppm corresponding to the **H^f** of the amine is in rapid protonic exchange with water so that a single broad singulet corresponding to the integration of H_f (4H) and residual H_2O (~ 5.3 H) is observed.

^{1}H NMR characterization of PEO-C_6-NCO after its synthesis (see Experimental section for the details of the synthesis):

After workup, the crude product was solubilized in DMSO-d_6 with a drop of benzylamine in order to quench the isocyanates moieties, and was then analyzed by ^{1}H NMR.

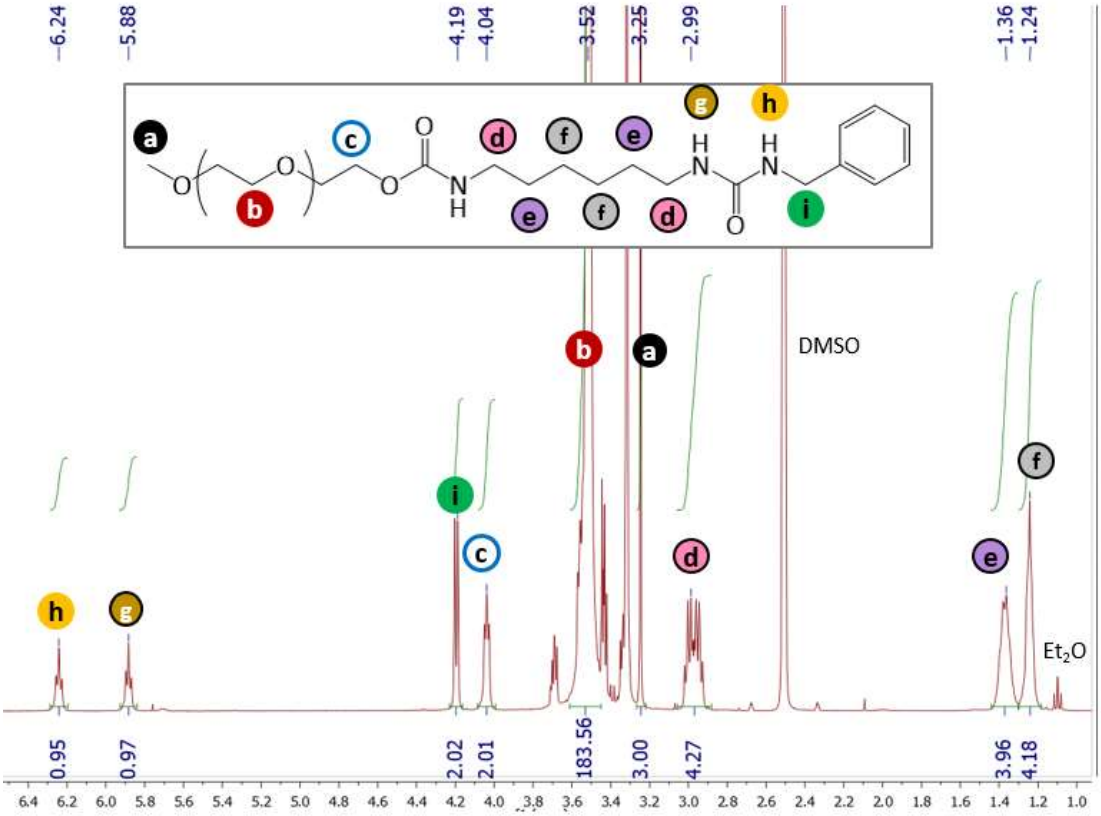

Figure C3-S6. ^{1}H NMR of PEO-C_6-Benzylurea

^{1}H NMR (DMSO-d_6, 400 MHz): δ (ppm) 6.24 (t, **H^{h}**, J_3 = 6.0 Hz, 1H), 5.88 (t, **H^{g}**, J_3 = 6.0 Hz, 1H), 4.19 (d, **H^{i}**, J_3 = 6.0 Hz, 2H), 4.04 (t, **H^{c}**, J_3 = 4.8 Hz, 2H), 3.52 (m, **H^{b}**, 180H = DP_n x 4H), 3.25 (s, **H^{a}**, 3H), 2.99 (m, **H^{d}+H$^{d'}$,** 2H+2H), 1.36 (m, **H^{e}+H$^{e'}$**, 2H+2H), 1.24 (m, **H^{f}+H$^{f'}$**, 2H+2H).

<u>Identification of the impurity during the synthesis of Azo-(U-PEO)$_2$:</u>

After workup during the synthesis of **Azo-(U-PEO)$_2$**, an impurity was observed by ^{1}H NMR. The formation of the latter is presumed to be through the hydrolysis of some isocyanates, yielding amine terminated PEO, which can then react with remaining isocyanate (see **Figure C3-S7**).

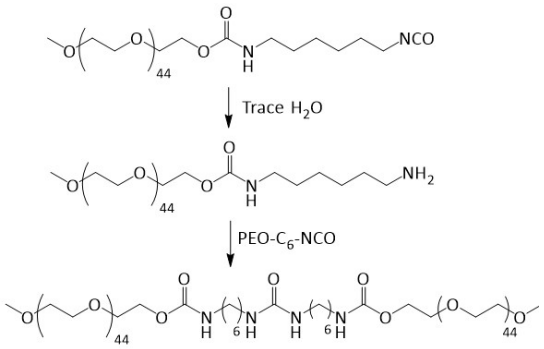

Figure C3-S7. Proposed formation of PEO-C_6-U-C_6-PEO through the hydrolysis of some isocyanate functions of PEO-C_6-NCO.

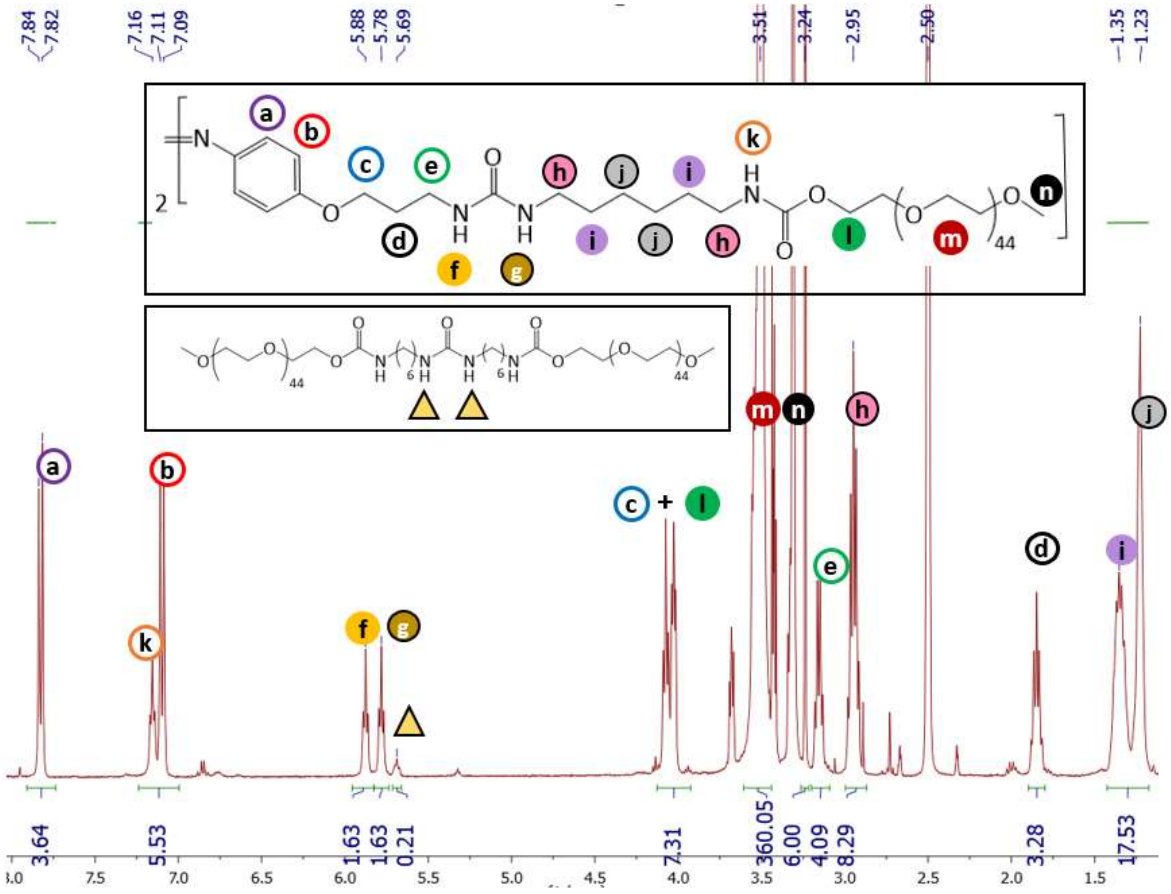

Figure C3-S8. ^{1}H NMR (in DMSO-d_6) of the crude product (**5**) with the impurity PEO-C_6-U-C_6-PEO.

Reference[1]: Wei, W., Tomohiro, T., Kodaka, M. & Okuno, H. Selective Synthesis and Kinetic Measurement of 1 : 1 and 2 : 2 Cyclic Azobenzene Units. 8979–8987 (2000) doi:10.1021/jo000926p.

2. Characterization of the self-assemblies in aqueous media

i. Direct dispersion in water.

LS measurements

Light scattering revealed a very weakly aggregated system, with an apparent molecular weight M_{app} = 3.10^5 g/mol, corresponding to an N_{agg} of approximately 70 (**Figure C3-S9**). The hydrodynamic radius R_h was also rather low, at 15 nm, and lack of angular dependence implied R_g < 20 nm. The solution was again analyzed after 10 days of aging at r.t., and LS measurements indicated that the system had not re-organized into nanocylinders. The only difference observed is that the initial sample contains a few ill-defined aggregates slightly increasing the scattered intensity at low q, whereas the sample after 10 days is cleaner, with none of these aggregates and a q-independent scattered intensity. The scattered intensity at high q and the R_h are identical at t_0 and after 10 days, implying no significant evolution of the extent of self-assembly over this period and certainly no formation of nanocylinders.

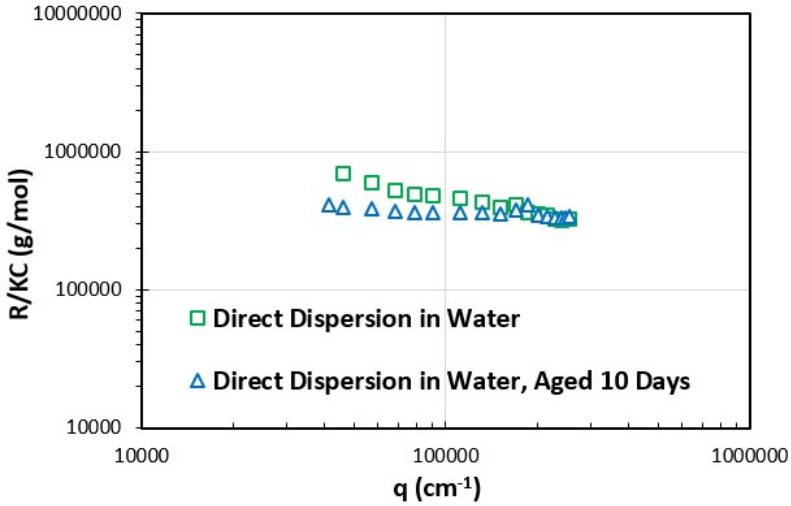

Figure C3-S9. LS data of a solution prepared by direct dissolution of **Azo-(U-PEO)$_2$** in water, and after 10 days. The solutions were filtered over 0.45 µm and loss of matter was found to be negligible, as measured using UV-Vis before and after filtration.

UV-Vis measurements

Photo-isomerization kinetics were carried out using a solution prepared by directly dissolving the polymer in water at 1 g/L. Irradiation was performed at different time intervals at 365 nm to trigger *trans* → *cis* isomerization and the isomerization was monitored using UV-Vis spectroscopy. Once the photo-stationary state was reached, photo-isomerization back to the *trans* isomer was performed by irradiating at 450 nm. Once the second photo-stationary state had been reached, the solution was heated at 80°C for 30 minutes to accelerate thermal relaxation.

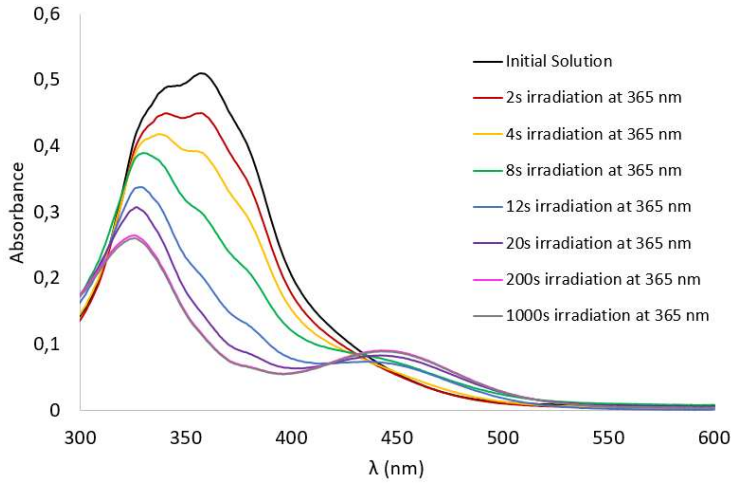

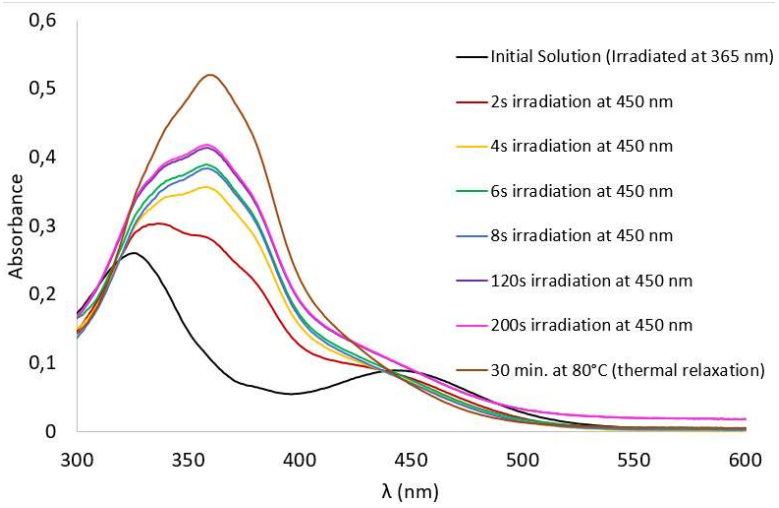

Figure C3-S10. Kinetics of photo-isomerization of a solution prepared by directly dissolving the polymer in water at 1 g/L. Top: *trans* → *cis* photo-isomerization with irradiation at 365 nm. Bottom: *cis* → *trans* photo-isomerization with a second irradiation at 450 nm.

ii. Water/DMSO route

Cryo-TEM images

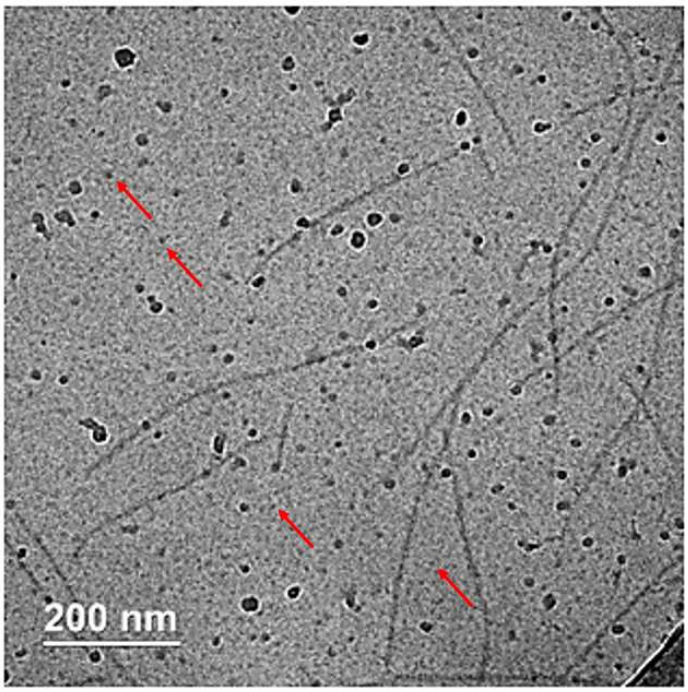

Figure C3-S11. Cryo-TEM images of the "water/DMSO" route solution prior to irradiation

As can be observed in **Figure C3-S11**, some very small spherical particles appear to be present in addition to the long nanocylinders. It suggests that part of the polymer does not form nanocylinders, but small spherical micelle-like structures. The amount of the latter cannot be estimated by cryo-TEM which is not a quantitative method. However, the length of the cylinders calculated either from the molecular weight of the cylinders assuming that

all the polymer forms nanocylinders (400 nm), or by fitting the light scattering data (520 nm, which makes no assumption on the concentration of polymers forming nanocylinders) or from the cryoTEM experiments (several hundreds nm) is in very good agreement. These results strongly suggest that the mass concentration of small spherical particles observed by cryoTEM is low compared to that of nanocylinders, which by the way explains why they are not detected by light scattering.

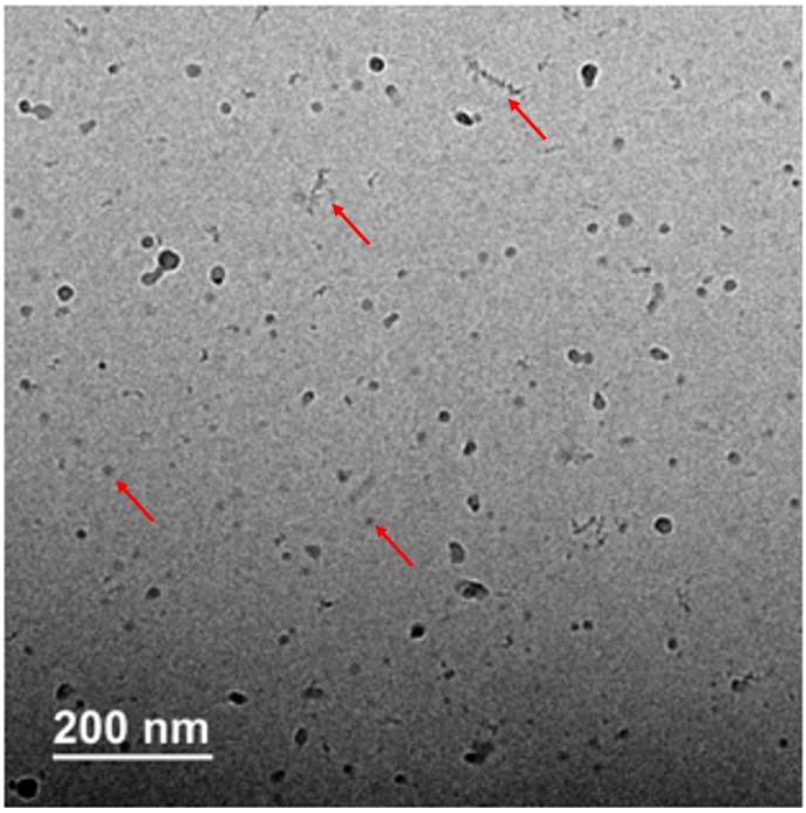

Figure C3-S12. Cryo-TEM images of the "water/DMSO" route solution after UV irradiation for 5 minutes at 365 nm.

As can be seen in **Figure C3-S12**, some small anisotropic particles can be observed, which may perhaps be small bits of disrupted nano-cylinders, as well as small spherical particles, which would be consistent with LS measurements. The larger, darker spherical dots are however sample pollution (ice crystals).

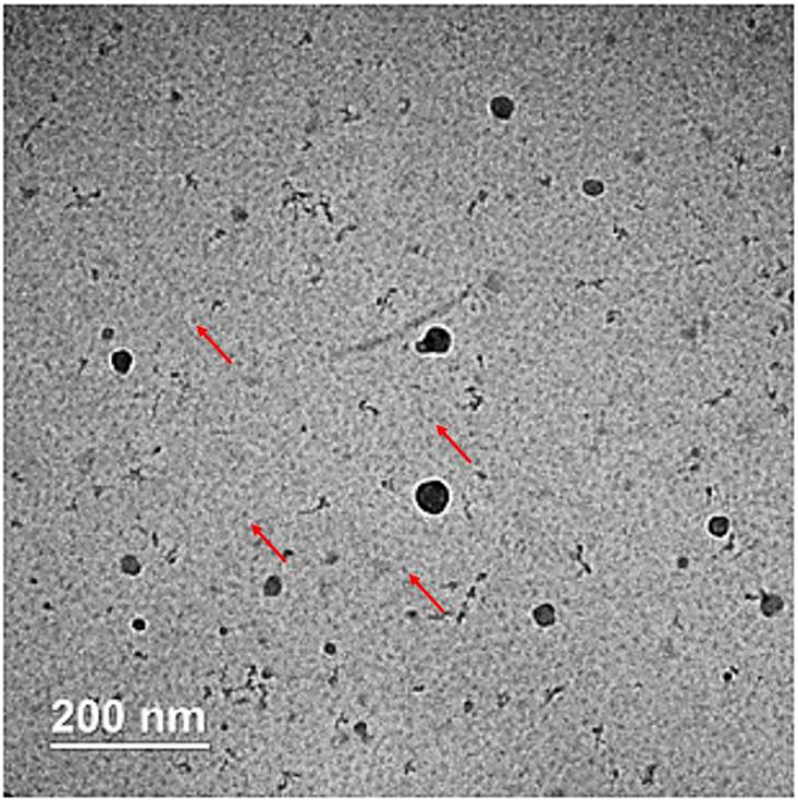

Figure C3-S13. Cryo-TEM images of the "water/DMSO" route solution after a first UV irradiation for 5 minutes at 365 nm followed by a second blue light irradiation for 5 minutes at 450 nm.

As can be seen in **Figure C3-S13**, still no nano-cylinders are present, however there are still some very small spherical particles. Once again, the larger, dark spots are pollution from ice crystals.

LS measurements

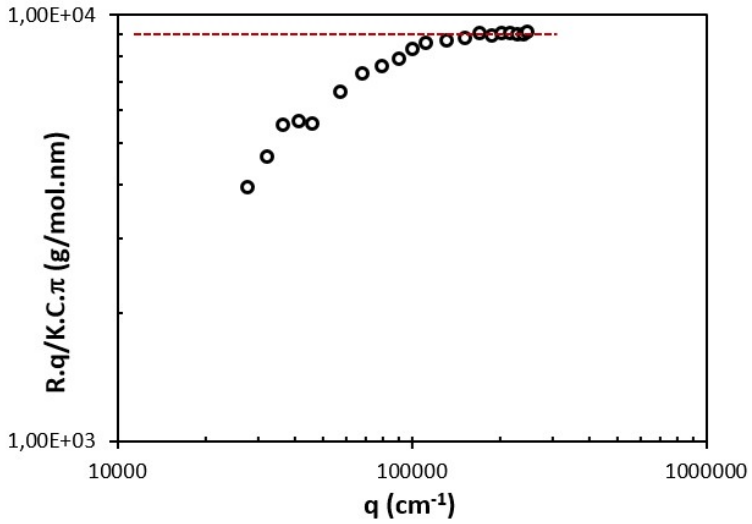

Figure C3-S14. LS data of a « water/DMSO » route solution before irradiation. R.q/K.C.π plotted as a function of q

Another experiment was conducted, which consisted in first irradiating with UV light the concentrated DMSO solution, followed by slow addition of water (**Figure C3-S15**). Overall, the scattered intensity did not show any angular dependence, and the weak Rh of 15 nm suggests a low extent of aggregation.

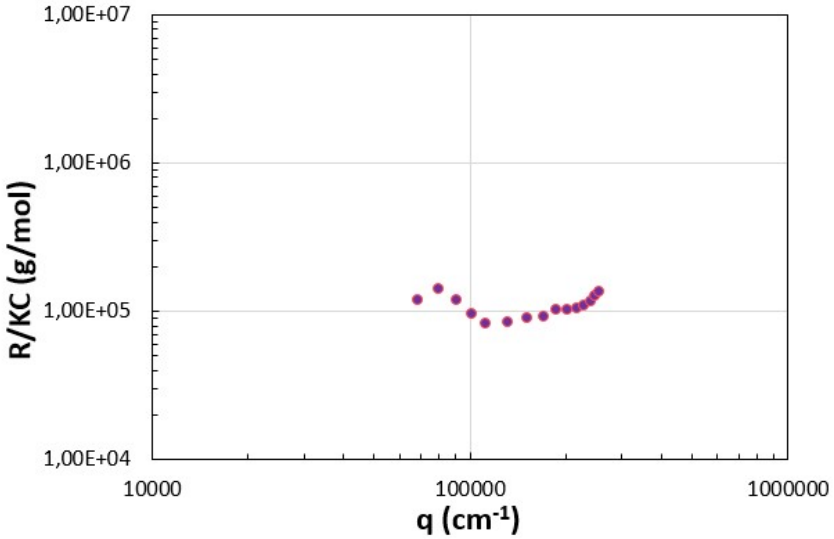

Figure C3-S15. LS data of a "water/DMSO" route solution, with UV (365 nm) irradiation of the initial DMSO solution

A few organic solvents were tested as substitutes for DMSO (**Figure C3-S16**). The protocol was identical to that of the "water/DMSO" route, with the only difference being the nature of the initial organic solvent. The "water/EtOH" route led to no angular dependence in LS, with a R_h of 15 nm, suggesting very weak aggregation. LS of "water/acetone" solution also led to no angular dependence, with a larger R_h of 50 nm, which is likely not representative of the sample, and is probably due to the presence of large ill-defined aggregates that were not removed during filtration (0,45 µm). Indeed, the scattered intensity if of the same order of magnitude for both solvents, albeit with more noise with acetone. In either cases, no nanocylinders appeared to be present.

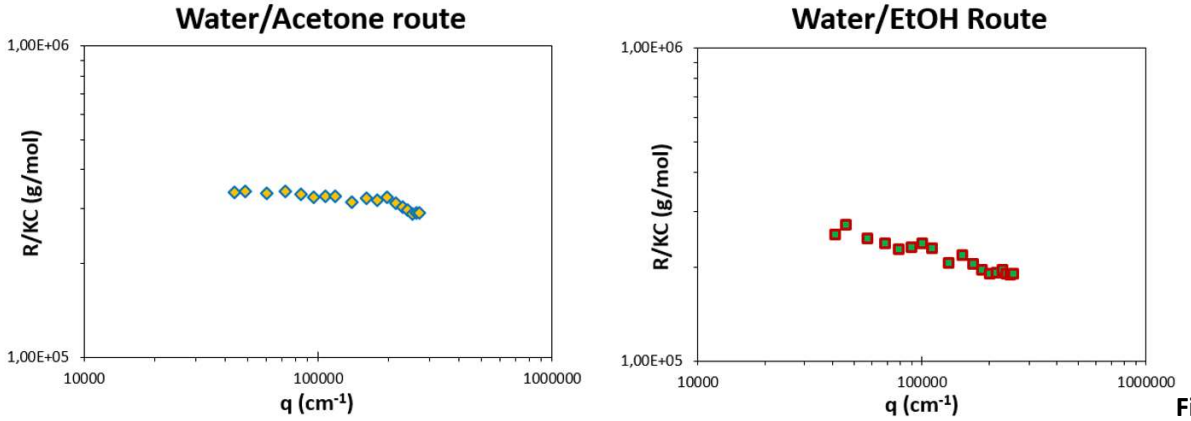

Figure C3-S16. Testing alternative organic solvents instead of DMSO, otherwise following the same protocol as the "water/DMSO" route.

<u>UV-Vis measurements</u>

An aqueous solution of nanocylinders was prepared following the « water/DMSO » route (0.9 g/L). It was irradiated with UV (365 nm) for 5 minutes to trigger photo-isomerization of *trans*-azobenzene to *cis*-azobenzene, and thermal relaxation (*cis* → *trans*) kinetics were monitored using UV-Vis spectroscopy. As can be seen in **Figure C3-S17**, the thermal relaxation was monitored by measuring the absorption spectra at 450 nm, a characteristic peak of the *cis* isomer, which was observed to gradually decrease upon thermal relaxation. The data were normalized, so that at t_0, the normalized absorbance is equal to 1 (and therefore $\ln(A)_{t0} = 0$), and so that after reaching steady-state, it is equal to 0. The data agree very well with a 1st order kinetic, with a rate constant k of $5{,}4.10^{-4}$ min^{-1}, corresponding to a half-life $t_{1/2}$ of approximately 1300 minutes (or around 22 hours).

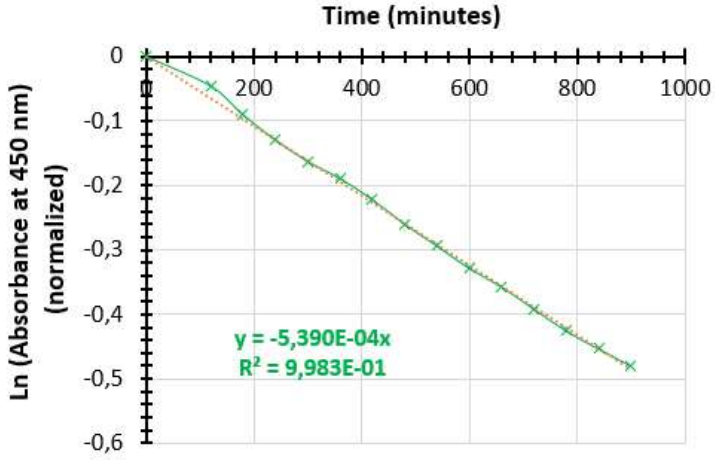

Figure C3-S17. Kinetic graph of the thermal relaxation at 20°C of a "water/DMSO" route (99/1 v/v) at 0.9 g/L solution after irradiation at 365 nm

A "water/DMSO" solution (99/1, 0.9 g/L) was subjected to irradiations at 365 and then 450 nm and then heated to 80°C for 30 minutes to accelerate thermal relaxation. The solutions were analyzed by UV-Vis spectroscopy, and the data can be found in **Figure C3-S18**. After thermal relaxation, virtually all of the initial *trans*-azobenzene is recovered.

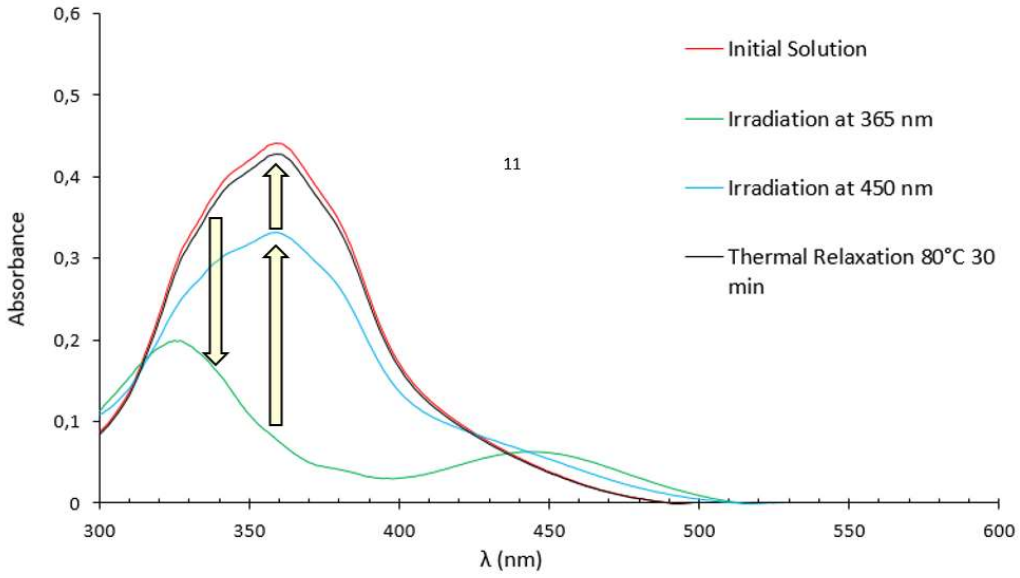

Figure C3-S18. UV-Vis spectra of a solution prepared following the "water/DMSO" route (99/1, 0.9 g/L), prior to irradiation (red curve), after irradiation at 365 nm (green curve), after a second irradiation at 450 nm (blue curve), and after thermal relaxation at 80°C for 30 minutes (black curve)

<u>Estimation of trans/cis ratio by ^{1}H NMR measurements after light irradiations</u>

Since the azobenzene core is insoluble in water (i.e. the polymer directly dissolved in D_2O shows no azobenzene peaks in ^{1}H NMR), ^{1}H NMR must be conducted in DMSO-d_6, which is a good solvent for both the polymer arms and the azobenzene core. Therefore, a solution was prepared following the "water/DMSO" route (99/1) at 0.9 g/L, and was subjected to UV irradiation at 365 nm until the photo-stationary state was reached. Then, a portion of this solution was subjected to a second irradiation at 450 nm, triggering *cis* → *trans* photo-isomerization. Both solutions were then quickly freeze-dried to remove water, solubilized in DMSO-d_6 and analyzed by ^{1}H NMR.

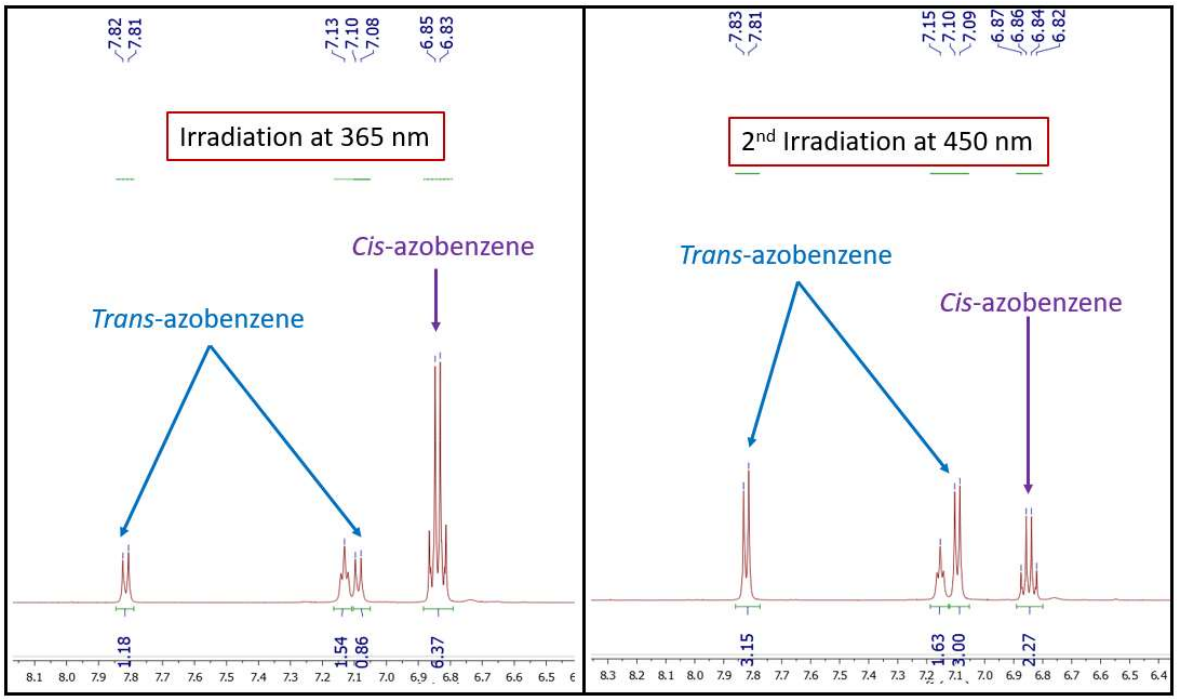

Figure C3-S19. ^{1}H NMR in DMSO-d_6 of the polymer after irradiation and freeze-drying

The amount of *trans* isomer can be calculated by dividing the integral values of the *trans*-azobenzene peaks by the sum of *trans* + *cis* peak integrals:

$\%_{trans}$ = (1.18 + 0.86)/(1.18 + 0.86 + 6.37) x 100 = **24.3 %**

And therefore: **following UV irradiation (365 nm)**

$\%_{cis}$ = 100 - $\%_{trans}$ = **75.7 %**

$\%_{trans}$ = (3.15 + 3.00)/(3.15 + 3.00 + 2.27) x 100 = **73.0 %**

And therefore: **following blue light irradiation (450 nm)**

$\%_{cis}$ = 100 - $\%_{trans}$ = **27.0 %**

These values are consistent with UV-Vis measurements which indicated that approximately 75% of *trans*-azobenzene is recovered after the two irradiations (as seen in **Figure C3-S18**).

V. Reproducibility issues encountered

The synthesis of Azo-(U-PEO)$_2$ was achieved in the spring of 2022, during which the physico-chemistry experiments were also conducted (as detailed in the article) and were reproducible. However, after the summer period, difficulties were encountered. Using exactly the same "water/DMSO" route protocol (99/1, 0.9 g/L), light scattering experiments indicated a barely aggregated system with no angular dependency (see **Figure C3-S20**). Several other solutions were prepared using the same conditions, but gave similar results.

About 8 months of experiments were dedicated to understand this phenomenon and decide whether we could publish the initial results.

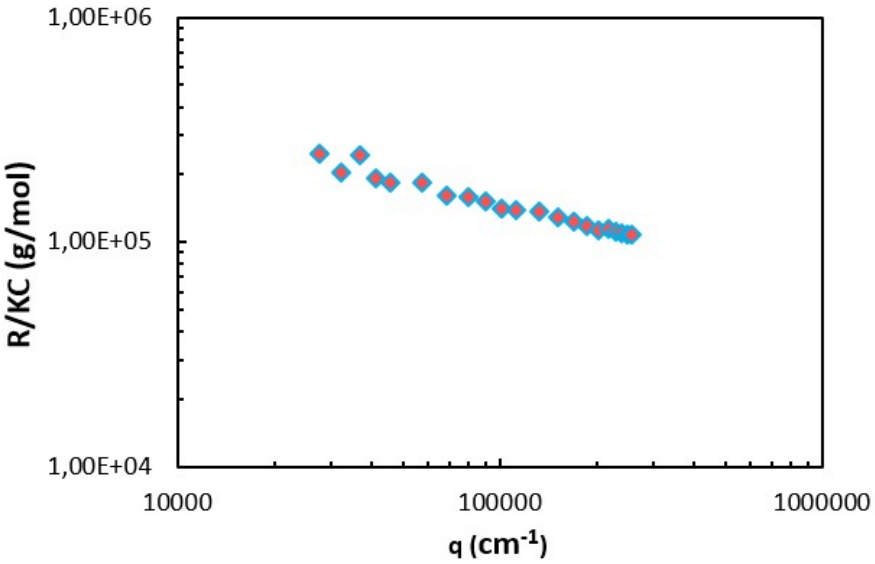

Figure C3-S20. LS data of a water/DMSO solution prepared after the summer of 2022, filtered over 0.45 µm. R_h = 12 nm

First, ^{1}H NMR and SEC experiments were conducted in order to verify if any degradation of the polymer had occurred. It is worthy to note that the polymer was stored in the dark at 20°C since it had been synthesized. As can be seen in **Figure C3-S21**, ^{1}H NMR conducted straight after the synthesis superimposes perfectly with the spectra done after the summer. SEC measurements after the summer indicated that the polymer was not degraded, with a molecular weight very close (slightly superior) to that of PEO_{4K}.

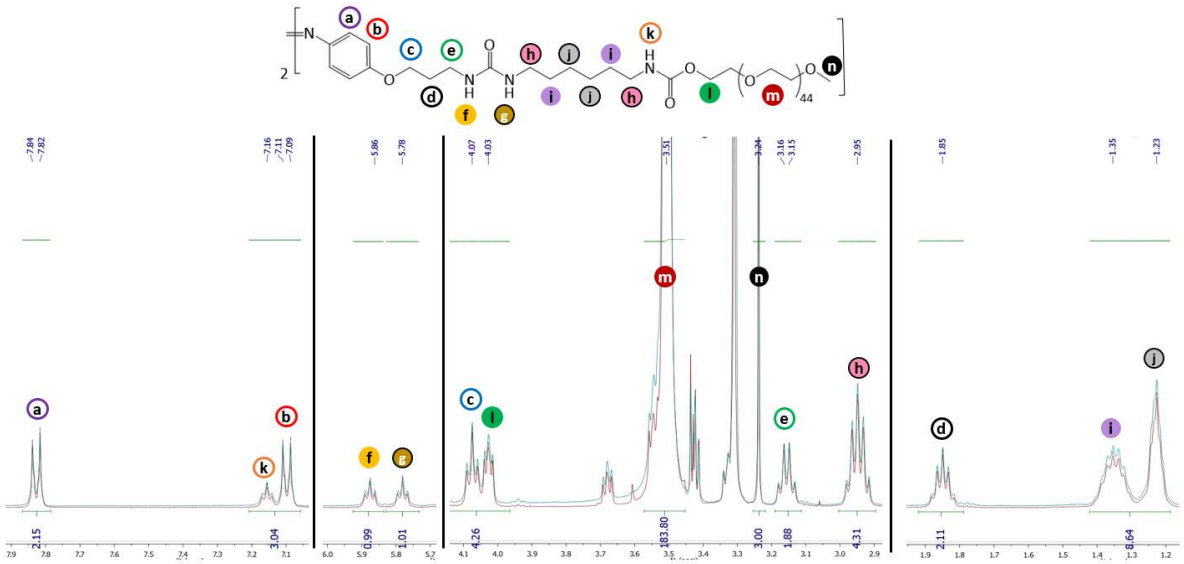

Figure C3-S21. ^{1}H NMR (DMSO-d_6, 400 MHz) spectra of Azo-(U-PEO)$_2$ after synthesis (red) and after the summer (blue)

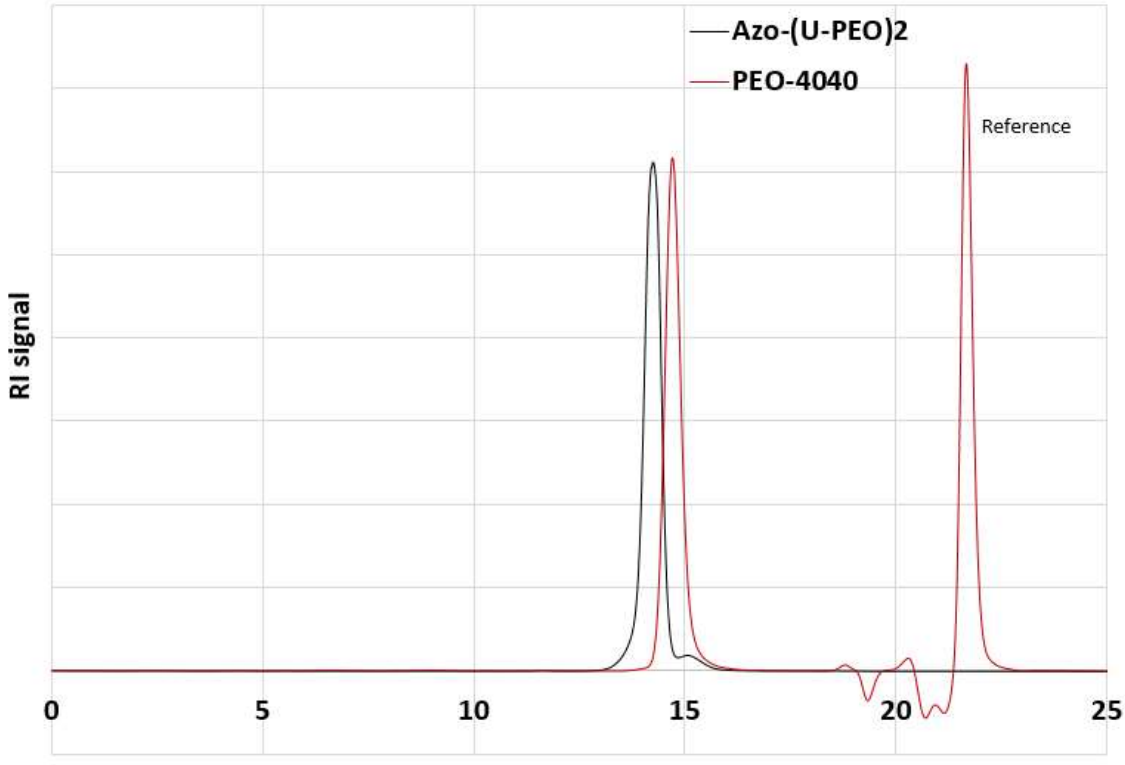

Sample	Retention time (min)	Mn (g/mol)	Mw (g/mol)	Polydispersity
Azo-(U-PEO)2	14,6	9470	10057	1,06
PEO4K	14,71	8311	8725	1,05

Figure C3-S22. SEC chromatogram in DMF (with 1 g/L LiBr) of Azo-(U-PEO)$_2$ (black curve) and of PEO$_{4K}$ (red curve). Molecular weights are calculated from a PMMA calibration.

Cryo-TEM measurements (carried out before the summer and the problems) suggests that the amount of nano-cylinders decreases during filtration over 0.45 µm. Since UV-Vis measurements indicated negligible loss of matter upon filtration of the solution, the decrease in observed nano-cylinders could be explained by a partial disruption of the assemblies during filtration (see **Figure C3-S23**).

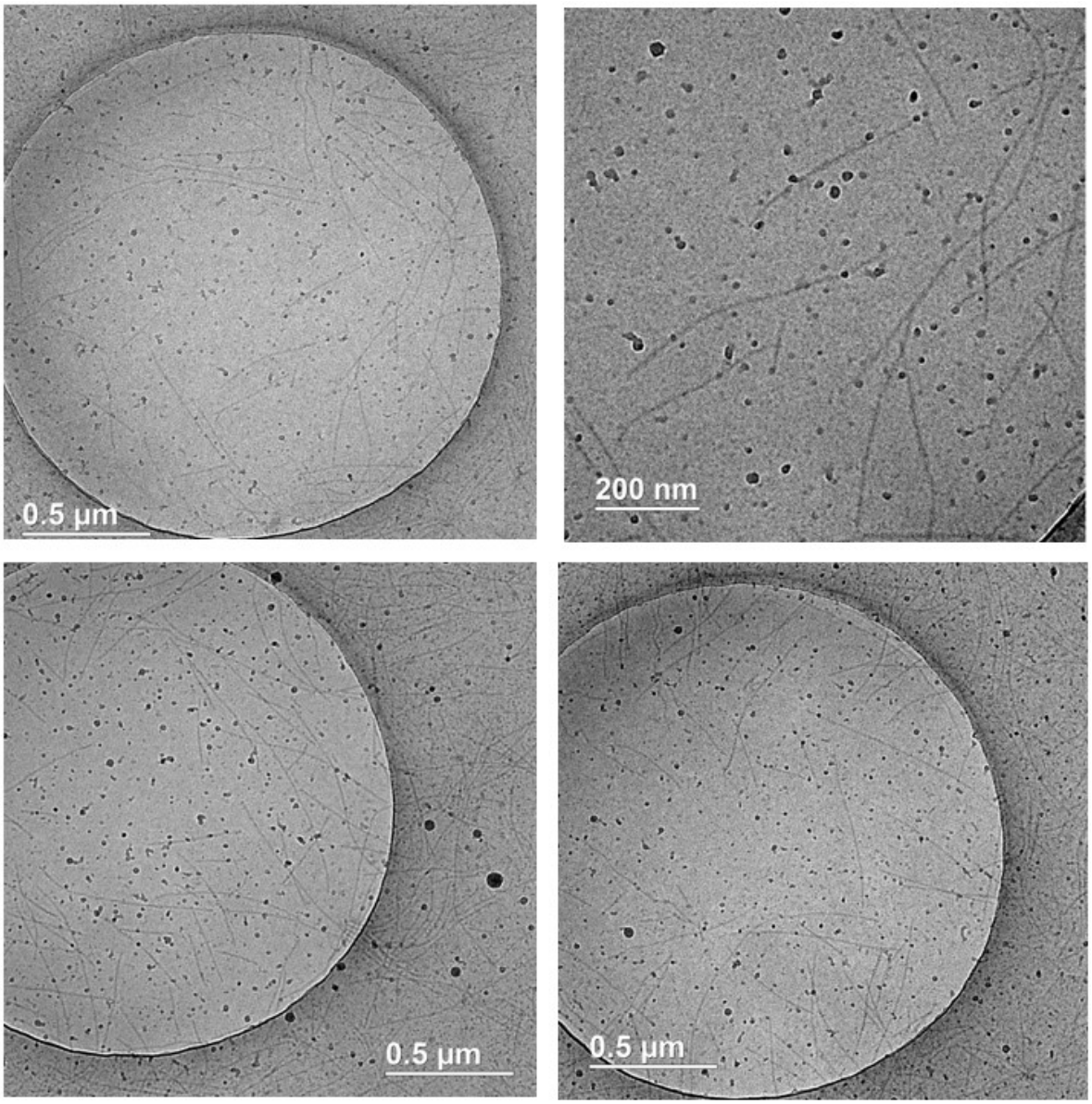

Figure C3-S23. Cryo-TEM images of a solution of Azo-(U-PEO)$_2$ prepared using the water/DMSO route (99/1, 1 g/L) before the summer, without filtration

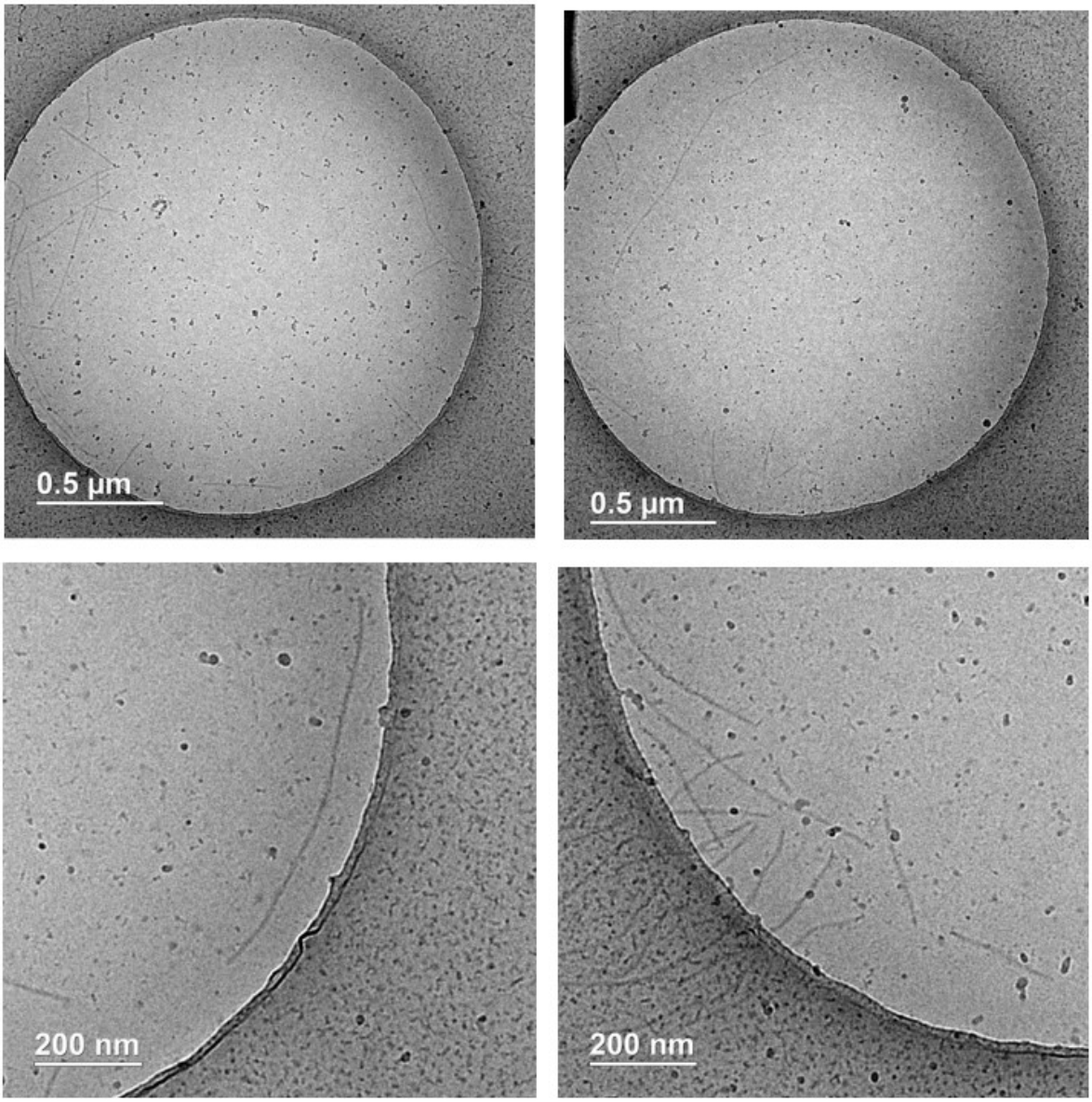

Figure C3-S24. Cryo-TEM images of a solution of Azo-(U-PEO)$_2$ prepared using the water/DMSO route (99/1, 1 g/L) before the summer, after filtration (0.45 µm)

In view of these results, another water/DMSO route solution was prepared (99/1, 1 g/L) with the aged sample (after summer 2022) and analyzed both by light scattering, after filtration over 0.8 µm (negligible loss of matter was observed by UV/Vis spectroscopy with this filter) and by cryoTEM (without filtration). As can be seen in **Figure C3-S25**, the static light scattering data reveal a weak extent of aggregation (M_{app} ~ 10^5 g/mol corresponding to N_{agg} ~ 20, instead of 800 on the fresh sample). However, the same solution analyzed by cryo-TEM without filtration revealed that lots of long nano-cylinders were present in the sample (see **Figure C3-S26**). The quality of the image was poor due to the formation of a thick vitrified water film, but the nano-cylinders are still clearly visible.

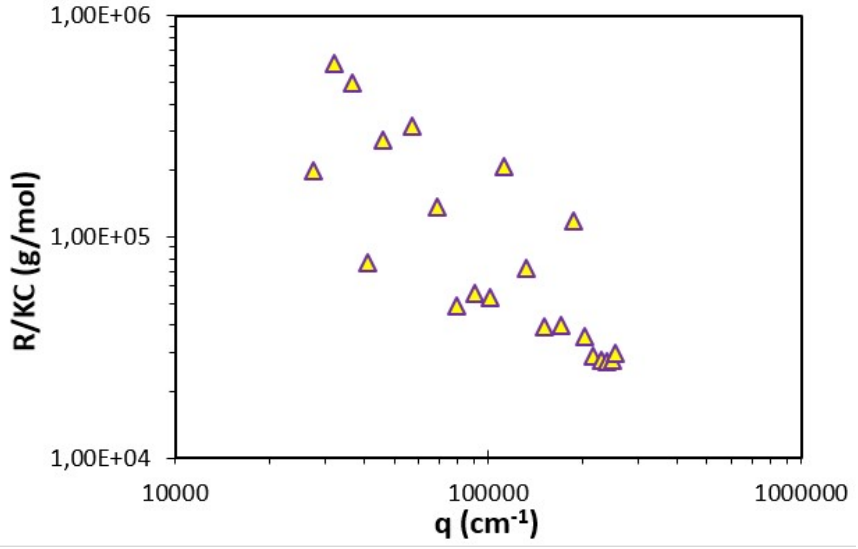

Figure C3-S25. LS data of an Azo-(U-PEO)2 solution prepared using the "water/DMSO" route (200 rpm stirring speed) after filtration over 0.8 µm.

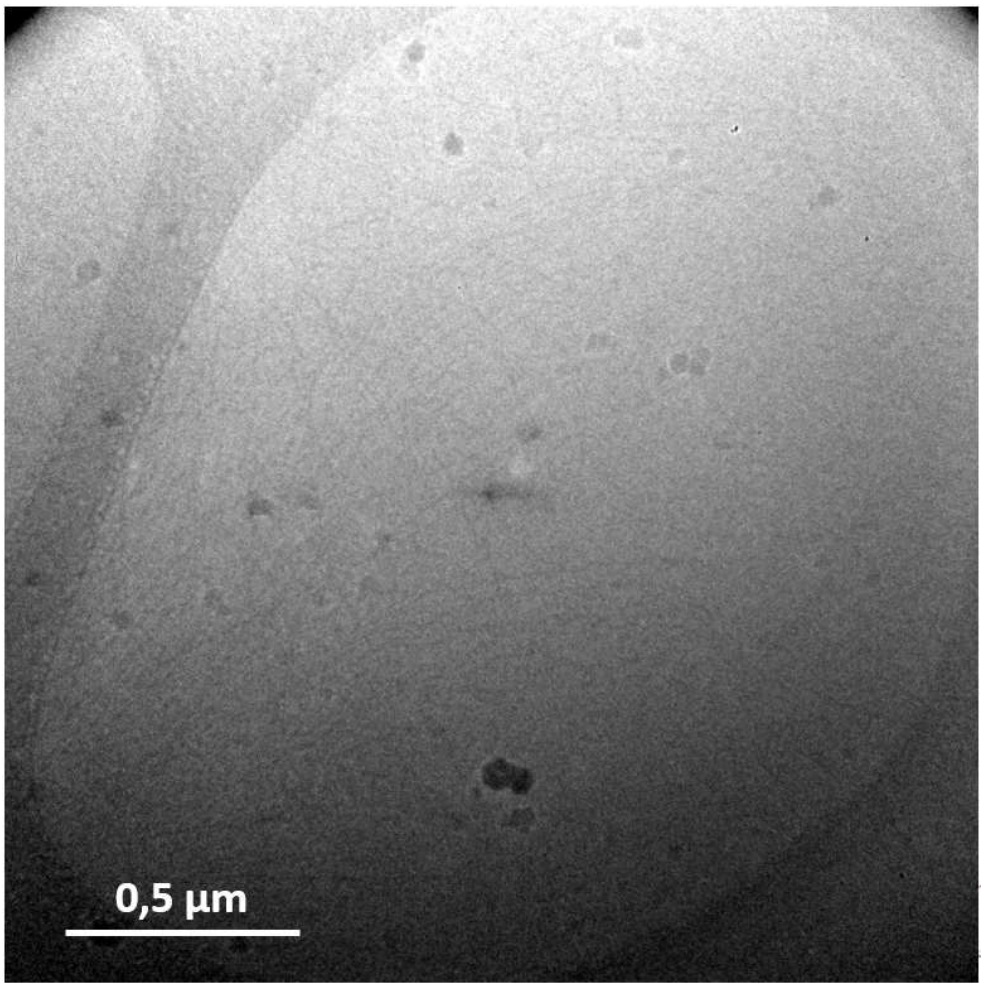

Figure C3-S26. Cryo-TEM image of the Azo-(U-PEO)$_2$ solution prepared using the "water/DMSO" route (200 rpm stirring speed) without filtration.

To confirm the formation of nanocylinders using the "DMSO-route" with the aged sample, another solution was prepared using the same protocole. Again, cryo-TEM confirmed the presence of many long nano-cylinders in the sample (see **Figure C3-S28**). However, filtration over a 0.8 µm filter resulted in 31% loss of matter according to UV-Vis and revealed the presence of very large objects with an angular dependency of the scattering intensity close to a q^{-2}; which would correspond to fractal objects. Filtration of the same (unfiltered) solution over a 0.45 µm filter resulted in 35% loss of matter and a strong decrease of the scattered intensity. The angular dependency was closer to a q^{-1}, but the shape of the curve was still very different from that obtained with the fresh polymer sample in spring 2022 (see **Figure C3-S27**).

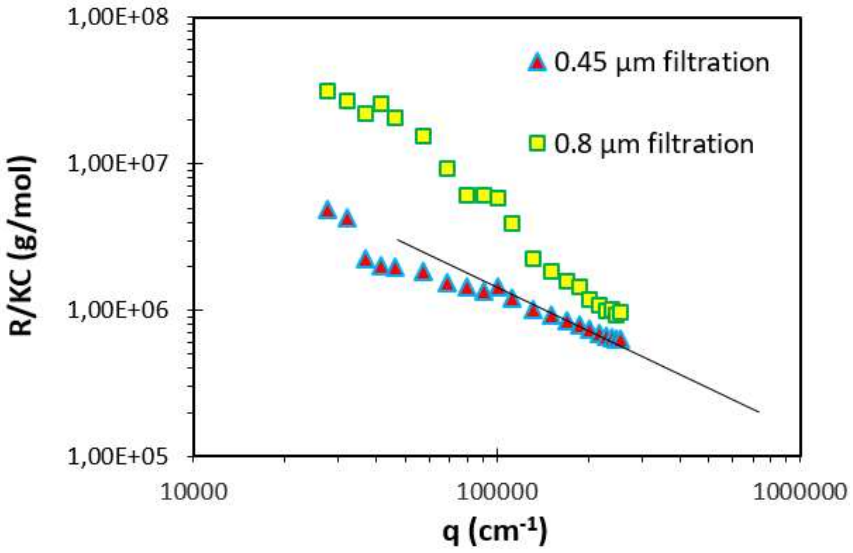

Figure C3-S27. LS data of an Azo-(U-PEO)$_2$ solution prepared using the "water/DMSO" route (200 rpm stirring speed) after filtration over 0.8 µm (orange curve, $R_h \approx$ 100-110 nm) or 0.45 µm (blue curve, $R_h \approx$ 50-60 nm). The black line is q^{-1} visual guide. The differences in concentration due to filtration were taken into account in the R/KC ratio.

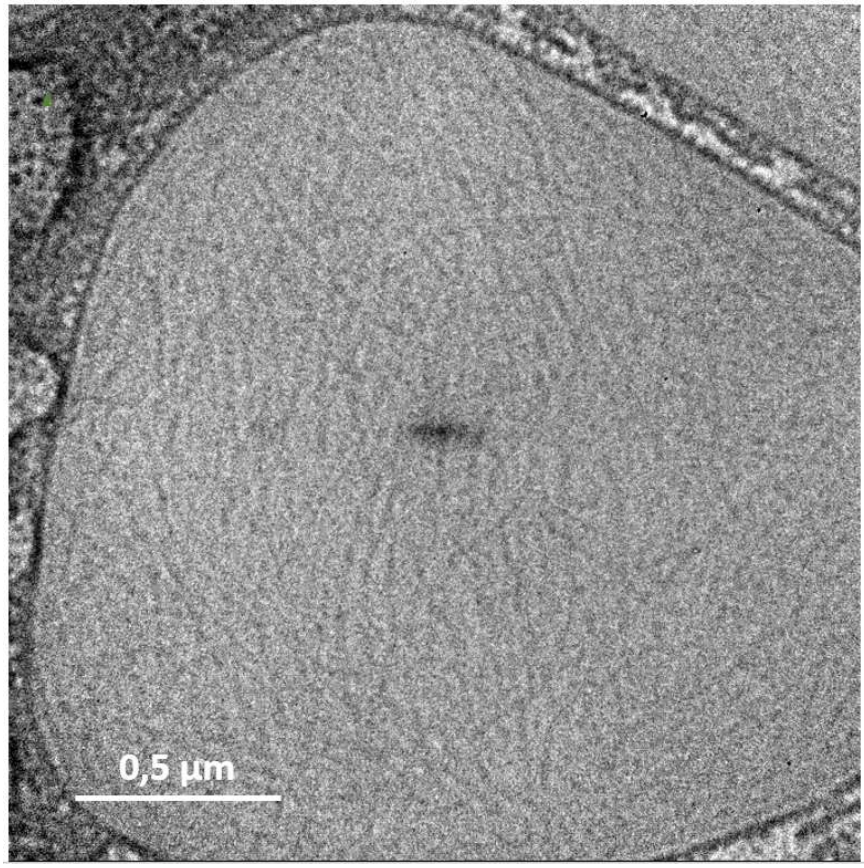

Figure C3-S28. Cryo-TEM image of the second Azo-(U-PEO)$_2$ solution prepared using the "water/DMSO" route (200 rpm stirring speed) without filtration.

From these results, it would appear that filtration strongly disrupted the nanocylinders, even more with the aged sample (after summer 2022) than with the fresh one (spring 2022). Additionnally, even though the filtration was performed as gently on possible (gravity-induced crossing of the filter over several minuted, without pushing with the syringe piston) and with different kinds of filters, different behaviors were observed by light scattering, ranging from the observation of small and weakly aggregated particles to large fractal aggregates. Unfortunately, filtration was compulsory for light scattering analysis in order to remove the unavoidable small fraction of dust or of large spurious aggregates which would otherwise dominate the light scattering signal because of their size and in spite of their low concentration. Light scattering was therefore no more reliable on the aged sample.

Still, cryoTEM did reveal the formation of long and numerous nanocylinders with the "DMSO-route", which made us confident that the conclusions presented in the article were reliable. We therefore decided to publish the light scattering and cryoTEM data obtained with the fresh sample. Some additionnal UV/Vis experiments were conducted with the aged samples and the conclusions we reached here were reliable in our opinion because nanocylinders were indeed present even for the aged sample according to cryoTEM.

We have currently no explanation why these reproducibility issue occurred. However, it is clear that they are not related to a chemical degradation of the molecule as shown by ^{1}H NMR and SEC. We actually believe that this has something to do with the frozen character of the self-assemblies in aqueous medium. Indeed, we have observed

with similar systems that a small proportion of water could induce aggregation of the polymers in water/DMSO solutions. It might then for example be possible that a slight change of the hygrometry of the sample over the course of the summer would change its behavior in DMSO, leading even to a small proportion of spurious aggregates causing partial aggregation of the nanocylinders into fractal aggregates and leading to irreproducible filtration and/or stronger disruption of the nanocylinders upon filtration. Because of a lack of time and material, we could not investigate this issue in more details.

We therefore decided not to investigate the effect of the parameters of the process (speed of addition of water, initial concentration of polymer in the DMSO solution, effect of temperature during the addition of water, mixtures of *cis* and *trans* Azo-(U-PEO)$_2$ in DMSO before addition of water…) on the characteristics of the samples as initially planned because we feared the results would be unreliable. Instead, we focused on the self-assembly of this polymer in organic solvents where we hoped the self-assemblies to be under thermodynamic equilibrium and therefore easier to handle. These results are presented in the next chapter. We note that they were conducted with the aged sample and still resulted in the formation of nanocylinders as observed by small angle neutron and X-ray scattering, which we consider as another proof that the aged Azo-(U-PEO)$_2$ sample was not degraded.

VI. Conclusions

In this chapter, the physico-chemical study of Azo-(U-PEO)$_2$ in aqueous media, using a combination of cryo-TEM, LS and UV-Vis, has been presented. Direct dispersion of the polymer in water did not lead to nano-cylinders. Instead small, weakly aggregated particles were obtained. On the other hand, using a so-called “water/DMSO” route led to the generation of long (several hundreds of nm in length) and polydisperse nano-cylinders, due to the presence of both the urea groups, providing strong H-bonds, and also alkyl spacers, that likely reinforce the self-assembly through hydrophobic interactions. The azobenzene could be photo-switched both from *trans* → *cis* and *cis* → *trans*, and photo-stationary states were reached within a matter of minutes. Photo-isomerization of trans-azobenzene to the non-planar *cis* configuration led to the disassembly of the nano-cylinders. Due to the out of thermodynamic equilibrium nature of the assemblies, isomerization back to the *trans* isomer did not lead to the recovery of the nano-cylinders, i.e. their disassembly was irreversible.

Aging of Azo-(U-PEO)$_2$ resulted in strong reproducibility issues observed by light scattering, preventing the characterization of the assemblies by this technique after several months. Still, cryoTEM proved the formation of nanocylinders even with the aged sample and led us to the conclusion that filtration, required for light scattering analysis, disrupted the nanocylinders formed by the aged sample more than was observed with the fresh sample. Although there is currently no explanation of these results, we believe that they are related to the frozen nature of the assemblies in aqueous medium which may lead to aggregation of the nanocylinders into more or less fractal aggregates difficult to remove by filtration without breaking the nanocylinders.

CHAPTER 4

Summary – Chapter 4

CHAPTER 4 – Physico-chemical study of Azo-(U-PEO)$_2$ in organic solvents

I. Introduction

In the third chapter, the self-assembly and light-responsiveness of Azo-(U-PEO)$_2$ was studied. The "water/DMSO" route led to the formation of long nano-cylinders that could be disrupted using light, but irreversibly. This was attributed to the fact that the system was out of thermodynamic equilibrium, due to the strong contribution of hydrophobic effects.

We therefore decided to investigate the physico-chemical properties of Azo-(U-PEO)$_2$ in toluene and chloroform, where solvophobic effects were much less present, leading to assemblies driven mainly by hydrogen bonding. Toluene and chloroform were selected as organic solvents due to their slightly different H-bond competitive ability and because they are good solvents of PEO chains. This study was done using a combination of small angle X-ray and neutron scattering measurements (SAXS and SANS). While light scattering and cryo-TEM measurements were possible with aqueous solutions, it was not the case for toluene and chloroform solutions. In LS, the contrast was too low. Moreover, cryo-TEM measurements were attempted with toluene solutions but with no success. This might be also due to a lack of contrast (it is rather difficult to observe carbon based objects in a carbon based solvent) and/or to the difficulty to prepare glassy toluene thin films by rapid cooling in liquid nitrogen as required for cryoTEM analysis.

The results are again presented in the form of an article. However, this chapter still deserves some work to be appropriate for publication. In particular, the SANS and SAXS data have been roughly fitted, but the fits are currently being improved to refine our conclusions.

The main result of this chapter is that, in the organic solvents, the assemblies were found to form spontaneously by direct dissolution and to exhibit reversible photo-induced disassembly, suggesting that they were formed under thermodynamic equilibrium. We attribute this result to the fact that solvophobic interactions are negligible in these solvents, contrary to water, allowing the assemblies to reach thermodynamic equilibrium and therefore reversible light-induced reorganization.

II. ARTICLE 2 - Photo-responsive supramolecular polymer bottle-brushes: the key role of interactions on self-assembly and responsiveness

Luke Harvey[a], Ralf Schweins[b], Isabelle Morfin[c], Gilbert Chahine[c], Guillaume Brotons[a], Laurent Bouteiller[d], Erwan Nicol[a*], Olivier Colombani[a*]

[a] *Institut des Molécules et Matériaux du Mans (IMMM), UMR 6283 CNRS, Le Mans Université, 72085 Le Mans, Cedex 9, France*

[b] *Institut Max von Laue-Paul Langevin, 71 Av. des Martyrs, F-38042 Grenoble, France*

[c] *Université Grenoble Alpes, LiPhy, F-38000, Grenoble, France*

[d] *Sorbonne Université, CNRS, Institut Parisien de Chimie Moléculaire, Equipe Chimie des Polymères, 4 Place Jussieu, F-75005 Paris, France*

ABSTRACT: We report the hydrogen bond-driven self-assembly of an azobenzene-bisurea decorated with poly(ethylene oxide) polymer arms into supramolecular nano-cylinders in different solvents. These nano-cylinders are rendered light-sensitive due to the presence of the azobenzene: exposure to UV light triggers photo-isomerization of the planar *trans*-azobenzene to non-planar *cis*-azobenzene, leading to disassembly. This effect was found to strongly depend on the solvent used. In water, the assembly was previously shown to be driven by both H-bonds and hydrophobic interactions, which rendered the system kinetically frozen, causing disassembly to be irreversible. Here, we report that in organic solvents, solvophobic interactions are suppressed, leading to reversible light-responsive dissociation. In toluene, light induced disassembly at 365 nm was only partial, while it was total in chloroform, which we attribute to weaker H-bonds between urea groups in the more competitive chloroform. Re-assembly occurred upon photo-isomerization of azobenzene back to its *trans* configuration under blue light irradiation (450 nm).

1. Introduction

Supramolecular polymer bottlebrushes (SPBs) consist in the 1D self-assembly of macromolecular building blocks composed of a self-assembling core with pendant polymer arms. Their formation is generally achieved in solution through cooperative and directional non covalent interactions, such as π-stacking or hydrogen-bonding, often complemented by the hydrophobic effect (in aqueous environment).[1,2] Compared to supramolecular 1D-nanostructures formed by small organic molecules[3], SPBs allow for introducing more diverse functionalities due to the large variety of polymers available, which is relevant for a wider panel of applications. For instance, using polymeric arms permits the synthesis of artificial light-harvesting supramolecular nanotubes by aligning chromophores along the 1D-assemblies allowing efficient Förster resonance energy transfer while avoiding aggregation-induced quenching of the chromophores[4]. The incompatibility between two polymer arms was also used to promote segregation of the arms on either side of cyclic peptide-polymer nanotubes, creating Janus SPBs able to form artificial pores when inserted in phospholipid membranes.[5] Other Janus SPBs were reported to efficiently stabilize oil-in-water emulsions.[6]

Due to the non-covalent nature of their backbone, SPBs are attractive candidates for the elaboration of stimuli-sensitive assemblies, whereby stimuli triggered disassembly can be achieved. While several examples of stimuli-sensitive SPBs have been reported[7–10], most rely on the polymer arms to impart responsiveness, which limits the versatility of the approach. Relying on the self-assembling core is therefore a more versatile approach. However, only a handful of studies achieved this, using stimuli such as pH[9], oxidation[7,10], host-guest chemistry[8], or light[11]. Light is a particularly attractive stimulus since it can be easily fine-tuned in terms of wavelength and intensity, allows a high spatio-temporal control, and is non-invasive. Light-responsive 1D-supramolecular self-assemblies based on small molecules have already been reported.[12–18] However, SPBs are more complicated to obtain than supramolecular 1D-nanostructures formed by small organic molecules due to steric hindrance of the polymer arms and the loss of conformational entropy which tend to hinder self-assembly.[19,20]

To the best of our knowledge, there are only two reported examples of light-triggered disassembly of SPBs in the literature, one of them relying again on the nature of the polymer arms to impart responsiveness.[21] In the other work, our group reported the synthesis, self-assembly in aqueous medium and light-triggered disassembly of a poly(ethylene oxide) (PEO)-based supramolecular precursor (Azo-(U-PEO)$_2$) (**Scheme C4-1**). This compound combined a photo-responsive azobenzene unit, hydrogen bonding ureas, C_6 alkyl spacers to reinforce the hydrogen bonding units in water through the solvophobic effect and PEO arms granting solubility both in aqueous medium and organic solvents. In aqueous solution and in the *trans* configuration of the azobenzene core, this polymer was shown to form thin (diameter = 10 nm) SPBs several hundreds of nanometers long. UV irradiation photo-isomerized a large portion of the azobenzene to *cis* configuration (~75%), triggering the disassembly of the nano-cylinders into small micellar structures. Blue-light irradiation switched back the azobenzene to their *trans* configuration, but did not induce the re-assembly into nano-cylinders because the assemblies were kinetically frozen (formed out of thermodynamic equilibrium).

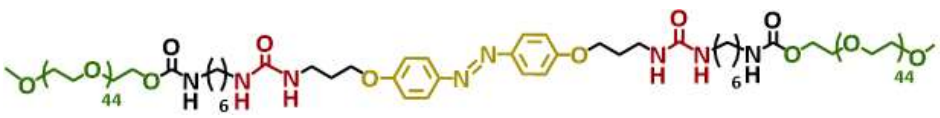

Scheme C4-1. Chemical structure of Azo-(U-PEO)$_2$

In the present study, we aimed at obtaining reversibly light-responsive supramolecular SPBs, which requires that the self-assemblies are formed under thermodynamic equilibrium. Based on the literature on polymer self-assembly in solution[16,17,22,23], we speculated that reducing solvophobic effects by switching from water to organic solvent would help forming SPB under thermodynamic equilibrium able to reversibly photo-switch. We therefore investigated the supramolecular 1D-self-assembly of Azo-(U-PEO)$_2$ in toluene and chloroform, organic solvents with different hydrogen bond competing abilities and displaying weak to no solvophobic effects, with the objective to obtain reversibly-light-responsive SPBs for the first time and investigate the role of the different types of interactions on the kinetic and thermodynamic characteristics of the assemblies.

2. Results

i. Self-assembly of *trans*-Azo-(U-PEO)$_2$ in chloroform and toluene.

The self-assembly of Azo-(U-PEO)$_2$ was studied in toluene and chloroform with the aim of forming SPBs in thermodynamic equilibrium able to reversible disassemble upon UV irradiation. Assemblies in these solvents were probed using a combination of small angle X-ray (SAXS) and neutron (SANS) scattering experiments.

Solutions were prepared by directly dissolving the polymer in deuterated solvent at C=10 g/L. It was verified that inter-particle interactions are negligible at this concentration, (see **Figure C4-S1**). SANS analysis of solutions in toluene-d_8 or $CDCl_3$ showed a q^{-1} angular dependency at low q values, which is typical for anisotropic 1D nano-cylinders, with lengths exceeding the q-range accessible by SANS ($q = 3\times10^{-3}$ Å^{-1}, L > 100 nm, see **Figure C4-S1** for details). This indicates that supramolecular nano-cylinders formed spontaneously in organic solvents contrary to what was observed in aqueous solution[11] and therefore suggests that the assemblies form under thermodynamic equilibrium. The data were fit using a cylinder model, which gave a radius of 5.3 nm in toluene-d_8 solution and 5.2 nm in $CDCl_3$ (data are shown in **Figure C4-1**). These values are quite similar to those previously obtained in aqueous medium with cryoTEM (radius ~ 5 nm)[11]. Note that the discrepancy in terms of scattered intensity between toluene-d_8 and $CDCl_3$ may be due to a lower contrast in chloroform and/or to differences in the self-assemblies.

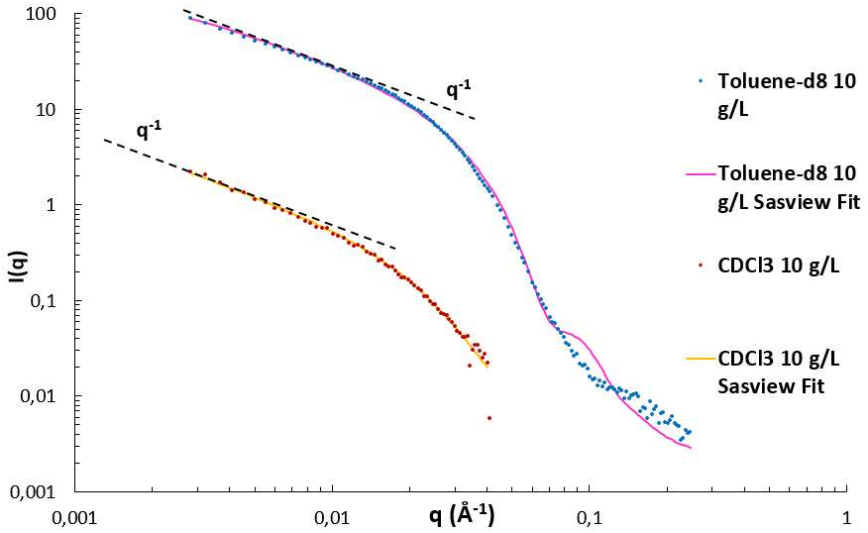

Figure C4-1. SANS data of Azo-(U-PEO)$_2$ in toluene-d$_8$ and CDCl$_3$ at 10 g/L (points) and their respective Sasview fits (solid lines). Due to low scattering intensity of the chloroform solution, data beyond q = 0.03 Å^{-1} was unreliable. The toluene solution was fit with L > 100 nm, r = 5.3 nm (lognormal distribution, PD = 0.163) and a polymer SLD = 3,35.10^{-6} Å^{-2} (solvent SLD = 5.664.10^{-6} Å^{-2}), while the chloroform-D solution was fit with L > 100 nm, r = 5.2 nm (lognormal distribution, PD = 0.151) and SLD = 3,05.10^{-6} Å^{-2} (solvent SLD = 3.16.10^{-6} Å^{-2}). The calculated SLD for PEO was 0.679.10^{-6} Å^{-2}, the fitted values are higher due to solvation of the PEO chains. The quality of the fit for toluene is clearly not satisfying at large q and deserves improving, as currently being done. The values found here however already give a fair estimation of the characteristics of the nanocylinders.

After having confirmed that Azo-(U-PEO)$_2$ self-assembles into SPB in CDCl$_3$ and toluene-d$_8$, its light-responsiveness was studied, first by probing the ability of the azobenzene unit to undergo photo-isomerization, and then by evaluating the impact of the photo-isomerization on the self-assembly.

ii. Probing the *trans* → *cis* and *cis* → *trans* photo-isomerizations by UV-vis and ^{1}H NMR.

Photo-isomerization kinetics were measured by using UV-Vis spectroscopy and *trans*/*cis* isomer ratios at the photo-stationary states were assessed by ^{1}H NMR experiments (**See Figures C4-S2-S5**).

In chloroform.

In chloroform, ^{1}H NMR indicated that 100% *trans*-Azo was present in the initial solution (see **Figure C4-S2**). The initial UV-Vis spectrum (**Figure C4-2)** showed a maximum of absorption in the UV domain at 360 nm, which corresponds to the π → π* transition of *trans*-Azo. Irradiating this solution with UV light (365 nm) triggered photo-isomerization to *cis*-Azo. This was evidenced by the progressive diminution of the intensity at 360 nm to ~10% of its initial value and to a change of this peak's shape. Concomitantly two new maxima appear, respectively at 320 and 450 nm, the former corresponding to the π → π* transition and the latter to the n → π* transition of *cis*-Azo. The kinetic plots of the photo-

isomerizations are presented in **Figure C4-S3**, and the kinetics in chloroform appeared to be similar to those in water. ^{1}H NMR indicated a *trans*/*cis* ratio of 10/90, consistent with UV-Vis (see **Figure C4-2**).

The chloroform solution was then irradiated a second time with blue light (450 nm) in order to trigger *cis* → *trans* photo-isomerization. The absorption band at 450 nm rapidly (photo-stationary state reached within less than 1 min) decreased while the UV maxima of the *trans*-Azo re-appeared (see **Figure C4-2**). Note that only 70% of the initial intensity at 360 nm was recovered, suggesting that not all of the azobenzenes were converted back to their *trans* configuration. This result was consistent with ^{1}H NMR which indicated a *trans*/*cis* ratio of 75/25 at steady-state after irradiation at 450 nm. This behavior was already observed in aqueous medium[11] and attributed to the fact that irradiation at 450 nm not only triggers the *cis*-*trans* isomerization, but also the *trans*-*cis* one, albeit with different quantum yields. The *trans*/*cis* photo-stationary state therefore depends on the respective quantum yields of both photo-isomerization mechanisms at 450 nm and does not correspond to 100% *trans*. Slightly heating the solution in the dark nevertheless allowed for 100% conversion to *trans*-Azo (see **Figure C4-2**), proving the reversibility of the transition. UV/blue light irradiation cycles were performed, and led to identical photo-stationary states, indicating that no degradation occurred during photo-isomerizations (see **Figure C4-S4**). Lastly, thermal relaxation kinetics of *cis*-Azo back to *trans*-Azo were monitored using UV-Vis, indicating a half-life of 11.5 hours at room temperature (20°C) (see **Figure C4-S5**). This relatively slow thermal relaxation allowed for reliable characterization of assemblies within the measurement timeframe.

In toluene.

The same experiments were repeated in toluene. However, in these conditions direct analysis of the toluene-d_8 solution by ^{1}H NMR was not possible because of a lack of resolution of the ^{1}H NMR spectrum in this solvent. This could be attributed to the poor solubility of the azobenzene self-assembling core (4,4'-dihydroxyazobenzene was indeed fully soluble in chloroform at 0.05 g/L, corresponding to the same molar concentration as for Azo-(U-PEO)$_2$ at 1 g/L, but only partially soluble in toluene) and/or to a strong self-assembly in toluene with slower exchange dynamics in this solvent than in $CDCl_3$. The resolution of the ^{1}H NMR spectra in aqueous medium was also poor, for the same potential reasons.[11] This technical issue was circumvented by irradiating in pure toluene-d_8 (to avoid any contribution of DMSO-d_6) and, then, adding 10 vol.% DMSO-d_6 to the solution prior to analysis, see **Figure C4-S6** for details. ^{1}H NMR confirmed that 100% *trans*-Azo was also initially present in toluene-d_8 (see **Figure C4-S6**). The initial solution showed a significant hypsochromic effect: the UV absorption maximum was shifted from 360 nm in chloroform to 325 nm in toluene (see **Figures C4-2 and C4-3**). Note that the maximum was also 360 nm in water or DMSO[11] (See **Figure C4-S7**). In order to determine if this effect was due to the solvent, 4,4'-dihydroxyazobenzene was selected as a model molecular azobenzene. UV-Vis analysis indicated that the maxima were close for this model compound in toluene, $CHCl_3$ and water (~ 355 +/- 5 nm nm) and slightly red-shifted in DMSO (~ 370 nm, see **Figure C4-S8**). This means that the hypsochromic shift observed with Azo-(U-PEO)$_2$ in toluene is not due to the solvent but to another effect. It is possible that the assembly in toluene induces a different environment compared to the unimer state or the assembly state in other solvents, thereby affecting its absorption spectrum.

Exposing this solution to UV irradiation (365 nm) again triggered *trans* → *cis* photo-isomerization, with the apparition of a band at 450 nm. The maximum at 325 nm simultaneously decreased, but with a much weaker deformation of the peak as the new maximum appearing upon *trans*-*cis* isomerization

was still observed at 320 nm as in chloroform. Because of the proximity of the maxima of the *trans* (325 nm) and the *cis* (320 nm) isomers, the *trans*/*cis* ratio after UV-irradiation at 365 nm was estimated using the value of the absorbance at 360 nm, where the contribution of the *cis*-isomer should be weaker. We stress that this methodology only gives a rough estimate of the *trans*/*cis* ratio which was ~ 25/75. These results were confirmed with ^{1}H NMR experiments in toluene-d_8/DMSO-d_6 90/10 (v/v) mixtures, giving a 30/70 ratio (see **Figure C4-S6**). We note that the *trans*/*cis* ratio at the photo-stationary state after irradiation at 365 nm is lower than in chloroform (**Figure C4-S2**) or DMSO (see **Figure C4-S9**) and of the same order of magnitude as in water.[11] Furthermore, *trans* → *cis* photo-isomerization kinetics in toluene were slower than in chloroform (**Figure C4-S3**). Both effects might be due to a stronger self-assembly in water (due to hydrophobic effects) or in toluene (due to strong hydrogen bonding in this weak hydrogen bond competitor) compared to chloroform (moderate H bond competitor) or DMSO (strong H bond competitor), slightly hindering photo-isomerization in the two former solvents. In fact, SANS measurements suggest that only very small objects were present in DMSO, probably unimers, since the scattering intensity was very weak and appeared to be dominated by large aggregates (see **Figure C4-S10**). The hindrance is not strong though as photo-isomerization still occurs to a large extent and remains quite fast in toluene or water. The slower and lower yielding isomerization in toluene may also be attributed to the hypsochromic effect, as the UV absorption maxima was further away from the irradiation wavelength.

Further irradiation at 450 nm led to recovery of the *trans* isomer, and in contrast to chloroform, ~100% of the initial intensity was recovered, indicating that the azobenzenes had almost quantitatively been isomerized back to their *trans* configuration (**Figure C4-3**). This observation could be related to the hypsochromic effect observed in toluene which might imply a change of the quantum yield of the *trans* → *cis* and *cis* → *trans* photo-isomerizations at 450 nm. Irradiation cycles were performed and photo-stationary states were again found to be reproducible (**Figure C4-S11**). Lastly, thermal relaxation was also found to be rather slow, with a half-life of 9.6 hours (see **Figure C4-S5**).

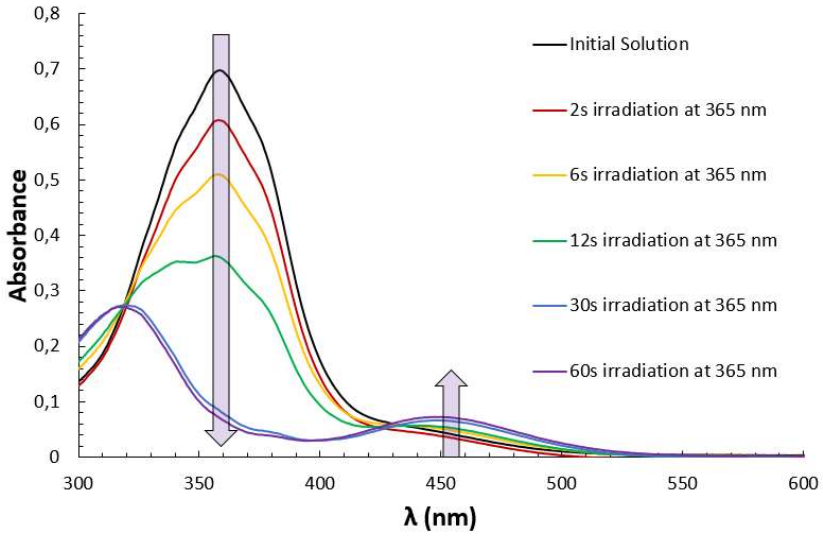

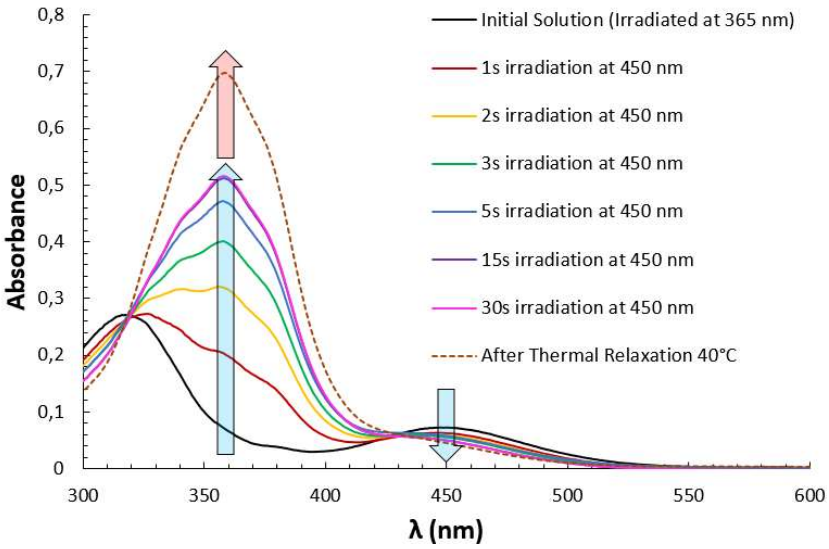

Figure C4-2. UV-Vis kinetics of photo-isomerization when irradiated with UV light (365 nm, top) and blue light (450 nm, bottom), followed by thermal relaxation at 40°C for 30 minutes (dotted line), at 1 g/L in $CHCl_3$

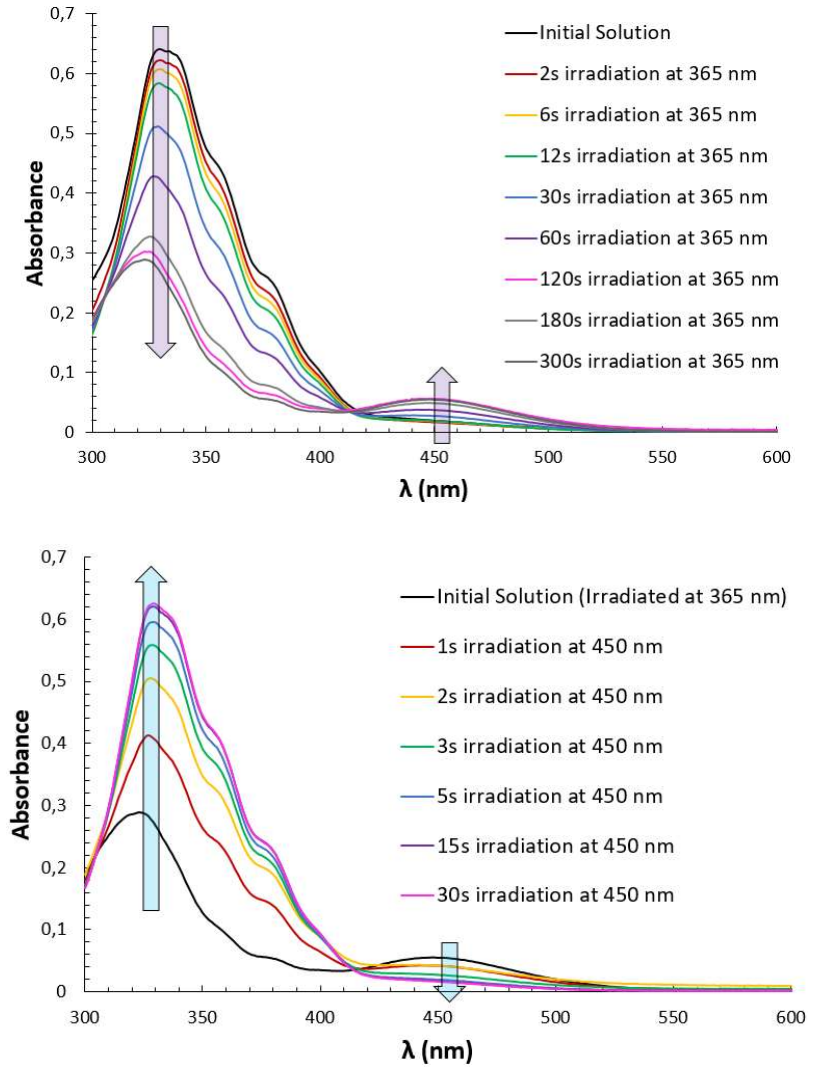

Figure C4-3. UV-Vis kinetics of photo-isomerization when irradiated with UV light (365 nm, top) and blue light (450 nm, bottom) at 1 g/L in toluene

iii. Impact of the photo-isomerizations on self-assembly in $CDCl_3$.

After irradiation of the chloroform solution at 365 nm, SANS showed a drastic change of the scattering profile (**Figure C4-4**): the q^{-1} dependency was somewhat lost and the scattering intensity showed a q^{-3} dependence at low q-values, suggesting that the signal was dominated by large aggregates. We stress that a few very large particles would be sufficient to explain the q^{-3} dependency at low q as already observed for other systems.[24] After substraction of the q^{-3} contribution, the remaining signal exhibited no q-dependency at low q, suggesting that the solution mainly contains very small particles. These data could indeed be fit using a Gaussian coil model, with a R_g = 4 nm; which could correspond to unimers or very small particles.

Irradiating with blue light (450 nm) led to recovery of the nano-cylinders with a q^{-1} dependence appearing again (**Figure C4-4**). Only 70% of the initial level of scattering was recovered though, consistent with the fact that only 70% of *trans*-azobenzene was recovered upon blue light irradiation.

As a conclusion, irradiation at 365 nm in $CDCl_3$ leads to almost quantitative *trans* → *cis* isomerization, accompanied by disruption of most nanocylinders (and a few large particles). More importantly, the photo-induced dissociation of the nanocylinders is to a great extent reversible in this solvent.

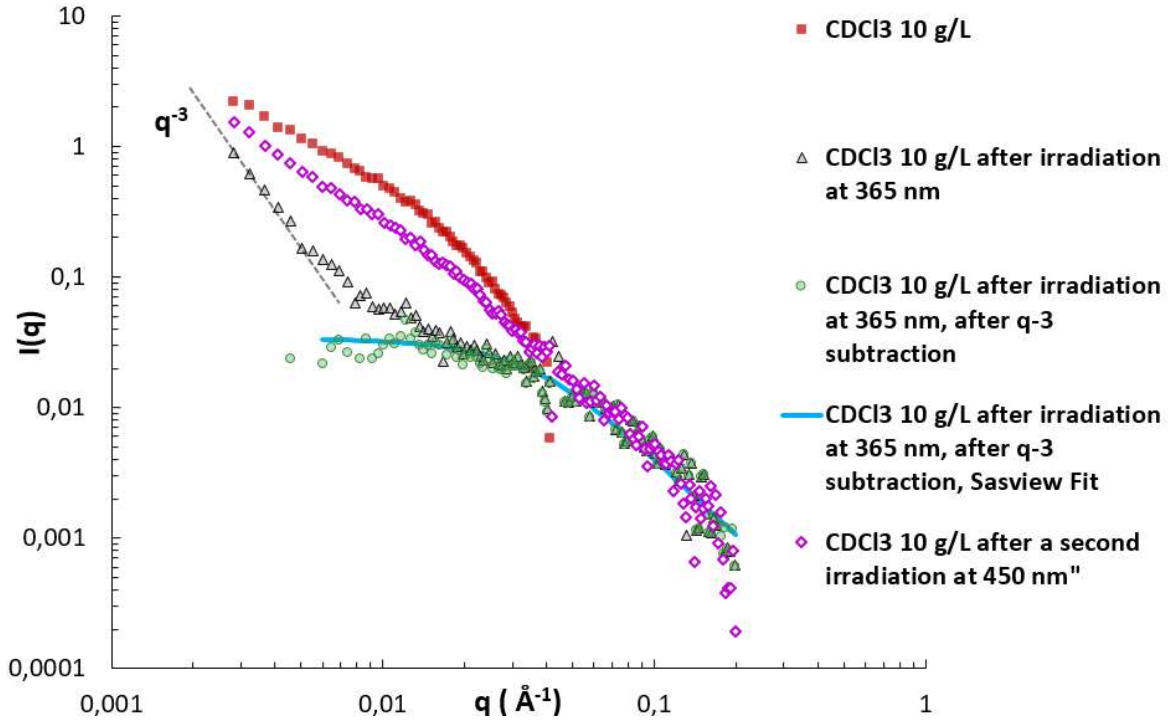

Figure C4-4. SANS data of a 10 g/L solution of Azo-(U-PEO)$_2$ in $CDCl_3$, prior to irradiation, after UV irradiation (365 nm), after subtracting the q^{-3} dependence (these data were fitted with a Gaussian coil Sasview fit, R_g = 4 nm), and after a second irradiation with blue light (450 nm).

iv. Impact of the photo-isomerizations on self-assembly in toluene.

In toluene-d_8, exposure to UV irradiation led to a decrease of the SANS scattered intensity to approx. 30% of the initial intensity (**Figure C4-5**). However, the q^{-1} angular dependence was conserved indicating that nanocylinders were still present after irradiation. Scattering intensity at high-q increased, suggesting that very small particles (such as unimers or small aggregates) were formed from the disrupted nano-cylinders. The q-range accessible by SANS does not allow determining whether the length of the nanocylinders was affected but the length is still at least > 100 nm as before irradiation. We note that light scattering would have allowed investigating the evolution of the length of the nanocylinders at larger scale, but the contrast of PEO in toluene was too low to allow light scattering measurements. Additionally, cryoTEM would have helped but our attempts to perform cryoTEM in this organic solvent proved unsuccessful.

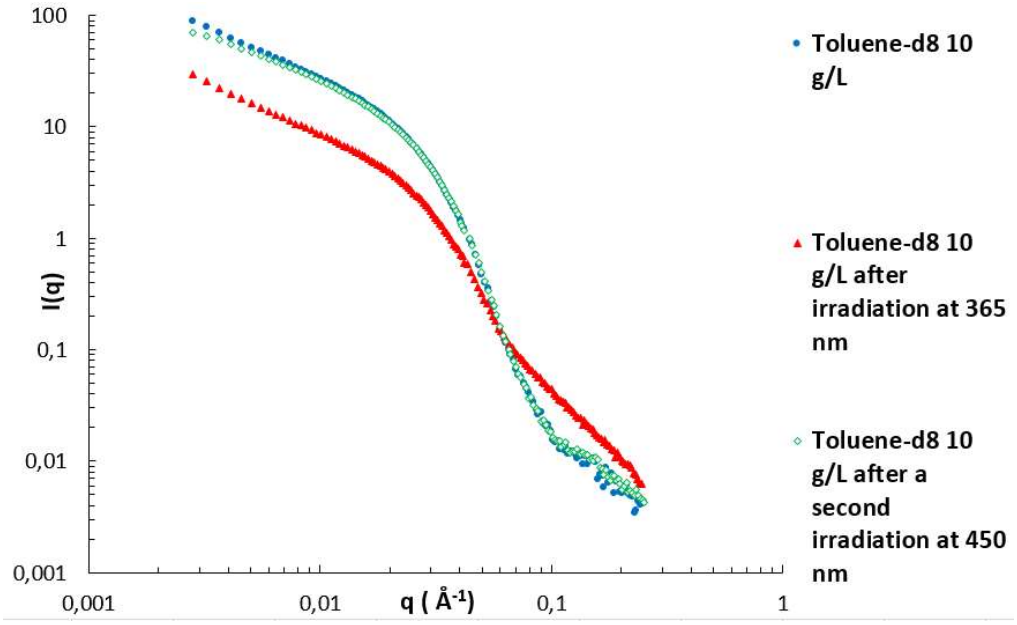

Figure C4-5. SANS data of the initial toluene solution at 10 g/L, after UV irradiation (365 nm), and after a second blue light irradiation (450 nm)

The photo-isomerization-induced disassembly was probed in more details by measuring kinetics of dissociation during exposure at 365 nm. Given the rapidity of the photo-isomerization described above, very fast scattering measurements were necessary; which was achieved using synchrotron SAXS in toluene-d_8. Note that the same experiments could not be conducted in chloroform as this solvent absorbs too much for SAXS experiments. The initial SAXS scattering profile of the *trans*-Azo-(U-PEO)$_2$ solutions in toluene-d_8 is consistent with what was observed by SANS (**Figure C4-S12**). As can be seen in **Figure C4-6 (top)**, the scattered intensity at 0.01 A^{-1} rapidly diminished during exposure to 365 nm irradiation, until it reached ~ 15% of the initial intensity. Additionally, the q^{-1} angular dependency is again maintained during irradiation at 365 nm, suggesting that nano-cylinders are still present when the *trans*/*cis* ratio becomes stable at the photo-stationary state (see **Figure C4-S12**) (according to the UV-vis and ^{1}H NMR measurements described above, which show the required time to reach the steady-

state and the cis/trans isomer ratios at the steady state, respectively). The initial decrease in scattered intensity could actually be fitted with 1st order kinetics (see **Figure C4-6, top, inset**). Surprisingly, the scattering signal was not stable, but oscillated between 15% and 30% of the initial scattering value at low q for the trans-Azo-(U-PEO)$_2$ (see **Figure C4-6, top).** Since thermal relaxation at r.t. was found to be slow, the oscillations cannot be explained by thermal recovery of *trans*-Azo.

In another measurement, the solution was irradiated with UV and then left in the dark (see **Figure C4-6, bottom**). After stopping irradiation and measuring in the dark, the SAXS scattering signal initially increases from 25% to ~50% of its initial value within 30 seconds, followed by a much slower increase. This much slower increase roughly followed 1st order kinetics (see **Figure C4-6, bottom, inset**), with a characteristic half-life of 13h, that is of the same order of magnitude as the thermal relaxation kinetics in the dark measured by UV-Vis (see **Figure C4-S5**).

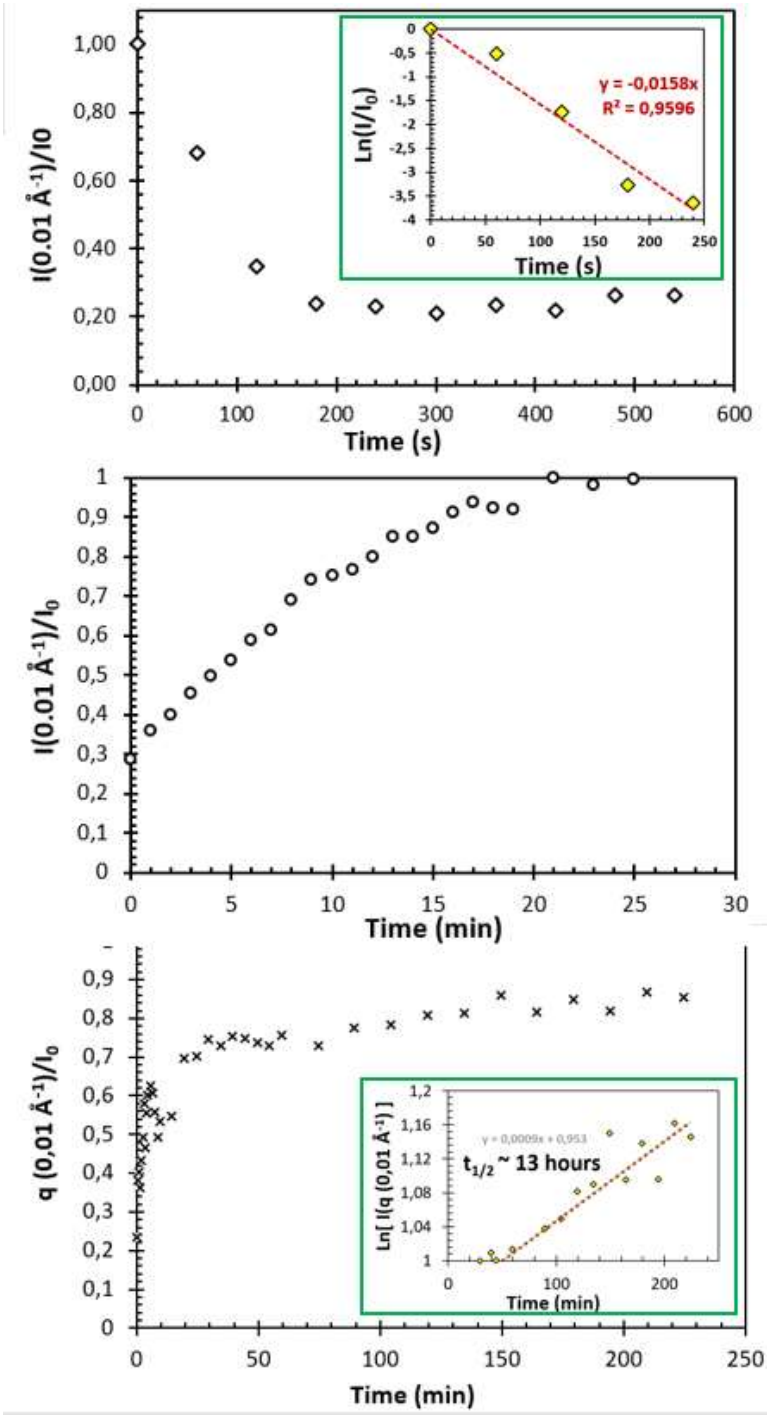

Figure C4-6. SAXS data of a 10 g/L solution of Azo-(U-PEO)$_2$ in toluene-d$_8$ during irradiation at 365 nm, with a kinetic plot inset (**top**), during a second irradiation at 450 nm (at 10% of LED max. power) (**middle**), and thermal relaxation following UV irradiation (365 nm), with a kinetic plot inset (of the data after the fast initial rise in scattered intensity) (**bottom**). The data plotted correspond to the scattering intensity at q = 0,01 Å^{-1} as a function of time normalized by its value before irradiation (i.e. I_{max} for the *trans*-isomer).

We hypothesize that, because not all Azo-(U-PEO)$_2$ molecules undergo *trans* → *cis* photo-isomerization, the formed *cis*-Azo-(U-PEO)$_2$, which probably do not (or hardly) self-assemble creates defects inside the supramolecular nanocylinders, cutting them into small bits or even unimers, consistent with similar mechanisms observed in the literature.[25] However, if the system is dynamic, the remaining *trans*-Azo-(U-PEO)$_2$ molecules should be able to gather and reassemble into supramolecular nanocylinders. Then, the scattered intensity measured by SANS at photo-stationary state under irradiation at 365 nm should correspond to 30% of the initial value (before irradiation) because 30% of *trans*-Azo-(U-PEO)$_2$ remain at steady state. This is exactly what is observed by SANS experiments in toluene-d$_8$ after irradiation at 365 nm, supporting this scenario.

Now, it must also be kept in mind that photo-isomerization is a continuous process with a different quantum yield for the *cis* and *trans* configurations. This implies that the *trans*-Azo-(U-PEO)$_2$ forming the nanocylinders should be continuously transformed into *cis*-Azo-(U-PEO)$_2$, leading to their disruption again, followed by their reformation. If the *trans* → *cis* photo-isomerization is faster than the reassembly of the *trans*-Azo-(U-PEO)$_2$ (which is highly probable as the photo-stationary state is reached within less than 1 min and polymers are known to reorganize rather slowly), the scattered intensity upon disruption of the nanocylinders might decrease even below 30% of the initial scattered intensity observed for all-*trans* molecules. This scenario could then explain the SAXS kinetic results with a decrease of the scattered intensity to 15% of the initial value, oscillation (due to permanent destruction and reformation of nanocylinders) and rapid increase of the scattered intensity after stopping irradiation (due to nanocylinders reformation without new destruction), followed by a much slower subsequent increase (due to slow thermal *cis*->*trans* isomerization). A schematic representation of the proposed mechanism is depicted in **Scheme C4-2**.

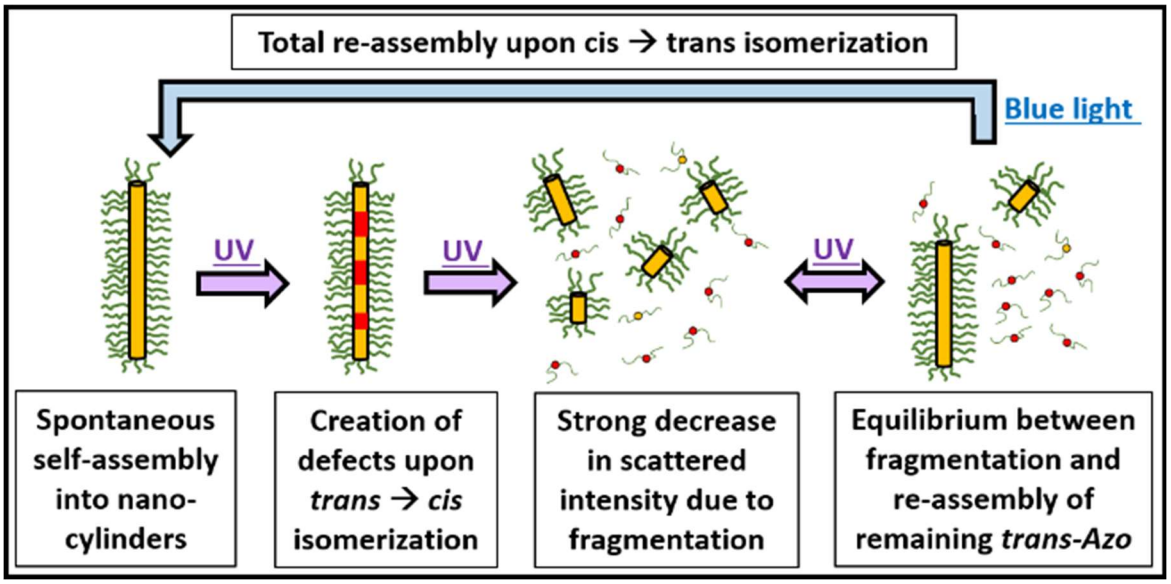

Scheme C4-2. Schematic representation of Azo-(U-PEO)$_2$ behavior in toluene upon UV light (365 nm) irradiation

Finally, irradiating the sample with blue light (450 nm) led to the recovery of the initial scattered intensity, suggesting the disassembly is perfectly reversible. These results are coherent with UV-Vis measurements, which showed that 100% of trans isomer was recovered after a UV – blue light

irradiation cycle. Irradiation cycles were also performed and monitored by SAXS, and the assembly/disassembly was found to be reproducible, which confirmed the fact that no degradation occurred (**Figure C4-S13**).

v. Summary: impact of the solvent on the extent of association and on the stimuli-responsiveness

Comparison of the results obtained in this work with those reported in our previous publication in aqueous medium suggests a strong impact of the solvent on the extent of self-assembly of Azo-(U-PEO)$_2$ and on its light responsiveness.

In our previous work, it was observed that *trans*-Azo-(U-PEO)$_2$ formed out-of-equilibrium SPBs in aqueous medium, requiring a complex "DMSO-route" to obtain the nanocylinders. These supramolecular structures could still undergo *trans* -> *cis* isomerization to a 25/75 ratio upon exposure to UV-light (365 nm); which led to their disruption into much smaller and mostly spherical particles. This disruption was however irreversible upon *cis*->*trans* back photo-isomerization at 450 nm; which we attributed to the kinetically frozen nature of the assemblies, likely induced by strong hydrophobic effects. These results are in agreement with work reported by Feringa et al., who showed that a stilbene-bisurea with oligo-PEO arms self-assembled in both water and toluene, with a Gibbs free energy two times higher in water, due to the hydrophobic effect, and isomerization was blocked in water at r.t. due to the great extent of assembly. Isomerization was also significantly blocked in toluene, with isomerization leading from 100% *trans* to just 33% *cis* isomer. [17] Additionally, in the field of amphiphilic block copolymers, it was reported that very strong hydrophobic effects can prevent supramolecular structures from reaching thermodynamic equilibrium and to be reversibly stimuli-responsive.[22]

In chloroform and toluene, Azo-(U-PEO)$_2$ spontaneously formed SPBs upon direct dissolution. The azobenzene units of Azo-(U-PEO)$_2$ were able to photo-isomerize from *trans* to *cis* and from *cis* back to *trans*, when exposed to UV (365 nm) and blue light (450 nm), respectively. In both cases, photo-isomerization at 365 nm triggered disassembly, but irradiation at 450 nm reversibly conducted to the reformation of the nanocylinders. In toluene, the disassembly was only partial, which we attribute to the fact that even after UV irradiation, some *trans* isomer is left (~25-30%, see **Figure C4-S2**), possibly due to strong H-bonding somewhat hindering photo-isomerization and/or to the shift of absorption maximum of the *trans* isomer modifying the quantum yield of photo-isomerization. We hypothesize that the remaining *trans*-Azo-(U-PEO)$_2$ was able to rapidly reorganize into new nanocylinders after disruption. The SPBs could be quantitatively recovered with blue light irradiation, since all of the azobenzenes photo-isomerized back to their *trans* configuration. In chloroform, on the other hand, near quantitative disruption of SPBs was achieved, which we attribute to the fact that chloroform is slightly more H-bond competing than toluene, thus weakening the assemblies. Re-assembly was also achieved upon blue light irradiation, although to a lesser extent than the initial solution, due to some *cis* isomer remaining after irradiation at 450 nm. All these results suggest that the supramolecular nanocylinders formed in toluene or chloroform by Azo-(U-PEO)$_2$ are under thermodynamic equilibrium, unlike what was observed in aqueous medium. This could be explained by the fact that the solvophobic effects were likely much weaker in these solvents, compared to water, and the assembly was mainly driven by H-bonding.

Finally, by comparison, no assembly occurred even for the *trans*-isomer in DMSO, which is a solvent exhibiting both a very strong hydrogen bond competing ability and a good solvation ability towards the azo-core. We therefore showed that by modifying the strength of the hydrogen bonds and of the solvophobic effects, we could tune the extent of self-assembly and the response to light of Azo-(U-PEO)$_2$ in solution, see **Scheme C4-3.**

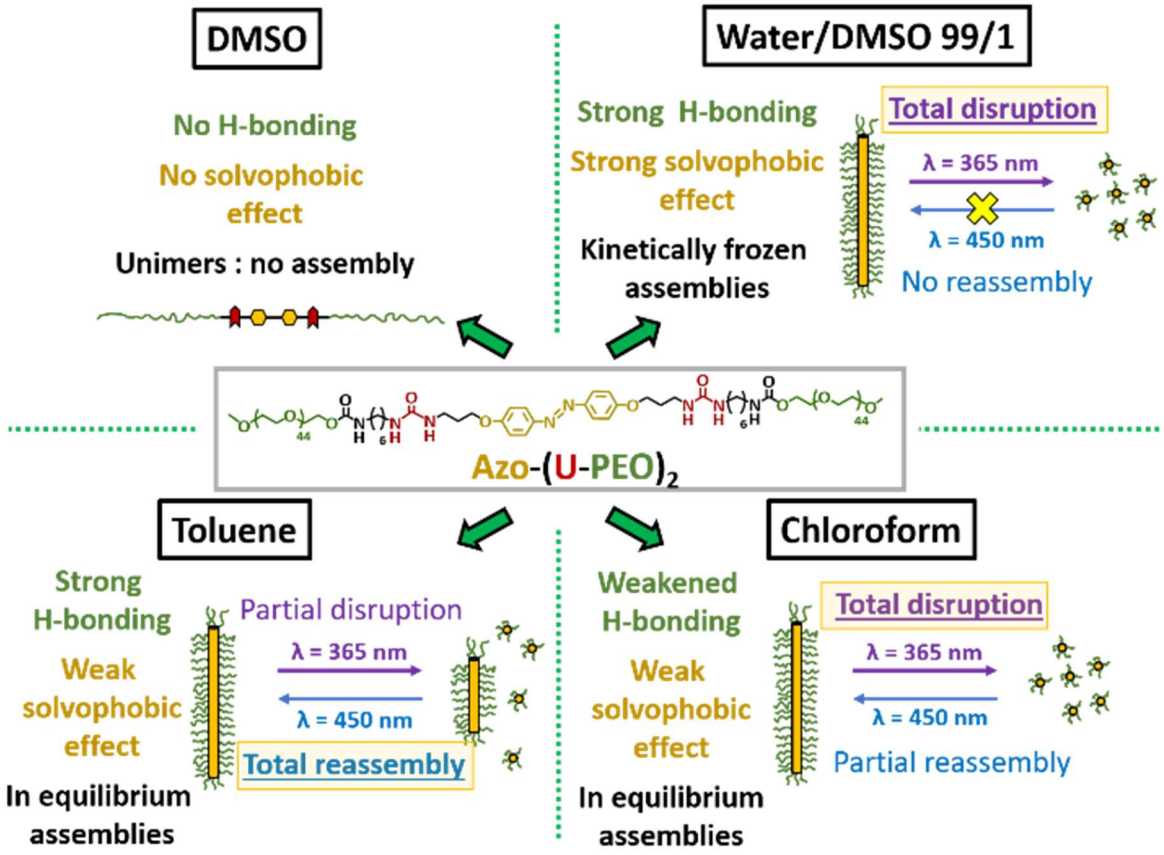

Scheme C4-3. Schematic representation of the different modes of self-assembly of Azo-(U-PEO)$_2$ in studied solvents.

3. Conclusions

Azo-(U-PEO)$_2$ is an azobenzene-bisurea self-assembling core decorated with PEO arms, providing solubility in water, chloroform, toluene and DMSO. This molecule was previously shown to self-assemble into long supramolecular nanocylinders in aqueous medium, which could be disrupted into small particles upon *trans-cis* photo-isomerization.[1] However, the self-assembled structures were frozen in aqueous medium, probably due to strong hydrophobic effects, requiring a complex assembly procedure to form the nanocylinders and causing the photo-induced disruption of the nanocylinders to be irreversible.

In this work, we showed that the formation of long supramolecular nanocylinders was also possible in chloroform and toluene, but that *trans* → *cis* photo-isomerization led to a reversible disassembly of the nanocylinders in these solvents. The amount of disrupted nanocylinders upon trans → cis photo-

isomerization was in perfect agreement with the percentage of *trans*-Azo-(U-PEO)$_2$ transformed into *cis*-Azo-(U-PEO)$_2$. The photo-isomerization was only partial in toluene, which might be due to a different quantum yield or to very strong hydrogen bonds in this solvent hindering partially the photo-isomerization. In chloroform, the *trans*->*cis* photo-isomerization and the disruption of the nanocylinders at 365 nm were quasi-quantitative. Finally, the strong solvating and hydrogen bond competing ability of DMSO prevented any self-assembly even of *trans*-Azo-(U-PEO)$_2$.

Reducing solvophobic effects, as was achieved in this work, led to supramolecular assemblies that were under equilibrium, leading to the first reversible light-triggered disassembly of SPBs to the best of our knowledge. These results highlight the importance of solvent choice when considering supramolecular self-assembly, particularly in the case of stimuli-sensitive systems.

4. Bibliography

1. Hartlieb, M., Mansfield, E. D. H. & Perrier, S. A guide to supramolecular polymerizations. *Polym Chem* **11**, 1083–1110 (2020).

2. Gruschwitz, F. V., Klein, T., Catrouillet, S. & Brendel, J. C. Supramolecular polymer bottlebrushes. *Chem. Commun.* **56**, 5079–5110 (2020).

3. Palmer, L. C. & Stupp, S. I. Molecular self-assembly into one-dimensional nanostructures. *Acc Chem Res* **41**, 1674–1684 (2008).

4. Song, Q., Goia, S., Yang, J., Hall, S. C. L., Staniforth, M., Stavros, V. G. & Perrier, S. Efficient Artificial Light-Harvesting System Based on Supramolecular Peptide Nanotubes in Water. *J Am Chem Soc* **143**, 382–389 (2021).

5. Danial, M., My-Nhi Tran, C., Young, P. G., Perrier, S. & Jolliffe, K. A. Janus cyclic peptide-polymer nanotubes. *Nat Commun* **4**, (2013).

6. Han, S., Pensec, S., Yilmaz, D., Lorthioir, C., Jestin, J., Guigner, J. M., Niepceron, F., Rieger, J., Stoffelbach, F., Nicol, E., Colombani, O. & Bouteiller, L. Straightforward preparation of supramolecular Janus nanorods by hydrogen bonding of end-functionalized polymers. *Nat Commun* **11**, 2–7 (2020).

7. Nicolas, C., Ghanem, T., Canevet, D., Sallé, M., Nicol, E., Gautier, C., Levillain, E., Niepceron, F. & Colombani, O. Oxidation-Sensitive Supramolecular Polymer Nanocylinders. *Macromolecules* **55**, 6167–6175 (2022).

8. Song, Q., Yang, J., Rho, J. Y. & Perrier, S. Supramolecular switching of the self-assembly of cyclic peptide-polymer conjugates: Via host-guest chemistry. *Chem. Commun.* **55**, 5291–5294 (2019).

9. Otter, R., Klinker, K., Spitzer, D., Schinnerer, M., Barz, M. & Besenius, P. Folding induced supramolecular assembly into pH-responsive nanorods with a protein repellent shell. *Chem. Commun.* **54**, 401–404 (2018).

10. Otter, R., Berac, C. M., Seiffert, S. & Besenius, P. Tuning the life-time of supramolecular hydrogels using ROS-responsive telechelic peptide-polymer conjugates. *Eur Polym J* **110**, 90–96 (2019).

11. Harvey, L., Guigner, J. M., Bouteiller, L., Nicol, E. & Colombani, O. Photo-responsive disassembly of supramolecular polymer bottlebrushes in water. *Polym Chem* 1–10 (2023) doi:10.1039/D3PY00963G.

12. Wang, C., Chen, Q., Sun, F., Zhang, D., Zhang, G., Huang, Y., Zhao, R. & Zhu, D. Multistimull responsive organogels based on a new gelator featuring tetrathiafulvalene and azobenzene groups: Reversible tuning of the gel-sol transition by redox reactions and light irradiation. *J Am Chem Soc* **132**, 3092–3096 (2010).

13. Velema, W. A., Stuart, M. C. A., Szymanski, W. & Feringa, B. L. Light-triggered self-assembly of a dichromonyl compound in water. *Chem. Commun.* **49**, 5001–5003 (2013).

14. Endo, M., Fukui, T., Jung, S. H., Yagai, S., Takeuchi, M. & Sugiyasu, K. Photoregulated Living Supramolecular Polymerization Established by Combining Energy Landscapes of Photoisomerization and Nucleation-Elongation Processes. *J Am Chem Soc* **138**, 14347–14353 (2016).

15. Xu, J. F., Chen, Y. Z., Wu, D., Wu, L. Z., Tung, C. H. & Yang, Q. Z. Photoresponsive hydrogen-bonded supramolecular polymers based on a stiff stilbene unit. *Angew. Chem. Int. Ed*. **52**, 9738–9742 (2013).

16. Xu, F., Pfeifer, L., Crespi, S., Leung, F. K. C., Stuart, M. C. A., Wezenberg, S. J. & Feringa, B. L. From Photoinduced Supramolecular Polymerization to Responsive Organogels. *J Am Chem Soc* **143**, 5990–5997 (2021).

17. Xu, F., Crespi, S., Pfeifer, L., Stuart, M. C. A. & Feringa, B. L. Mechanistic Insight into Supramolecular Polymerization in Water Tunable by Molecular Geometry. *CCS Chemistry* **4**, 2212–2220 (2022).

18. Fuentes, E., Gerth, M., Berrocal, J. A., Matera, C., Gorostiza, P., Voets, I. K., Pujals, S. & Albertazzi, L. An Azobenzene-Based Single-Component Supramolecular Polymer Responsive to Multiple Stimuli in Water. *J Am Chem Soc* **142**, 10069–10078 (2020).

19. Catrouillet, S., Fonteneau, C., Bouteiller, L., Delorme, N., Nicol, E., Nicolai, T., Pensec, S. & Colombani, O. Competition between steric hindrance and hydrogen bonding in the formation of supramolecular bottle brush polymers. *Macromolecules* **46**, 7911–7919 (2013).

20. Han, S., Mellot, G., Pensec, S., Rieger, J., Stoffelbach, F., Nicol, E., Colombani, O., Jestin, J. & Bouteiller, L. Crucial Role of the Spacer in Tuning the Length of Self-Assembled Nanorods. *Macromolecules* **53**, 427–433 (2020).

21. Yang, J., Song, J. I., Song, Q., Rho, J. Y., Mansfield, E. D. H., Hall, S. C. L., Sambrook, M., Huang, F. & Perrier, S. Hierarchical Self-Assembled Photo-Responsive Tubisomes from a Cyclic Peptide-Bridged Amphiphilic Block Copolymer. *Angew. Chem. Int. Ed.* **59**, 8860–8863 (2020).

22. Nicolai, T., Colombani, O. & Chassenieux, C. Dynamic polymeric micelles versus frozen nanoparticles formed by block copolymers. *Soft Matter* **6**, 3111–3118 (2010).

23. Crippa, M., Perego, C., de Marco, A. L. & Pavan, G. M. Molecular communications in complex systems of dynamic supramolecular polymers. *Nat Commun* **13**, 1–12 (2022).

24. Choisnet, T., Canevet, D., Sallé, M., Nicol, E., Niepceron, F., Jestin, J. & Colombani, O. Robust supramolecular nanocylinders of naphthalene diimide in water. *Chem. Commun.* **55**, 9519–9522 (2019).

25. Bochicchio, D., Kwangmettatam, S., Kudernac, T. & Pavan, G. M. How Defects Control the Out-of-Equilibrium Dissipative Evolution of a Supramolecular Tubule. *ACS Nano* **13**, 4322–4334 (2019).

III. SUPPORTING INFORMATION – ARTICLE 2

Photo-responsive supramolecular polymer bottle-brushes: the key role of interactions on self-assembly and responsiveness

1. Materials

Deuterated solvents (toluene-d_8, $CDCl_3$, DMSO-d_6 and D_2O) and standard solvents were purchased from Aldrich.

2. Methods

Nuclear magnetic resonance (NMR). ^1H NMR spectra were recorded on either a Bruker DPX-200 or Bruker AC-400 spectrometer, using deuterated chloroform ($CDCl_3$) or dimethyl sulfoxide (DMSO-d_6), and toluene-d_8/DMSO-d_6 mixtures as solvents. Chemical shifts (δ) are expressed in parts per million (ppm) relative to the reference (tetramethylsilane (TMS), δ = 0 ppm). Multiplicities are reported as follows: singlet (s), doublet (d), triplet (t), quadruplet (q), quintet (qt), sextet (sext), multiplet (m), and broad signal (br s).

Light irradiations. LED irradiations were carried out using a Thor Labs DC2200 High-Power LED Driver, with Thor Labs M365LP1 and Thor Labs M450LP1 LEDs, operating at 365 nm and 450 nm, respectively. The LEDs were linked to the driver using a waveguide. Irradiation of solutions was carried out with the waveguide placed 4.5 cm above the solution for UV-Vis measurements. The LED irradiance at this distance was measured using a Thor Labs PM160T optical power meter, and the irradiances were measured as follows: 215 $mW.cm^{-2}$ for the 365 nm LED and 515 $mW.cm^{-2}$ for the 450 nm LED. Irradiations during SAXS analysis were achieved by placing the LED setup on the beamline, with the LED waveguide at approximately 5 cm from the quartz capillary.

UV-Vis absorption spectroscopy. UV-Vis spectra were measured on a Jasco V760 spectrometer using glass cuvettes with an optical pathway of 1 mm at room temperature.

Small angle neutron scattering (SANS). SANS measurements were performed at the Institut Laue-Langevin (ILL, Grenoble, France), on the small angle neutron scattering instrument D22. A circular neutron beam was used (diameter of 13 mm). The D22 instrument uses two detectors: a front detector, at a fixed distance of 1.4 m (relative to the sample), as well as a rear detector. Measurements were achieved using a sample to detector distances at 4 m (collimation), using a neutron wavelength of 6 Å. This setup allowed for probing over a wide q-range: 0.0026 $Å^{-1}$ to 0.6424 $Å^{-1}$. Neutron detection was achieved using two ^3He detectors (multi-tube detector consisting of vertically aligned Reuter-Stokes tubes, with 128 tubes for the rear and 96 tubes for the front detector, all with a diameter of 8 mm and a pixel size of 8 mm x 8 mm). Acquired detector images were treated using GRASP software,

to correct for the transmission of the direct beam, to scale to absolute intensity, and to azimuthally average. Scattering contribution of the empty cell and solvent were subtracted from the scattering curves.

Small angle X-ray scattering (SAXS). X-ray scattering experiments were performed using the WAXS-SAXS setup at the D2AM beamline of the European Synchrotron Radiation Facility (ESRF, Grenoble, France). The samples were probed with a monochromatic X-ray of 12 keV (λ = 1 Å). The scattering intensity was simultaneously measured using two-dimensional WAXS and SAXS pixel detectors (XPAD-WOS and D5). The sample-detector distances were respectively 3.29 m allowing to cover scattering vector ranges of $q = 3.10^{-3}$ to $2{,}4.10^{-1}$ $Å^{-1}$. q-range and radial averaging were determined measuring Ag and LaB_6 standards. Glassy carbon was used as reference to obtain the scattered intensity in absolute unit. Jupyter notebook script was used to perform the radial averaging, correct for the transmission, and obtain the I(q) data.

3. Characterizations

i. SANS – 5 vs 10 g/L toluene solutions

In order to verify that inter-particle interactions were negligible at 10 g/L, a 5 g/L solution was also prepared and analyzed by SANS (**Figure C4-S1**). I/C was plotted as a function of q, and the two scattering curves were nearly identical, indicating that 10 g/L solution are sufficiently dilute.

Furthermore, the length of the assemblies was not accessible with the available q-range. The minimum length of the nanocylinders was determined based on the fact that in this q-range, if $R_g > 1/q$, then $R_g > 30$ nm. Assuming that the length L of the nanocylinders is large compared to their diameter (thin nanocylinders), $R_g = L/12^{0.5}$. It follows that L>100 nm. The assumption L >> d is then verified.

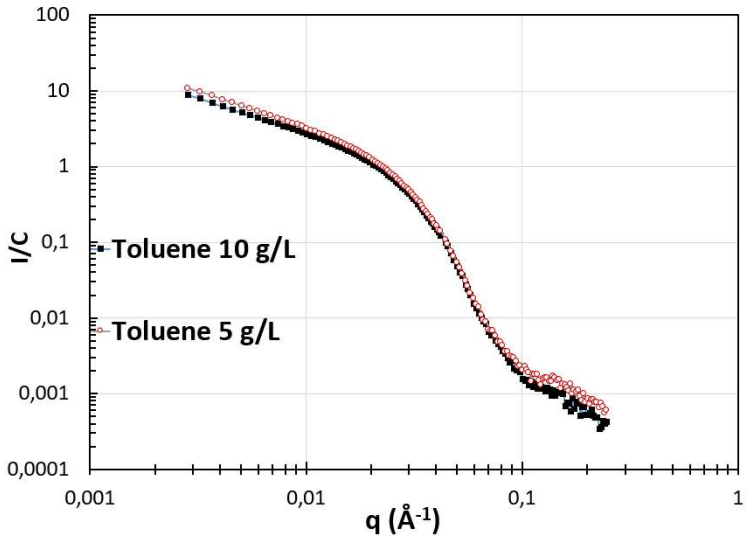

Figure C4-S1. SANS data of 10 and 5 g/L solutions in toluene-d8, normalized by the concentration.

ii. ^{1}H NMR – *trans*/*cis* isomer ratios in chloroform

The *trans*/*cis* isomer ratios at the photo-stationary states were determined by ^{1}H NMR (**Figure S2**).

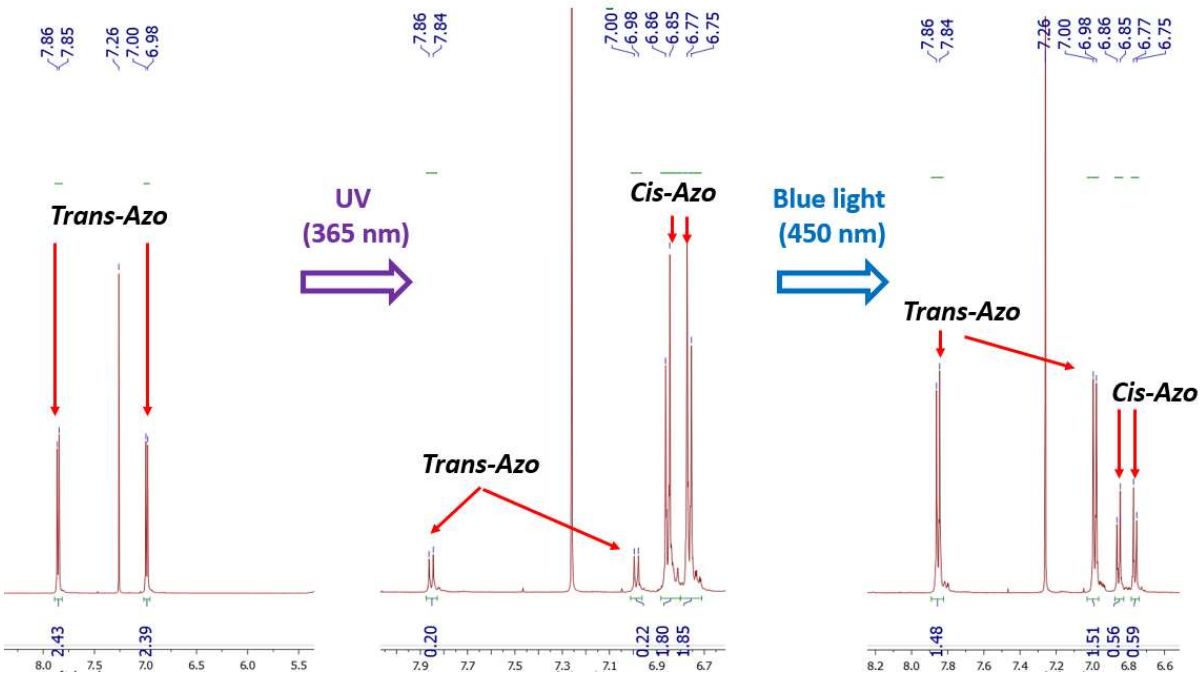

Figure C4-S2. ^{1}H NMR of Azo-(U-PEO)$_2$ in $CDCl_3$ prior to irradiation (left), after UV irradiation (365 nm, middle) and after a second irradiation with blue light (450 nm, right). Integral reference set on the terminal PEO methoxy group (3H).

<u>After UV irradiation (365 nm):</u>

$\%_{trans}$ = (0.20 + 0.22)/(0.20 + 0.22 + 1.80 + 1.85) x 100 = **10 % ,** and $\%_{cis}$ = 100 - $\%_{trans}$ = **90 in chloroform**

<u>After blue light irradiation (450 nm):</u>

$\%_{trans}$ = (1.48 + 1.51)/(1.48 + 1.51 + 0.56 + 0.59) x 100 = **72 % ,** and $\%_{cis}$ = 100 - $\%_{trans}$ = **28% in chloroform**

iii. UV-Vis – Kinetic plots of photo-isomerization in toluene, chloroform and water

Kinetic plots of photo-isomerizations in toluene, chloroform and water/DMSO 99/1 are presented in **Figure C4-S3**.

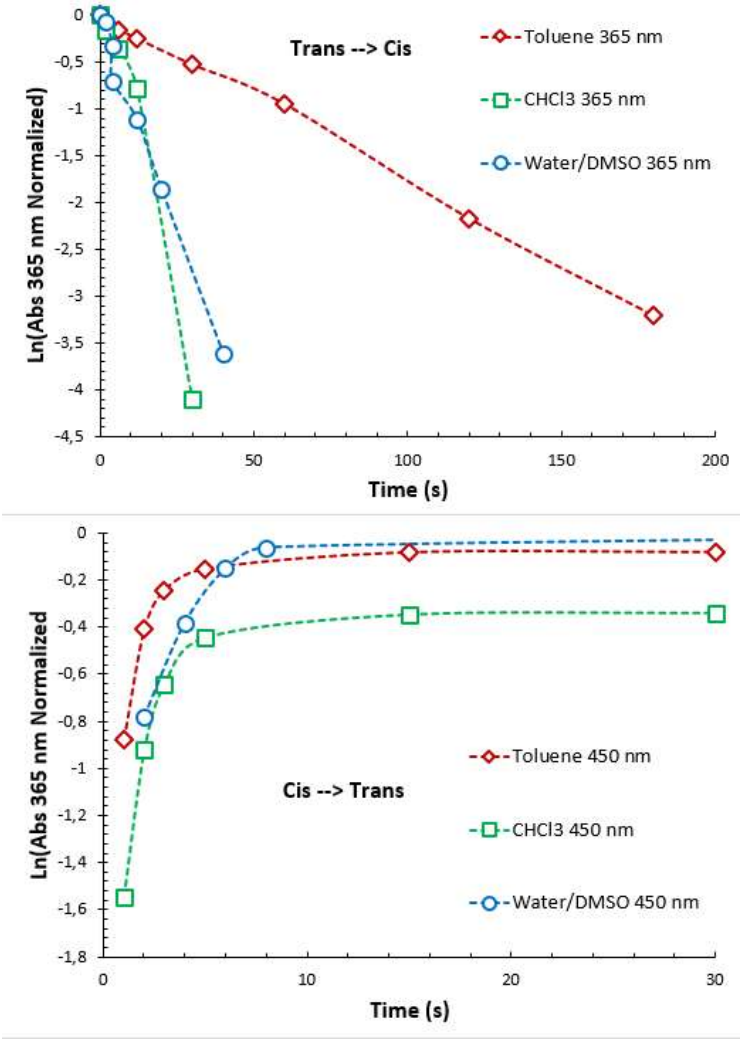

Figure C4-S3. Photo-isomerization kinetics measured by UV-Vis in toluene, chloroform and water/DMSO 99/1 (v/v) at 1 g/L during *trans* → *cis* photo-isomerization (top) and *cis* → *trans* photo-isomerization (bottom). Dashed lines a guide for the eye.

iv. UV-Vis – Irradiation cycles of chloroform solution

1 g/L solution of Azo-(U-PEO)$_2$ were prepared in chloroform, and subjected to UV (365 nm) and blue light (450 nm) irradiation cycles, see **Figure C4-S4**, and only 70% of *trans*-Azo is recovered after a cycle.

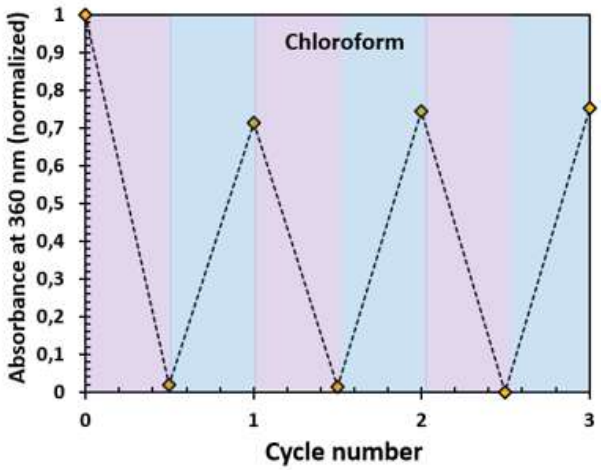

Figure C4-S4. UV/blue light (365 nm, 450 nm, respectively) irradiation cycles, monitored by UV-Vis, in chloroform at 1 g/L.

v. UV-Vis – thermal relaxation of chloroform and toluene solutions

Chloroform and toluene solutions were irradiated with UV light (365 nm) and then thermal relaxation in the dark (at 20°C) was monitored by UV-Vis (**Figure C4-S5**).

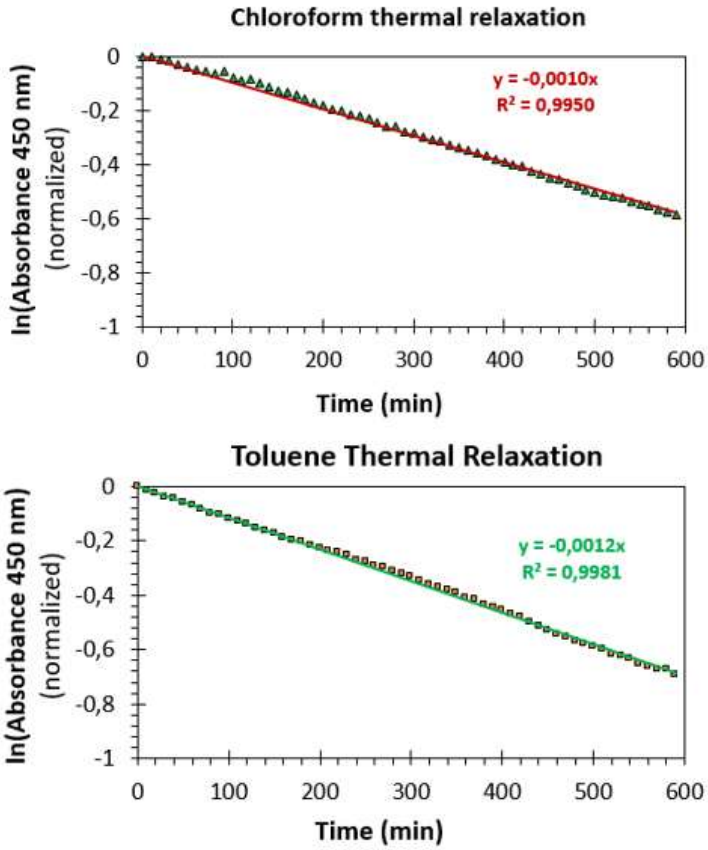

Figure C4-S5. UV-Vis measurements of thermal relaxation at 1 g/L in chloroform (**top**) and toluene (**bottom**) following UV irradiation (365 nm), with linear regressions (solid lines).

Half-lives $t_{1/2}$ were calculated from $t_{1/2} = \ln(2)/k$ with k being the 1st order rate constant, i.e. the slope of the linear regression curves (absolute value).

So $t_{1/2} = \ln(2) / 0.0010 = 11.5$ hours for chloroform

And $t_{1/2} = \ln(2) / 0.0012 = 9.6$ hours for toluene

vi. ^{1}H NMR – *trans/cis* isomer ratios in toluene

The *trans*/*cis* isomer ratios in toluene were assessed by ^{1}H NMR. However, in pure toluene-d_8, the spectrum was insufficiently resolved (likely due to the extent of aggregation). To remedy this, 10 vol% DMSO-d_6 was added prior to analysis (but after irradiation), in the aim of disrupting assemblies to gain resolution while not affecting isomer ratios (**Figure C4-S6**). Adding more DMSO (10 vol%) did not affect the measured isomer ratios (data not shown).

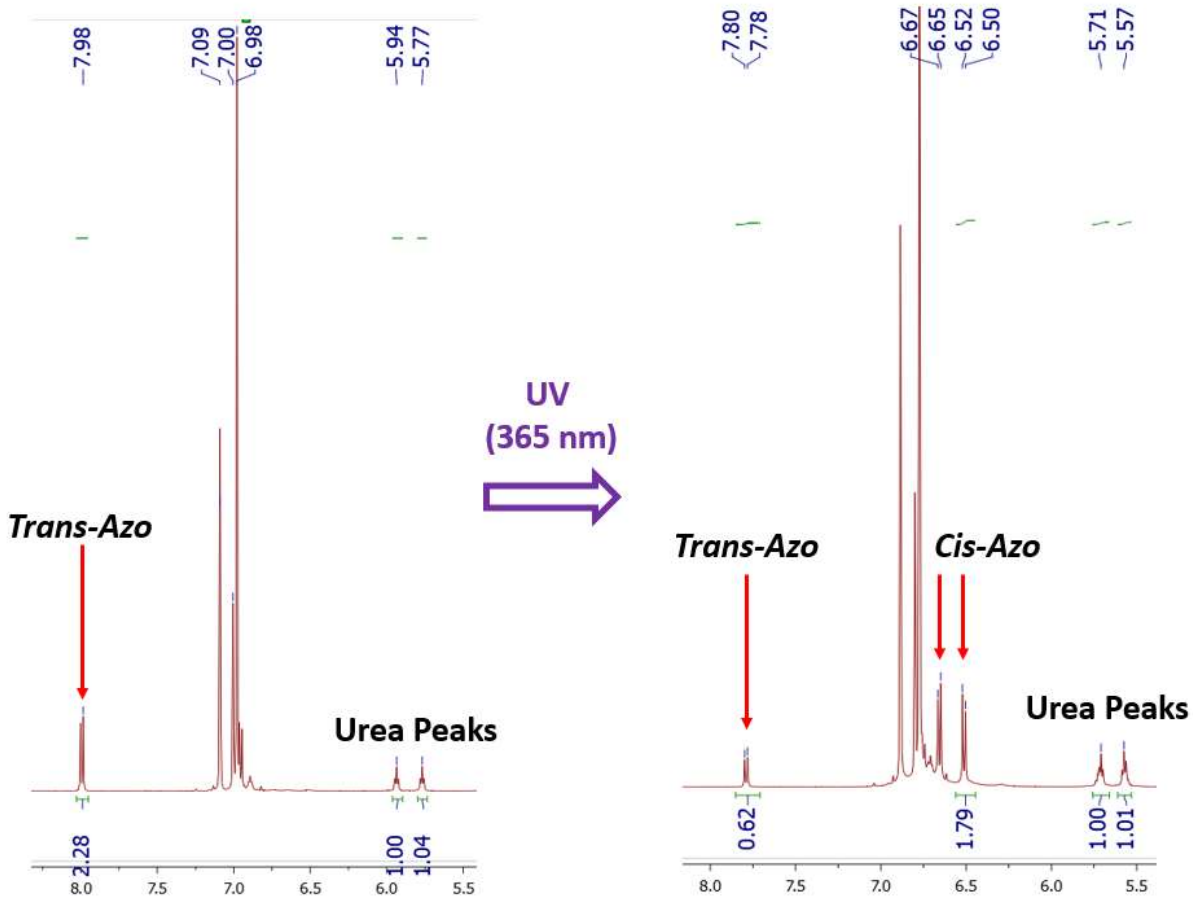

Figure C4-S6. ^{1}H NMR of Azo-(U-PEO)$_2$ in toluene-d_8 / DMSO-d_6 90/10, prior to irradiation (left), after UV irradiation (365 nm, right). Integral reference set on the terminal PEO methoxy group (3H).

$\%_{trans}$ = (0.62)/(0.62 + 1.79) x 100 = **26 % ,** and $\%_{cis}$ = 100 - $\%_{trans}$ = **74%** **in toluene after UV irradiation**

$\%_{trans}$ = **100%**, since 100% trans-Azo was initially present, and after the two irradiations, the initial UV-Vis spectra was recovered **in toluene** (see **Figure C4-S11**).

vii. UV-Vis – Comparison of spectra in different solvents

A comparison of the UV-Vis spectra of Azo-(U-PEO)$_2$ in different solvents is presented in **Figure C4-S7**.

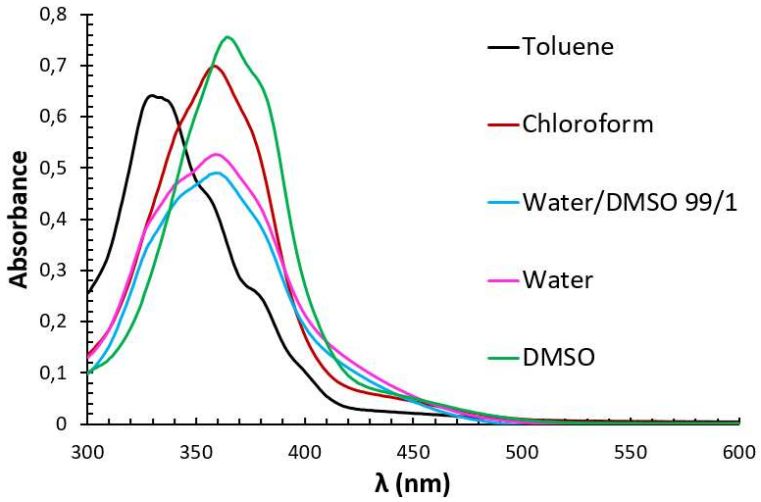

Figure C4-S7. UV-Vis spectra of Azo-(U-PEO)$_2$ in different solvents, prior to any irradiation. The solutions were prepared at 1 g/L, except for the "Water/DMSO 99/1" which was prepared at 0.9 g/L (data was normalized to 1 g/L).

viii. UV-Vis – Spectra of molecular azobenzene in different solvents

A comparison of 4,4'-dihydroxyazobenzene UV-Vis spectra in different solvents (at 0.048 g/L, which corresponds to the same molar concentration of azobenzene as a 1 g/L solution of Azo-(U-PEO)$_2$) is presented in **Figure C4-S8**. Note that this compound was only partially soluble in water, chloroform and toluene, therefore the real concentration in these solvents is lower than 0.048 g/L.

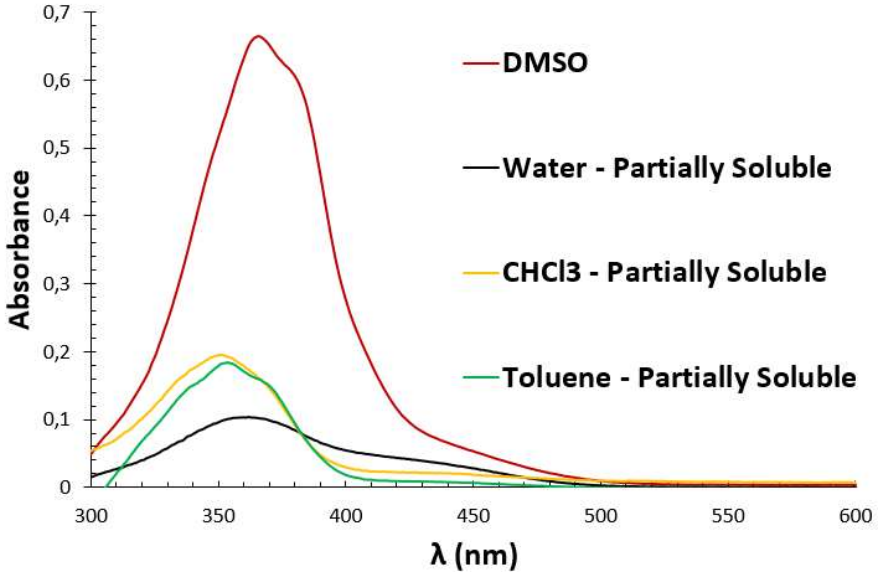

Figure C4-S8. UV/Vis spectra of 4,4'-dihydroxyazobenzene in water, DMSO, chloroform and toluene, at 0.048 g/L (equivalent to the same molar concentration as Azo-(U-PEO)$_2$ at 1 g/L). The compound was only partially soluble in water and toluene.

ix. ^{1}H NMR – *trans*/*cis* isomer ratios in DMSO

The *trans*/*cis* isomer ratio after UV irradiation in DMSO was determined by ^{1}H NMR (**Figure C4-S9**). It should be noted that in this solvent, a small amount (< 10%) of *cis*-isomer was present in the initial solution.

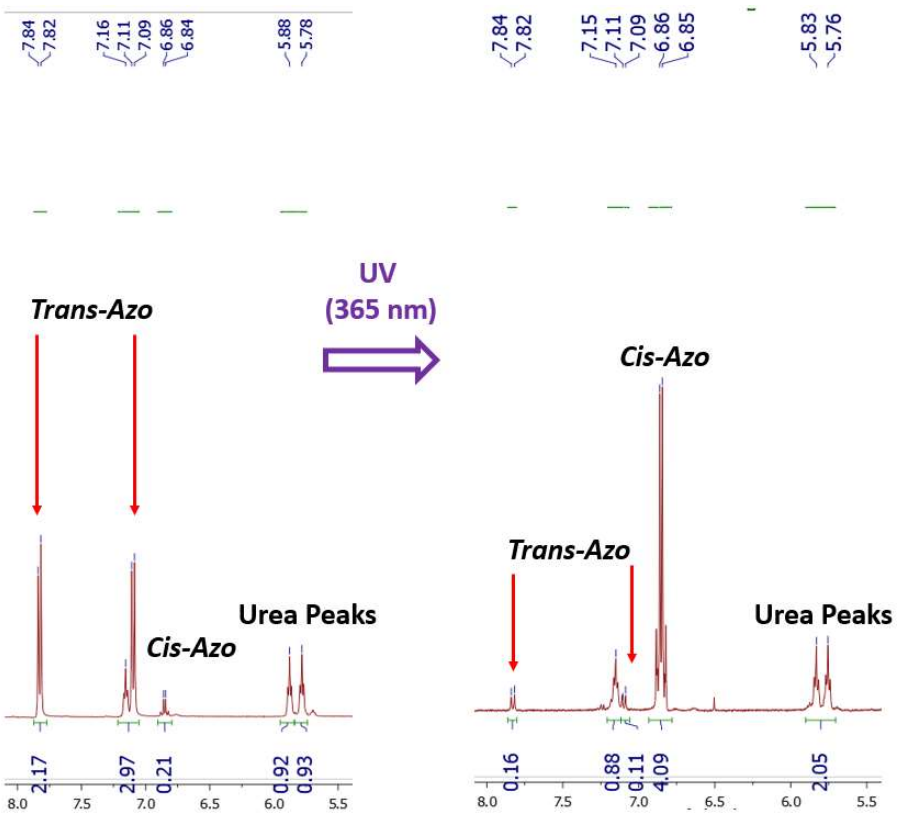

Figure C4-S9. ^{1}H NMR of Azo-(U-PEO)$_2$ in DMSO-d$_6$ prior to irradiation (left) and after UV irradiation (365 nm, right). Note that the signal at 7.16 ppm corresponds to the urethane protons. Integral reference set on the terminal PEO methoxy group (3H).

$\%_{trans}$ = (0.16 + 0.19)/(0.16 + 0.19 + 4.09) x 100 = **8 % ,** and $\%_{cis}$ = 100 - $\%_{trans}$ = **92% in DMSO after UV irradiation**

x. SANS – DMSO-d$_6$ solution

A 10 g/L solution in DMSO-d$_6$ was analyzed by SANS (**Figure C4-S20**) and the scattering intensity was very weak (which cannot be explained by a weak contrast since the theoretical contrast ($SLD_{polymer}$ – $SLD_{solvent}$)^2 of the polymer in DMSO is similar to that in toluene, 21 vs 25 10^{-12} Å^{-4}, respectively). A sharp increase of the scattering intensity at low q suggests that large aggregates are present, dominating the signal at low q, but there amount is low considering that the signal is dominated by small particles at high q.

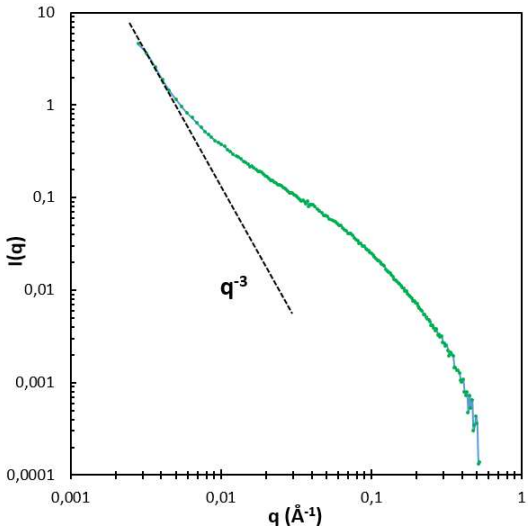

Figure C4-S10. SANS data of a 10 g/L solution in DMSO-d_6.

xi. UV-Vis – Irradiation cycles in toluene

A 1 g/L solution of Azo-(U-PEO)$_2$ was prepared in toluene, and subjected to UV (365 nm) and blue light (450 nm) irradiation cycles, see **Figure C4-S11.** Near quantitative recovery of the *trans* isomer was achieved following blue light irradiations.

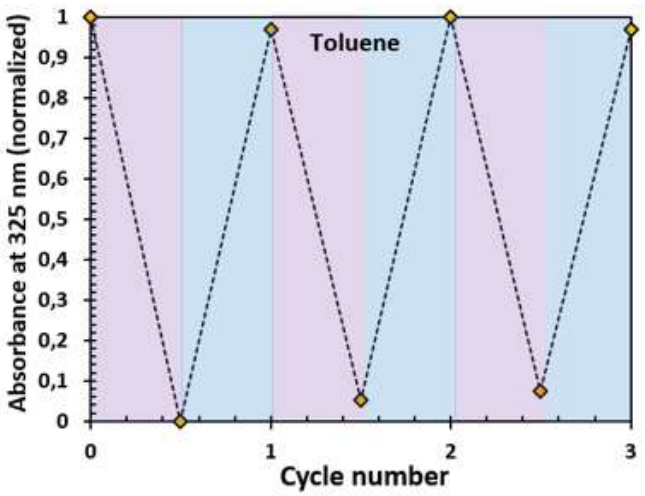

Figure C4-S11. UV/blue light (365 nm, 450 nm, respectively) irradiation cycles, monitored by UV-Vis, toluene (top right) at 1 g/L.

xii. SAXS – Scattering curves during photo-isomerization in toluene

SAXS scattering curves of a 10 g/L toluene solution during 365 nm irradiation, followed by 450 nm irradiation, are presented in **Figure C4-S12.** The q^{-1} angular dependence was conserved during UV irradiation, consistent with SANS measurements.

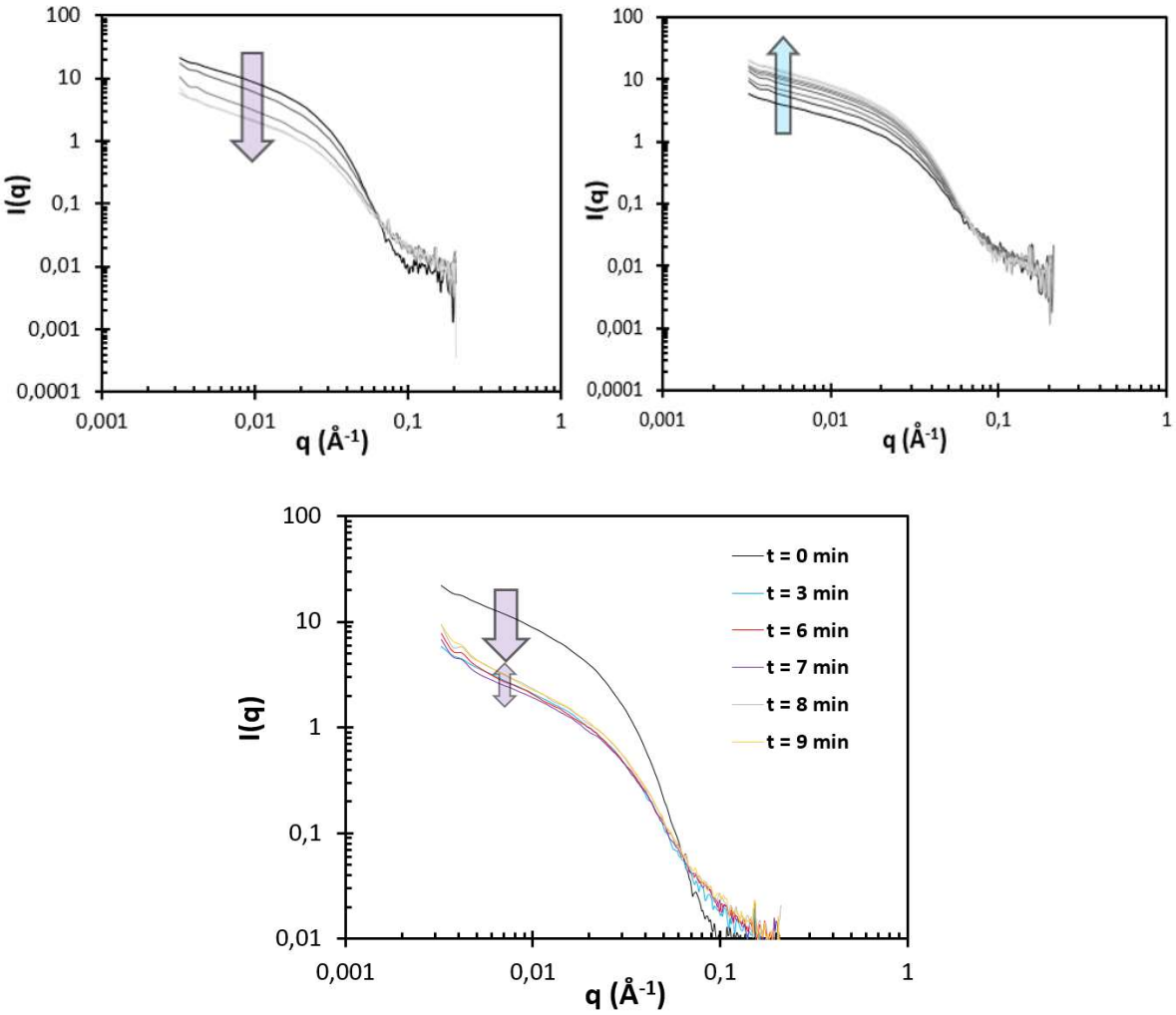

Figure C4-S12. SAXS data of a toluene solution (10 g/L) during UV irradiation (365 nm), 1 minute between each scan (**top left**), and during a second blue light irradiation (450 nm at 10% of max. LED power), 2 minutes between each scan (**top right**). Some SAXS scattering curves of the experiment monitoring thermal relaxation following UV irradiation are presented in the bottom graph, which correspond to the same data as the ones presented in **Figure 6, bottom**.

xiii. SAXS – Photo-isomerization cycles in toluene

A toluene solution (10 g/L) underwent irradiation cycles (365 nm followed by 450 nm and so forth) during SAXS analysis, and as can be seen in **Figure C4-S13**, the cycles were rather reproducible.

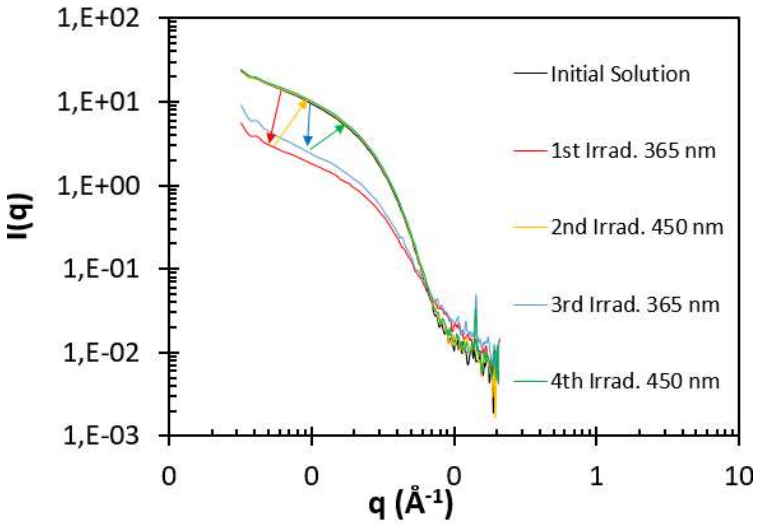

Figure C4-S13. SAXS irradiation cycles of a chloroform solution (10 g/L), arrows are for visual aid.

References

1. Harvey, L., Guigner, J. M., Bouteiller, L., Nicol, E. & Colombani, O. Photo-responsive disassembly of supramolecular polymer bottlebrushes in water. *Polym Chem* (Accepted, 2023) doi: 10.1039/D3PY00963G.

CONCLUSIONS AND PERSPECTIVES

The aim of this work was to synthesize polymer precursors capable of self-assembling into supramolecular nano-cylinders which could be reversibly disassembled in solution using light as a trigger. Firstly, the bibliographic state of the art showed the relevance of using supramolecular chemistry; and while several examples of light triggered disassembly of 1D nano-structures involving the self-assembly of small organic molecules have been reported, only one example of photo-triggered disassembly of supramolecular polymer bottlebrushes (with long polymer arms) had been reported by Perrier's group, which relied on the nature of the polymer arms for responsiveness and was also intrinsically irreversible. Therefore, a more versatile approach was employed for this work, where the responsiveness is imparted by the self-assembling core rather than the polymer arms. In light of the bibliographic review, H-bonding was selected as driving force for supramolecular self-assembly, due to its relatively high strength and directionality, while an azobenzene motif was chosen to impart light-responsiveness.

To achieve this, Azo-(U-PEO)$_2$ was designed and synthesized. This polymer is composed of a light-responsive self-assembling core: a light-responsive azobenzene core was functionalized with two urea moieties, which are H-bond promoting groups. Poly-(ethylene oxide) polymer arms were linked to this core with short alkyl spacers; the polymer arms provide solubility in water and some organic solvents, while the alkyl spacers protect the self-assembling core from H-bond competing solvents (such as water) and even reinforce assembly through the hydrophobic effect.

Initial attempts in synthesizing this compound relied on a convergent strategy, involving a final urea generating coupling step between an azobenzene diamine core and aliphatic amine terminated PEO. While the synthesis of the latter synthons was successfully achieved, several syntheses for the critical coupling step were explored during this project, including triphosgene and carbamate based routes, which rely on the generation of isocyanate in situ, but were ultimately unsuccessful. This could be attributed to two main reasons: 1) these reactions are generally carried out with aromatic amines, which stabilize intermediates, and 2) the reactivity of an amine on the end of a polymer is quite reduced in comparison to a molecular equivalent. While there may be other routes which exist for synthesizing ureas from aliphatic amines; we did not have the time to test any other ones. Lastly, it should be noted that in our case, reaction conditions that can be employed are somewhat limited, since an excess of neither the azobenzene nor the PEO can be used, as the former would lead to mono-functionalized azobenzene, and the latter would lead to an excess of unreacted PEO which would be difficult to remove during purification. Since generating aliphatic isocyanate appeared to be challenging, an alternative route was studied, using diisocyanates. The synthesis using an aliphatic C_6 diisocyanate (HMDI) yielded the desired product, despite purification being somewhat tedious. On the other hand, attempts at reproducing the same synthesis but with shorter (C_4) and longer (C_8) diisocyanates were unsuccessful, for reasons not entirely clear.

In water, direct dispersion of the polymer led to small, weakly aggregated particles, which were far from the desired anisotropic 1D nano-cylinders. An alternative protocol was then tested: the "water/DMSO" route. This consisted in first dissolving the polymer at high concentration in DMSO, a solvent in which the polymer is in unimer state. Water was then slowly added, triggering self-assembly into long nano-cylinders through a combination of cooperative H-bonding and hydrophobic effects.

Photo-isomerization of the azobenzene cores was possible to a large extent (70%) in spite of self-assembly, and UV irradiation, which triggered photo-isomerization to non-planar *cis*-Azo, led to the near quantitative disassembly of the nano-cylinders. While irradiating with blue light did lead to recovery of the initial, planar *trans*-Azo, this was not accompanied by re-assembly into nano-cylinders. This was attributed to the fact that the system was out of thermodynamic equilibrium (i.e. kinetically frozen), most likely due to the strong contribution of hydrophobic effects, and therefore unable to reorganize into nanocylinders after *cis* -> *trans* isomerization.

In organic solvents, such as chloroform and toluene, direct dispersion of the polymer led to the formation of nano-cylinders, suggesting that the system is in thermodynamic equilibrium. In chloroform, total disassembly occurred, but only partial re-assembly, due to remaining *cis*-Azo. In toluene, only partial disassembly occurred (~70% of the SPBs were disrupted), which is coherent with the fact that there was 25-30% of trans isomer still remaining after UV irradiation. It is possible that the photo-isomerization was somewhat blocked due to stronger self-assembly than in chloroform. Indeed, chloroform is more H-bond competitive than toluene and may have somewhat weakened the assemblies. It is worthy to note that in DMSO, where the polymer is in unimer state, UV irradiation leads to near quantitative formation of the *cis* isomer, further suggesting that it was the self-assembly which led to lower *cis*/*trans* ratios after UV irradiation in toluene.

Therefore, the main objective of this work was accomplished, as reversible light-triggered disassembly of supramolecular polymer nano-cylinders was achieved. To further the study, it would be desirable to achieve reversible light-triggered disassembly of SPBs in water. It may perhaps be possible to achieve this by reducing hydrophobic effects, therefore synthesizing an Azo-(U-PEO)$_2$ with shorter alkyl chains may be interesting. This could potentially be achieved using a diisocyanate based synthesis with a shorter diisocyanate.

It would also be interesting to understand the role of the polymer arms in the self-assembling properties. To study the impact of the polymer arms in a more versatile manner, the synthesis of a RAFT agent (such as Azo-(U-TTC)$_2$) would be an attractive strategy. Longer and/or bulkier polymer arms may hinder self-assembly, allowing for a certain control over nano-cylinder length.

These studies could ultimately allow access to light responsive Pickering emulsions, where reversible demulsification may be achieved. The RAFT agent would allow for the synthesis of copolymer arms, and for fine tuning its affinity with the water and oil phases.

It may also be possible to generate light-responsive Janus nano-cylinders, by combining asymmetric and complementary self-assembling motifs (such as tris-ureas) with azobenzene units. Such systems could potentially stabilize emulsions even more than non-Janus assemblies.

Lastly, such systems could potentially be functionalized for given applications, such as catalysis or to interact with specific molecules, such as proteins.

COLLEGE DOCTORAL PAYS DE LA LOIRE
ED MATIERE, MOLECULES MATERIAUX ET GEOSCIENCES

Le Mans Université

Titre : Elaboration de nano-cylindres supramoléculaires photo-stimulables en solution

Mots clés : Azobenzene, Bis-urée, Auto-assemblage, Chimie supramoleculaire, Photo-stimulable

L'objectif de ce travail a été d'élaborer des nano-cylindres supramoléculaires qui peuvent être réversiblement désassemblés en utilisant la lumière comme stimulus. A cette fin, Azo-(U-PEO)$_2$ a été conçu et synthétisé. C'est un polymère composé d'un coeur azobenzène-bis-urée photo-sensible et auto-associative, auquel deux bras poly(oxyde d'ethylène) (POE) sont liés par le biais de deux courtes chaines alkyles. Tant que les azobenzènes, photo-sensibles, sont dans leur configuration *trans*, plane, ce polymère peut être auto-assemblé en nano-cylindres par liaisons hydrogène directionnelles et coopératives entre unités urée.

Dans l'eau, le polymère peutt être auto-assemblé en longs nano-cylindres de plusieurs centaines de nanomètres de longs, en le solubilisant dans le DMSO puis en ajoutant de l'eau, déclenchant l'auto-assemblage. L'irradiation UV provoque la photo-isomérisation des azobenzènes en leur configuration *cis*, non planaire, qui mène au désassemblage des nano-cylindres. Une irradiation avec de la lumière bleue permet de reformer l'isomère initial trans, mais ne mène pas à la reformation des nano-cylindres. Ceci peut être expliqué par le fait que les assemblages sont cinétiquement figés à cause des effets hydrophobes.

Dans le toluène et le chloroforme, où il y a beaucoup moins d'effets solvophobes, le polymère s'auto-assemble spontanément en nano-cylindres, suggérant que le système est à l'équilibre thermodynamique. L'irradiation UV mène à un désassemblage partiel dans le toluène et total dans le chloroforme. L'irradiation avec de la lumière bleue mène au ré-assemblage total dans le toluène, mais seulement partiel dans le chloroforme.

Pour conclure, l'objectif principal de ce projet a été accompli, et représente le premier exemple de désassemblage réversible photo-induit de nano-cylindres supramoléculaires décorés de bras polymères.

Title: Elaboration of photo-responsive supramolecular nano-cylinders in solution

Key-words: Azobenzene, Bis-urea, Self-assembly, Supramolecular chemistry, Light-responsive

The aim of this work was to elaborate supramolecular nano-cylinders that may be reversibly disrupted using light as a trigger. To this end, Azo-(U-PEO)$_2$ was designed and synthesized. This is a polymer composed of a light-responsive azobenzene bisurea self-assembling core, linked to two poly(ethylene oxide) (PEO) arms with short alkyl chains. As long as the photo-responsive azobenzenes were in their planar *trans* configuration, this polymer could be self-assembled into nano-cylinders through directional and cooperative hydrogen bonding between urea units.

In water, the polymer could be self-assembled into long nano-cylinders of several hundreds of nanometers in length, by first dissolving it in DMSO, followed by water addition, triggering self-assembly. UV irradiation triggered photo-isomerizing of the azobenzene units to their non-planar *cis* configuration, leading to the disruption of the nano-cylinders. While blue light irradiation did lead to recovery of the initial trans isomer, this was not accompanied by the re-assembly of the nano-cylinders. This could be explained by the kinetically frozen nature of the assemblies, due to hydrophobic effects.

In toluene and chloroform, where there were far fewer solvophobic effects, the polymer self-assembled spontaneously into nano-cylinders, suggesting that the system was at thermodynamic equilibrium. UV irradiation led to partial disassembly in toluene, while it was total in chloroform. Blue light irradiation led to total re-assembly in toluene, and only partial re-assembly in chloroform.

To summarize, the main aim of this project was achieved, and represents the first example of reversible light-triggered disassembly of supramolecular polymer decorated nano-cylinders.